

Bentonite Seal Properties in Saline Water

NWMO TR-2018-20

December 2018

David Dixon¹, Alex Man², Santosh Rimal¹, Jeff Stone¹, Greg Siemens³

¹ Golder Associates Limited: Winnipeg, MB; Mississauga, ON; Saskatoon, SK

² Scatliff, Miller and Murray, Winnipeg MB;

³ Royal Military College, Kingston, ON

nwmo

NUCLEAR WASTE
MANAGEMENT
ORGANIZATION

SOCIÉTÉ DE GESTION
DES DÉCHETS
NUCLÉAIRES

Nuclear Waste Management Organization

22 St. Clair Avenue East, 6th Floor

Toronto, Ontario

M4T 2S3

Canada

Tel: 416-934-9814

Web: www.nwmo.ca

Bentonite Seal Properties in Saline Water

NWMO TR-2018-20

December 2018

**David Dixon¹, Alex Man², Santosh Rimal¹, Jeff Stone¹,
Greg Siemens³**

¹ Golder Associates Limited: Winnipeg, MB; Mississauga, ON; Saskatoon, SK

² Scatliff, Miller and Murray, Winnipeg, MB

³ Royal Military College, Kingston, ON

This report has been prepared under contract to NWMO. The report has been reviewed by NWMO, but the views and conclusions are those of the authors and do not necessarily represent those of the NWMO.

All copyright and intellectual property rights belong to NWMO.

Document History

Title:	Bentonite Seal Properties in Saline Water		
Report Number:	NWMO TR-2018-20		
Revision:	R000	Date:	December 2018
¹ Golder Associates Limited; ² Scatliff, Miller and Murray; ³ Royal Military College			
Authored by:	David Dixon ¹ , Alex Man ² , Santosh Rimal ¹ , Jeff Stone ¹ , Greg Siemens ³		
Verified by:	Frank Barone <i>Frank Barone</i>		
Approved by:	Jeff Stone <i>J Stone</i>		
Nuclear Waste Management Organization			
Reviewed by:	Ken Birch		
Accepted by:	Paul Gierszewski		

Revision Summary		
Revision Number	Date	Description of Changes/Improvements
R00	2019-05	Initial issue

ABSTRACT

Title: Bentonite Seal Properties in Saline Water
Report No.: NWMO TR-2018-20
Author(s): David Dixon¹, Alex Man², Santosh Rimal¹, Jeff Stone¹, Greg Siemens³
Company: ¹Golder Associates Ltd., ²Scatliff, Miller and Murray, ³Royal Military College of Canada
Date: December 2018

Abstract

This document presents the latest results of laboratory testing of 1) a mixture of 70% MX80 bentonite clay and 30% graded sand being considered for use as a shaft sealing material, and 2) 100% bentonite for use as buffer ($>1.4 \text{ Mg/m}^3$ minimum compacted dry density) and also in the form of highly compacted bentonite (HCB) blocks ($>1.7 \text{ Mg/m}^3$ compacted dry density). These materials are being considered for sealing purposes in a deep geological repository located at a nominal depth of 500 m below ground surface and potentially in a sedimentary rock environment. The pore fluid compositions that could be encountered at such depths require that the bentonite-based materials be capable of maintaining their hydro-mechanical properties under a wide range of conditions.

In order to begin the process of qualifying potential materials for use, as well as to identify what behavioural parameters are particularly sensitive to conditions such as groundwater salinity and density, the material characterisation study described in this document was completed.

The bentonite-sand material was tested to evaluate its basic physical (compaction) and mineralogical properties as well as its hydro-mechanical properties including hydraulic conductivity, swelling pressure, shear strength, air permeability, suction-moisture behaviour and thermal conductivity. Laboratory prepared reference solutions containing approximately 0 g/L, 11 g/L, 223 g/L and 335 g/L total dissolved solids were used in the testing in order to determine what effects salinity would have on the post-placement behaviour of this material.

Testing of the basic index properties confirmed that the behaviour of bentonite-based materials is substantially affected by the pore fluid it is exposed to. These data also provide a measure of the degree of variability that can be expected when different laboratories are used for chemical and mineralogical evaluation or the same laboratory and operator conduct basic index tests on identical materials. These values provide a means to begin evaluation of what level of confidence can be applied to other more complex parameters associated with modelling the longer-term hydro-mechanical evolution of clay-based engineered barriers materials.

TABLE OF CONTENTS

ABSTRACT	iii
LIST OF TABLES	vii
LIST OF FIGURES	viii
1. INTRODUCTION.....	1
2. CHEMICAL AND MINERALOGICAL CHARACTERIZATION	4
2.1 COMPOSITION OF REFERENCE WATER SOLUTIONS.....	4
2.2 DESCRIPTION OF SAND AND CLAY MATERIALS	5
2.2.1 Quartz Sand	5
2.2.2 MX80 Bentonite.....	5
2.3 MINERALOGICAL AND CHEMICAL CHARACTERISATION	7
2.3.1 Methods and Materials	7
2.3.2 MX80 Bentonite: XRD and XRF Analyses of As-received Material	7
2.3.3 Bentonite After Brine-Soaking	10
2.3.4 Quartz Sand Analyses.....	14
3. COMPACTION TESTING	16
4. CONSISTENCY (ATTERBERG) LIMITS	20
5. FREE SWELL INDEX	22
6. SWELLING PRESSURE AND HYDRAULIC CONDUCTIVITY TESTING.....	23
6.1 BACKGROUND.....	23
6.2 SWELLING PRESSURE.....	26
6.2.1 Directly Measured Swelling Pressure	26
6.2.2 Swelling Pressures Derived from One-Dimensional Consolidation Testing.....	30
6.3 HYDRAULIC CONDUCTIVITY.....	30
6.3.1 Directly Measured Hydraulic Conductivity.....	30
6.3.2 Hydraulic Conductivity Derived from Oedometer Test Data.....	34
6.3.3 Permeability Parameter	34
6.4 DISCUSSION.....	36
7. SHRINKAGE, SOIL WATER CHARACTERISTIC CURVES AND AIR PERMEABILITY	40
7.1 BACKGROUND AND APPROACH TO TESTING	40
7.2 SHRINKAGE TESTS	40
7.2.1 Background and Test Method.....	40
7.2.2 Shrinkage Behaviour of MX80 and MX80-Sand Specimens	42
7.3 SOIL-WATER CHARACTERISTIC CURVES (SWCC)	48
7.3.1 Background and Testing Method.....	48
7.3.2 SWCC Test Results	51
7.3.3 Comparison of SWCC Behavior of MX80 and BSM Materials	56

7.4 AIR PERMEABILITY (AP) MEASUREMENTS	58
7.4.1 Background and Testing Method	58
7.4.2 Air Permeability Test Results.....	59
7.4.3 Summary of Air Permeability Testing.....	65
7.5 SWCC and Air Conductivity Results Summary.....	67
8. MECHANICAL PROPERTIES TESTING	69
8.1 BACKGROUND.....	69
8.2 ISOTROPIC TRIAXIAL CONSOLIDATION TESTS (K, κ, λ).....	69
8.2.1 Isotropic Consolidation Test Setup	69
8.2.2 Isotropic Consolidation Test Results (K, κ and λ).....	71
8.3 ISOTROPICALLY CONSOLIDATED UNDRAINED (CI\bar{U}) TRIAXIAL TESTS (G).....	72
8.3.1 CI \bar{U} Test Setup.....	72
8.3.2 CI \bar{U} Test Results (G)	74
8.4 ISOTROPICALLY CONSOLIDATED DRAINED (CID) TRIAXIAL TESTS	76
8.4.1 CID Test Setup.....	76
8.4.2 CID Test Results (E).....	76
8.5 TRIAXIAL SHEAR STRENGTH AND YIELD LOCUS.....	78
8.6 SUMMARY OF STRESS-STRAIN BEHAVIOUR DETERMINED BY TRIAXIAL TESTING	81
8.7 ONE-DIMENSIONAL CONSOLIDATION (OEDOMETER) TESTS	83
8.7.1 Oedometer Test Setup	83
8.7.2 Oedometer Test Results.....	85
8.7.3 Summary of One-Dimensional Consolidation Test Results.....	87
8.8 SUMMARY OF MECHANICAL PROPERTIES	88
9. THERMAL PROPERTIES TESTING	92
9.1 BACKGROUND.....	92
9.2 THERMAL TESTING SETUP.....	92
9.2.1 Thermal Constants Analyzer (TPS1500) Description.....	92
9.2.2 Testing Method.....	93
9.2.3 Calculation of Thermal Properties.....	94
9.3 RESULTS OF THERMAL CHARACTERIZATION TESTING.....	96
9.4 SUMMARY OF THERMAL CHARACTERIZATION TESTS.....	99
10. SUMMARY: COMPILATION OF PARAMETER VALUES	100
11. CLOSURE	110
REFERENCES	111
APPENDIX A: CHEMICAL COMPOSITION OF SALINE SOLUTIONS.....	113
APPENDIX B: RESULTS OF XRD AND XRF ANALYSES OF MINERALS TESTED.....	122
APPENDIX C: MODIFIED COMPACTION TEST DATA.....	139
APPENDIX D: CORRECTION FOR SALT CONTENT IN SATURATED SOIL.....	141

APPENDIX E : SWELLING PRESSURE AND HYDRAULIC CONDUCTIVITY TEST DATA	143
APPENDIX F: DRYING VOLUME CHANGE (SHRINKAGE) DATA.....	145
APPENDIX G: SOIL WATER CHARACTERISTIC CURVE (SWCC) DATA.....	154
APPENDIX H: AIR PERMEABILITY TEST DATA.....	162
APPENDIX I: TRIAXIAL TEST RESULTS.....	168
APPENDIX J: UNIAXIAL CONSOLIDATION (OEDOMETER) TEST RESULTS.....	189
APPENDIX K: THERMAL PROPERTIES MEASUREMENTS.....	204

LIST OF TABLES

	Page
Table 1.1: Testing Matrix for Current Study	2
Table 2.1: Target Concentrations for Reference Solutions as Specified by NWMO.....	4
Table 2.2: Salts Added to Reach Target Concentrations in the Reference Solutions	4
Table 2.3: Measured Versus Target Concentrations for the Major Cations and Anions in the Reference Solutions.....	5
Table 2.4: Semi-Quantitative X-Ray Diffraction Results for Bulk MX80 Bentonite	8
Table 2.5: Major Oxides Composition of Source MX80 Bentonite by XRF.....	10
Table 2.6: Semi-Quantitative X-Ray Diffraction Results for MX80 Bentonite After 18 Months Exposure to SR-Sh Brine	12
Table 2.7: Major Oxides Composition of MX80 Bentonite After Brine Exposure as Determined by XRF	13
Table 2.8: Semi-Quantitative X-ray Diffraction Results for Sand	14
Table 2.9: Major Oxides Composition of Sand Determined by XRF	15
Table 3.1: Maximum Density Achieved Using Modified Compaction Effort for MX80	17
Table 3.2: Maximum Density Achieved Using Modified Compaction Effort for 70:30 BSM	17
Table 4.1: Consistency Limits for MX80 Bentonite (ASTM-D4318-10)	20
Table 4.2: Consistency Limits for Screened BSM (ASTM-D4318-10).....	21
Table 5.1: Free Swell Test Results for MX80 and 70:30 BSM (ASTM-D-5890-11)	22
Table 6.1: Hydraulic Conductivity Equations from Best-Fit Lines (based on EMDD values)	31
Table 6.2: Fluid Densities, Viscosities and Conversion Factors to Calculate Permeability.....	35
Table 6.3: Hydraulic Conductivity (k) and Permeability (K) Calculated from Best-Fit Lines.....	35
Table 6.4: Regression Equations Describing Swelling Pressure and Hydraulic Properties of MX80 and 70:30 MX80:Sand Materials.....	39
Table 7.1: Fitting Parameters Used to Describe Shrinkage Behaviour of MX80 and BSM.....	48
Table 7.2: Fitting Parameters Used to Generate SWCCs for MX80 and BSM.....	57
Table 7.3: Fitting Parameters Used to Derive Air Permeability Trendlines.....	66
Table 8.1: Bulk Modulus (K) and elastic-plastic parameters (κ and λ)	71
Table 8.2: Shear Modulus (G) Results	74
Table 8.3: Young's Modulus (E) Results	78
Table 8.4: Summary of Shear Strength Test Results.....	79
Table 8.5: Summary of mechanical properties parameters derived from triaxial testing	82
Table 8.6: Summary of Oedometer Test Results.....	89
Table 10.1: Summary of Materials Properties and Behaviour Data (MX80 at $\sim 1.5 \text{ Mg/m}^3$ Dry Density, EMDD = 1.35 Mg/m^3).....	104
Table 10.2: Summary of Materials Properties and Behaviour Data (MX80 at $\sim 1.7 \text{ Mg/m}^3$ Dry Density, EMDD = 1.56 Mg/m^3).....	106
Table 10.3: Summary of Properties and Behaviour Data (70:30 MX80:Sand at $\sim 1.7 \text{ Mg/m}^3$ Dry Density; EMDD $\sim 1.37 \text{ Mg/m}^3$).....	108

LIST OF FIGURES

	Page
Figure 2.1: Grain Size Distribution Curve for Sand	6
Figure.2.2: Grain Size Distribution Curve for MX80 Bentonite	6
Figure 2.3: Desalinization of MX80 Specimens Using Dialysis Membranes	11
Figure 3.1 : Miniature Compaction Device (Priyanto et al. 2013)	18
Figure 3.2: Compaction Curves for MX80 Bentonite Obtained Using Miniature Compaction Device.....	18
Figure 3.3: Miniature Compaction Curves for 70:30 BSM Obtained Using Miniature Compaction Device.....	19
Figure 6.1: Test Cells and Flow Gauges Used to Measure Swelling Pressure and Hydraulic Conductivity (from Priyanto et al. 2013)	24
Figure 6.2: Swelling Pressures Measured for MX80 Bentonite (circled data are replicates)	28
Figure 6.3: Effect of Pore Fluid Salinity on Swelling Pressure of MX80 Systems.....	29
Figure 6.4: Hydraulic Conductivity Measurements for MX80 Bentonite.	32
Figure 6.5: Comparison of New MX80 Bentonite and BSM Hydraulic Conductivity Data to Literature Values.....	33
Figure 6.6: Water permeability as a Function of EMDD and Pore Fluid Salinity.....	36
Figure 6.7: Swelling Pressure and Hydraulic Conductivity Best-Fit Lines and Comparison to Data Presented by Baumgartner et al. (2006) (dashed lines)	38
Figure 7.1: Photograph Showing Shrinkage Specimen (Fredlund et al. 2012).....	42
Figure 7.2: Drying Shrinkage and Density Change of MX80 and MX80-Sand Specimens.....	44
Figure 7.3: Shrinkage Behaviour of MX80 at 1.5 Mg/m ³ Dry Density in DW, SR-L and SR-Sh Pore Fluids	45
Figure 7.4: Shrinkage Behaviour of 70% MX80 : 30% Sand at ~1.8 g/cc Dry Density in DW, CR10, SR-L & SR-Sh Pore Fluids.....	46
Figure 7.5: Comparison of Shrinkage Behaviour of MX80 and 70:30 Bentonite:Sand	47
Figure 7.6: GCTS Apparatus Used to Measure the SWCC in Low Suction Range and MX80 SWCC Specimen in Ring After Test.....	49
Figure 7.7: WP4 Device Used to Measure the SWCC in the High-Suction Range and Example of Specimen Used in Testing.....	50
Figure 7.8: SWCC Curves for MX80 Bentonite at 1.5 Mg/m ³ Dry Density.....	53
Figure 7.9: Comparison of Saturation – Capillary Pressure Behaviour of MX80.....	54
Figure 7.10: SWCC Curves for BSM Material at ~1.8 Mg/m ³ Dry Density	55
Figure 7.11: Comparison of Saturation – Capillary Pressure Behaviour of BSM.....	56
Figure 7.12: Comparison of SWCCs of BSM and MX80.....	57
Figure 7.13: Specimen Installed in Triaxial Cell for Air Permeability Testing and Test Apparatus in Operation	58
Figure 7.14: Air Conductivity and Air Permeability of MX80 Bentonite at ~1.5 Mg/m ³ Dry Density (DW and SR-L Solutions)	61
Figure 7.15: Air Conductivity and Air Permeability of MX80 Bentonite at ~1.5 Mg/m ³ Dry Density (SR-Sh Solution)	62
Figure 7.16: Air Conductivity and Air Permeability of 70:30 MX80:Sand at ~1.8 Mg/m ³ Dry Density (DW and CR10 Solutions)	63
Figure 7.17: Air Conductivity and Air Permeability of 70:30 MX80:Sand at ~1.8 Mg/m ³ Dry Density (SR-L & SR-Sh Solutions)	64
Figure 7.18: Air Conductivity and Air Permeability of MX80 and BSM	65
Figure 7.19: Comparison of Current Air Conductivity Results to Barone et al. (2014).....	66

Figure 7.20: Summary of Fitted Air Permeability Results Based on Water Saturation	68
Figure 7.21: Summary of Fitted Air Permeability Results Based on Capillary Pressure.....	68
Figure 8.1: Triaxial Test Apparatus at Golder's Mississauga Laboratory	70
Figure 8.2: Isotropic Consolidation Test Results	72
Figure 8.3: Triaxial Test Apparatus used at RMC.....	73
Figure 8.4: Stress-Strain Curves from CI \bar{U} Tests	75
Figure 8.5: Stress-Strain Curves from CID Tests	77
Figure 8.6: p', q Plots from Triaxial Tests	80
Figure 8.7: Lever-Arm Oedometers Used in 1-D Consolidation Testing.	84
Figure 8.8: Derivation of the Parameters of C _c , C _s (sometimes referred to as C _r) in 1D Consolidation Tests and the Lambda and Kappa Parameters from Triaxial Testing. (Figure from Priyanto et al. 2013).	84
Figure 8.9: Consolidation Tests Showing Effect of Salinity on Rebound Behaviour.....	86
Figure 8.10: Effect of Pore Fluid Composition on Volume Compressibility (mv) and Swelling Index (C _s) Properties of 70:30 MX80:Sand Specimens and 100% MX80 clay.	90
Figure 8.11: Effect of Pore Fluid Composition on Consolidation (C _c) and Swelling (C _r) Properties of 70:30 MX80:Sand Specimens and 100% MX80 Clay.....	91
Figure 9.1: Hot Disk Sensor Used in Current Thermal Testing	93
Figure 9.2: Thermal Test Setup Showing Sensor and Specimen installation.....	94
Figure 9.3: Specific Heat of MX80 and 200 Mesh Wyoming Bentonite Compacted Using Fresh Water.	97
Figure 9.4: Thermal Conductivity of MX80 Bentonite and 200 Mesh Wyoming Bentonite Compacted Using Fresh Water (average of three readings).	98
Figure 9.5: Thermal Diffusivity of MX80 and 200 Mesh Wyoming Bentonite Compacted Using Fresh Water (average of three readings).....	98

1. INTRODUCTION

The Nuclear Waste Management Organization (NWMO) is responsible for the long-term management of Canada's used nuclear fuel. The purpose of this project is to provide material properties data to support the optimization and safety assessment of bentonite-based materials that are proposed for sealing purposes in a deep geological repository (DGR).

The geotechnical testing program described in this document focused on characterizing two bentonite-based reference sealing materials under a range of pore fluid salinities and dry densities. Bentonite-based materials included 1) a mixture of 70% MX80 bentonite clay and 30% graded sand for a shaft sealing material (compacted to 1.7 to 1.8 Mg/m³ dry density), and 2) 100% bentonite for buffer in a sedimentary environment, compacted to (a) 1.4 Mg/m³ minimum dry density, and (b) as highly compacted bentonite (HCB) blocks (>1.7 Mg/m³ dry density). These materials need to have appropriate mineralogical, chemical and hydro-mechanical properties in order to ensure that the backfilled openings do not become preferential pathways for movement of gas or contaminants following repository closure.

The 70:30 bentonite: sand mixture (BSM) and 100% bentonites examined in this study were tested using four pore fluids. The pore fluids used were predefined with regards to both their ionic composition as well as their total dissolved solids (TDS) concentrations and consisted of deionized water (DW), CR-10 (~11 g/L TDS), SR-L (~223 g/L TDS) and SR-Sh (~335 g/L TDS).

The following properties were determined for the bentonite-based sealing materials using the four pore fluids defined by NWMO:

- Compaction/fabrication properties of the materials (to Modified Proctor density);
- Consistency limits (Atterberg Limits) and free swell tests;
- Density of as-fabricated material;
- Moisture content of as-fabricated material;
- Mineralogical/chemical composition to approximately the 1 wt% level, including three independent measurements of montmorillonite content using different laboratories;
- Mineralogical/chemical composition of the materials exposed to brine for an extended period of time;
- Swelling pressure;
- Saturated hydraulic conductivity;
- Two phase gas/water properties, specifically the capillary pressure function (or soil-water characteristic curve (SWCC)) and relative permeability function, measured over a range of saturations that include the as-fabricated and fully saturated condition;
- Mechanical parameters including Shear Modulus (G), Bulk Modulus (K) and Young's Modulus (E); and
- Thermal properties including thermal conductivity and specific heat capacity.

These tests were typically done in triplicate to allow for assessment of data reproducibility. A listing of tests and replicates completed is provided in Table 1.1.

Table 1.1: Testing Matrix for Current Study

No.	Tests / Parameters	70:30 Bentonite:Sand				100% Bentonite			HCB ¹	
		Test Fluid					DW	SR-L	SR-Sh	DW
1	Compaction Properties ²	√ (3)	√ (3)	√ (3)	√ (3)	√ (3)	√ (3)	√ (3)	-	-
2	Initial mineralogical composition ³	-	-	-	√ (3)	-	-	-	-	-
3	As-fabricated chemical composition ³	-	-	-	√ (3)	-	-	-	-	-
4	Mineralogy after brine exposure ³	-	-	-	√ (3)	-	-	-	-	-
5	Composition after brine exposure ³	-	-	-	√ (3)	-	-	-	-	-
6	Consistency limits ⁴	√ (3)	√ (3)	√ (3)	√ (3)	√ (3)	√ (3)	√ (3)	-	-
7	Free swell	√ (3)	√ (3)	√ (3)	√ (3)	√ (3)	√ (3)	√ (3)	-	-
8	Saturated swelling pressure	√ (1)*	√ (3)	√ (3)	√ (3)	√ (1)*	√ (3)	√ (3)	√ (1)*	√ (3)
9	Saturated hydraulic conductivity	√ (1)*	√ (3)	√ (3)	√ (3)	√ (1)*	√ (3)	√ (3)	√ (1)*	√ (3)
10	Gas permeability, K_g ⁵	√ (3)	√ (3)	√ (3)	√ (3)	√ (3)	√ (3)	√ (3)	-	-
11	Capillary pressure, SWCC ⁵	√ (3)	√ (3)	√ (3)	√ (3)	√ (3)	√ (3)	√ (3)	-	-
12	Triaxial isotropic consolidation (K, κ , λ) ⁶	√ (1)	√ (1)	√ (1)	√ (1)	√ (1)	√ (1)	√ (1)	-	-
13	1D-Consolidation tests (m_v , C_c , C_s) ⁷	√ (3)	√ (3)	√ (3)	√ (3)	√ (3)	√ (3)	√ (3)	-	-
14	Triaxial undrained shearing (CIU) (G) ⁸	√ (1)	-	-	-	-	-	-	√ (1)	-
15	Triaxial drained shearing (CID) (E) as-fabricated ⁹	√ (3)	-	-	-	-	-	-	√ (3)	-
16	Thermal properties (0 to 100 % saturation) ¹⁰	-	-	-	-	√ (3)	-	-	√ (3)	-

Notes: Values in brackets are number of replicates required and colours indicate laboratory that was to complete the work (Blue = Royal Military College (RMC) lab, Red = Golder labs).

* Large database exists, if first test was consistent with existing data, no replicates were planned.

¹ HCB – Highly Compacted Bentonite blocks with dry density of 1.7 Mg/m³ or greater.

² Modified Proctor curve composed of more than 6 points.

³ Three specimens exposed to SR-Sh brine were tested to check for mineralogical or chemical changes.

⁴ Also known as Atterberg Limits.

⁵ Gas permeability and capillary pressure curves (Soil Water Characteristic Curve or SWCC) constructed using multiple points at saturations ranging from as-fabricated to fully-saturated.

⁶ Isotropic consolidation tests split between RMC's and Golder's laboratories. Only one specimen per condition due to very long saturation times. Tests provide Bulk Modulus (K), elastic-plastic κ and λ parameters. At the end of test the specimens were sheared to provide a point on the strength envelope.

⁷ 1D consolidation following ASTM Standards for oedometer tests to provide volume compressibility (m_v), Swelling Index (C_s) and Compression Index (C_c).

⁸ CI \bar{U} tests on DW and CR-10 specimens done at RMC in high pressure cells (6 MPa cell pressure). Since pore water pressure measurements are required for CI \bar{U} tests. Due to very long saturation periods expected for these specimens, only one specimen was tested. These tests were used to determine the Shear Modulus (G) since $\epsilon_v = \epsilon_s$ when there is no volume change (i.e. undrained).

⁹ CID tests done on as-fabricated specimens, consolidated isotropically at the expected swelling pressure of the material to prevent decreases in density, and then sheared under drained conditions with zero back pressure at the as-fabricated moisture content. Tests were used to determine Young's Modulus (E).

¹⁰ Thermal conductivity and specific heat capacity on specimens at target saturations of 0%, 5%, 10%, 15%, 20%, 30%, 40%, 50%, 60%, 80% and 100%.

The materials selected for examination in this testing program to determine their hydraulic, mechanical, suction-moisture and gas transport characteristics are of a nature that tests are technically challenging to complete and can require long testing times. Table 1.1 lists all the tests conducted and the number of replicates of each completed as part of this work. In addition to the tests listed in Table 1.1, activities such as the identification of sources of supply and development of formulations for the sand component to be blended with the MX-80 bentonite in order to produce the 70:30 bentonite: sand mixture (BSM) specified for testing were completed prior to the initiation of testing. The saline solutions used in the testing program also required development of dry component formulations that would result in fluids meeting total dissolved solids (TDS) and ionic composition specifications.

2. CHEMICAL AND MINERALOGICAL CHARACTERIZATION

2.1 COMPOSITION OF REFERENCE WATER SOLUTIONS

As part of the program guidelines provided by NWMO, target concentrations were set for solutes in each of the reference solutions used (Table 2.1). The redox potential (E_h) although provided, is not a parameter that can be readily maintained in a laboratory and was not deemed as relevant to the behavioural properties being evaluated in this study. The pH of each of the solutions was checked to ensure that they closely matched the target values and adjusted as necessary.

Table 2.1: Target Concentrations for Reference Solutions as Specified by NWMO

Parameter	CR-10	SR-L	SR-Sh
pH	7.0	'neutral'	'neutral'
Na	1900	46000	55200
Ca	2130	19400	48100
K	15	17600	19500
Mg	60	4860	6080
Cl	6100	135100	205600
SO ₄	1000	480	96
TDS	11205	223440	334576

Note: Units are in mg/L, except for pH.

Table 2.2 presents the formulations used to prepare the reference solutions for this study. A comparison of the measured and target solute concentrations for the prepared reference solutions is provided in Table 2.3. The differences between target and determined values are attributable to analytical uncertainty associated with the increasing degree of dilution required for chemical analyses by ion chromatography/mass spectrometry as ionic concentrations increase. The detailed analytical laboratory results for the test batches of each solution are provided in Appendix A and are summarized below.

Table 2.2: Salts Added to Reach Target Concentrations in the Reference Solutions

Salt	Units	Amount of Salt Added		
		CR-10	SR-L	SR-Sh
NaCl	g/L	4.85	116.89	140.26
KCl	g/L	nil	33.55	37.28
CaCl ₂ – 2H ₂ O	g/L	6.32	70.55	176.37
MgCl ₂ – 2H ₂ O	g/L	0.59	40.64	50.80
CaSO ₄ – 2H ₂ O	g/L	1.72	1.04	0.17

Table 2.3: Measured Versus Target Concentrations for the Major Cations and Anions in the Reference Solutions

Parameter	Measured Concentration in Prepared Solution			Target Concentrations (from Table 2.1)		
	CR-10	SR-L	SR-Sh	CR-10	SR-L	SR-Sh
pH	7.88	6.73	6.43	7.0	'neutral'	'neutral'
Sodium	1.85	43.5	51.7	1.9	46	55.2
Calcium	2.03	20.3	45.0	2.13	19.4	48.1
Potassium	0.085	18.0	20.8	0.015	17.6	19.5
Magnesium	0.067	4.53	5.66	0.06	4.86	6.08
Chloride	6.08	138.0	204.0	6.1	135.1	205.6
Sulphate	0.923	0.83	<0.75	1.0	0.48	0.096
Total	11.0	225.0	327.0	11.21	223.44	334.58
Fluid density (g/cc)				1.0058	1.1528	1.2186

Note: Concentration units are g/L except for pH and final density.

2.2 DESCRIPTION OF SAND AND CLAY MATERIALS

2.2.1 Quartz Sand

The sand used in this study was a size-blended material that falls within the tolerance limits predefined by NWMO at the start of this project (SA440 in Figure 2.1). The sand was required to be water-washed natural sand of glacio-fluvial origin. It is dominated by sub-round quartz with minor feldspar and trace non-silicates (e.g. calcite). The results of a sieve analysis on the sand selected for use in this study are presented in Figure 2.1 and show a fine to medium grain size that meets the size and gradation requirements set for this component. The detailed mineralogical and chemical composition of this component is presented in Section 2.3.

2.2.2 MX80 Bentonite

The bentonite used in this study is MX80 Bentonite (from Wyoming, USA) manufactured by American Colloid Company and supplied directly by Colloid Environmental Technological Company (CETCO). This material was used, as-supplied with no modification of its granularity or properties other than water content (materials were oven dried at 110°C to remove excess water prior to preparation of test specimens).

As bentonite is a mined-dried-milled product that will disaggregate in water to form a fine-grained mass of partially colloidal material, conduct of wet sieve analysis is not a particularly useful analysis. Of more importance to the application considered in this study is the granularity of the as-received materials. MX80 is a milled material with a target grain-size of 80 mesh (US Sieve Size) which is 0.177 mm (0.0070 inches) post milling. It is intended to have only a limited size range with few fines or coarse particles. As a means of determining if the as-received materials met these targets, a dry sieve analysis was done. This involved passing the bulk material through a series of mechanical sieves (8, 16, 30, 50, 80, 200 mesh), no crushing,

drying or other pre-treatment were done and so results describe the as-received materials. Figure 2.2 provides the resulting grain size distribution curve for MX80. The bentonite was ~87% retained between the 30 and 80 mesh screens, ~12% smaller than 0.177 mm and materials coarser than 0.6 mm making up approximately 1%. These results are entirely consistent with the 80 mesh target granularity for this material.

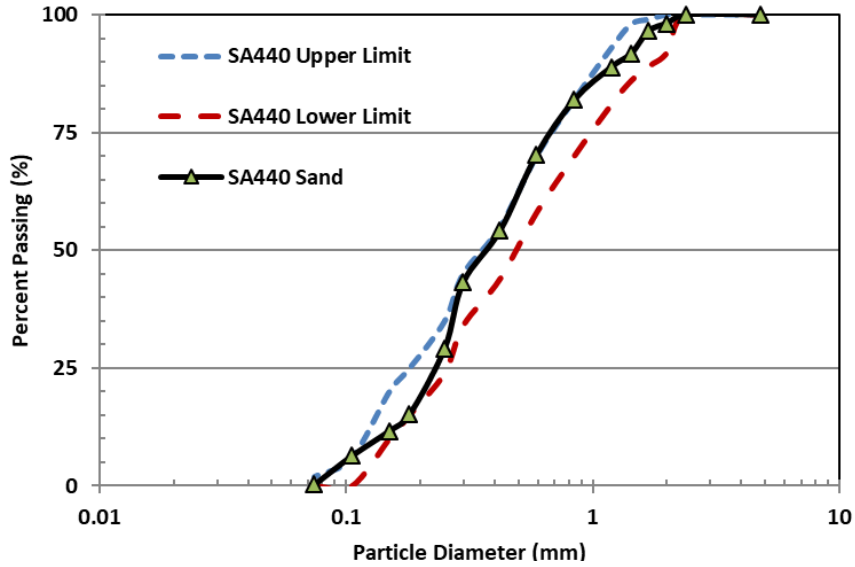


Figure 2.1: Grain Size Distribution Curve for Sand

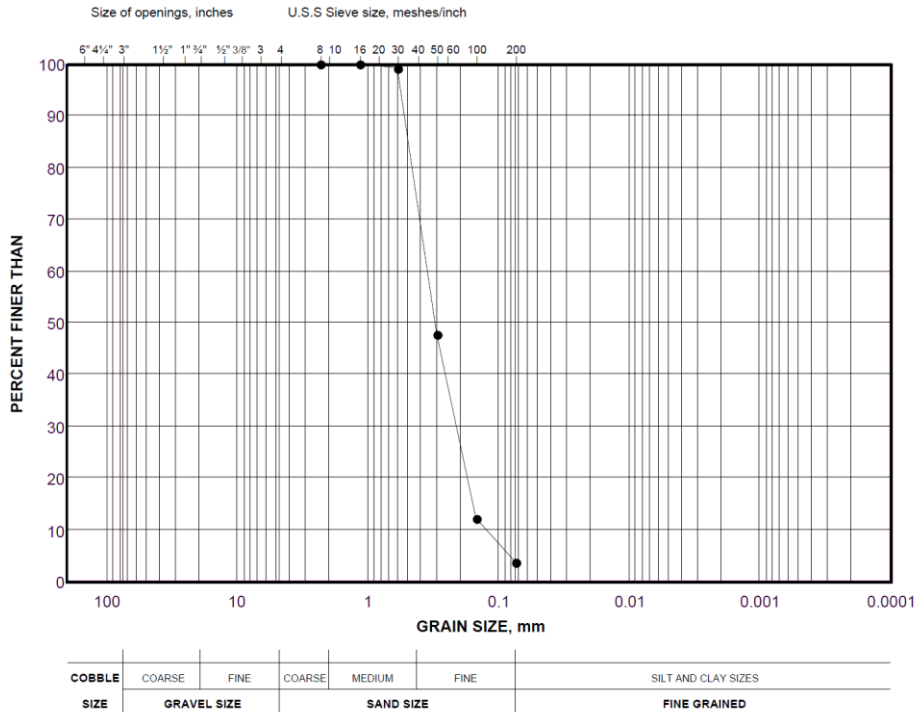


Figure.2.2: Grain Size Distribution Curve for MX80 Bentonite

2.3 MINERALOGICAL AND CHEMICAL CHARACTERISATION

2.3.1 Methods and Materials

The mineralogical and chemical composition of each material used (MX80 bentonite and sand) was verified by X-ray diffraction (XRD) and X-Ray fluorescence (XRF). The use of XRD on a blend of bentonite and sand was not deemed to be an appropriate method of confirming mineralogical composition. This is due to the very strong reflection/diffraction characteristics of crystalline minerals such as quartz and feldspars as well as their much larger size (mm versus μm), relative to the clay minerals. Analysis of such a material would require separation of the coarse (quartz sand) and fine components (clay and any quartz powder) in order to conduct the analysis on subsequently crushed materials. The results of the two analyses would then need to be combined to provide an estimate of the bulk composition. Therefore, it is simpler and likely more accurate to analyse the two components separately. The small sample size associated with XRD means that there will be an uncertainty regarding the actual quantity of quartz grains present (large, coarse textured) in a sand-clay mixture, leading to difficulty in obtaining a truly representative subsample for analysis. Mineralogical and chemical analyses of the individual components (bentonite and sand), therefore provides a much better measure of the overall bulk composition of this subsequently blended material.

The MX80 bentonite is a hydrous aluminum silicate comprised of clay minerals of the smectite group including montmorillonite, nontronite and sodium aluminum silicate hydroxide. This material has been used extensively for more than 30 years as a reference product for application in sealing of nuclear fuel waste repositories. As a result, there is a large body of mineralogical and chemical data available for this material. Being a natural material, it varies compositionally, making exact definition of mineralogical composition problematic, especially given the known presence of x-ray invisible amorphous mineral phases which result in an over-estimate of the crystalline mineral content. Literature does however provide a well-established range in mineralogical composition for the MX80 product. It is reported to consist of between 75 and 90% smectite clay minerals (Karnland 2010).

Of more limited use in terms of establishing mineralogical composition are the results of major oxide analyses (by XRF) of the soil. It should be noted that this analytical tool does not provide a direct means of determining the smectite (or any other mineral) content but does provide an indication of the overall elemental composition. All MX80 products should exhibit similar elemental composition and so deviations from the norm could be used to identify changes in material composition and product quality. This is however a topic that requires more extensive study before it could be used as part of routine analyses. The analytical reports, including quality checks provided by the three laboratories used in this testing are in Appendix B.

2.3.2 MX80 Bentonite: XRD and XRF Analyses of As-received Material

Commercial mineralogical analytical laboratories were used to provide a basic mineralogical check on the MX80 bentonite and sand used in this study. As required for this project, three qualified and registered laboratories (James Hutton Institute, Saskatchewan Research Council (SRC) and Activation Laboratories) were selected and subsamples of the same batch of clay were submitted for random orientation bulk powder analysis. The XRD results for MX80 bentonite are presented in Table 2.4. The detailed analytical reports provided by the laboratories are provided in Appendix B.

Identification of specific mineral contents within the smectite group (e.g. montmorillonite, nontronite) provided by this means analysis can be problematic as the clay minerals vary considerably in crystallinity and are extremely fine-grained. On the other hand, certain non-clay minerals such as quartz, muscovite, plagioclase feldspar, and K-feldspar are readily identifiable. The XRD analysis on the as-received bentonite indicates an average quantity of approximately 87% montmorillonite.

XRD Analysis

The XRD data for MX80 bentonite provided in Table 2.4, shows that this material is clearly montmorillonite-dominated. There is a notable range in the results reported for montmorillonite content (79-95%) with an average of 87%. This is consistent with the range reported in literature and likely reflects the best sensitivity available for this method. The range can be attributed to sample preparation (a more oriented sample will provide a higher montmorillonite value) and perhaps the method used by the software used in calculating mineral contents. The traces associated with the XRD analyses are provided in Appendix B as part of the laboratory reports. These data highlight the challenges in assessing bentonite materials for small (<10%) changes in montmorillonite content. It should also be noted that the semi-quantitative analyses are generally not able to determine minor mineral proportioning to an accuracy greater than approximately $\pm 1\%$ and swelling clay composition is accurate to $\sim \pm 5\%$ (Karnland et al. 2006).

Table 2.4: Semi-Quantitative X-Ray Diffraction Results for Bulk MX80 Bentonite

	Activation Labs	Hutton Institute	SRC	Average or range	SKB (2006) XRD	SKB (2006) Chemical
Mineral	(%)	(%)	(%)	(%)		
Montmorillonite	94.8	88.5	79	87.4 \pm 8.0	81.1-85.8	83.5
Calcite	2.2	3	3.6	2.9 \pm 0.7	0.1-0.5	0.2
Dolomite	-	TR	-	TR	-	-
Quartz	1.6	2.3	3.5	2.5 \pm 1.0	4.6-7*	6.1
Biotite	1.4	-	-	<1.4	-	-
Muscovite (+illite)	-	0.3	7.1	0.3-7.1	2.1-3.9	3.5
Plagioclase	TR	0	6.8	0-6.8	1.8-4.2	2.9
K-Feldspar	TR	3	-	<3	0.3-2.1*	1.5
Siderite	-	1.9	-	<2	-	-
Pyrite	-	0.6	-	<0.6	0.5-0.6	0.6
Gypsum	-	0.4	-	<0.4	0.5-1.3	0.9
Iron minerals**	-	-	-	-	0.8-2.6	1.1
Total	100	100	100	99.9		

Note: TR = trace; '-' = not detected

* values are sum of polymorphs of the indicated mineral group (e.g. quartz, cristobalite and tridymite; microcline and orthoclase feldspars)

** sum of iron minerals goethite, hematite, magnetite and lepidocrocite

It should also be noted that the results provided are for bulk materials. Bentonite is known to contain quantities of x-ray invisible (amorphous) materials (e.g. iron-oxides, hydroxides, silica). The presence of x-ray amorphous materials in MX80 bentonite was noted by Olsson and Karnland (2009) and Karnland (2010) and represent an unquantified mineral component. Of particular interest are the amorphous iron and silica components that have the potential to affect

the behaviour of the bentonite. These amorphous materials are not accounted for in semi-quantitative XRD analyses and so depending on their quantity, discernible over-estimation of the proportion of crystalline minerals in a clay mass may occur (Kaufhold et al. 2002). This poorly crystalline state of many of the iron-based minerals is indicated by the range of analytical values for the various iron-based minerals (e.g. siderite, goethite, Hematite, magnetite and Lepidocrocite), which is taken to be indicative of their generally poor crystallinity.

Based on the combination of uncertain x-ray-invisible minerals and a generally accepted $\pm 5\%$ accuracy in the measured montmorillonite content, there is a considerable uncertainty regarding the actual amount of this mineral present. A montmorillonite content at the lower end of the range of XRD-derived mineralogical analyses (80%) was therefore selected for use in subsequent behavioural analyses in the current study. An item of note in the mineralogical characterisation work was the difficulty in finding analytical services that are able to accurately quantify smectite mineral content. This is an issue that will need to be addressed as part of development of a bentonite quality-control program.

XRF Analysis

The same bentonite samples that were used in the XRD analyses also underwent XRF analysis. A total of four XRF analyses were completed on MX80 and the results of these analyses are presented in Table 2.5. For comparison purposes Table 2.5 also contains data reported for MX80 bentonite in other studies spanning almost 2 decades (Dixon 1994; Dixon and Miller 1995; Karnland et al. 2006 and Kiviranta and Kumpulainen 2011).

While the as-received data values for the XRF analyses, provided in Table 2.5 show some scatter in the results obtained for “identical” specimens, these differences can to a large extent be attributed to differences in the water content reported for the specimens tested (expressed as LOI (loss on ignition)). The LOI component includes water, organic matter and carbonate that is removed by heating. Differences in LOI can be attributed to laboratory conditions present prior to drying (high humidity will change absorbed water. In order to address analytical uncertainty, the data was processed to eliminate the LOI component and expressed as percentage of oxides based on total mass less the LOI. While there is still a degree of uncertainty, this approach reduces the data scatter and allows for comparison of the results based on a consistent initial water content (0%). Comparison of the current studies measurements to previously published (and subsequently adjusted using the same method), indicates that the MX80 bentonite used in this study is very close in composition to previously reported materials. The detailed tabulation of the individual tests used in determining literature XRF-generated chemical compositions is provided in Appendix B.

The only discernible differences in the current material from literature information is related to a slight reduction in sodium, silica and an increase in calcium and iron. They may represent a slightly higher iron-mineral content in the newer MX80 and a slight reduction in the layer silicates present. The changes are however so small as to be attributable to analytical variability.

Table 2.5: Major Oxides Composition of Source MX80 Bentonite by XRF

	Activation Labs	Adjusted value	Hutton Institute	Adjusted value	SRC 1	Adjusted value	SRC 2	Adjusted value	Average Adj. Value	STDev	Adjusted literature values***
Oxides											
Na ₂ O	1.87	2.30	1.98	2.41	1.49	1.78	1.56	1.88	2.09	0.27	2.53
MgO	3.16	3.88	3.09	3.77	2.25	2.68	2.26	2.72	3.26	0.56	3.30
Al ₂ O ₃	18.57	22.82	18.24	22.24	18.80	22.43	18.80	22.65	22.54	0.22	21.78
SiO ₂	51.46	63.23	51.76	63.11	54.40	64.92	53.10	63.98	63.81	0.72	66.31
P ₂ O ₅	0.10	0.12	0.07	0.09	0.06	0.07	0.06	0.07	0.09	0.02	tr
K ₂ O	0.16	0.20	0.61	0.74	0.43	0.51	0.41	0.49	0.49	0.19	0.55
CaO	2.07	2.54	2.21	2.69	1.82	2.17	1.87	2.25	2.42	0.21	1.21
TiO ₂	0.16	0.20	0.16	0.20	0.19	0.22	0.18	0.21	0.21	0.01	0.18
MnO	0.02	0.02	<0.05	0.06	0.03	0.03	0.03	0.03	0.02	0.02	-
V ₂ O ₅	<0.003	-	<0.05	0.06	-	-	-	-	-	-	-
Cr ₂ O ₃	<0.001	-	<0.05	0.06	-	-	-	-	-	-	-
Fe ₂ O ₃	3.78	4.64	3.86	4.71	4.20	5.01	4.59	5.53	4.97	0.35	3.74
FeO	-	-	-	-	-	-	-	-	-	-	tr
C	-	-	-	-	-	-	-	-	-	-	0.11
S	-	-	-	-	0.16	0.19	0.17	0.20	0.10	0.10	0.22
LOI*	17.41	17.62	17.19	17.33	15.80	15.86	15.90	16.08	16.72	-	
Total	98.8	99.9	99.2	100.1	99.6	100.0	98.9	100.0	100.0	-	99.9

* Loss on ignition (heating to 1000C). This removes all water, carbonate, gypsum and organic matter from the specimen.

** Data from Karnland et al. 2006; Kiviranta & Kumpulainen 2011, Dixon 1994, Dixon and Miller 1995

*** Data expressed as % of total non-LOI oxide content. Adjusted value = measured value / (measured total) / (1-Adj LOI).

2.3.3 Bentonite After Brine-Soaking

This project also required determination of mineralogical composition after extended exposure to an SR-Sh environment. The effects of an approximately two-year long soaking of loose bentonite clay in a SR-Sh brine was examined. Loose bentonite (125 g) was placed in an air-tight container, the SR-Sh brine (325 g) was added and the materials were well mixed and then left undisturbed at room temperature for a period of approximately 18 months. The MX80-brine mixture immediately separated leaving a clear supernatant above the clay solids. The container was reopened only for end-of-test analysis.

The results of mineralogical and chemical analyses of the bentonite clay will be strongly affected by the presence of salts in the specimen. During drying, dissolved salts will precipitate out as highly crystalline forms that could make semi-quantitative analyses by XRD difficult. There would also be difficulties in entirely drying the specimens as the resultant concentrated brine would tend to remain at least in-part as a semi-liquid when dried at 110°C. Similarly, the presence of the TDS would make chemical analyses of the specimens via XRF difficult since it would not be possible to separate out TDS components and mineral components. These potential complications to post-test analysis of the MX80 required that a means to selectively remove the salts component be identified.

The most commonly used and effective means of accomplishing this is the use of dialysis membranes to contain the clay-brine materials while allowing the salts to diffuse out into a low TDS bulk solution. Removal of excess salts and water from the sample was accomplished by

allowing ionic diffusion through a semi-permeable membrane. A total of ~60 g of soil solids was placed in each of the diffusion bags shown in Figure 2.3 and allowed to soak in 2L of deionized water. The salinity of the external solution was monitored through use of a conductivity probe and once equilibrium was achieved the external solution was changed. It should be noted that electrical conductivity measurements were done for indication purposes only and no specification existed regarding acceptable values. The result was a stepwise reduction in the TDS concentration in the external solution with each change (and also the TDS within the specimen). Solution changes occurred four times and at the end of this process, the TDS concentration was ~0.1 g/L (<200uS). The specimens were then oven dried at 110°C, crushed to powder, subdivided and sent off for XRD/XRF using the same analytical technique (and laboratories) as were used in the initial material assessment. This powder was then subdivided and submitted to the same analytical laboratories selected for conduct of the original x-ray diffraction and XRF analyses (see Section 2.3.2).



Figure 2.3: Desalination of MX80 Specimens Using Dialysis Membranes

XRD Analysis

The same laboratories were used for conduct of XRD analysis of the brine-soaked bentonite as were used for the initial characterisations (section 2.3.2). This will provide maximum comparability of the results since there will be no addition of new preparation or analytical laboratory-induced testing unknowns to the analyses.

It should be noted that even though every effort was made to avoid any material loss or alteration during desalination there are several changes potentially induced in the treated materials. These include the following: change in granularity (breakdown of mineral aggregations) due to soaking, drying and crushing of treated material; loss of soluble components (e.g. gypsum, oxides and perhaps fine carbonates during soaking in salt or desalination). This may also result in cleaner mineral surfaces and change in diffraction pattern due to change in the way fine-grained powder is oriented. Of importance also is the exchanging of the initially present sodium ions on the bentonite's surface exchange sites with the more strongly sorbing calcium and magnesium ions provided by the SR-Sh solution (see

Table 2.3). These ions will alter the spacings of the smectite layer and hence may slightly influence the results of the XRD analyses.

The results of the XRD analyses done after brine soaking are provided in Table 2.6 and copies of the analytical laboratory reports are provided in Appendix B. These analyses show no discernible change in the montmorillonite content as the result of brine exposure. The range in the quantity of secondary (>2 %) and trace (< 2 %) minerals identified in the post-brine-exposure specimens are also very similar to those determined in the original bulk material. Minor differences can be attributed to several factors, including dissolution or relocation of amorphous coatings originally present on mineral surfaces (resulting in change in x-ray diffraction intensities), dissolution of minor mineral components into the bulk solutions (e.g. gypsum, fine carbonates, hydroxides) and the small size of the specimens tested. Given the inherent uncertainties related to x-ray diffraction analysis, the results for the desalinated material mineralogy show that it has not undergone any discernible change in its composition.

Table 2.6: Semi-Quantitative X-Ray Diffraction Results for MX80 Bentonite After 18 Months Exposure to SR-Sh Brine

Mineral	Activation Labs (%)	Hutton Institute (%)	SRC (%)	Brine Average (%)	Original Bentonite*	SRC ⁺ (%)
Montmorillonite	84.6	88.6±4.8	90.9	88.0	87.4±8	87.8
Calcite	3.1	4.3±1.7	0.3	2.6	2.9±0.7	0.8
Dolomite	-	-	-	--	TR	-
Quartz	2.4	1.4±1.1	0.4	1.4	2.5±1	0.4
Biotite	1.7	-	-	TR	<1.4	-
Muscovite (illite)	-	1.8±1.2	8.2	3.3	0.3-7.1	<u>11.2⁺⁺</u>
Plagioclase	8.3 ^{**}	0.3	-	3	0-6.8	-
K-Feldspar	-	1.2±1.1	-	<2.3	<3	-
Siderite	-	1.9±1.3	-	<3.2	<2	-
Pyrite	-	0.4	-	TR	<0.6	-
Gypsum	-	-	-	--	<0.4	-
Rutile	-	-	0.2	TR		-
Total	100.1	100	100	100	99.9	100

Note: TR = trace; - not detected

+ "B" analysis using x-ray analysis for partially oriented specimen.

++ SRC value is consistently higher than other analytical labs, however the smectite content determined by all labs is similar.

* bulk material, average of three analyses. See Table 2.4

** feldspar reported as bulk content rather than specific mineral phases

Table 2.6 also contains the results of an XRD analysis using a slightly different preparation method (resulting in a semi-oriented specimen). This method is intended to provide for a better identification of clay minerals such as montmorillonite. The montmorillonite-type minerals identified using this method are not much different than for the random orientation specimens, but minor minerals identified and quantified are discernibly different for the two methods. These

results highlight the need for use of very consistent methodology when undertaking semi-quantitative mineralogical analyses and the challenges associated with quantitative analyses.

XRF Analysis

The same laboratories were used for conduct of the XRF analysis of the brine-soaked bentonite as were used in the initial characterisation (Section 2.3.2). As is the case for the XRD analyses, use of the same labs will provide maximum comparability of the results since there will be no addition of new preparation or testing unknowns to the analyses. The results of the XRF analyses provided by the analytical laboratories are summarized in Table 2.7 and are also normalized to show the oxide composition with the LOI component removed. The analytical laboratory reports and comparative information from literature are provided in Appendix B.

Table 2.7: Major Oxides Composition of MX80 Bentonite After Brine Exposure as Determined by XRF

	Activation Labs	Adjusted Value**	Hutton Institute	Adjusted Value**	SRC 1	Adj. Value**	Raw Data Average	Avg. Adj. Value**	Std Dev. Adj. Data	Adj. Initial Material**	Adj. Lit. data**
Oxides	(wt %)	(wt %)	(wt %)	(wt %)	(wt %)	(wt %)	(wt %)	(wt %)	(wt %)	(wt %)	(wt %)
Na ₂ O	0.45	0.54	0.23	0.25	0.22	0.28	0.30	0.36	0.16	2.09	2.53
MgO	3.03	3.65	3.14	3.44	2.24	2.87	2.80	3.32	0.40	3.26	3.30
Al ₂ O ₃	18.22	21.97	20.60	22.58	15.96	20.47	18.26	21.67	1.09	22.54	21.78
SiO ₂	51.35	61.93	58.56	64.18	50.54	64.81	53.48	63.64	1.52	63.81	66.31
P ₂ O ₅	0.07	0.08	0.06	0.07	0.07	0.09	0.07	0.08	0.01	0.09	tr
K ₂ O	1.17	1.41	1.19	1.30	1.02	1.31	1.13	1.34	0.06	0.49	0.55
CaO	3.35	4.04	3.14	3.44	3.14	4.03	3.21	3.84	0.34	2.42	1.21
TiO ₂	0.16	0.19	0.18	0.20	0.19	0.24	0.18	0.21	0.03	0.21	0.18
MnO	0.03	0.03	0.02	0.02	0.03	0.04	0.03	0.03	0.01	0.02	-
V ₂ O ₅	-	-	-	-	-	-	-	-	-	-	-
Cr ₂ O ₃	-	-	-	-	-	-	-	-	-	-	-
Fe ₂ O ₃	5.09	6.14	3.97	4.35	4.48	5.75	4.51	5.41	0.94	4.97	3.74
FeO	-	-	-	-	-	-	-	-	-	-	tr
C	-	-	-	-	-	-	-	-	-	-	0.11
S	-	-	-	-	0.09	0.12	0.03	0.04	-	0.10	0.22
LOI*	16.68	16.75	8.46	8.49	22.02	22.02	15.72	15.75		16.72	
Total	99.6	100.0	99.7	99.8	100.0	100.0	99.7	99.9		100.0	99.9

Note: Values shown in red are where pre-soaking and post-soaking analyses are discernibly different.

Yellow highlighted columns are pre- and post-soaking results adjusted to remove LOI.

* Loss on Ignition (heating to 1000C). This removes all water, carbonate, gypsum and organic matter from the specimens.

** Data expressed as % of total non-LOI oxide content. Adjusted value = measured value / (1-LOI/100) / (1-Adj LOI).

As per the previous discussion related to XRD analyses, the brine-soaked specimens may be slightly affected by the soaking in the SR-Sh solution, primarily as the result of dissolution and loss of soluble components such as salt, gypsum, fine-grained (amorphous) oxides and carbonates during the soaking and subsequent desalinization process and thereby be lost to the analytical process. Also of potential significance with respect to XRF analysis is the exchange of the absorbed cations originally present on the montmorillonite clay particles (initially mostly sodium) for the more strongly sorbing calcium and magnesium cations provided by the groundwater. Given the very high surface area of montmorillonite (up to ~800 m²/g) and high CEC (85-90 meq/100g), this exchange process may explain the discernible decrease in the

sodium (lower) and increase in the calcium and magnesium contents. Determining the detailed mechanisms associated with changes in cation content are complex and beyond the scope of the current study to assess. Also of note in the results provided in Table 2.7 are consistently higher potassium content values in the brine-soaked samples, this is also likely due to ion-exchange on the particle surfaces resulting in release of potassium rather than any mineralogical alteration.

These results highlight the need for establishment of methods of analysis that are consistent and the importance of not setting unreasonably tight limits to acceptable levels of the various components of bentonite. Use of this type of analysis for quality control purposes requires careful determination of the natural variability of the materials themselves and the analytical methods used to determine them.

2.3.4 Quartz Sand Analyses

XRD Analysis

The mineralogical analysis of the sand component used in this project is summarized in Table 2.8. This material is a quartz (~75%) and feldspar (~24%) material with less than 1.5% of other trace minerals. This means that the material resulting from blending of sand and MX80 should not have a substantial quantity (<3%) of readily soluble or altered non-clay minerals present. It should be noted again that as for the bentonite samples, the XRD analyses of the sand do not identify the presence or quantity of non-crystalline (amorphous) minerals. Detailed results and analytical traces are provided in Appendix B.

Table 2.8: Semi-Quantitative X-ray Diffraction Results for Sand

Mineral	Activation Labs (%)	Hutton Institute (%)	SRC 1 (%)	SRC 2 (%)	Average (%)	Standard Deviation (%)
Montmorillonite	-	-	-	-	-	
Calcite	-	0.7	-	-	<0.7	
Dolomite	-	tr	-	-	Tr	
Quartz	75.9	81.7	73	71.5	75.4	5.5
Biotite	-	-	-	-	-	
Muscovite	-	-	-	-	-	
Plagioclase Feldspar	15.5	10.9	17	17.2	15.0	3.6
K Feldspar	8.6	6	9.9	12.4	9.4	3.2
Siderite	-	-	-	-	-	
Pyrite	-	-	-	-	-	
Gypsum	-	-	-	-	-	
Amphibole	-	0.7	-	-	<0.7	
Total	100	100	99.9	101.1	99.9	

- Not detected, quantity is too small to identify

XRF Analyses

The sand samples were also subjected to XRF in order to determine their cation compositions (Table 2.9). In total four analyses were provided, including a re-run by SRC which provides an indication of the repeatability of results in a single laboratory for the same specimen. The overall XRF results show very consistent values were obtained by all the laboratories with only a small range in results. This is consistent with what would be expected in a homogeneous material with only a limited range of minerals present.

Table 2.9: Major Oxides Composition of Sand Determined by XRF

Oxides	Activation Labs (%)	Hutton Institute (%)	SRC 1 (%)	SRC2 (%)	Average (%)	Standard Deviation (%)
Na ₂ O	1.03	1.1	1.52	1.32	1.32	0.25
MgO	0.3	0.32	0.55	0.43	0.43	0.12
Al ₂ O ₃	4.84	4.51	6.93	5.82	5.82	1.15
SiO ₂	89.38	90.22	86.1	87.93	87.93	1.90
P ₂ O ₅	0.05	0.05	0.1	0.08	0.08	0.03
K ₂ O	0.09	1.27	1.69	1.19	1.19	0.66
CaO	1.11	1.08	1.94	1.52	1.52	0.42
TiO ₂	0.09	0.09	0.12	0.11	0.11	0.02
Mn ₃ O ₄	0.016	0.05	0.04	0.04	0.04	0.01
V ₂ O ₅	0.003	0.05	-	-	-	
Cr ₂ O ₃	0.001	0.05	-	-	-	
Fe ₂ O ₃	1.22	0.9	1.07	1.06	1.06	0.11
S	-	-	0.03	0.03	0.03	
LOI	1.03	0.93	-	0.98	0.98	
Total	99.2	100.6	100.1	100.01	100.01	0.53

- oxide not identified or too low to be detected LOI is loss on ignition

3. COMPACTION TESTING

The bentonite-sand samples used in compaction testing were prepared using sufficient quantities of the bentonite and sand for conduct of each compaction series per solution type. The bentonite and sand were dried in a 105°C oven and allowed to cool to room temperature in a sealed mixing bowl. Bentonite and 70:30 BSM by dry mass were prepared in small batches by weighing the mineral components out and manually homogenizing them. Small dry mix batches were moisture conditioned using the reference solutions (DW, CR-10, SR-L and SR-Sh). The bentonite-only tests (MX80) were completed using the same procedure excepting that there was no sand addition. This procedure ensures that there is no dilution of the salinity of the pore water by the presence of water in the as-received materials. Each of the batches was stepwise moistened by misting. Batches were not dried back due to high salts concentration in the saline specimens. The misted material was further mixed to ensure uniform moisture distribution and stored in an air-tight container for at least 24 hours between preparation and conduct of compaction tests.

It is necessary to recognize that there is the presence of a considerable mass of salt in the pore fluid of the saline specimens and that correction of masses, degree of saturation and densities obtained during specimen manufacture and dismantling will be necessary for tests such as compaction, swelling pressure, hydraulic conductivity and deformation properties. Moisture content typically reported in this document is based on oven drying to 105°C as per ASTM D2216 standard, but again the high salt content will mean that there is some water still present as part of this brine that will not be removed by this drying.

The compaction density versus water content relationship was obtained using the mini-proctor procedures described in Dixon, Gray and Thomas (1985) and Priyanto et al. (2013), and correlates to Modified Proctor Method ASTM D1557 as specified by NWMO. From the compaction characterisation test, it is possible to identify the moisture content at which the backfill will achieve its maximum dry density for a given energy input. The device used is shown in Figure 3.1 and was acquired from Canadian Nuclear Laboratories (CNL) in order to conduct this testing. As this density will be affected by the chemistry of the water used for the compaction, the compaction density versus water content relationship was obtained for each of the reference solutions.

The results of the compaction testing for the MX80 bentonite and 70:30 BSM are presented in Figure 3.2 and Figure 3.3 respectively. Zero Air Voids (ZAV) lines (representing full solution saturation of the soil pore voids), are calculated for both MX80 bentonite and 70:30 BSM. The maximum compaction density and gravimetric water content obtained using each reference solution are summarised in Table 3.1 and Table 3.2. The difference between the maximum compacted density for the specimens shown in Figure 3.2 and provided in Table 3.1 is due to the need to apply a correction to the results of the miniature compaction device in order to determine the maximum compaction density. As derived by Dixon et al. (1985) the maximum compacted dry density measured using the miniature compaction method can be used to generate the modified compaction maximum density (Modified Proctor), expressed in Mg/m³ or g/cm³ as follows:

$$\rho_d (\text{modified proctor}) = 0.98 \rho_d (\text{mini}) + 0.11 \quad (R^2 = 0.995)$$

The detailed data associated with these tables and figures are provided in Appendix C. The values presented are for conditions where the mass of pore water salts that was left behind in

the oven drying process has been deducted from the soil solids mass when calculating density and water content. The measured values of the maximum dry density for the compaction tests are used with the correlation presented in Dixon et al. (1985) to generate the modified proctor density for each material. Low optimum water content and low salinity conditions means that the effects of salt mass on the calculated densities is very small, however, it will be of importance in the tests using SR-L and SR-Sh pore waters. These differences are important when predicting the swelling and hydraulic behaviour of bentonite-based materials as both of these parameters are dependent on compacted density of the soil particles.

Table 3.1: Maximum Density Achieved Using Modified Compaction Effort for MX80

Compaction Water	Estimated Maximum Dry Density (Mg/m ³)	Estimated Optimum Gravimetric Water Content (%)	Estimated Porosity of Material at Maximum Dry Density
Deionized Water	1.72	17.4	0.374
CR10	1.71	18.6	0.377
SR-L	1.73	19.8	0.369
SR-Sh	1.71	18.0	0.379

Note: values calculated using a salt correction method provided in Appendix D and adjusted for correlation to ASTM D1557.

Table 3.2: Maximum Density Achieved Using Modified Compaction Effort for 70:30 BSM

Compaction Water	Estimated Maximum Dry Density (Mg/m ³)	Estimated Optimum Gravimetric Water Content (%)	Estimated Porosity of Material at Maximum Dry Density
Deionized Water	1.94	15.0	0.286
CR10	1.91	13.7	0.299
SR-L	1.93	13.6	0.293
SR-Sh	1.90	14.4	0.302

Note: values calculated using a salt correction method provided in Appendix D and adjusted for correlation to ASTM D1557.

A parameter of importance in subsequent evaluation of laboratory tests is the total porosity (n) of each compacted test specimen. The total porosity represents the combined volume of voids per unit total volume of the compacted sample and is calculated as shown below for a system containing no soluble salts component:

$$n = 1 - \frac{\rho_d}{G_s \rho_w}$$

where,

- n = total porosity;
- ρ_d = compacted dry density (not including soluble salt component);
- G_s = specific gravity of mineral particles (assumed to be 2.72 for MX80 bentonite and assumed to be 2.70 for the 70:30 BSM); and
- ρ_w = density of water (1.0 for DW).

The resulting porosity values at Maximum Dry Density presented in Table 3.1 range from about 0.37 to 0.38 for MX80 bentonite. The resulting porosity values at Maximum Dry Density presented in Table 3.2 range from about 0.29 to 0.30 for the 70:30 BSM.



Figure 3.1 : Miniature Compaction Device (Priyanto et al. 2013)

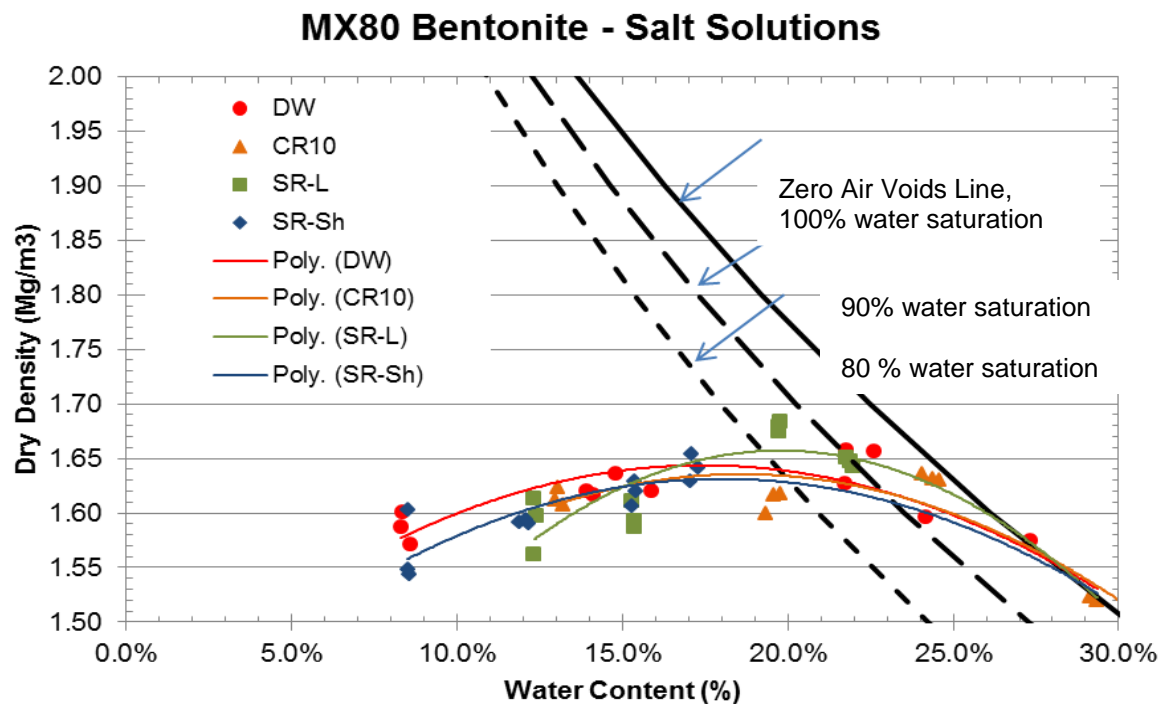


Figure 3.2: Compaction Curves for MX80 Bentonite Obtained Using Miniature Compaction Device

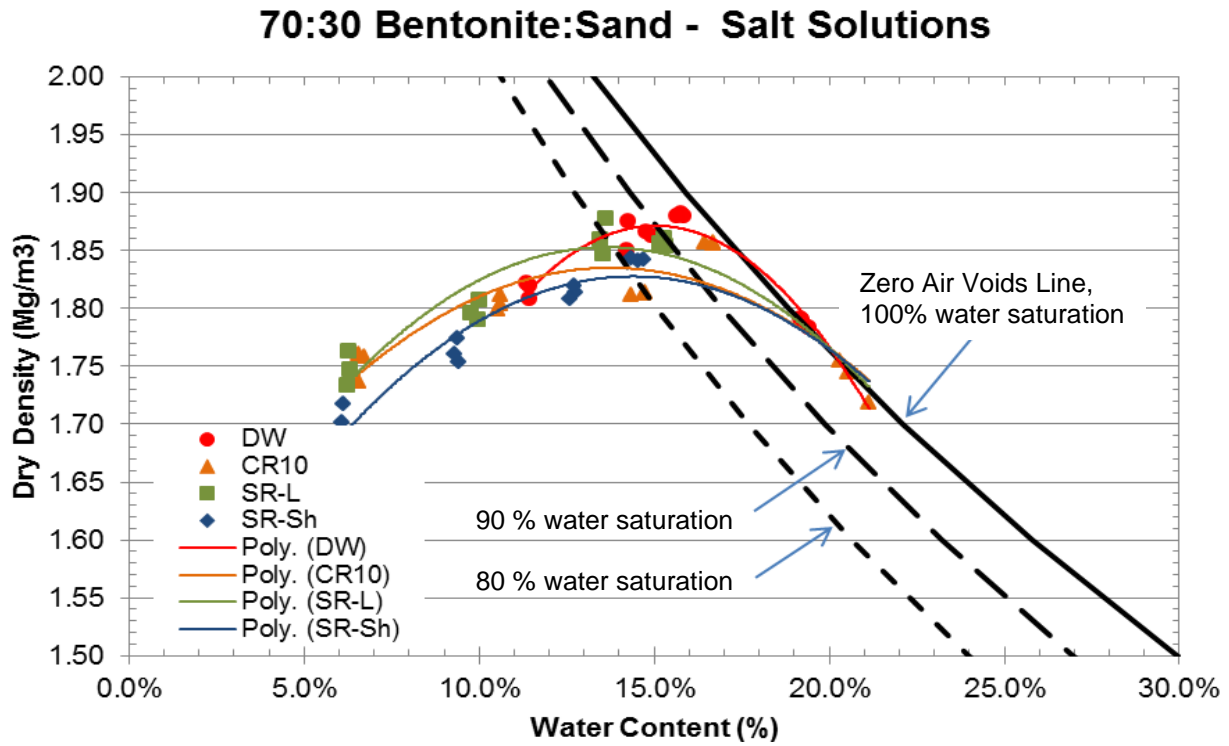


Figure 3.3: Miniature Compaction Curves for 70:30 BSM Obtained Using Miniature Compaction Device

4. CONSISTENCY (ATTERBERG) LIMITS

Consistency limit tests are a standard ASTM test (ASTM-D4318-10) and this methodology was followed in this testing program. Consistency limits were completed in triplicate on each material using each of the pore fluids.

The data generated by triplicate tests of the MX80 bentonite is presented in Table 4.1 and Table 4.2 contains the results of testing the 70:30 BSM mixture. It should be noted that use of the standard test method ASTM-D-4318-10 for conduct of consistency limit tests requires the removal of any material exceeding 0.425 mm (40 mesh sieve). As a result, the bentonite-sand material tested was not a 70:30 mixture since a large proportion (~50%) of the sand component had to be removed. The 70:30 test results are therefore more of a measure of what consistency of results can be obtained when using an 85:15 mix of MX80 and fine sand.

The data show the large influence of fluid composition on the liquid limit of the bentonite and 70:30 BSM. The effect of pore fluid composition is less on the plastic limit. The tests completed also show the influence of non-swelling minerals (sand) on the consistency limits. The sieved 70:30 material had a discernibly lower liquid limit for each of the solutions tested, particularly for the material tested using fresh water. The influence was less substantial for the saline systems, again illustrating the effects of pore fluid salinity on loose bentonite-based materials.

Table 4.1: Consistency Limits for MX80 Bentonite (ASTM-D4318-10)

Sample	Water Content Based on ASTM D-2216		
	LL	PL	PI
B-DW-1	352.4	32.5	319.9
B-DW-2	367.8	33.1	334.7
B-DW-3	331.0	33.2	297.8
<i>Average</i>	350.4	32.9	317.5
<i>Std Dev</i>	18.5	0.4	18.6
B-CR-10	Testing not part of Matrix	-	-
B-SR-L-1	52.3	26.2	26.1
B-SR-L-2	51.5	27.7	23.8
B-SR-L-3	51.5	28.2	23.3
<i>Average</i>	51.8	27.4	24.4
<i>Std Dev</i>	0.5	1.0	1.5
B-SR-SH-1	48.6	26.7	21.9
B-SR-SH-2	47.6	27.1	20.5
B-SR-SH-3	47.7	27.7	20.0
<i>Average</i>	48.0	27.2	20.8
<i>Std Dev</i>	0.6	0.5	1.0

Note: LL = Liquid Limit; PL = Plastic Limit; PI = Plasticity Index

Table 4.2: Consistency Limits for Screened BSM (ASTM-D4318-10)

Water Content Based on ASTM D-2216			
Sample	LL⁺	PL⁺	PI
BS-DW-1	289.0	28.8	260.2
BS-DW-2	280.0	28.6	251.4
BS-DW-3	256.8	26.4	230.4
<i>Average</i>	275.3	27.9	247.3
<i>Std Dev</i>	16.6	1.3	15.3
BS-CR-10-1	91.6	27.9	63.7
BS-CR-10-2	91.7	28.6	63.1
BS-CR-10-3	92.8	30.7	62.1
<i>Average</i>	92.0	29.1	63.0
<i>Std Dev</i>	0.7	1.5	0.8
BS-SR-L-1	47.6	24.2	23.4
BS-SR-L-2	46.9	24.6	22.3
BS-SR-L-3	46.9	25.9	21.0
<i>Average</i>	47.1	24.9	22.2
<i>Std Dev</i>	0.4	0.9	1.2
BS-SR-SH-1	42.0	22.6	19.4
BS-SR-SH-2	41.8	23.6	18.2
BS-SR-SH-3	42.1	23.0	19.1
<i>Average</i>	42.0	23.1	18.9
<i>Std Dev</i>	0.2	0.5	0.6

Note: LL = Liquid Limit; PL = Plastic Limit; PI = Plasticity Index

⁺ Conduct of ASTM D-4318-10 requires removal of coarse (>0.425 mm) particles from the soil specimen.

5. FREE SWELL INDEX

The Free Swell Index (FSI) of clay is a measure of the ability of the material to swell under conditions of no confinement and unlimited supply of water (ASTM D-5890-11). There are two material formulations (100% bentonite and 70:30 BSM) and four pore fluids in this program. Each free swell test was completed in triplicate for all combinations of material and pore fluid. The FSI is normally expressed as the volume in millilitres in a water-filled volumetric cylinder occupied by 2 grams of loose, oven-dried clay (it is sometimes also expressed in terms of mL/g or cc/g). For the 70:30 BSM, materials the sand component was not ground to reduce its coarseness prior to testing. Tests were done to determine the behaviour of the as-mixed blend. The required test matrix was completed, and the results are summarized in Table 5.1.

The free swell tests clearly show the result of saline conditions on the swelling capacity of bentonite-based materials. The MX80 material shows the very high swelling capacity expected of it under freshwater conditions and this capacity is rapidly decreased as salinity of a solution it is in contact increases, even when the salinity is as low as 11 g/L (CR-10). The BSM shows the same pattern of free swell reduction as was observed for the bentonite-only material. The blended material also shows a consistently lower free-swell volume than was observed for the clay-only system, a result of the reduced swelling clay component.

Table 5.1: Free Swell Test Results for MX80 and 70:30 BSM (ASTM-D-5890-11)

100% MX80 Bentonite	Free Swell Index (cc/g)	70:30 bentonite:sand	Free Swell Index (cc/g)
Distilled Water	17.50	Distilled Water	9.25
Distilled Water	15.75	Distilled Water	9.50
Distilled Water	15.75	Distilled Water	9.50
Average, Stdev	16.33±0.8	Average	9.42±0.1
CR10	3.75	CR10	2.75
CR10	3.25	CR10	2.50
CR10	3.75	CR10	2.75
Average, Stdev	3.58±0.2	Average	2.67±0.1
SR-L	2.25	SR-L	2.00
SR-L	2.00	SR-L	1.75
SR-L	2.00	SR-L	2.00
Average, Stdev	2.08±0.1	Average	1.92±0.1
SR-Sh	2.00	SR-Sh	1.50
SR-Sh	1.50	SR-Sh	1.50
SR-Sh	2.00	SR-Sh	1.50
Average, Stdev	1.83±0.2	Average	1.50

6. SWELLING PRESSURE AND HYDRAULIC CONDUCTIVITY TESTING

6.1 BACKGROUND

There are no national (or international) standard test procedures for the conduct of confined swelling pressure measurements on swelling clays of the type studied in this project. The basic methodology used in most previous testing of these materials involved rigid confinement and measurement of reaction forces and water movement through the specimens (Dixon et al. 1995, Priyanto et al. 2013). The same approach was used in the current testing program.

A considerable body of information is available on a variety of bentonite products from numerous laboratories that use similar testing methodologies. A concern related to use of this information in setting performance expectations is that many of these data are associated with bentonite materials that have been incompletely characterised mineralogically or are for tests done using pore fluid compositions other than those of interest to NWMO.

For comparison purposes, a literature-derived database was generated for MX80 bentonites and data collected in the course of this study was compared to those data. There still exists uncertainty regarding absolute comparability as the literature tests involve materials provided over many years from a natural deposit. Hence there is a degree of variability associated with the composition of these materials, even within the same mill run. The current study is intended in part to determine just what can be attributed to various test methods and what might be the result of material variability. It should also be noted that there is only a limited body of pre-existing data for materials tested at very high pore fluid salinity. The current testing program therefore provides much needed data on behaviour under brine groundwater conditions.

The swelling pressure measurements were done using a specially constructed, rigid-walled test cell constructed from salt resistant stainless steel (Figure 6.1). The size of the specimens was small (~32 mm diameter x ~10 mm height). These cells are identical in design to those used for previous studies completed by Dixon (1995), Dixon et al. (1990, 1995), Priyanto et al. (2013) and follow the same basic construction as those used by other researchers examining bentonite materials. The flow gauges used were sourced from Atomic Energy of Canada Ltd. (AECL) as part of their laboratory equipment recycling process and were re-installed in the Golder Laboratory in Winnipeg. Specimens were installed at >90% initial degree of saturation and percolated at gradients in excess of 1000 until saturation was achieved (ongoing water outflow from the top of the test cell). During the entire test, the vertical force on a confining piston was monitored and on achieving steady-state pressure conditions the swelling pressure could be determined based on application of the effective stress concept to the measurements (swelling pressure = total pressure – hydraulic pressure).

In addition to the data generated by rigidly confined specimens, further data can be extracted from uniaxial compression tests (oedometers), conducted to provide deformation parameters for these materials (see Section 8). The nature of one-dimensional compression testing involves application of a series of constant known vertical loads on a laterally confined (rigid) cylindrical specimen of soil. For bentonite materials, this load results in compression (if load is higher than swelling pressure) or expansion (if load is insufficient to prevent swelling). By determining the density of the specimen on completion of a load increment it is possible to provide an estimate of the swelling pressure. For the purposes of the current study only a limited number of load-increments were selected for use in data comparison. These were the increments where the

highest four or five load increments (at loads above the determined preconsolidation pressure) were applied and did not include any unloading data. The reason for this method of data selection is that initial deformation measurements can be affected by the initial specimen strain as any non-homogeneities present in the as-built specimen are accommodated by volume changes. Effects induced by compaction of the specimens (e.g. preconsolidation pressure) are minimized through use of values obtained at loads exceeding the preconsolidation pressure, and so measurements obtained at low loads that may not be representative of an equilibrated specimen are excluded. This equilibration process is particularly important in testing of swelling clay materials where the specimen actively resists the compressive load. In addition, as the specimen is unloaded and swells, there is the potential for the specimen to undergo fabric changes as the plate-like clay particles re-arrange in response to load changes. Hence unloading data may not be representative of what would be experienced in a system where internal particle movement is limited.



Figure 6.1: Test Cells and Flow Gauges Used to Measure Swelling Pressure and Hydraulic Conductivity (from Priyanto et al. 2013)

At the same time as a swelling pressure testing was occurring, water movement into the cell was monitored and the hydraulic conductivity of the specimen was calculated once outflow from the cell was established. Where end-of-test measurements of the specimens indicated that the pre-established density requirements had not been met (see Table 1.1), tests were redone. Each of the density and pore fluid specimens identified for testing in this study were done in triplicate so as to provide some measure of the “intrinsic” variability of the values obtained using identical source materials. Construction of exactly identical specimens is not possible since

each test will exhibit some post-installation change in specimen height (rebound as the result of unloading). As a result, there were some tests that did not fall within the pre-set density requirements (e.g. 1.4 to 1.5 Mg/m³; 1.7 to 1.8 Mg/m³ dry density) and replacement tests were undertaken. As a result of this, a considerable number of new data values were generated, all of which can be used when generating density-hydraulic conductivity trendlines.

Numerical methods also exist to estimate the hydraulic conductivity of specimens tested in a lever-arm oedometer (where volume change is allowed to occur under defined confining loads). Calculation of swelling pressure and hydraulic conductivity from oedometer tests of bentonite-based materials have been presented previously by Dixon and Gray (1985) and also Barone et al. (2014) and indicated that swelling pressure and hydraulic conductivity values obtained using this method are generally comparable to the fixed-volume tests, but an exact match is not usually achieved. The consolidation testing done as part of this testing program were intended primarily to provide deformation parameters but could also be used to try and generate additional swelling pressure and hydraulic conductivity data. The results of those analyses are presented in Section 6.3.2.

Presentation of data and development of behavioural understanding and models related to many of the parameters of interest in bentonite-based materials is difficult if the data is compared based on the basis of dry density. This is particularly the case if materials contain a non-bentonite component as behaviour is strongly linked to the swelling clay component. In previous work, a means of normalizing data presentation such that variations in bentonite content (due to presence of a sand component) and also smectite content of the bentonite itself was developed. This involves use of the parameter known as Effective Montmorillonite Dry Density (EMDD) described by Baumgartner and Snider (2002); Priyanto et al. (2013), and Barone et al. (2014). EMDD is defined as the mass of swelling clay minerals present in a sample divided by the combined volumes of voids and swelling clay minerals (e.g. montmorillonite). Non-swelling clays and other mineral components are treated as inert filler and their mass and volume are subtracted from the system. Calculation of EMDD therefore requires that the swelling clay component be accurately known. The nature of non-smectite component does not really matter provided that its composition is known and it does not chemically or mechanically alter the behaviour of the swelling clay. The EMDD concept predicts that the smectite-rich materials will follow generic EMDD-K relationships, based on the salinity of the percolating fluid and the smectite content of the material being tested. The formulation of the equation used to convert from conventional dry density to EMDD (Priyanto et al. 2013) is provided below:

$$\text{EMDD} = \rho_{\text{md}} = \frac{M_m}{(V_m + V_v)} = \frac{f_m \cdot f_c \cdot \rho_d}{\left[1 - \left(\frac{(1 - f_c) \cdot \rho_d}{G_a \cdot \rho_w} \right) - \left(\frac{(1 - f_m) \cdot f_c \cdot \rho_d}{G_n \cdot \rho_w} \right) \right]}$$

where: ρ_d = dry density of soil (kg/m³);
 ρ_w = density of water (kg/m³);
 f_c = mass fraction of clay in dry solids;
 f_m = mass fraction of montmorillonite in clay fraction f_c ;
 G_a = specific gravity of aggregate solid;
 G_n = specific gravity of non-montmorillonite component in clay;

- G_s = specific gravity of soil solid;
 G_{mc} = specific gravity of montmorillonite
 M_m = mass of montmorillonite component (kg);
 V_m = volume occupied by montmorillonite component (m^3); and
 V_v = volume of void (m^3).

The following values were used to calculate EMDD for the 70-30 bentonite-sand mixture for this study: $f_m = 0.8$, $f_c = 0.7$, $G_a = G_s = G_n = 2.65$ and $G_m = 2.716$.

The current study was intentionally designed to minimize the effect of variation in swelling clay content (same batch of MX80 bentonite was used for all testing and all materials were predried at 110°C before being weighed for use). As result the data generated should therefore be unaffected by mineralogical factors or inaccurate mass proportioning of solids and liquids.

BSM was also examined in this study and unless EMDD is used, separate behavioural trends would need to be developed for these materials. Preparation of specimens for testing involved careful pre-test blending of small batches of pre-weighed clay and sand, with particular care taken to homogenize the specimens before compaction. This process will have minimized uncertainty regarding homogeneity of each specimen.

6.2 SWELLING PRESSURE

6.2.1 Directly Measured Swelling Pressure

The densities specified were at or near the anticipated as-placed density for sealing system components in NWMO's DGR concepts. As described above, a series of at least three replicate tests were completed to measure swelling pressure and hydraulic conductivity for each specified material, density and pore fluid composition (Table 1.1), in an attempt to provide an indication of the intrinsic variability in laboratory-generated data.

In order to get a better sense of the comparability of the data collected as part of the current study, the data presented in Figure 6.2 has been plotted together with literature data for MX80 materials (Figure 6.3). A complete tabulation of the test swelling pressure values collected in this study are provided in Appendix E. The data presented in Figure 6.3 includes plots of both dry density and EMDD for MX80 only and 70-30 BSM, clearly showing how EMDD normalizes the relationship allowing for comparison of behaviour. While the compilation of new with literature data presented in Figure 6.3 re-introduces uncertainties regarding the mineralogical composition of the previously reported MX80 materials, the database is still limited to this single product and provides an indication of variability over an extended period as the data spans an almost 30 year period of material supply.

The plot provided in Figure 6.2 for low pore fluid salinity (CR-10) conditions, shows good clustering of the values obtained for the replicate tests done on three materials of interest. The new data does not however show a clear differentiation in the values obtained for the freshwater and CR-10 solutions. This may be a function of the relatively low salinity of the CR-10 solution and the presence of soluble salts naturally occurring in the bentonite clay (which will result in a >0 g/L TDS concentration in the DW systems) or may be a function of the limitations of the test method used. When the new data is combined with literature-sourced measurements for MX80

bentonite, a slight offset of CR-10 (lower swelling pressure) from the freshwater trend line is evident (Figure 6.3).

At higher salinities (>100 g/L TDS), there is clearly a reduced swelling pressure developed by MX80 for a given EMDD relative to what was seen at lower pore fluid salinity (Figure 6.3). The scatter in the data collected for replicate tests (Figure 6.2), seems slightly higher at high salinity and may be a function of the lower magnitude of the swelling pressure being more difficult to measure using the techniques available. There is no clear trend for increasing TDS to influence swelling pressure for a given EMDD once approximately 150 g/L is exceeded, although as EMDD increases so does the swelling pressure. This would seem to indicate that the effect of salinity on swelling pressure for a given density condition is not substantial once salinity exceeds approximately 150 g/L (i.e. the surface charge on clay particles is overwhelmed by ions in solution once ~150 g/L is achieved). If this is the case, then the prediction of system behaviour becomes easier as a single, conservative relationship between EMDD and swelling pressure could be assumed in environments where TDS exceeds ~150 g/L.

The data collected in the current study shows good comparability to previously completed NWMO work (e.g. Priyanto et al. 2013; Barone et al. 2014) as well as to other literature collected and presented in those reports. The new, extended database (especially for high salinity conditions), allows for better interpretation of the role of pore fluid salinity in determining the swelling pressure of a bentonite-based material. There does not seem to be a discernibly different amount of data scatter between the current study and that reported in literature, indicative of a consistent product over many years.

The data presented in Figure 6.3 includes data presented by Priyanto et al. 2013; Barone et al. 2014 and was analysed using a power regression function and the maximum R^2 values shown were determined for each data set by varying the y-axis intercepts in order to generate the best possible R^2 . Using this technique, the regression lines intersected the y-axis (EMDD = 0) at values of 0.04 to 3 kPa (brine solution and DW respectively). The data available generally does not extend below EMDD values of 0.5 Mg/m³ and reference EMDD values for sealing materials of interest to NWMO in this study lie between ~1.35 and ~1.67 Mg/m³. Hence extension of the regression lines to low densities is not particularly relevant to this study but do demonstrate anticipated material behaviour should the density of placed materials locally decrease slightly following installation (e.g. as the result of material erosion or swelling to occupy other voids).

The data for low salinity systems generated in the current study shows good comparability to literature values, although it generally trends towards the lower end of the range of data scatter. This trend is consistent for both DW and CR-10 pore fluids. There is also a separation of the swelling pressure-EMDD trend lines that indicate that the slightly saline CR-10 can be expected to show slightly lower swelling pressures than DW systems, particularly as the EMDD decreases. At high EMDD values (>1.3 Mg/m³), the difference in swelling pressure developed in DW or CR-10 systems becomes indistinguishable.

The swelling pressures developed in high TDS environments are consistently and substantially lower than observed for low TDS systems. The TDS conditions appear to systematically influence (reduce) the swelling pressure developed at any EMDD as TDS increases to approximately 100 g/L but further changes beyond this TDS level are not clearly observed. This is potentially significant as it would allow for a single relationship to be used for EMDD and

swelling pressure for any condition where TDS > 100 g/L. The validity of this needs to be confirmed through examination of differing TDS concentrations and ionic compositions.

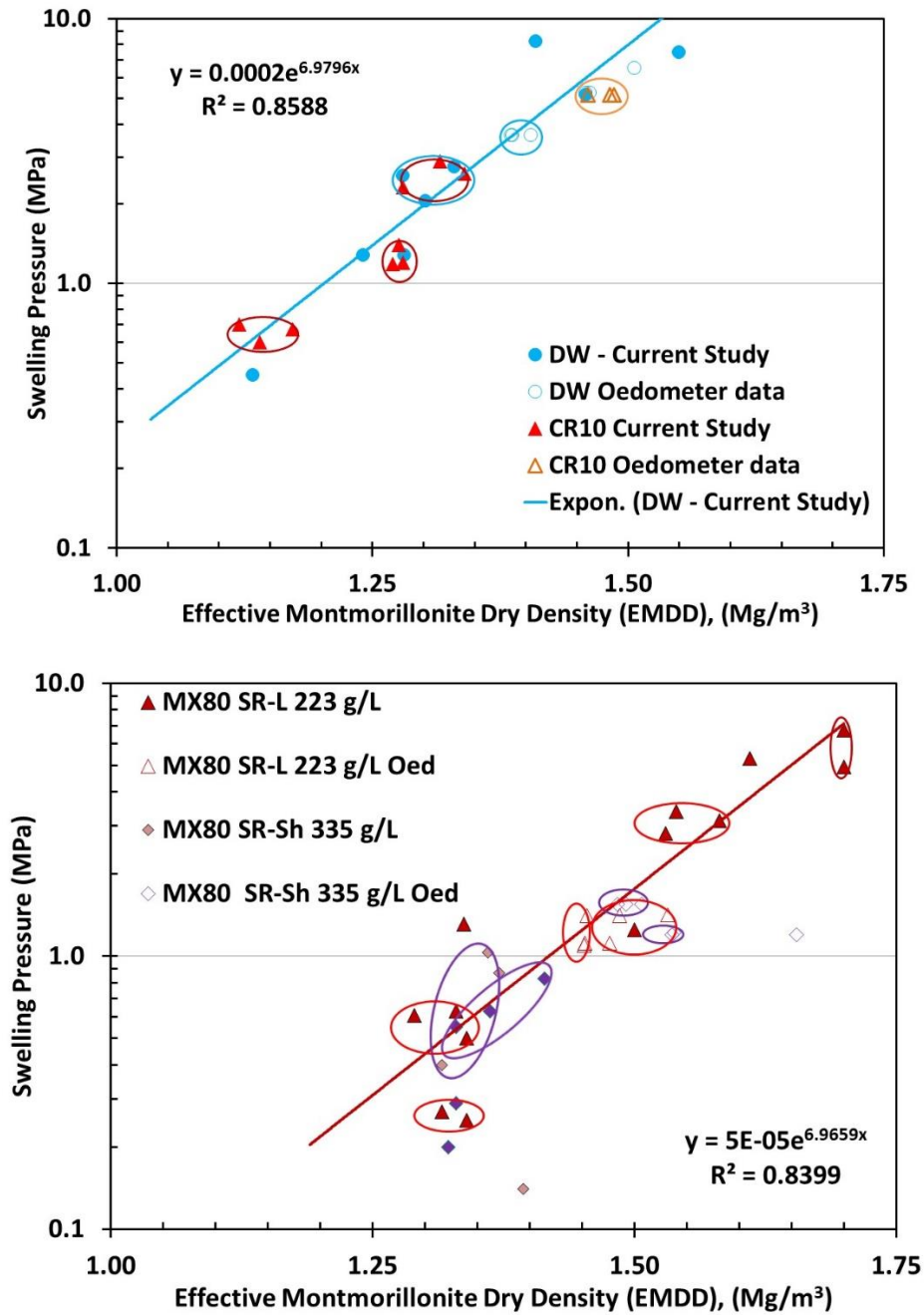


Figure 6.2: Swelling Pressures Measured for MX80 Bentonite (circled data are replicates)

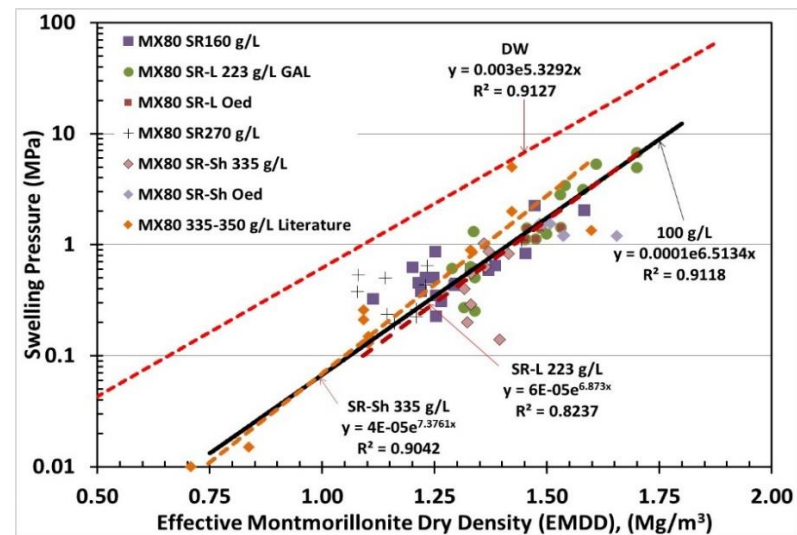
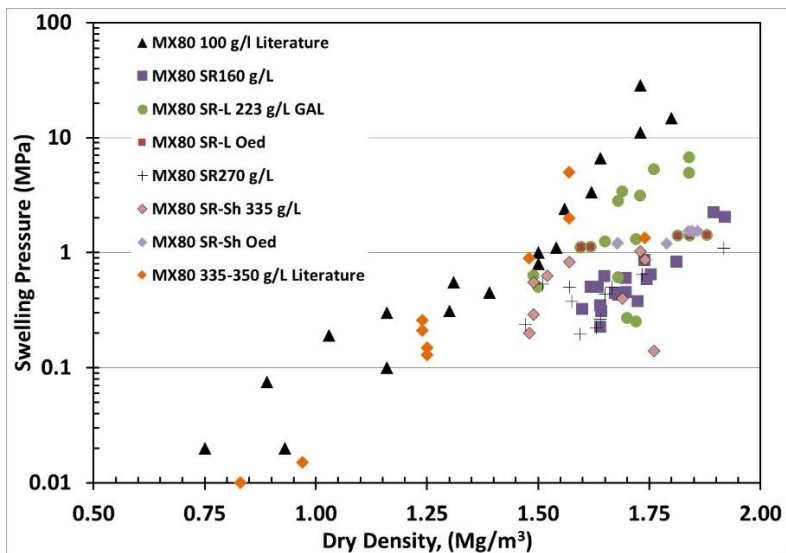
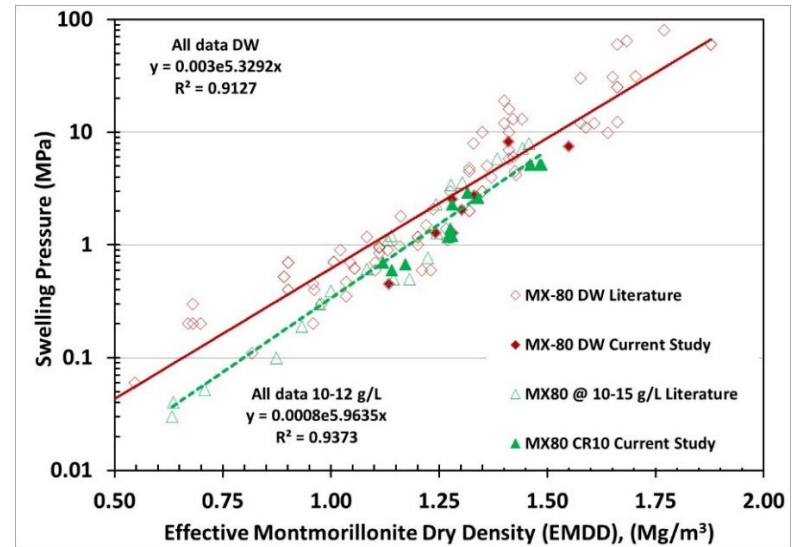
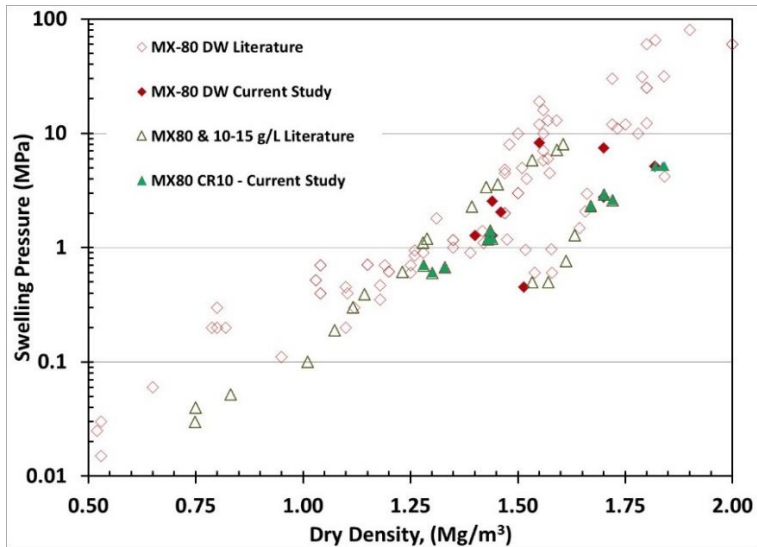


Figure 6.3: Effect of Pore Fluid Salinity on Swelling Pressure of MX80 Systems

6.2.2 Swelling Pressures Derived from One-Dimensional Consolidation Testing

One of the tests undertaken as part of this materials characterization study was one-dimensional consolidation using lever-arm oedometers (see Section 8). These tests are primarily intended to provide deformation parameters for the bentonite and bentonite-sand materials. These data can however also be used to provide additional swelling pressure information. As the tests involve applying a known load to upper surface of a specimen and then monitoring the strain (expansion or consolidation) of the specimen under that load pressure-density information is generated. Previous studies comparing swelling pressure data collected in this manner with those collected from triaxial tests and conventional rigidly confined swelling pressure tests indicate that the data should be comparable (Dixon 1986; Barone et al. 2014).

Swelling pressure values extracted from the one-dimensional consolidation tests that were completed (testing and analysis) during 2015 is provided in Appendix E, together with that collected from rigidly confined tests (Section 6.2.1). The plots of swelling pressure versus density provided as Figure 6.2 and Figure 6.3 include the lever-arm oedometer data (oed) and shows how well these measurements compare with those collected using rigidly confined specimens.

6.3 HYDRAULIC CONDUCTIVITY

6.3.1 Directly Measured Hydraulic Conductivity

As described above, the tests to measure swelling pressure in the rigidly confined cells also allowed for measurement of the hydraulic conductivity at the density and fluid compositions of interest to NWMO. Also, as per the swelling pressure tests, the hydraulic conductivity measurements provide an indication of the potential variability in laboratory-generated data.

Testing of hydraulic conductivity at high pore fluid salinity is challenging due to the aggressiveness of the salts on testing equipment. Collection of reliable data requires particular care to ensure that the test equipment is not compromised in the course of testing. As part of this testing process, each test cell was visually inspected prior to installing a new specimen and frequent visual inspection was done to ensure no adverse processes (corrosion-induced leakage or salt-precipitation causing blockage) were affecting the testing equipment.

As was the case with the swelling pressure testing described in Section 6.2, hydraulic conductivity testing involved three replicate tests for each material, dry density and pore fluid composition listed in Table 1.1. As noted previously, there is some deviation in the actual end-of-test densities measured for these tests relative to their target values. These changes are attributed to minor vertical expansive stain of the restraint system as pressure developed within the rigid-walled cells. There were however three tests completed within each of the density ranges and pore fluid compositions defined for the testing program (MX80 at 1.4 to 1.5 Mg/m³ and >1.7 Mg/m³ and 70:30 MX80 - sand at >1.7 Mg/m³ dry density).

Figure 6.4 presents the hydraulic conductivities measured in the current study using direct flow testing (left side of figure) and derived via calculation from oedometer tests (right side of figure), with each replicate group of tests circled for ease of reference. From these data it can be observed that:

- At low salinity (DW and CR-10) the data generated for the bentonite and bentonite-sand materials showed a relatively low degree of data scatter for replicate specimens, approximately one-half order of magnitude range in the directly-measured hydraulic conductivity values for a given EMDD. The data also followed the EMDD-K relationship previously observed for similar MX80 materials (Figure 6.5). As was observed for the swelling pressure measurements, there is only a slight difference in the behaviour of the DW and CR-10 systems, CR-10 is only slightly more permeable at a given EMDD (Figure 6.5); and
- At high salinity (SR-L and SR-Sh), the directly measured hydraulic conductivity data followed established patterns with respect to EMDD and hydraulic conductivity with, as expected, high salinity systems showing substantially higher K values than were observed for low salinity systems. The degree of data scatter is also slightly greater for the saline systems, almost an order of magnitude for a given EMDD (Figure 6.4). This is consistent with the scatter observed in swelling pressure values
- It is difficult to differentiate the EMDD-K behaviour based on pore fluid salinity for specimens having a TDS > ~100 g/L (Figure 6.5).

Figure 6.5 presents the results of the current testing series in combination with the extensive available body of literature-derived hydraulic conductivity data for MX80 and MX80-aggregate systems. These data clearly show how hydraulic behaviour is affected by both density and pore fluid salinity. The difficulty in using the specimen density to assess hydraulic behaviour is shown as is the benefit of using the normalizing EMDD parameter to describe behaviour. From these data, regression equations describing the changes in hydraulic conductivity with density for the various solutions have been generated (Table 6.1).

Appendix E contains the full tabulation of the hydraulic conductivities measured. The data presented in Figure 6.5 was used to generate regression lines and equations that allow for numerical estimation of hydraulic conductivity for a given EMDD and pore fluid salinity condition. From these equations it is possible to generate estimates for the hydraulic conductivity and intrinsic permeability of MX80 and MX80-sand systems (see Section 6.3.3).

Table 6.1: Hydraulic Conductivity Equations from Best-Fit Lines (based on EMDD values)

	DW**	CR10	SR-L	SR-Sh***
Regression equation (power-fit)	$k=6E-13*EMDD^{-4.635}$	$k=1E-12*EMDD^{-6.55}$	$k=2E-10*EMDD^{-16.78}$	$K \leq 2E-9*EMDD^{-15.07}$
R ²	0.7218	0.6912	0.7589	---

* Hydraulic conductivity expressed in m/s.

** Equation derived from best-fit line for all MX80 data available including literature sources

*** Equation from >300 g/L values in Figure 6.5 and represent conservative bounds for high salinity systems.

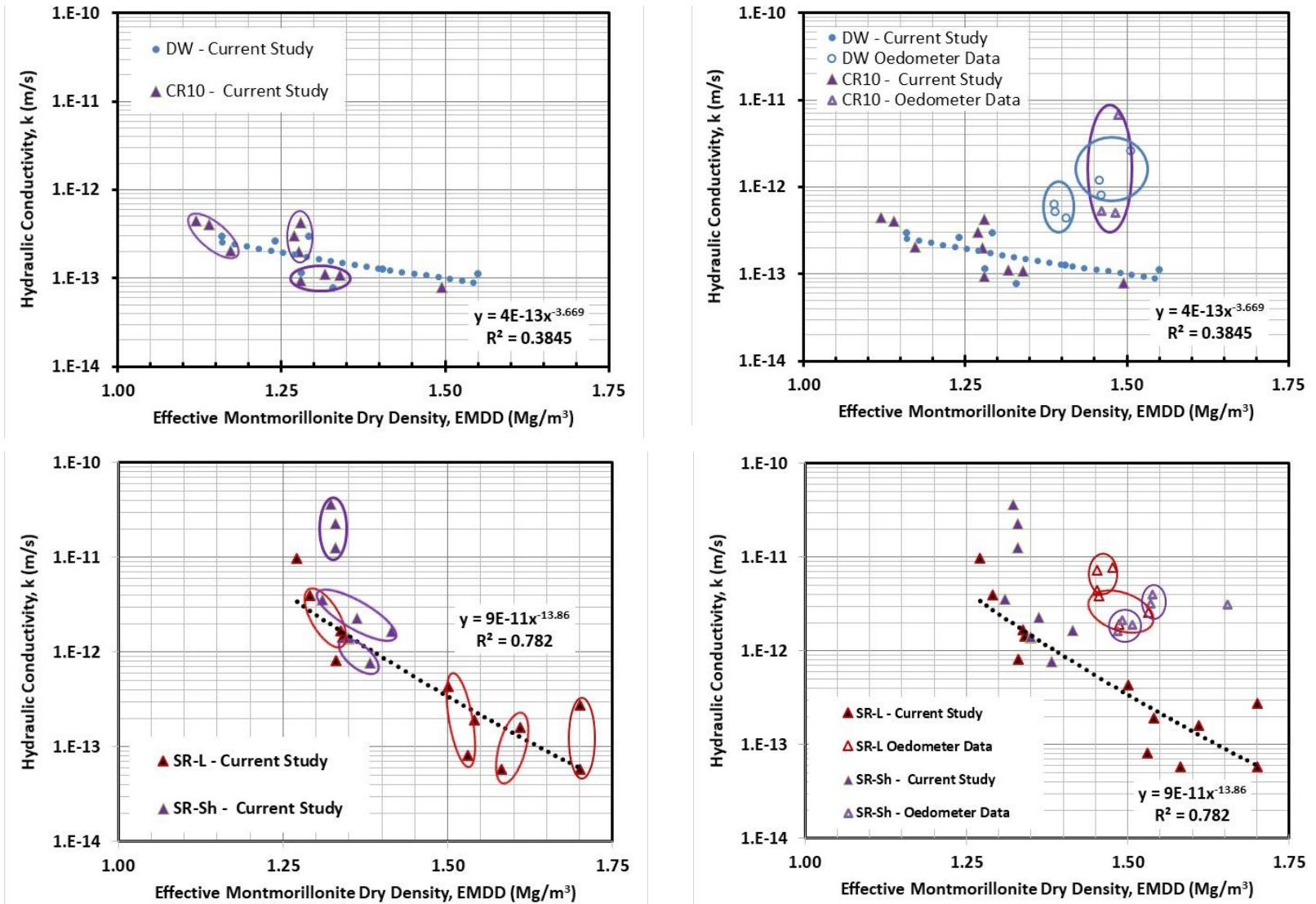


Figure 6.4: Hydraulic Conductivity Measurements for MX80 Bentonite.
 (Circled data points identify replicate tests).

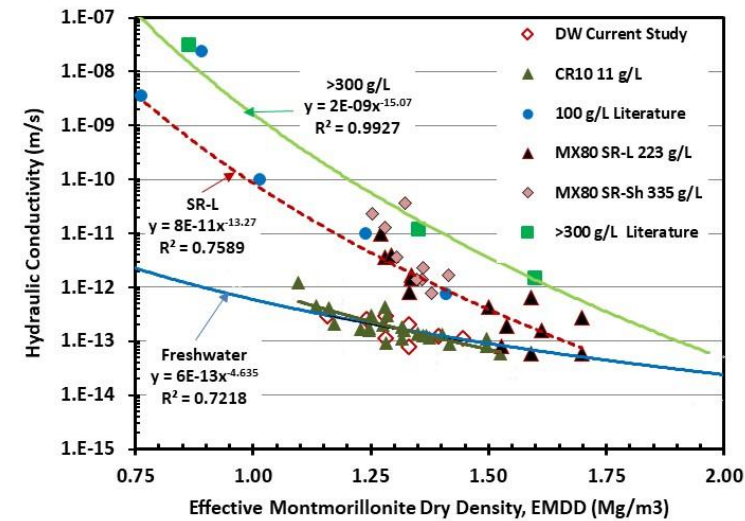
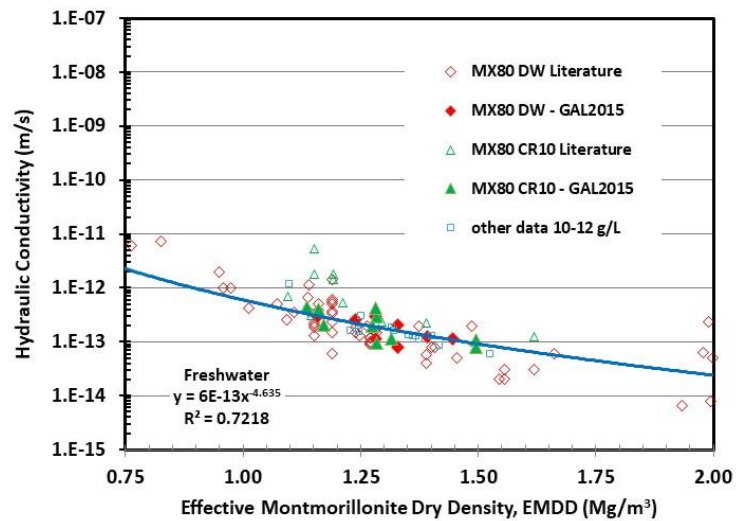
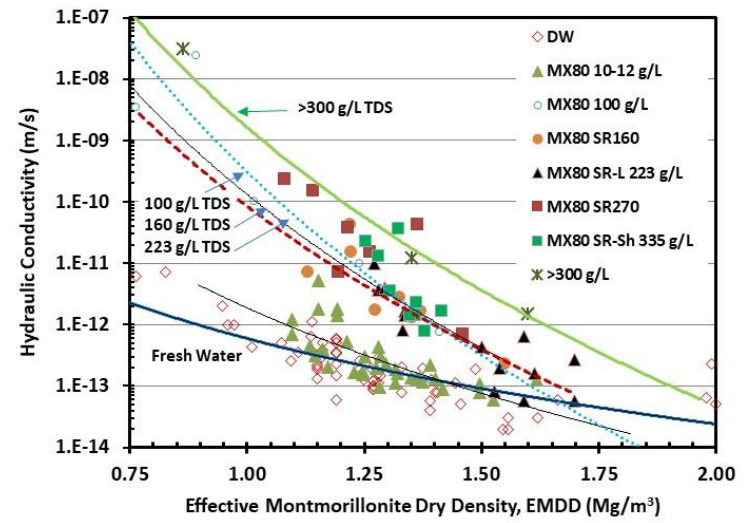
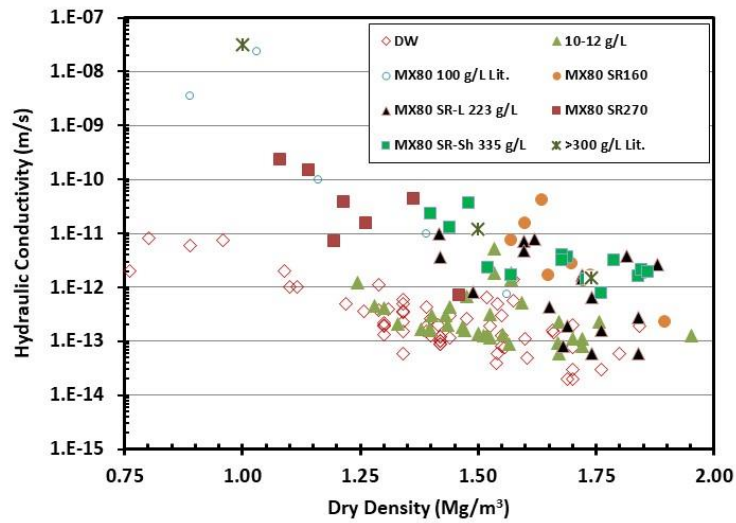


Figure 6.5: Comparison of New MX80 Bentonite and BSM Hydraulic Conductivity Data to Literature Values
 (Data presented is for directly measured hydraulic conductivity tests only)

6.3.2 Hydraulic Conductivity Derived from Oedometer Test Data

In addition to directly measured flow rates, it is possible to estimate hydraulic conductivity from the results of uniaxial consolidation (1-D) test measurements. Figure 6.4 includes the hydraulic conductivity (k) values calculated from the oedometer tests as compared to direct flow measurement data for exactly the same materials.

The calculated hydraulic conductivity determined from the oedometer tests using low salinity (DW and CR-10) and high salinity (SR-L and SR-Sh) pore fluids differ notably from that observed for direct flow measurements:

- There is a clear difference in the hydraulic conductivity measured by testing using fixed-volume, rigid-walled permeameters and the oedometer tests where specimen volume strain occurs. The oedometers seem to show an approximately 1 order of magnitude higher hydraulic conductivity relative the permeameters. There are several potential explanations for this, including the effects of specimen strain on pore structure and hence water movement, as well as the fact that hydraulic conductivity is a calculated value rather than being directly measured. When the two data sets to be separated as in Figure 6.4, the permeameter data shows a smaller degree of scatter and a clearly defined relationship between hydraulic conductivity and EMDD.
- The hydraulic conductivity values calculated for DW and CR-10 systems are very similar. The data for systems having low salinity have hydraulic conductivity values are $\sim 1/2$ to 1 order of magnitude higher than those determined using conventional permeability tests (Figure 6.4). The conduct of three replicate tests for each salinity condition confirms that this difference is real as the 1-D tests provided very reproducible data for each pore fluid type. This systematic difference in values may be a function of the effects of clay particle surface charge on water movement and differences in how water moves under mechanically-induced gradients. It should also be noted that the 1-D tests use the consolidation test parameter (m_v) to calculate the hydraulic conductivity. If this parameter's value is not accurately defined, the resulting calculated hydraulic conductivity will change substantially.
- At high salinity, the hydraulic conductivity values obtained from the consolidation tests (Figure 6.4) show consistent results but again the hydraulic conductivity calculated from consolidation tests is typically $\sim 1/2$ to 1 order of magnitude higher than directly measured values.

These observations highlight the challenges encountered when trying to assess material behaviour when different testing methods are used to determine the same parameter. What is clear from the comparison of the direct flow-type and derived from consolidation test values is that for the range of densities of interest to NWMO, the hydraulic conductivity will remain well below 10^{-10} m/s, the generally accepted limit where mass transport becomes diffusion-dominated.

6.3.3 Permeability Parameter

Literature also presents hydraulic flow values in terms of permeability (K), in m^2 rather than hydraulic conductivity (k) in m/s and in some cases numerical models require use of this parameter. Permeability K (or intrinsic permeability), takes into account factors such as solution density (ρ in kg/m^3), g is gravitational acceleration of 9.81 ms^{-2} and dynamic viscosity (μ in $kg\text{-}s^{-1}m^{-1}$) and is defined as follows:

$$K = k\mu / \rho g$$

When converting the measured hydraulic conductivity to permeability values in saline systems both the solution density as well as its viscosity is required. For the solutions considered in this study the density of the solutions was measured and values are presented in Table 6.3. There were no values available for viscosity of the mixed ion solutions used and so estimates for NaCl and CaCl₂ solutions of similar TDS values were obtained from literature and an average of the two values used. This is the same approach as was used in the study by Barone et al. (2014).

Based on the fluid properties provided in Table 6.2 for materials at approximately 20°C, permeability values can also be derived by applying the multipliers provided in Table 6.2. Permeability values have been generated for each of the tests completed and are included in the data summary tables provided in Appendix E.

Table 6.2: Fluid Densities, Viscosities and Conversion Factors to Calculate Permeability

NWMO Fluid	TDS (g/L)	Fluid Density (g/L)	Viscosity (kg/ms)	k to K multiplier ($\mu / \rho g$)
DW	0	1	0.0010	1.019E-7
CR10	11	1.0058	0.00102	1.035E-7
SR160	155	1.110	0.00179	1.644E-7
SR270	272	1.186	0.0020	1.719E-7
SR-L	223	1.1528	0.00188*	1.6753E-7*
SR-Sh	335	1.2186	0.00223*	1.9228E-7*

* Value estimated from extrapolation of previously used values for DW, CR-10, SR-160 and SR-270 (Barone et al. 2014).

Table 6.3: Hydraulic Conductivity (k) and Permeability (K) Calculated from Best-Fit Lines

Material	Dry Density (Mg/m ³)		EMDD (Mg/m ³)	DW* k (m/s) K (m ²)	CR10 k (m/s) K (m ²)	SR-L k (m/s) K (m ²)	SR-Sh** k (m/s) K (m ²)
MX80	1.5	k K	1.353	1.47E-13 1.50E-20	1.38E-13 1.43E-20	1.45E-12 2.43E-19	≤2.1E-11 4.04E-18
MX80	1.6	k K	1.456	1.05E-13 1.07E-20	8.5E-14 8.8E-21	5.47E-13 9.16E-20	≤6.95E-12 1.34E-18
MX80	1.7	k K	1.560	7.64E-14 7.79E-21	5.4E-14 5.59E-21	2.19E-13 3.67E-20	≤2.46E-12 4.73E-19
MX80	1.8	k K	1.667	5.46E-14 5.56E-21	3.5E-14 3.62E-21	9.1E-14 1.52E-20	≤9.1E-13 1.75E-19
70:30 BSM	1.7	k K	1.327	1.62E-13 1.65E-20	1.57E-13 1.62E-20	1.87E-12 3.13E-19	≤2.8E-11 5.38E-18
70:30 BSM	1.8	k K	1.439	1.11E-13 1.13E-20	9.2E-14 9.52E-21	6.39E-13 1.07E-20	≤8.30E-12 1.60E-18

* Equation from best-fit line for all MX80 data available including literature sources

** Equation from 300 g/L values in Figure 6.5 and represent conservative bounds for high salinity.

K is calculated using conversion multipliers provided in Table 6.2.

Figure 6.6 presents permeability of MX80 materials as a function of EMDD and porefluid salinity. The low (<11 g/L) TDS bentonites show limited effect of EMDD on permeability, decreasing less than a half order of magnitude over the range of 1.1 to 1.6 Mg/m³ EMDD. Under high TDS conditions the permeability showed a stronger influence of EMDD on permeability with approximately 2-orders of magnitude change (reduction) in permeability for the same change in EMDD. As with hydraulic conductivity for a given EMDD the permeability under saline porefluid conditions is consistently higher under saline conditions. The difference between freshwater and saline permeability decreases with increasing density and at EMDD in the order of 1700 kg/m³, permeability is essentially the same in freshwater and brine groundwater conditions. This can be attributed to the very low porosity available for flow and very limited volume of unstructured water in either system.

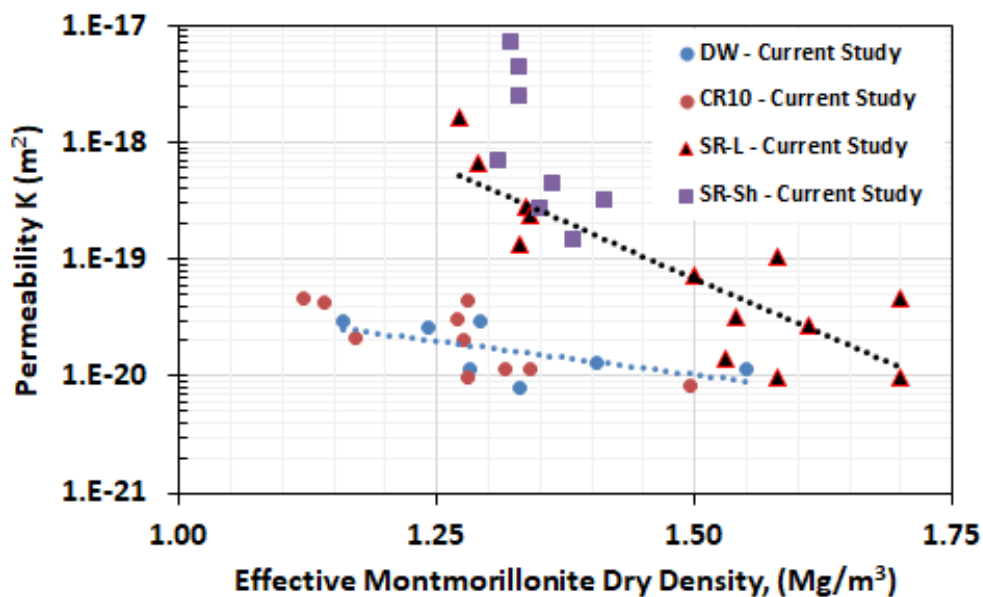


Figure 6.6: Water permeability as a Function of EMDD and Pore Fluid Salinity

6.4 DISCUSSION

The current testing program has provided a substantial body of data for bentonite-based materials tested at very high pore fluid salinity (223-335 g/L TDS). Literature does not contain very much information for swelling pressure or hydraulic conductivity under these conditions and so the current work has allowed a better sense of the effects of high TDS conditions on material behaviour to be developed.

Swelling pressure and hydraulic conductivity testing indicates that scatter in values for these parameters with respect to density are likely functions of intrinsic variability in the matrix of the compacted materials or test method limitations. As of the completion of this testing program, the data is showing the following:

- Replication of tests using identical testing materials and pore fluids did not generate a discernibly different degree of data scatter than was observed in previously completed

tests or what is reported in the literature for the same clay product (MX80) by a considerable number of researchers;

- For both swelling pressure and hydraulic conductivity tests, a range of approximately half an order of magnitude exists from the best-fit line's value for a given density;
- Swelling pressure will increase with increasing EMDD;
- Swelling pressure will decrease with increasing pore fluid TDS, up until a concentration of approximately 100 g/L is reached;
- Swelling pressure at a given density is not discernibly affected with changes in pore fluid concentration beyond approximately 100 g/L TDS;
- Hydraulic conductivity will decrease with increasing EMDD;
- Hydraulic conductivity will increase at a given density with increasing pore fluid TDS, up until approximately 100 g/L TDS is reached;
- Hydraulic conductivity at a given density is not discernibly affected by increasing pore fluid salinity beyond approximately 100 g/L TDS;
- Swelling pressure measurements obtained from rigidly confined specimens are generally comparable to those obtained from 1-D consolidation (oedometer) tests;
- Hydraulic conductivity measured from rigidly confined specimens is not comparable to those calculated from 1-D consolidation (oedometer) tests where low pore fluid salinity exists (0-12 g/L TDS). The oedometer tests tend to produce hydraulic conductivity values that are approximately one order of magnitude higher than those obtained from the fixed volume tests under these conditions; and
- Hydraulic conductivity derived from testing using rigidly confined, fixed-volume specimens are generally comparable to those calculated from 1-D consolidation (oedometer) tests where high pore fluid salinity exists (>100 g/L TDS).

Based on the observations provided above and using the data collected in this study and from literature sources, the swelling pressure and hydraulic conductivity and permeability behaviour of the MX80 and BSM materials can be described via regression equations. From these it is possible to define values for each of these parameters based on the EMDD of the materials of interest and the salinity of the fluids they are in contact with. Table 6.4 presents the equations and reference values developed from direct measurement (oedometer data was not used for reasons discussed previously), included for comparison are the equations provided by Baumgartner (2006). The Baumgartner (2006) regression equations includes some of the same data used in the current regression analysis and so similarity should be expected. Figure 6.7 compares the earlier data regression data of Baumgartner (2006) (as dashed lines) to the new ones and shows that although there have been slight changes in the trend-lines, they are very comparable. Baumgartner (2006) predicted swelling pressures of approximately 2 to 3 times that of the more recent testing and literature sources. Hydraulic conductivity values are generally comparable, although literature data seem to indicate higher values in very saline conditions. There is only a limited quantity of data at such high salinities and so drawing firm comparative conclusions regarding swelling pressure and hydraulic conductivity is difficult. It should be noted that the regression equations provided are considered representative for EMDD conditions greater than approximately 0.75 Mg/m^3 , lower density conditions may not be accurately described. The target EMDD range for materials examined in this study was 1.35 to 1.67 Mg/m^3 and so were within the bounds represented by the equations in Table 6.4.

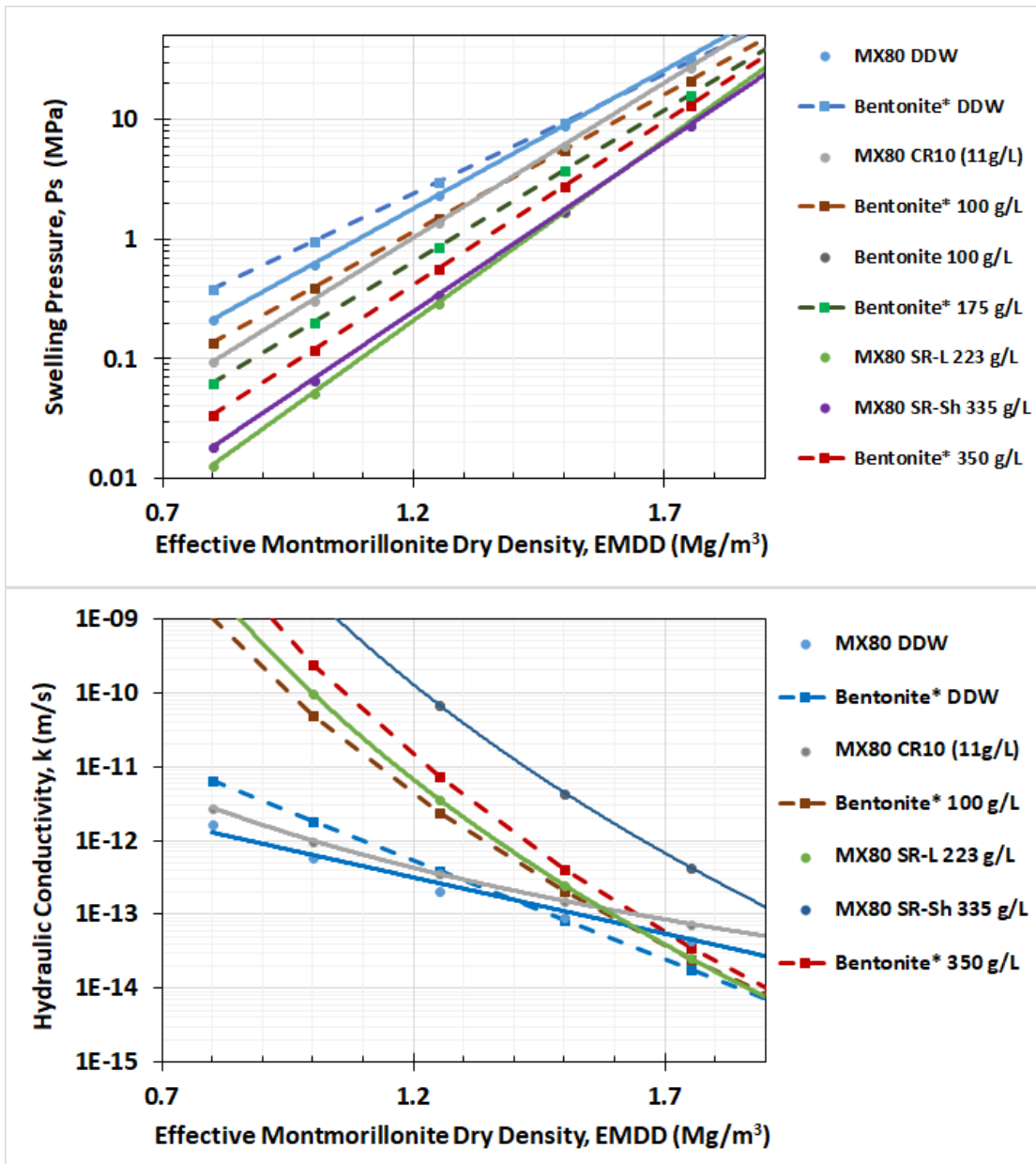


Figure 6.7: Swelling Pressure and Hydraulic Conductivity Best-Fit Lines and Comparison to Data Presented by Baumgartner et al. (2006) (dashed lines)

Table 6.4: Regression Equations Describing Swelling Pressure and Hydraulic Properties of MX80 and 70:30 MX80:Sand Materials

Pore Fluid (g/L)	Swelling Pressure (MPa) *	R ²	Hydraulic Conductivity** (m/s)	R ²
DW	$0.003 * e^{5.329 * EMDD}$	0.913	$6E-13 * EMDD^{-4.635}$	0.722
DW ⁺	$0.01 e^{4.58 EMDD}$		$9E-10 e^{-6.18 EMDD}$	
CR10 (11)	$0.0008 e^{5.9635 * EMDD}$	0.937	$1E-12 * EMDD^{-6.552}$	0.691
100 ⁺	$2 \times 10^{-3} e^{5.3 EMDD}$	0.912	$5.1E-11 * EMDD^{-13.6}$	
100	$1 \times 10^{-4} e^{6.5134 EMDD}$		$3E-10 EMDD^{-16.97}$	0.922
SR-L (223)	$5E-5 \times e^{6.9442 * EMDD}$	0.824	$1E-10 * EMDD^{-14.76}$	0.730
300-350	$5E-5 \times e^{7.255 EMDD}$	0.904	$2E-9 \times EMDD^{-15.07}$	0.993
350 ⁺	$2.3E-4 \times e^{6.26 EMDD}$		$2.5E-10 \times EMDD^{-15.8}$	
SR-Sh (335)	$0.0001 e^{6.5134 * EMDD}$	0.919	$2E-9 * EMDD^{-15.07}$	-----

(equations based on summary of available data for directly measured values)

+ Equations from Baumgartner (2006)

* The swelling pressure for SR-Sh is essentially identical to that for SR-L and other materials >100 g/L TDS. Measured values are generally within ½-order of magnitude from trendline predictions.

** The hydraulic conductivity for SR-Sh is based on data for materials >300 g/L and provides a conservative bound to behaviour.

*** The permeability provided for SR-Sh is based on data for materials >300 g/L and provides a conservative bound to behaviour.

7. SHRINKAGE, SOIL WATER CHARACTERISTIC CURVES AND AIR PERMEABILITY

7.1 BACKGROUND AND APPROACH TO TESTING

The characterization of air permeability involves five interrelated components:

1. sample preparation;
2. shrinkage curve tests (Section 7.2);
3. soil-water characteristic curve (SWCC) tests (Section 7.3);
4. air permeability (AP) tests (Section 7.4); and
5. derivation of a numerical relationship that describes the relative air permeability as a function of saturation.

The conduct of each of the material preparation and subsequent testing requires highly specialized equipment and testing procedures in order to accommodate the materials and pore fluids examined in this study. Previous studies to determine some of these parameters were completed by Barone et al. (2014). The method and equipment used to obtain the required data are described as part of discussion of each test in Sections 7.2 through 7.4.

Each of the specimens used in the SWCC, shrinkage and air permeability tests were prepared to a pre-calculated density and moisture (or saturation) state. These specimens were built and tested in triplicate in order to provide greater confidence in the reproducibility of the results as well as to gain an indication of what degree of variability of readings might be observed for essentially identical specimens.

7.2 SHRINKAGE TESTS

7.2.1 Background and Test Method

Shrinkage curve tests are used to measure the relationship between void ratio (e) (volume change) and water content during de-saturation and are used to interpret the volume-mass relationship in the SWCC test results (to compute the relationship between degree of saturation and soil suction). The specific testing matrix completed in this study is provided in Table 1.1 and represents three material specifications and four pore fluid compositions with each test done in triplicate.

The results of the triplicate tests on each material and pore fluid combination were combined to provide one shrinkage curve for each specimen type. Shrinkage tests previously reported by Barone et al. (2014) were done using small sub-specimens cut from larger compacted masses of material. This approach was not used in the current study as it was found to make accurate measurement of specimen volume difficult as well as inducing specimen disturbance during subsample extraction. In the current study, each specimen was larger than previously used (initial volume of $\sim 20 \text{ cm}^3$ versus 15 cm^3) and were individually manufactured from fresh material of known moisture content by compaction in a rigid-walled mold and then extracting an intact specimen (Figure 7.1). As previously, the specimens were then exposed to the laboratory environment ($\sim 20 \text{ }^\circ\text{C}$ and ambient humidity conditions) and water was allowed to evaporate (or sorb) naturally with the mass and volume of each specimen measured at least once per day. On reaching mass and volume steady-state, they were oven dried at $50 \text{ }^\circ\text{C}$ until mass and volume equilibrium was once again achieved. A final oven-drying step at $105 \text{ }^\circ\text{C}$ was completed and the final mass and volume was determined for each specimen. Drying at $105 \text{ }^\circ\text{C}$ was done

in order to remove as much of the non-structural water as possible and to confirm that volume change was complete.

The presence of brine pore fluid in the SR-L and SR-Sh specimens is a complicating factor regarding interpretation of system behaviour. In a high humidity environment, the brine may actually absorb water from the atmosphere resulting in an increasing water content and decreasing porefluid salinity. When drying occurs, the pore fluid will be lost more slowly due to the increasing suction caused by gradually increasing pore fluid salinity. Additionally, when weight loss occurs, only the water component is lost, salts remain behind. This means that as drying progresses the salinity of the remaining pore fluid is steadily increasing, which will affect subsequent behaviour and complicate interpretation (e.g. solution density changing and hence saturation is difficult to assess) as well as affecting the suction present within the specimen (the greater the salinity the greater the suction applied to the air adjacent to the specimen). Ultimately when dried at 105°C there will be considerable quantity of salts (mostly as solids), present in the specimen's pores and also some water will remain associated with these salts.

For the purposes of discussing and presenting the results of the current study, any salts component present as a precipitate is not considered to be part of the solids component of the specimen. The void volume occupied by any precipitated salts or viscous brine is considered to remain a component of the voids and not influence the porosity. Similarly, although specimens were weighed at the end of testing and oven drying, these specimens contain salt solids and also a hydrated brine component. Porosity calculations are therefore based on the known start of test mineral component masses.

As noted by Barone et al. (2014) *"The rate-and-magnitude of drying shrinkage is primarily influenced by the key parameters of:*

- *Density to which the sample is compacted: This will define the porosity of the sample and hence the volume that is potentially available to be involved in any volume change. In most soils there is a porosity below which further drying will not result in further shrinkage;*
- *Surface area available for evaporation/condensation: This will determine the rate and manner in which water can be lost from the block, larger blocks will lose moisture more slowly due to the distance required for moisture to move to the surface and subsequently evaporate. This will also affect the shrinkage magnitude since other macro-processes such as cracking may be more evident in larger blocks than small ones;*
- *Relative humidity of the surrounding atmosphere: The surrounding atmospheric conditions will strongly affect the drying and shrinkage behavior. The presence of low-humidity atmospheric conditions will tend to accelerate drying, give the blocks less opportunity to adjust to moisture loss without inducing cracks or substantial volume change. In contrast, where the atmosphere is very humid, there may actually be a water uptake (and swelling) by the backfill in response to the higher suction present in the soil pore space.*
- *Salinity of the water present in the pores: This parameter has several important influences on the volume and moisture evolution of the shaft backfill. Under low salinity conditions the processes listed above in bullets 1 through 3 will dominate the samples drying behavior. At high porewater salinity (e.g. SR160 and SR270), the salts will play a very important role in defining how the volume of compacted materials will change. Both of these solutions contain very high TDS contents, which mean they have a very high suction present in the internal pores and will also influence their immediate surroundings. These materials will tend to lose moisture much more slowly than low salinity materials. "*

7.2.2 Shrinkage Behaviour of MX80 and MX80-Sand Specimens

The volume change behaviour on drying of the MX80 and MX80-sand materials was determined by conduct of drying tests on disk-shaped specimens that were compacted in a rigid-walled mold and then extruded for testing (Figure 7.1). This provided specimens of known initial dry density and fluid content (in brine systems fluid content is a more accurate definition since the fluid was a high TDS solution rather than the low/no TDS usually assumed when describing water content).



Figure 7.1: Photograph Showing Shrinkage Specimen (Fredlund et al. 2012)

The laboratory data is first presented in terms of volume change with time, water content and density during the three drying stages (Figure 7.2).

The data shown in Figure 7.2 is shown in greater detail in Figure 7.3 through Figure 7.5 for the MX80 specimens compacted to an initial dry density of $\sim 1.5 \text{ Mg/m}^3$ and MX80 – sand specimens compacted to an initial dry density of $\sim 1.8 \text{ Mg/m}^3$ respectively. In Figures 7.3 and Figure 7.4 all three replicate specimen measurements are presented in terms of void ratio (e), showing how low the range of observed volume changes. The data for all systems examined in this study are then presented in Figure 7.5 as best-fit regression lines. These data show that shrinkage behaviour is strongly influenced by the density, composition and pore fluid present in the materials tested. The laboratory data associated with the individual tests summarized in Figure 7.2 through Figure 7.5 are provided in Appendix F.

The best-fit curves for the drying shrinkage tests completed on MX80 and BSM materials were generated using the method described by Fredlund et al. (2002). The equations and fitting parameters used to generate these lines are provided in Equation 7.1 and 7-2 and Table 7.1 respectively.

“The shrinkage curve has the form of a hyperbolic curve. Fredlund et al. (1997, 2002) proposed an equation to best-fit data for the shrinkage curve. The equation has parameters with physical meaning and is of the following form:

$$e(w) = a_{sh} \left[\frac{w^{c_{sh}}}{b_{sh}^{c_{sh}}} + 1 \right]^{\left(\frac{1}{c_{sh}} \right)} \quad (7-1)$$

where: a_{sh} = the minimum void ratio (e_{min}), b_{sh} = slope of the line of tangency, (e.g., drying from saturated conditions), c_{sh} = curvature of the shrinkage curve, and w = gravimetric water content. The ratio,

$$\frac{a_{sh}}{b_{sh}} = \frac{G_s}{S} \quad (7-2)$$

is a constant for a specific soil; G_s is the specific gravity and S is the degree of saturation. Once the minimum void ratio of the soil is known, it is possible to estimate the remaining parameters required for the designation of the shrinkage curve. The minimum void ratio the soil can attain is defined by the variable, a_{sh} . The c_{sh} parameter provides the remaining shape of the shrinkage curve. The curvature of the shrinkage curve is controlled by varying the c_{sh} parameter.”

There are two patterns of behaviour observed in the shrinkage test results. The BSM and MX80 materials show different behaviours as follows:

Pattern 1: Dense 70-30 MX80-sand material

- This material exhibits very limited drying shrinkage (<8.5%) for low salinity conditions (DW and CR10) and an even smaller shrinkage (~7-8%) when high salinity (SR-L and SR-Sh) pore fluid is present.
- The final dry density (based on the mass of non-soluble minerals and end-of-test volume), on completion of desiccation at 105°C is in the range of 1.92 to 1.95 Mg/m³.
- The limited shrinkage in the MX80-sand materials is attributable to the low initial void ratio, which will limit subsequent shrinkage volume available (minerals come into direct contact, restricting any further volume change), and
- The presence of precipitated or minimally-hydrated salt in the pore spaces as drying occurs in those systems having brine pore fluid will also limit the physical shrinkage.
- Shrinkage in systems having SR-L (~225 g/L TDS) and SR-Sh (~335 g/L TDS) were essentially identical. Changing salinity within this range is not likely to affect shrinkage behaviour of this material.

Pattern 2: MX80 at 1.5 Mg/m³.

- The lower density (initial dry density ~1.5 Mg/m³) MX80 bentonite specimens exhibited much larger shrinkage on drying than the denser bentonite-sand systems.
- A higher end-of-drying dry density (based on non-soluble mineral mass) was observed for the freshwater specimens (~1.95 Mg/m³) versus ~1.8 to 1.85 Mg/m³ for the brine systems.
- These specimens showed a greater influence of pore fluid composition on shrinkage. Specimens constructed using freshwater exhibited a drying volume change in the order of 23%, while MX80 specimens having high salinity pore fluid (SR-L and SR-Sh), exhibited drying shrinkage in the order of 18%, consistently less than observed for freshwater.
- The difference in shrinkage behaviour due to salinity is attributed to the effects of salt crystal precipitation, and/or formation of a very viscous hydrated salt slurry in the

specimen pores as the bentonite lost water during drying. Once present, these salt crystals/fluids will prevent/limit volume change and so saline systems will show a smaller degree of volume change relative to fresh (low salinity) systems.

The shrinkage behaviour observed for the current BSM is similar to that reported by Barone et al. (2014) for specimens of lower initial dry density (~ 1.5 to 1.65 Mg/m^3). In Barone et al. (2014) there was a similar strong effect of porefluid TDS on shrinkage capacity. Brine systems shrank from 7.5 to 10% while CR10 and freshwater systems exhibited approximately 15% and 20% shrinkage respectively. There would appear to be slight differences in the final dry density obtained in the current tests versus those of Barone et al. (2014). These may be attributable to slight differences in the bentonite granularity, smectite content of the bentonite, grain size distribution of the sand component and also the different saline solutions used as well as the much lower initial density of the materials examined by Barone et al. (2014).

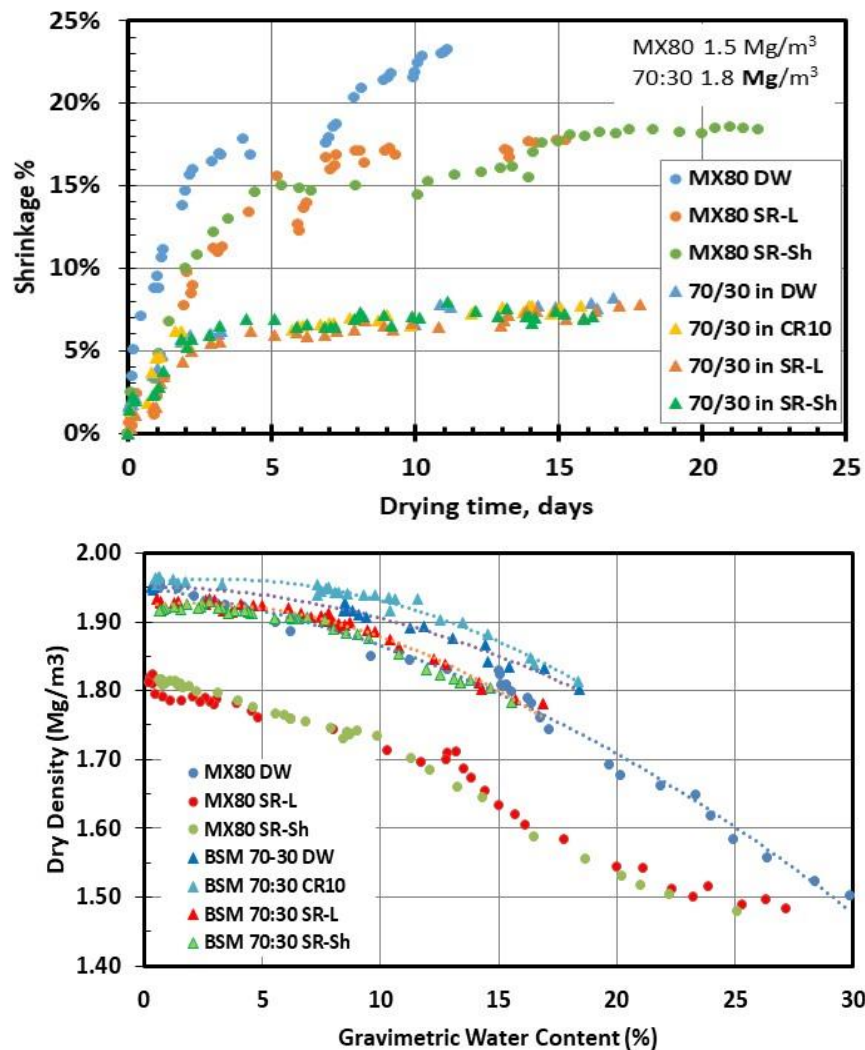


Figure 7.2: Drying Shrinkage and Density Change of MX80 and MX80-Sand Specimens

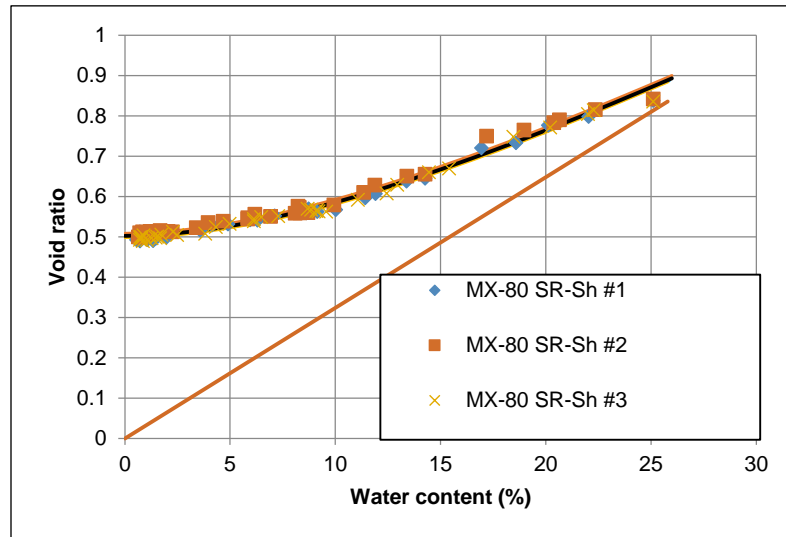
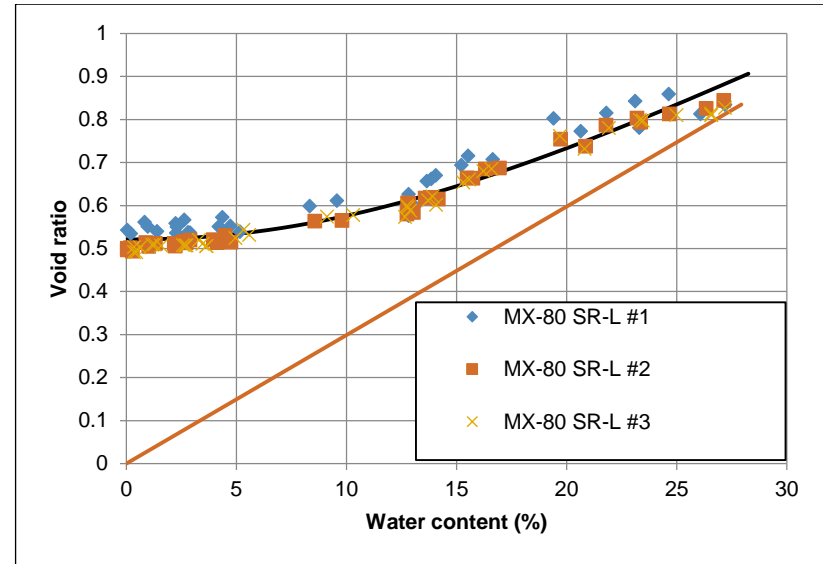
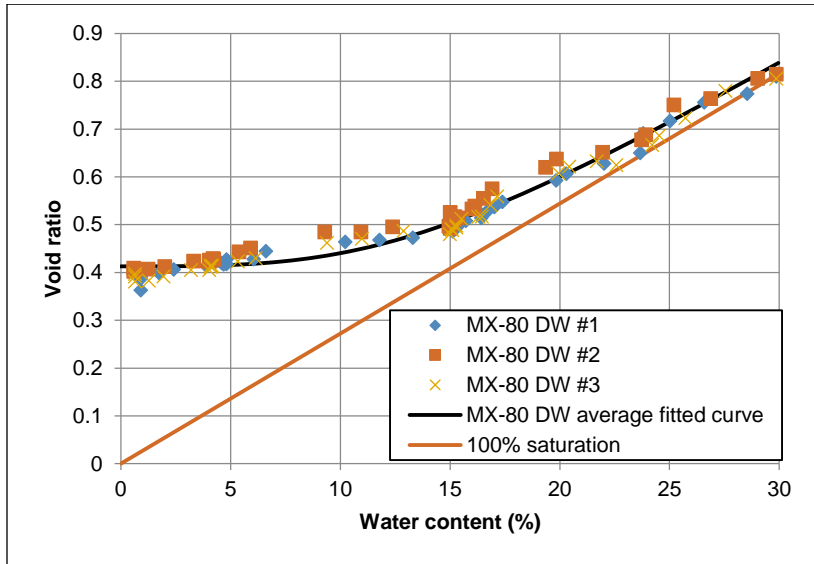


Figure 7.3: Shrinkage Behaviour of MX80 at 1.5 Mg/m³ Dry Density in DW, SR-L and SR-Sh Pore Fluids

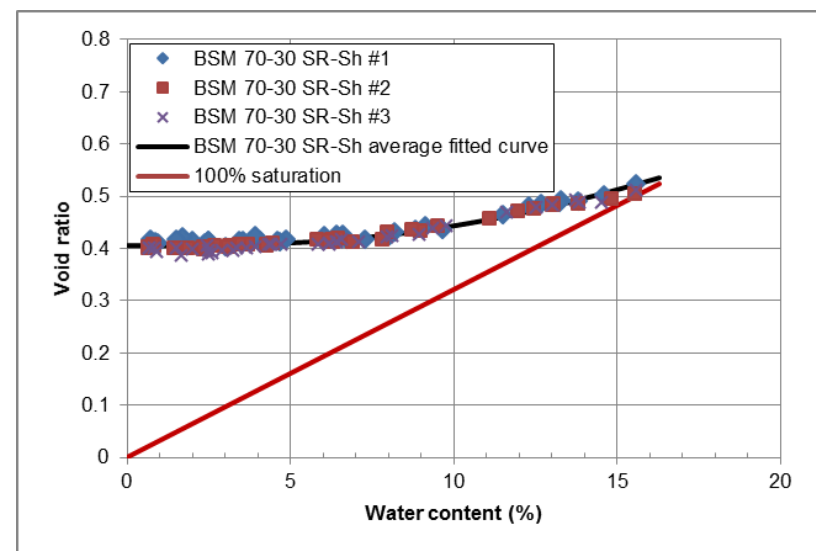
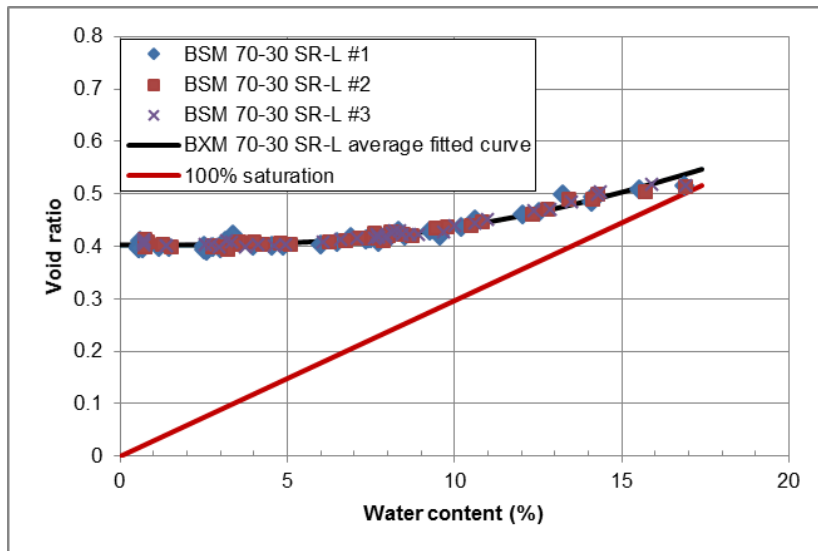
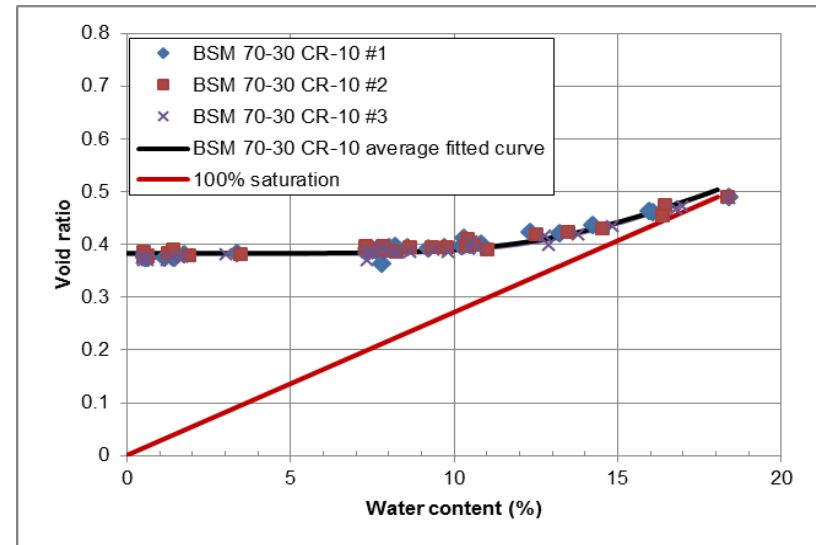
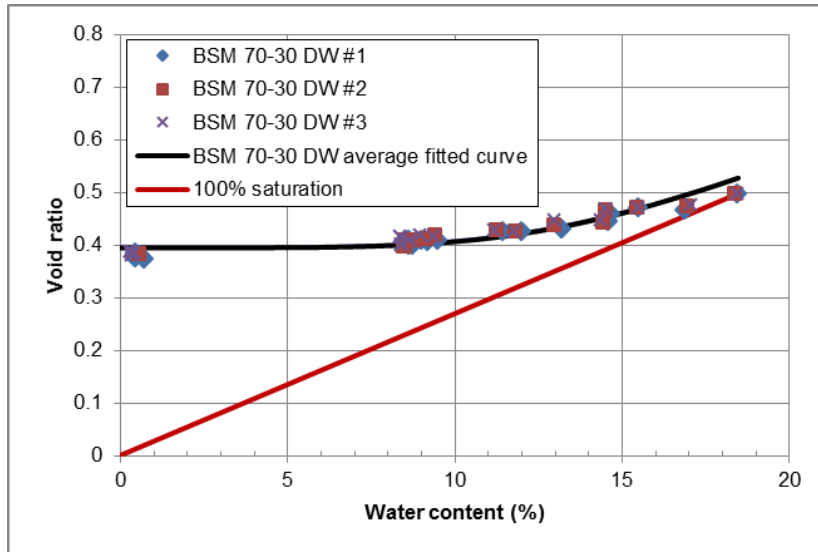


Figure 7.4: Shrinkage Behaviour of 70% MX80 : 30% Sand at ~1.8 g/cc Dry Density in DW, CR10, SR-L & SR-Sh Pore Fluids

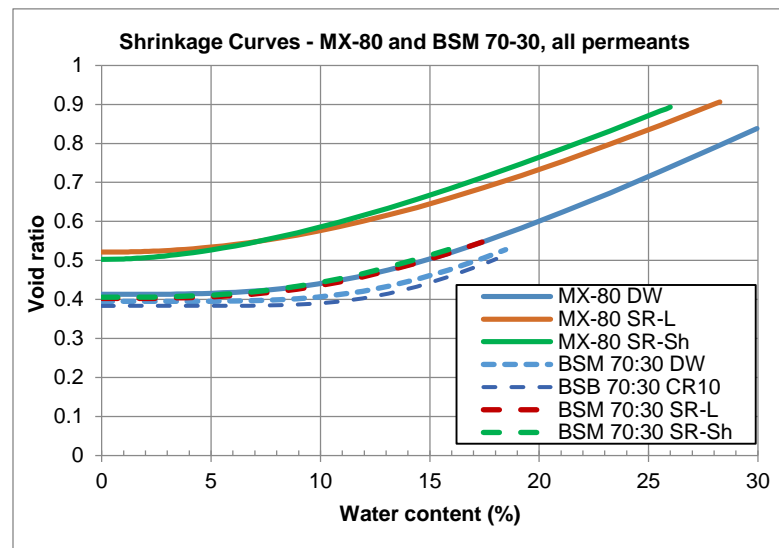
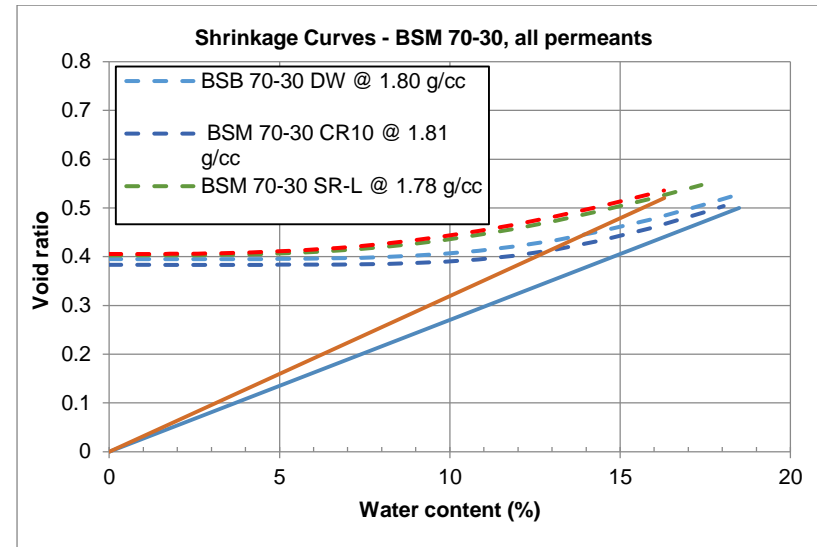
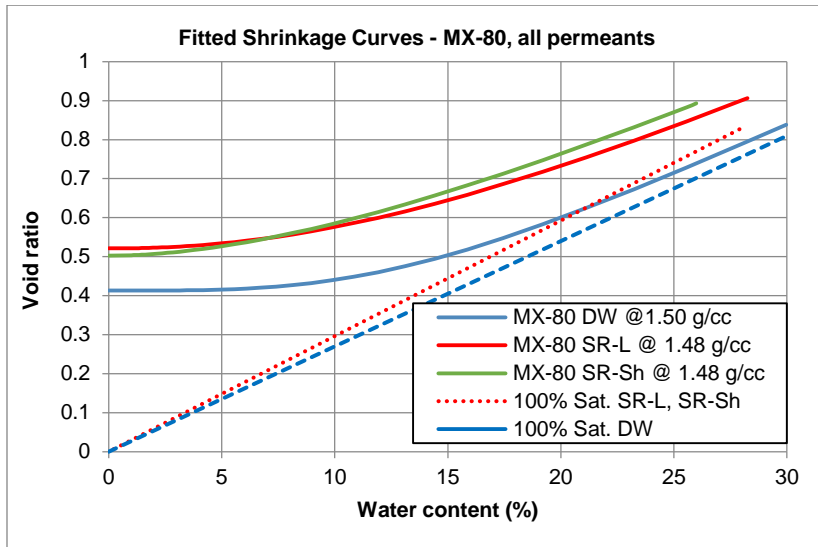


Figure 7.5: Comparison of Shrinkage Behaviour of MX80 and 70:30 Bentonite:Sand

Table 7.1: Fitting Parameters Used to Describe Shrinkage Behaviour of MX80 and BSM

Material	Fitting Parameter		
	a_{sh}	b_{sh}	c_{sh}
MX80 DW	0.41	0.15	3.38
MX80 SR-L	0.52	0.19	2.17
MX80 SR-Sh	0.50	0.18	1.83
BSM 70:30 DW	0.39	0.15	4.90
BSM 70:30 CR10	0.38	0.14	6.13
BSM 70:30 SR-L	0.40	0.15	3.14
BSM 70:30 SR-Sh	0.41	0.15	2.94

(values based on average of 3 measurements)

7.3 SOIL-WATER CHARACTERISTIC CURVES (SWCC)

7.3.1 Background and Testing Method

The soil-water characteristic curve (SWCC) test measures the relationship between the quantity of water in a soil and the negative pore water pressure, or soil suction that is holding this water in place. The suction tests undertaken as part of this study are necessary for assessing the water retention (resistance to desaturation), water uptake and storage capacity of the bentonite materials. The SWCC is typically presented in terms of degree of fluid saturation versus capillary pressure or saturation versus suction but can also be presented as gravimetric or volumetric water content versus suction. For the purposes of data analysis, it is assumed that the capillary pressure (resistance of soil capillaries to desaturation (suction)) is equal to the air pressure used to induce desaturation in the GCTS device and that the relative humidity in the air immediately above the specimens (as per WP4 device reading) is a measure of the total suction in the specimen itself. The measured SWCC, shrinkage curve data (shrinkage information presented in Section 7.2), and the specific gravity of the material are then combined to determine the relationship between degree of saturation and suction.

For this testing program, two methods were used to measure the complete SWCC. The first method used a GCTS Fredlund SWCC pressure cell to measure the lower portion of the SWCC, from 200 to 1500 kPa. The second method used a WP4 to measure the upper portion of the SWCC, from about 20,000 to 300,000 kPa. Data from the two methods can be combined to form the complete SWCC, from a saturated to a desaturated state.

GCTS Device

The low suction ranges (200-1500 kPa) were measured using the axis translation method by pressurizing a single soil specimen in a GCTS Fredlund SWCC pressure cell. The cell and associated pressure system were developed by Geotechnical Consulting and Testing Systems (GCTS) and are shown in Figure 7.6, together with an example of the type of specimen tested.

The GCTS apparatus has the ability to apply a vertical stress to the specimen and is preferred over traditional pressure cells for the type of materials being tested in this study. For each series of measurements (three replicates were done for each material and pore fluid), one saturated 64 mm diameter by 20 mm high specimen for each pore water solution material was compacted directly into stainless steel testing rings. Each specimen was placed on a 15 bar, high air entry ceramic stone for testing in the low suction range. The specimen was then subjected to a vertical confining stress of 500 kPa followed by the step-wise application of the appropriate suctions; namely 200, 450, 700, 1000 and 1450 kPa. At each of these suctions, fluid was allowed to drain from, or in some cases, enter into the specimen. In cases where the SWCC specimen took on fluid, and therefore swelled, rather than drain fluid, a maximum volume increase of 0.5% was allowed, after which the applied suction was increased.

In low- or non-bentonite soils with a low air-entry value, a significant quantity of fluid usually drains out of the specimen at suctions less than 1500 kPa, and in some cases, the specimen can be nearly dry. In fine-grained clay soils and in particular soils having substantial swelling clay content, the air-entry value is generally significantly greater, and a substantial suction can be required before specimen desaturation begins. The latter behavior was seen in all the materials tested for this program, with no significant drainage observed for suctions <1500 kPa.

In terms of water uptake in a rigidly confined system (constant volume), the behaviour of the specimen can be described in terms of change in water content with applied gas pressure. For materials located below the SWCC line (dry side) at a particular degree of water saturation, they will not lose capillary water until the capillary pressure exceeds that indicated by the line. Similarly, for situations where a specimen is on wet-side of the line, a specimen will lose water until it reaches the degree of saturation marking the equilibration of moisture-suction behaviour (intersection of SWCC line). This will be discussed in more detail in Section 7.3.2.



Figure 7.6: GCTS Apparatus Used to Measure the SWCC in Low Suction Range and MX80 SWCC Specimen in Ring After Test.

WP4 Device

The high suction range was measured in the WP4 device, shown in Figure 7.7. The WP4 measures suction by determining the relative humidity of the air above the sample in the closed chamber (an AOAC-approved method; also conforms to ASTM 6836). The instrument determines the relative humidity using the chilled mirror method, once the sample comes into equilibrium with the vapour in the sealed chamber. A tiny mirror in the chamber is chilled until dew just starts to form on it. At the dewpoint, the WP4 measures mirror and sample temperature with 0.001°C accuracy. The relative humidity environment can be converted to an equivalent suction value through the use of the Lord Kelvin equation. The WP4 is calibrated using saturated salt solutions to an accuracy of ± 100 kPa. The instrument will maintain good accuracy for suctions as low as 1,000 kPa, but in the current study was used over the range of $\sim 20,000$ to 250,000 kPa.

In order to conduct measurements in the WP4 device, specimens of known density and fluid content were produced (see Figure 7.7). Each specimen was placed in a testing cup that fit into the Lexan™ sample drawer on the WP4. The sample drawer was closed and sealed prior to start of measurement. On completion of each measurement, the specimen was removed and a new one was installed.

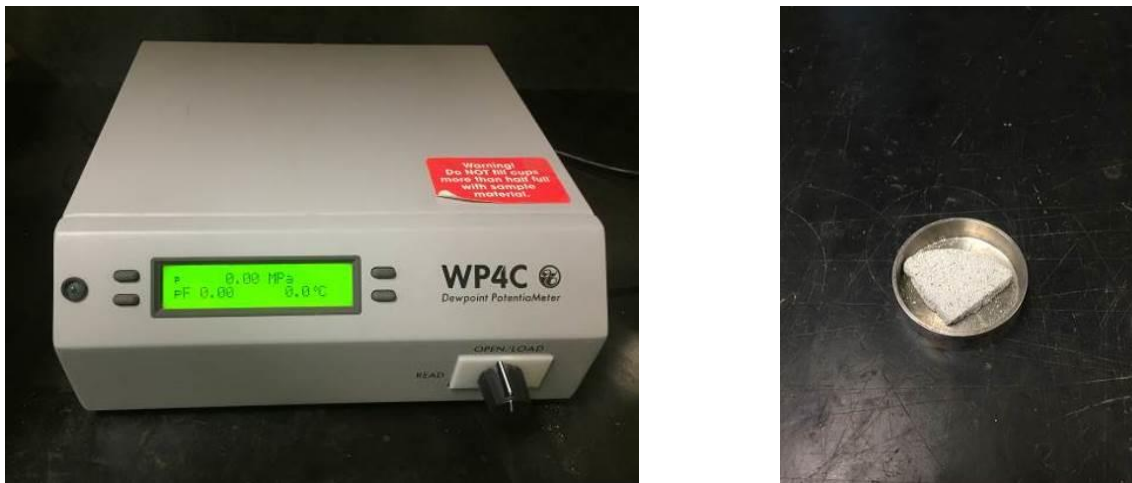


Figure 7.7: WP4 Device Used to Measure the SWCC in the High-Suction Range and Example of Specimen Used in Testing.

The data generated using the GCTS and WP4 devices are combined to generate a plot of saturation versus capillary pressure (actual values are negative pressure (suction) but are expressed as positive values). These data were then fitted using the van Genuchten curve fitting model to generate SWCC curves using fitting parameters provided in Table 7.2. These curves are defined by Equations 7.3 and 7.4:

$$P_c = (1 / \alpha) (S_{ec}^{-1/m} - 1)^{1/n} \quad (7.3)$$

$$S_{ec} = (S_i - S_{lr}) / (1 - S_{lr}) \quad (7.4)$$

where:

P_c	= capillary pressure, Pa;
S_{ec}	= effective saturation (volume ratio);
S_l	= liquid saturation (volume ratio);
S_{lr}	= residual liquid saturation (volume ratio);
α	= van Genuchten fitting parameter (1/Pa);
m	= van Genuchten fitting parameter (unitless); and
n	= van Genuchten fitting parameter (unitless).

It should be noted that since we are dealing with suctions rather than pressures, the equation above generates values that are negative. A summary of the van Genuchten parameters generated to describe the SWCC behaviour of BSM and MX80 bentonite are provided in Section 7.3.3.

7.3.2 SWCC Test Results

SWCC curves were generated for MX80 at about 1.5 Mg/m³ dry density and for BSM at about 1.8 Mg/m³ dry density. A summary of the data and discussion of the meaning of the results are provided below with the full set of data collected as part of SWCC testing provided in Appendix G.

MX80 at ~1.5 Mg/m³ dry density: All permeants

Figure 7.8 shows the plots of the average saturation versus capillary pressure for MX80 materials prepared to an initial dry density of ~1.5 Mg/m³. These graphs indicate that the air-entry value for materials containing each of the three permeants was greater than 1500 kPa, and that insignificant desaturation occurred below this suction.

Deionized Water

In the DW specimens all the materials tested had an initial degree of saturation of >95%. While the data suggests either a slight change in degree of saturation at the low capillary pressures (i.e. increase or decrease in saturation), this is more to do with the combination of specimen volume change and fluid flow into the specimen (i.e. specimens swelling under the 500 kPa vertical stress) and minute measurement inaccuracies. This very slight appearance of an increase or decrease in saturation would not be considered significant.

The DW specimens show a shallower pressure-saturation curve than was observed for the high salinity SR-L and SR-Sh systems. This may be attributable to the electrochemical interactions on the particle level. In a low TDS system, there is a considerable level of water structuring and adsorption associated with the surface of the clay particles. This “bound” or “adsorbed” water will be more strongly held within the specimen than would be the case in a material or system where there is little or no bound water (e.g. sand or non-smectite systems). The result of the bound water would be a more gradual desaturation behaviour, as was observed in these tests.

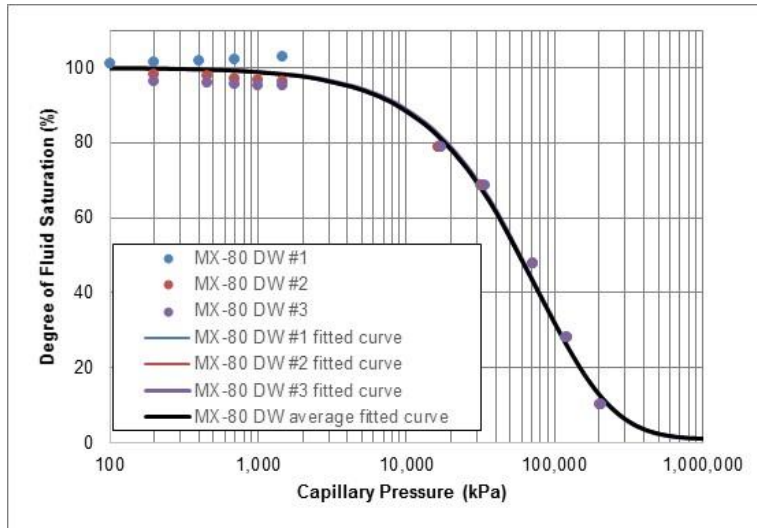
SR-L and SR-Sh

The air-entry values for the brine (SR-L and SR-Sh) systems seem to be consistently higher than were observed for the DW specimens for all six tests completed in this study. This may in part be attributable to the much higher viscosity of the brine solutions relative to DW. There may also be a different pore structure in the DW and brine systems, resulting in differences in the air-entry and desaturation behaviour of DW and brine systems.

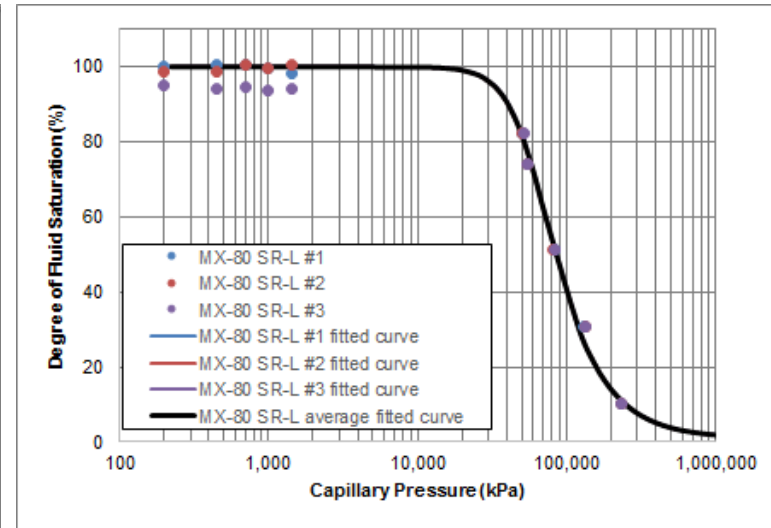
Once desaturation of the specimen begins, the slope of the capillary pressure – saturation plot is much steeper than for the fresh water systems, indicative of a more rapid loss of water for a given capillary pressure. This can also be expressed as a lower suction being present in the saline systems than in the freshwater ones (suction \approx capillary pressure). An explanation of the observed more rapid loss of fluid with increasing capillary pressure is associated with the electrochemical conditions within the soil-fluid system. The brine fluid interacts with the smectite (e.g. montmorillonite) minerals, resulting in reduction in the electrochemical bonding situation (less adsorbed (bonded) water). The result of this interaction is that the pore fluid may be more easily pushed out of the specimens, even though the brine solution will be more viscous than bulk, low salinity water. Other as-yet undetermined factors may also contribute to the difference in the behaviour of low salinity and high salinity systems.

Figure 7.9 shows the curves generated for the MX80 specimens in terms of capillary pressure versus fluid saturation (axes reversed from Figure 7.8). This plot shows the very similar behaviour of the brine pore fluid systems and the less abrupt desaturation behaviour of the DW system. Once fluid saturation falls below $\sim 40\%$ the suction-moisture behaviour is similar.

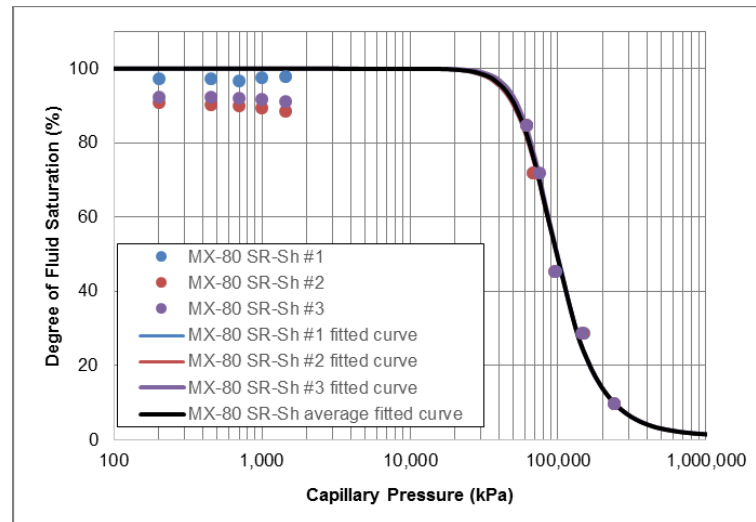
Figure 7.10 shows the plots of the average saturation versus capillary pressure for BSM materials prepared to an initial dry density of $\sim 1.8 \text{ Mg/m}^3$ using DW, CR10, SR-L and SR-Sh as pore fluid. As with the MX80 materials, these data indicate that the air-entry values for each of these materials was greater than 1500 kPa.



MX80 DW



MX80 SR-L



MX80 SR-Sh

Figure 7.8: SWCC Curves for MX80 Bentonite at 1.5 Mg/m³ Dry Density

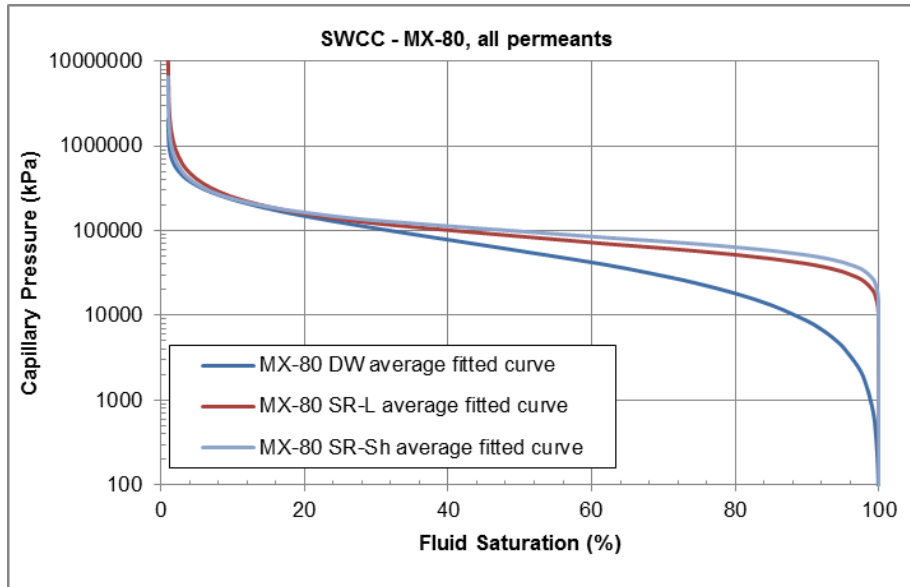


Figure 7.9: Comparison of Saturation – Capillary Pressure Behaviour of MX80

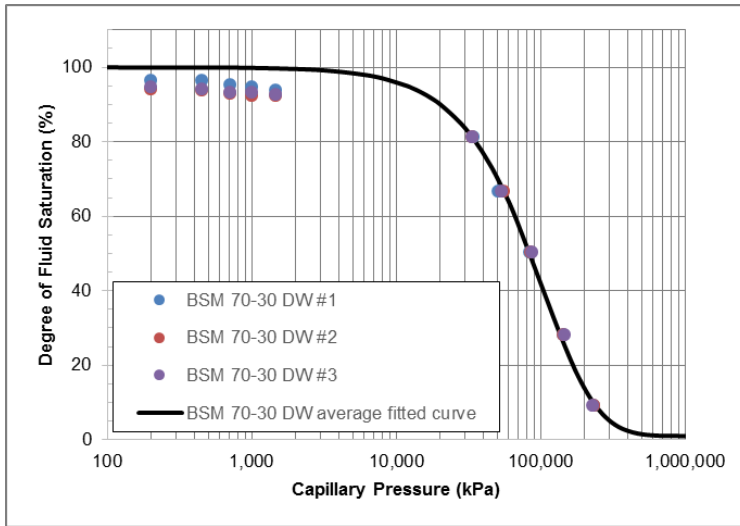
Deionized Water and CR10 Solution

As was observed for the MX80 specimens, the DW and CR10 specimens show a very slight change in degree of saturation in the low capillary pressure range. These would also be considered insignificant. The as-built degree of water saturation in these specimens was 94-97% (DW) and >98% (CR10). As with the MX80 systems, the low-salinity BSM material exhibits a shallower slope than observed for materials containing a brine pore fluid. The data generated by the replicate tests shows an excellent degree of reproducibility, providing confidence in the ability of this test method to generate consistent results.

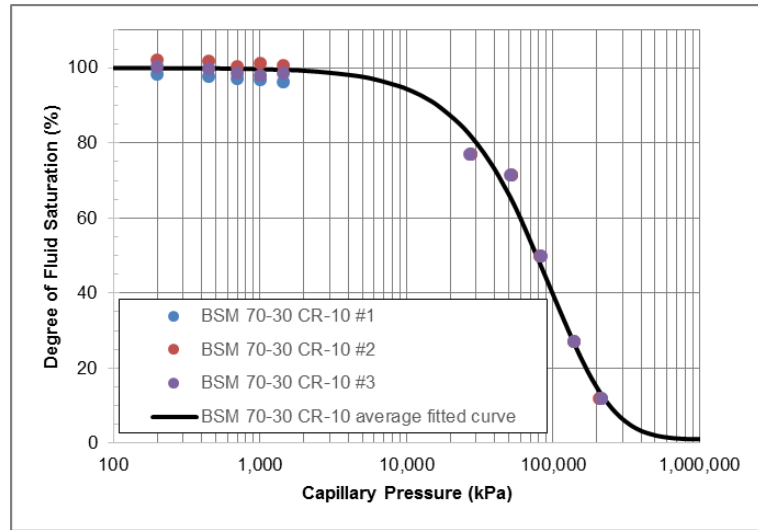
SR-L and SR-Sh Brine Solutions

The BSM materials constructed using brine pore fluids (SR-L and SR-Sh) had initial degrees of saturation of 96-98% and 92-98% respectively. Again, these degrees of initial saturation are considered to be sufficient to ensure that these specimens behave as saturated materials with respect to their subsequent suction-moisture evolution. As with the DW materials, the brine systems showed a slight tendency to have higher degree of saturation at lower applied capillary pressures but as for the low salinity specimens this represented less than a 2% change and is not significant with respect to defining the SWCC.

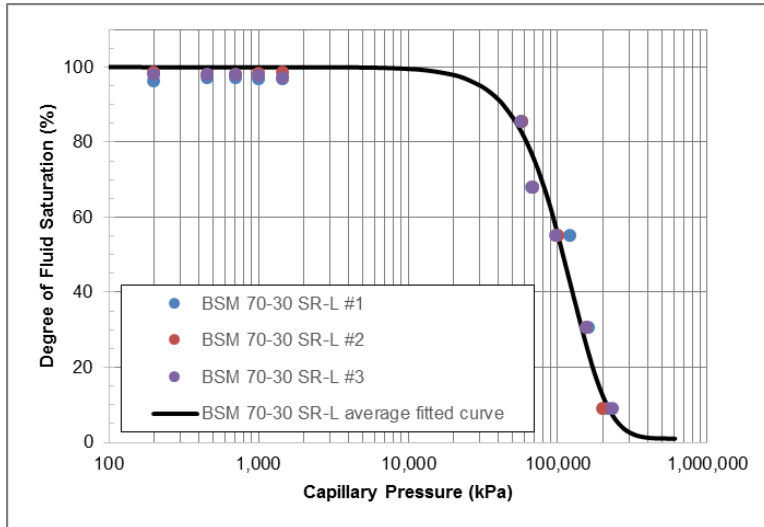
Figure 7.11 presents the results of the capillary pressure – saturation testing and again shows the excellent reproducibility of the test results. The capillary pressure – saturation plots for the brine systems show a much steeper desaturation curve than for the low salinity systems, again this is consistent with what was observed for the MX80 systems. The data also shows very consistent behaviour for the low- and high- TDS systems.



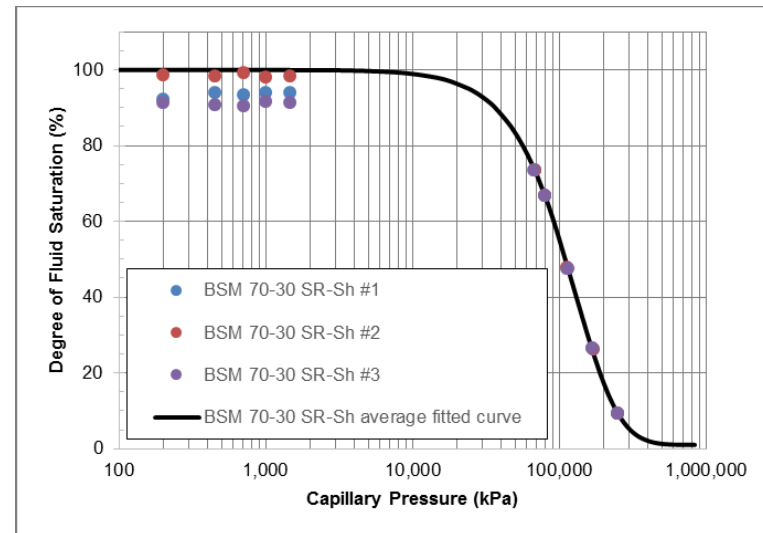
BSM – DW



BSM – CR10



BSM – SR-L



BSM – SR-Sh

Figure 7.10: SWCC Curves for BSM Material at $\sim 1.8 \text{ Mg/m}^3$ Dry Density

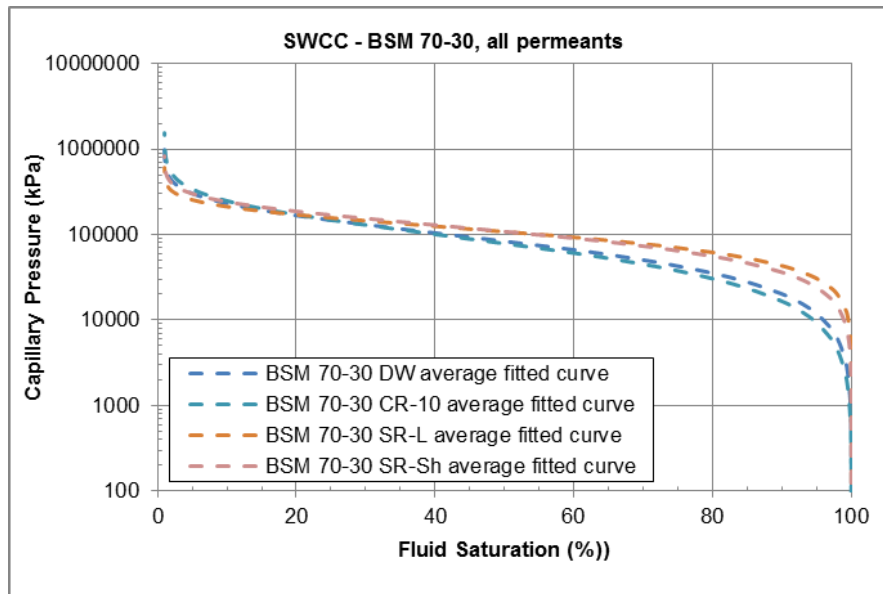


Figure 7.11: Comparison of Saturation – Capillary Pressure Behaviour of BSM

7.3.3 Comparison of SWCC Behavior of MX80 and BSM Materials

The SWCC curves for MX80 and BSM are shown in Figure 7.12 and show that the suction-moisture behaviour of MX80 and BSM are discernibly different. The freshwater bentonite-only system shows a notably more gradual loss of moisture with increasing capillary pressure (suction) than is evident in the BSM system. The brine systems all show similar SWCC curves.

As discussed previously:

1. The likely reason for the differences in the SWCC behaviour of the MX80 and BSM materials at low salinity is related to differences in the pore-size and pore-size distribution in these materials.
2. The reason for the differences in the behaviour of saline systems (and similar behaviour for MX80 and BSM systems at high salinity) can be attributed to a combination of pore-structure and electro-chemical interactions between the pore fluid and the swelling clay components. As well salt solution will increasingly resist loss of moisture as drying occurs

The data generated in the course of this testing have all be fitted using the van Genuchten curve fitting function provided as Equations 7.2 and 7.3. The fitting functions are forced to the 100% saturation line for the range of capillary pressures where no desaturation was observed (typically saturation >90% and capillary pressure below ~1500 kPa). The data plots clearly showed that the specimens were not able to lose moisture at low pressure and saturation levels above that level. This behavior can be observed in each of Figures 7.8 through Figure 7.12. The fitting parameters used to generate the van Genuchten – type curves for the SWCC are provided in Table 7.2 The parameter values derived by Barone et al. (2014) differ from those of the current study. This is attributed to differences in: the densities of the materials tests, the porefluid salinity, and perhaps also the texture and mineralogical composition of the bentonite used and the number of data points available for use in numerical analysis. These difference

result in slight changes in the fitting parameter values but the curve shape and values generated are very similar.

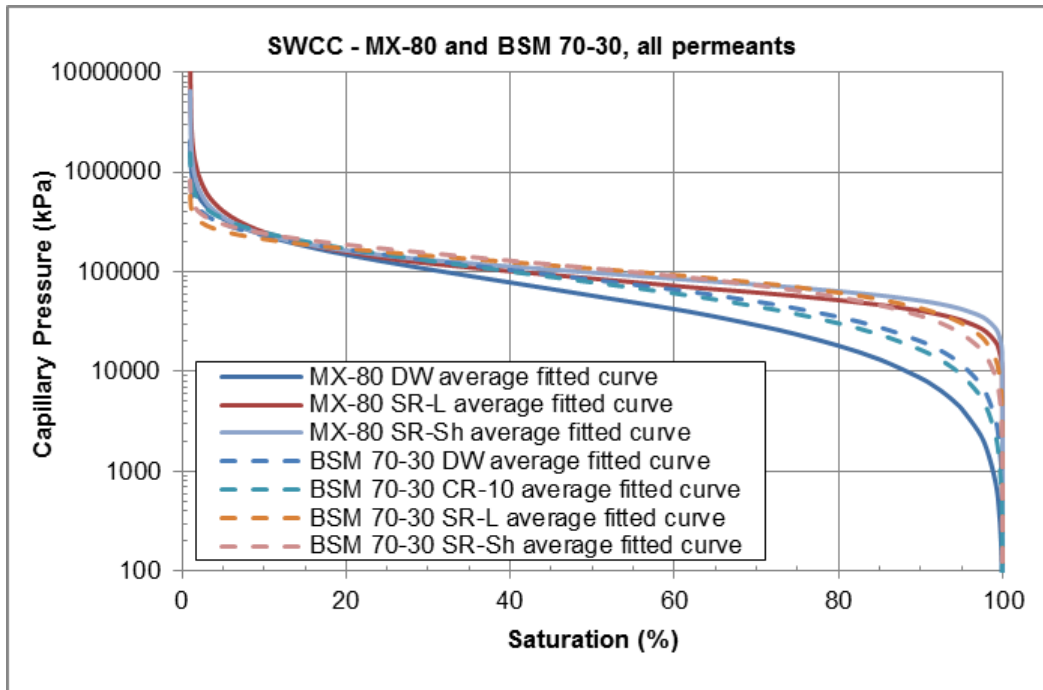


Figure 7.12: Comparison of SWCCs of BSM and MX80

Table 7.2: Fitting Parameters Used to Generate SWCCs for MX80 and BSM.

Current Study	m	n	α (1/Pa)	S_{ir}
MX80 at $\sim 1.5 \text{ Mg/m}^3$				
DW	4.66	1.02	2.91E-9	0.01
SR-L	0.47	3.57	1.68E-8	0.01
SR-Sh	0.52	3.99	1.35E-8	0.01
BSM 70:30 at $\sim 1.8 \text{ Mg/m}^3$				
DW	5.90	1.36	2.60E-9	0.01
CR10	4.37	1.25	3.18E-9	0.01
SR-L	4.70	2.11	3.87E-9	0.01
SR-Sh	4.90	1.77	3.15E-9	0.01
Barone et al. (2014) for 70:30 MX80:Sand at $\sim 1.8 \text{ Mg/m}^3$				
DI water	0.84	0.95	2.5E-8	0.01
CR10	0.80	1.10	2.0E-8	0.01
SR160	0.83	1.1	1.7E-8	0.01
SR270	1.00	1.40	1.2E-8	0.01

7.4 AIR PERMEABILITY (AP) MEASUREMENTS

7.4.1 Background and Testing Method

Air permeability, K (AP used for K in text discussions in order to make clearly differentiate between air and water permeability as both have their values presented in m^2) were made on unsaturated specimens of the reference clay using the specified pore fluids. Testing was done in triplicate using the device shown in Figure 7.13. It should be noted that the convention for expressing air permeability uses K (in m^2) and an also used value, air conductivity (expressed as AC in this report), uses the symbol k (expressed in m/s).

Specimens prepared to pre-defined degrees of saturation and dry density were installed in triaxial cells and confined through application of a fluid pressure on its perimeter. The use of specimens of this type provided a means of accurately knowing the degree of saturation and also provides a material of more uniform degree of saturation than can be accomplished through either saturation or desaturation via the specimen ends. This technique also allows for a more conventional confining pressure to be used on the perimeter of the specimen. Any other technique would require cell pressures capable of restraining the swelling pressure of the specimen, a technically difficult and extremely time intensive process and would result in heterogeneous specimen density and saturation conditions. Once the pre-built specimens were installed and confined using the external cell pressure, the specimen was exposed to a higher gas pressure at one end than the other and the rate of gas movement into the specimen is monitored. Through measurement of gas inflow into the specimen it is possible to calculate the gas permeability, providing a single point in the permeability-saturation curve for the material and pore fluid being examined. To develop a representative curve for use in defining the saturation-permeability relationship, a minimum of five measurements at substantially different degrees of saturation (10-80%) were completed. To confirm the reproducibility of the results, each series of tests were repeated three times.



Figure 7.13: Specimen Installed in Triaxial Cell for Air Permeability Testing and Test Apparatus in Operation

The tests completed provide AP values at a degree of saturation from 80% to 10%, corresponding to approximately optimum water content conditions down to near the residual degree of saturation. The data were then fitted to a two-phase flow characterisation curve using the Van Genuchten (1980) - type relationship to provide values extending beyond the range of saturation examined. Air conductivity (AC), expressed in m/s were also determined from these tests. Air conductivity is derived by simple multiplication of the AP value by 6.40 E+05.

The fitted air permeability curves have been generated using the van Genuchten-Mualem-Luckner model. These curves can be given by:

$$k_{rg} = (1 - S_{ek})^{1/3} (1 - S_{ek}^{1/m})^{2m} \quad (7.5)$$

$$S_{ek} = (S_l - S_{lr}) / (1 - S_{lr} - S_{gr}) \quad (7.6)$$

where:

- k_{rg} = gas phase relative permeability (ratio);
- k_g = gas phase permeability (m²);
- S_{ek} = effective saturation (volume ratio);
- S_l = liquid saturation (volume ratio);
- S_{lr} = residual liquid saturation (volume ratio);
- S_{gr} = residual gas saturation (volume ratio); and
- m = van Genuchten fitting parameter (unitless).

The gas permeability can be calculated by multiplication with the relative permeability (k_{rg}):

$$k_g = k_{rg} * k \quad (7.7)$$

7.4.2 Air Permeability Test Results

Tests were completed on seven different systems. Two soil materials (MX80 at 1.5 Mg/m³ dry density and a 70:30 MX80:sand blend at approximately 1.8 Mg/m³ dry density) were used and these were prepared using four different pore fluids.(no tests done using the CR10 solution and MX80 as per project instructions).

The AP and AC test results for each test are presented in Figure 7.14 through 7.17. The replicate tests produced very comparable results, providing confidence in the reproducibility of the results with consistent method used. The AP data shows the expected pattern of decreasing AP with increasing degree of liquid saturation and a trend towards rapidly decreasing permeability as the saturation increases beyond ~75%. This is consistent with the expected change from interconnected air voids to isolated air pockets above this fluid saturation level. The AP and AC data for each test are provided in Appendix H.

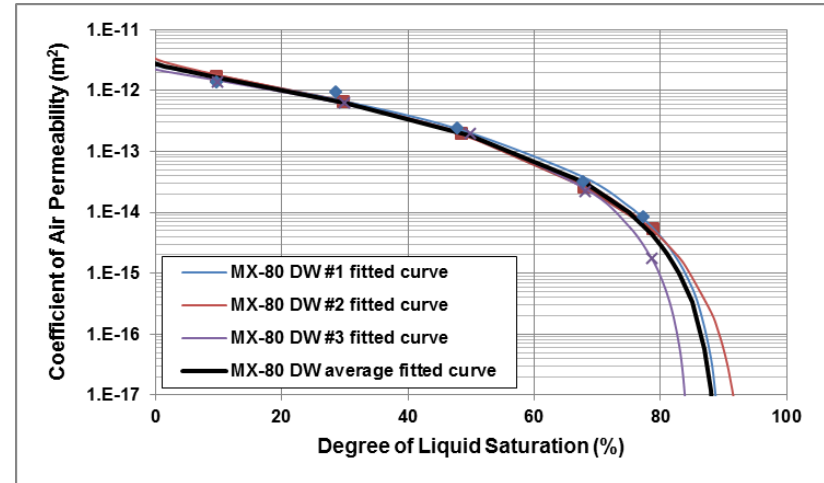
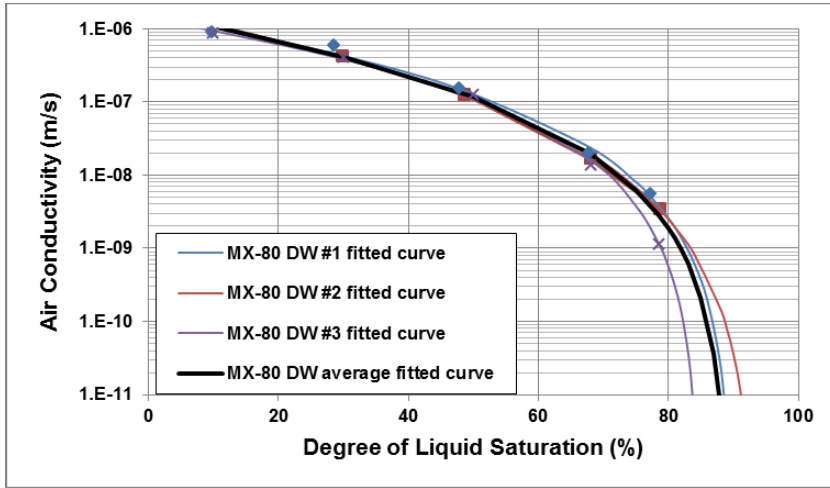
The AP tests completed as part of the current materials properties testing activities provided triplicate measurements of AP for each of the materials and pore fluids of interest to NWMO. The data showed a very high degree of reproducibility and very limited range of data scatter. The greatest degree of data scatter (typically ~ 0.5 order of magnitude from mean), was associated with the highest degrees of water saturation examined (approximately 80%) and reflects the inherent challenges of measuring very low air permeabilities (<10⁻¹⁵ m²) in systems having little to no interconnected air voids. The degree of variability in the replicate tests is summarized in the Figures and Tables provided in Appendix H.

Figure 7.18 presents the best-fit (using Van Genuchten fitting functions), air permeability and air conductivity plots for each of the materials and pore fluids. These plots both show the rapid decrease in the ability of air to move through these materials once degree of fluid saturation increases beyond approximately 75%. As noted previously, 70 to 75% water saturation is the point at which the air-filled pores begin to become discontinuous and air movement through the soil becomes more and more restricted as saturation increases.

The behaviour of the two materials (MX80 and MX80-sand mix) is clearly different with the $\sim 1.5 \text{ Mg/m}^3$ dry density MX80 having an air permeability at least one order of magnitude higher than the $\sim 1.8 \text{ Mg/m}^3$ 70:30 MX80:Sand mixture. The same trend is evident for air conductivity. This offset in values between the two materials is attributable to the different porosities (and perhaps pore size distribution) of bentonite-only versus bentonite-sand systems. The MX80 material has a porosity (volume voids / total volume) of ~ 0.45 while the MX80-sand material has a porosity of ~ 0.35 . This difference could result in easier air movement through the MX80 (where more pore space exists and hence a greater potential to have interconnected air-filled pores) for a given degree of saturation.

The data also indicates a slight change in the AP and AC with changing fluid, the values are slightly lower on average as pore fluid TDS increases. This could be attributed to the changes in fluid viscosity in the pore spaces. The higher the TDS, the more viscous is the fluid, potentially resulting in greater fluid resistance to air intrusion into and movement through fluid-filled pores.

MX80-DW



MX80-SR-L

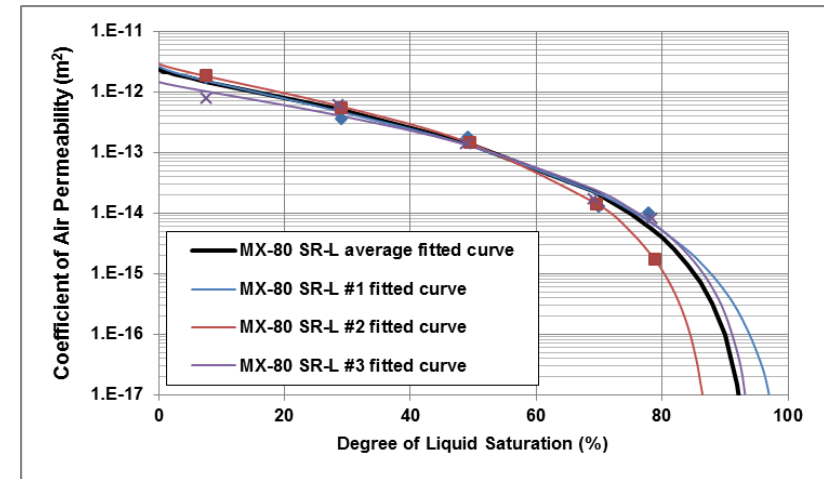
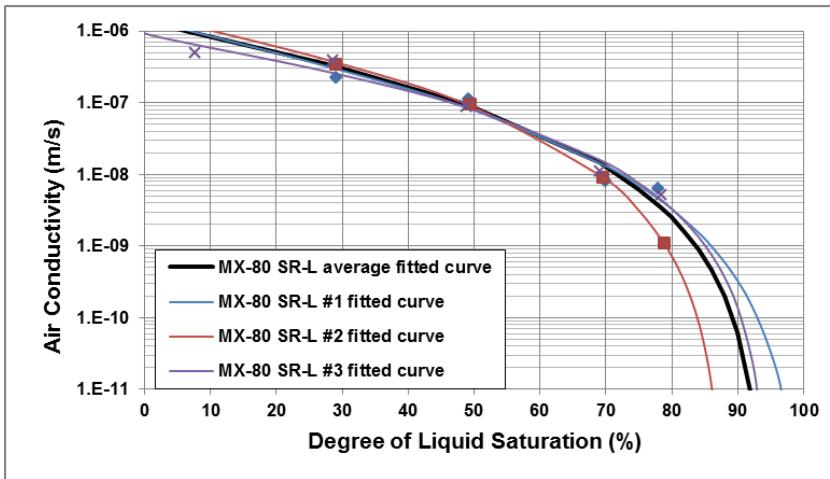


Figure 7.14: Air Conductivity and Air Permeability of MX80 Bentonite at ~1.5 Mg/m³ Dry Density (DW and SR-L Solutions)

MX80-SR-SH

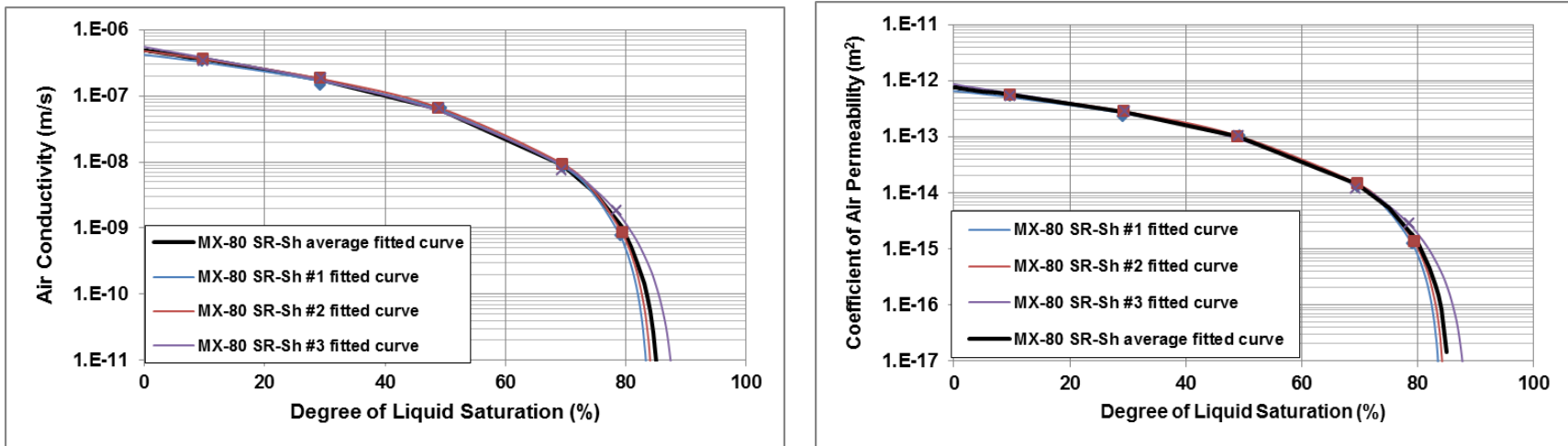
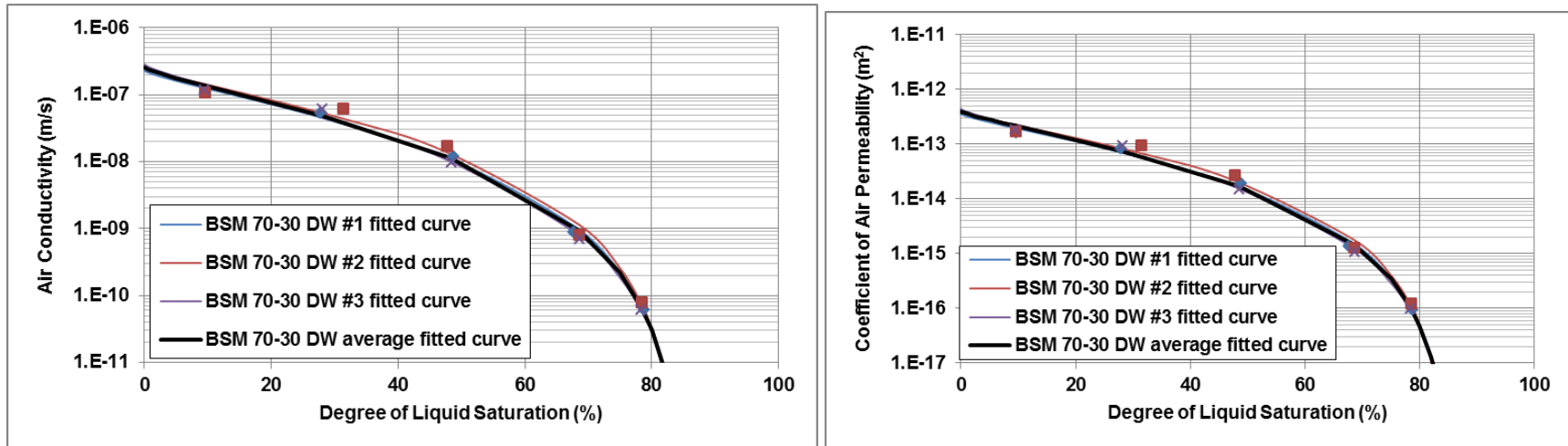


Figure 7.15: Air Conductivity and Air Permeability of MX80 Bentonite at ~1.5 Mg/m³ Dry Density (SR-Sh Solution)

BSB 70-30 DW



BSB 70-30 CR10

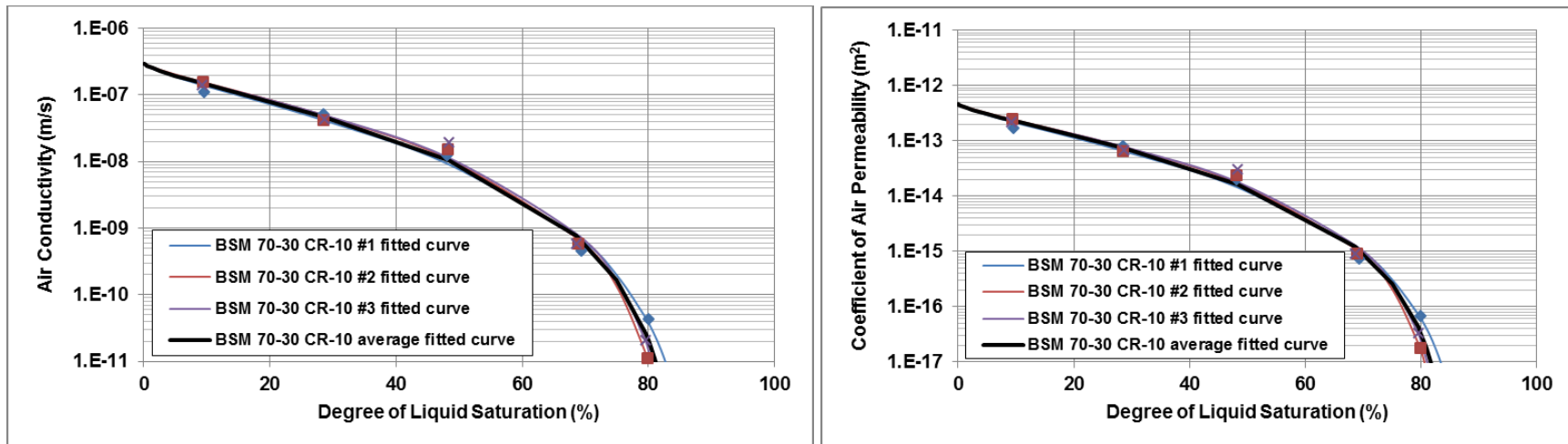
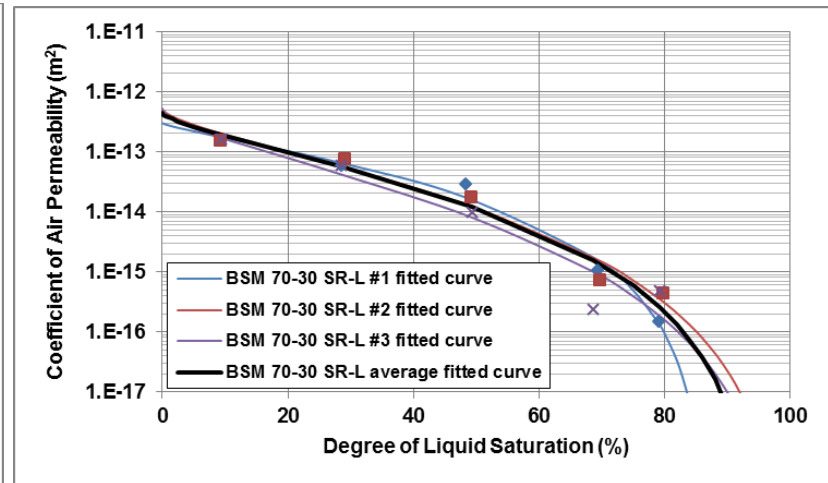
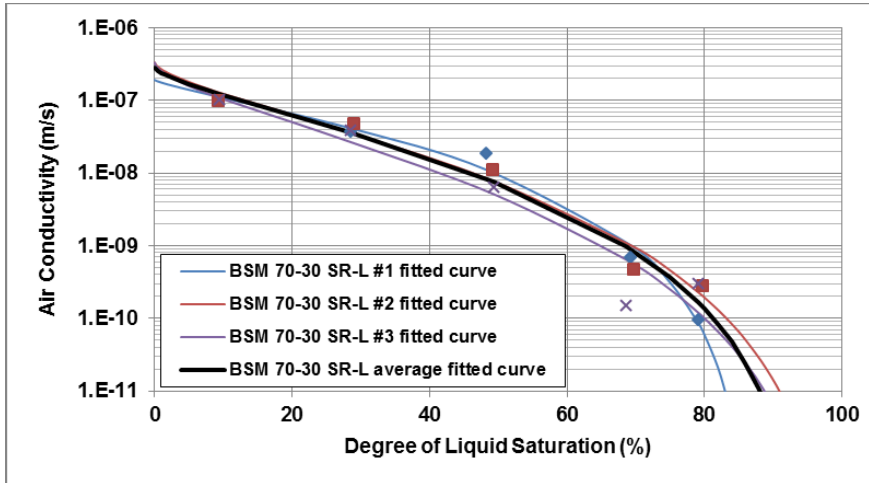


Figure 7.16: Air Conductivity and Air Permeability of 70:30 MX80:Sand at ~1.8 Mg/m³ Dry Density (DW and CR10 Solutions)

BSB 70-30 SR-L



BSB 70-30 SR-Sh

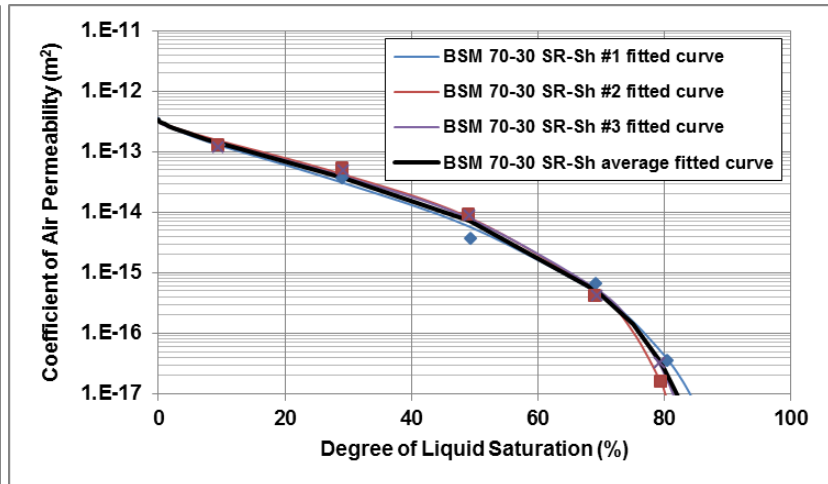
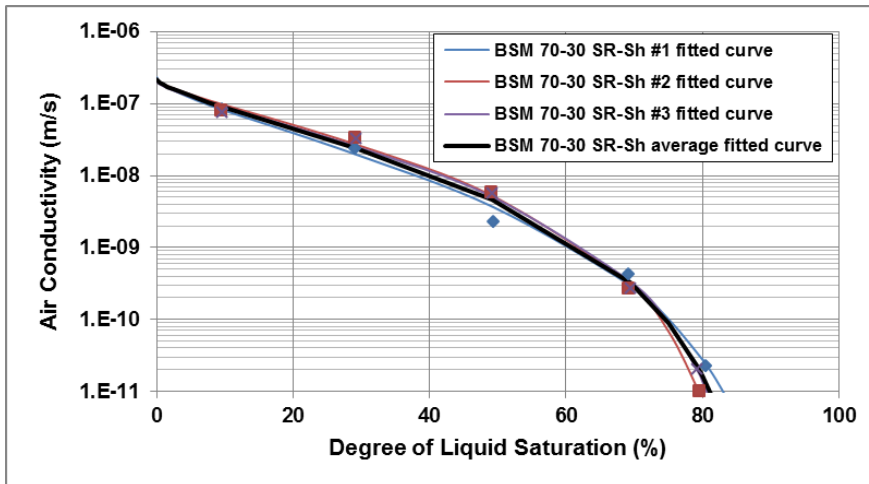


Figure 7.17: Air Conductivity and Air Permeability of 70:30 MX80:Sand at ~1.8 Mg/m³ Dry Density (SR-L & SR-Sh Solutions)

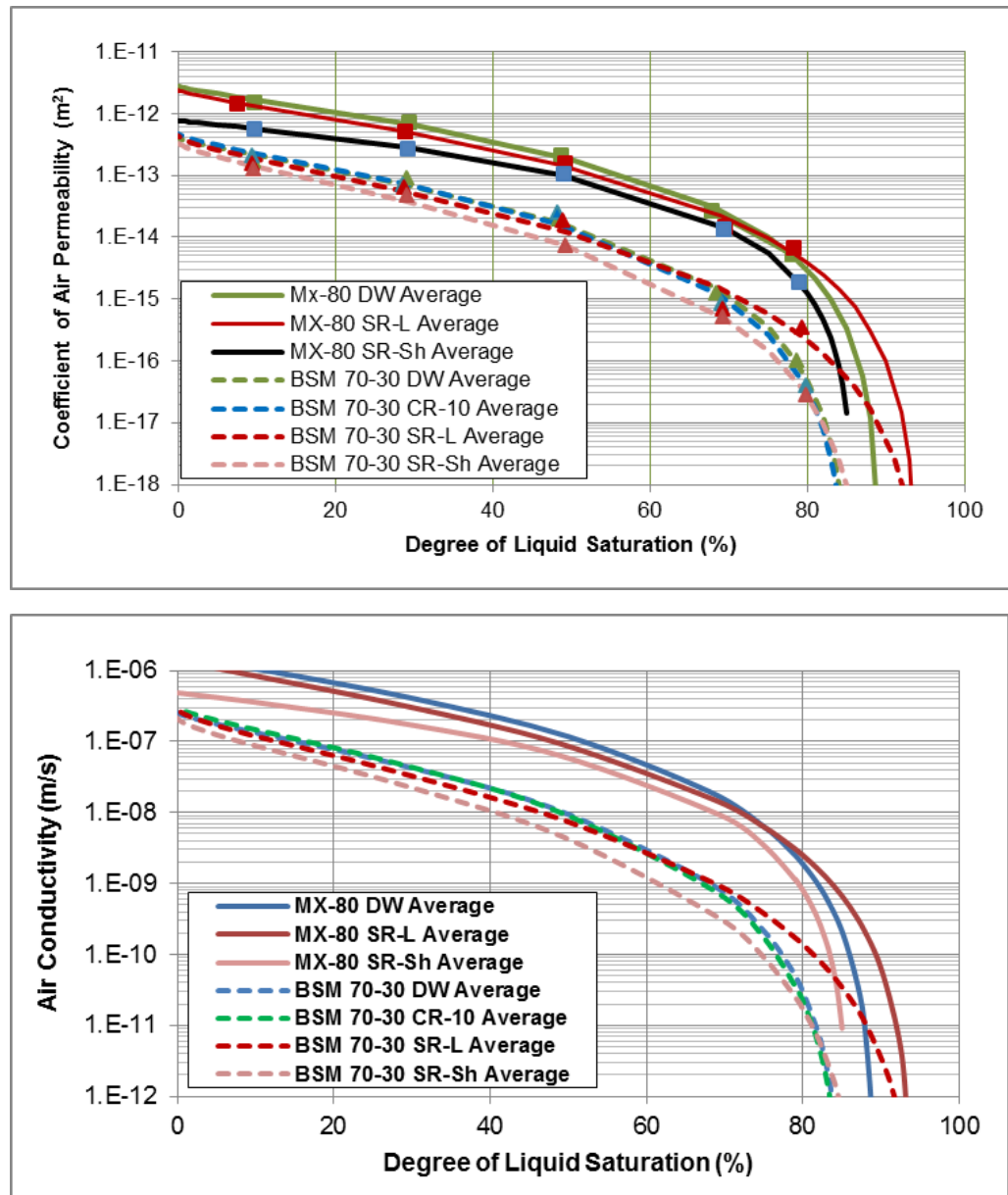


Figure 7.18: Air Conductivity and Air Permeability of MX80 and BSM

7.4.3 Summary of Air Permeability Testing

For the purposes of comparison with other measurements, the air conductivity data presented by Barone et al. (2014) has been plotted with the trendlines for the current study in Figure 7.19 and included in the fitting parameters generated and provided in Table 7.3. These tests were conducted using MX80 bentonite compacted to a dry density of between 1.7 and 1.85 Mg/m³ using DW, CR10 and saline solutions SR160 (~160 g/L TDS) and SR270 (~270 g/L TDS).

These data show very comparable results to those of the current study compacted to similar dry density and having very similar porosities (current ~33-35% and ~27-34% for Barone et al. (2014)). The data of Barone et al. (2014) for the same 70:30 BSM also exhibited similar slight

decrease in observed AC values with increasing pore fluid salinity. From these data it can be concluded that the AC and AP of MX80 and the 70:30 MX80:sand materials is determined by the porosity (dry density) and degree of saturation of the systems. The clay:sand ratio and pore fluid TDS of these materials play secondary roles in determining the movement of air. As noted previously for the SWCC curve fits, the parameter values reported in Barone et al. (2014) differ slightly from those of the current study, again this is attributed to differences in the number and range of data values available for use in curve fittings as well a differences in the materials used. The result are slightly different curve fitting equations but the results are comparable.

Table 7.3: Fitting Parameters Used to Derive Air Permeability Trendlines

Current Study	m	S_{gr}	K_a (m/s)	S_{ir}
MX80 at ~1.5 Mg/m ³				
DW	1.24	0.11	1.759E-06	0
SR-L	1.34	0.06	1.513E-06	0
SR-Sh	1.02	0.14	4.872E-07	0
BSM 70:30 at ~1.8 Mg/m ³				
DW	1.34	0.14	2.557E-07	0
CR10	1.40	0.15	2.97E-07	0
SR-L	1.57	0.04	2.856E-07	0
SR-Sh	1.54	0.12	2.181E-07	0
Barone et al. (2014) for BSM 70:30 at 1.75-1.85 Mg/m ³				
DI water	1.19	0.01	1.0E-07	0
CR10	1.30	0.01	1.4E-07	0
SR160	1.08	0.10	5.0E-08	0
SR270	0.90	0.10	3.0E-08	0

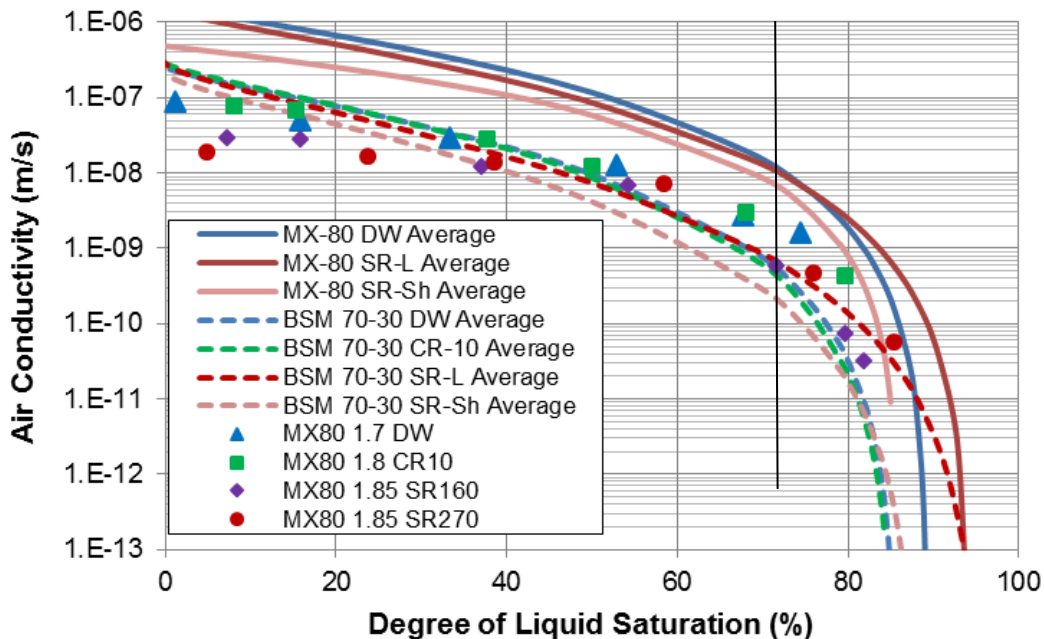


Figure 7.19: Comparison of Current Air Conductivity Results to Barone et al. (2014)
(Barone et al. (2014) are shown as solid symbols, current tests as dashed and solid lines)

7.5 SWCC and Air Conductivity Results Summary

Summaries of the air conductivity results are provided in Figures 7.19 through 7.21 and detailed data is provided in Appendix H.

Key observations from the Shrinkage, SWCC and AC measurements are as follows:

- Figure 7.19 shows the same data as in Figure 7.20, but Figure 7.19 includes previously measured (Barone et al. 2014), AC versus saturation data for BSM compacted to $\sim 1.8 \text{ Mg/m}^3$ (current study MX80 also has dry density of $\sim 1.8 \text{ Mg/m}^3$). The data shows good comparability to current study.
- Figure 7.20 shows the AC results based on degree of fluid saturation (volume of liquid/total volume of non-solids). These results indicate that the bentonite-sand materials have a lower air conductivity than the MX80 clay, and that materials with high TDS have a slightly lower air permeability than observed for low TDS systems.

In Figure 7.20, a vertical line has been drawn at the 75% degree of saturation mark for reference purposes. It appears that at approximately this saturation state, the soil pores containing air become discontinuous and the ability of air to move through the soil becomes increasingly restricted. However, it should also be noted that for saturations less than $\sim 75\%$, the difference in air permeability between high TDS and low TDS materials of the same composition, was less than about half order of magnitude. As noted previously, if air permeability values (m^2) are needed they can be derived by dividing AC (m/s) by $6.40 \text{ E}+05$.

Figure 7.21 shows the air conductivity results based on capillary pressure and incorporate the results of the SWCC's (which were based on degree of saturation). In Figure 7.21 it can be observed that:

- at low ($< \sim 20\%$) saturation, where the suction is $> \sim 200,000 \text{ kPa}$, the air conductivity of MX80 at $\sim 1.5 \text{ Mg/m}^3$ dry density is higher by as much as an order of magnitude than for the BSM at $\sim 1.8 \text{ Mg/m}^3$. This might be attributable to the greater drying shrinkage potential for the clay-only systems (possibly resulting in more microcracks as the result of desiccation) or pore size distribution differences in the two materials.
- The void ratio of the two systems is also very different (~ 0.81 for MX80 at 1.5 Mg/m^3 versus ~ 0.54 for BSM at 1.8 Mg/m^3) and so shrinkage and AC at similar degrees of fluid saturation would be expected to be different. (BSM has lower e , lower AC and lower shrinkage than MX80).
- The AC of specimens having a high TDS pore fluid are lower than for similar materials having a low TDS pore fluid (particularly for systems having low suction (higher degrees of saturation)).
- The MX80 materials show a much greater range in their suction-moisture and suction-air conductivity properties as the result of pore fluid TDS conditions than do BSM materials.

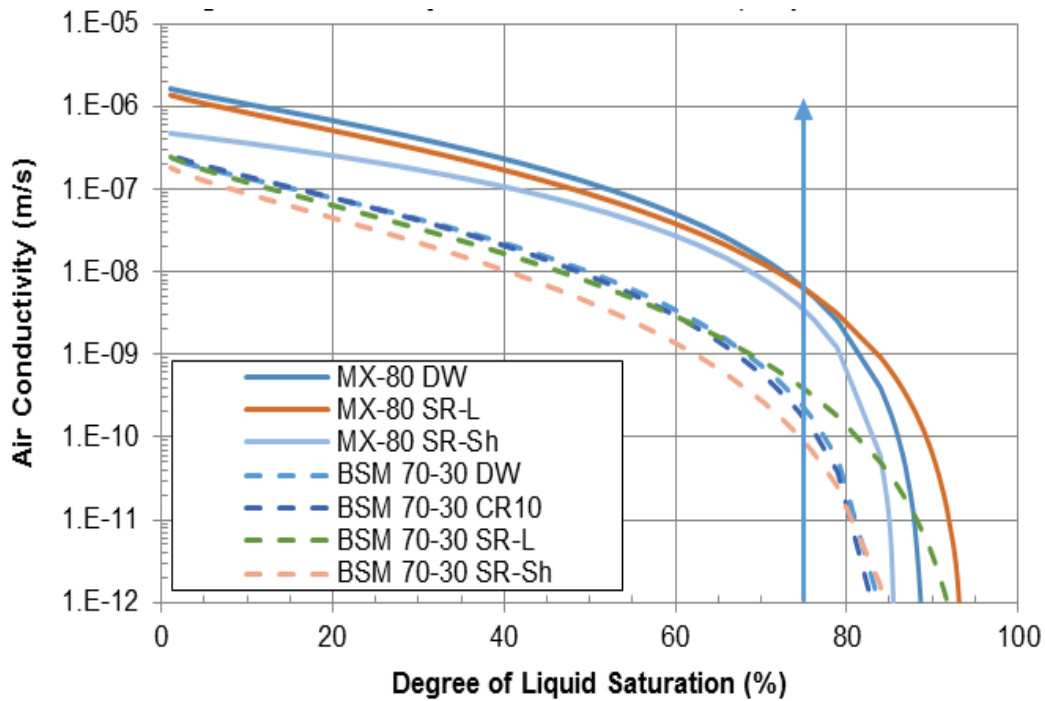


Figure 7.20: Summary of Fitted Air Permeability Results Based on Water Saturation
(using average of 3 readings)

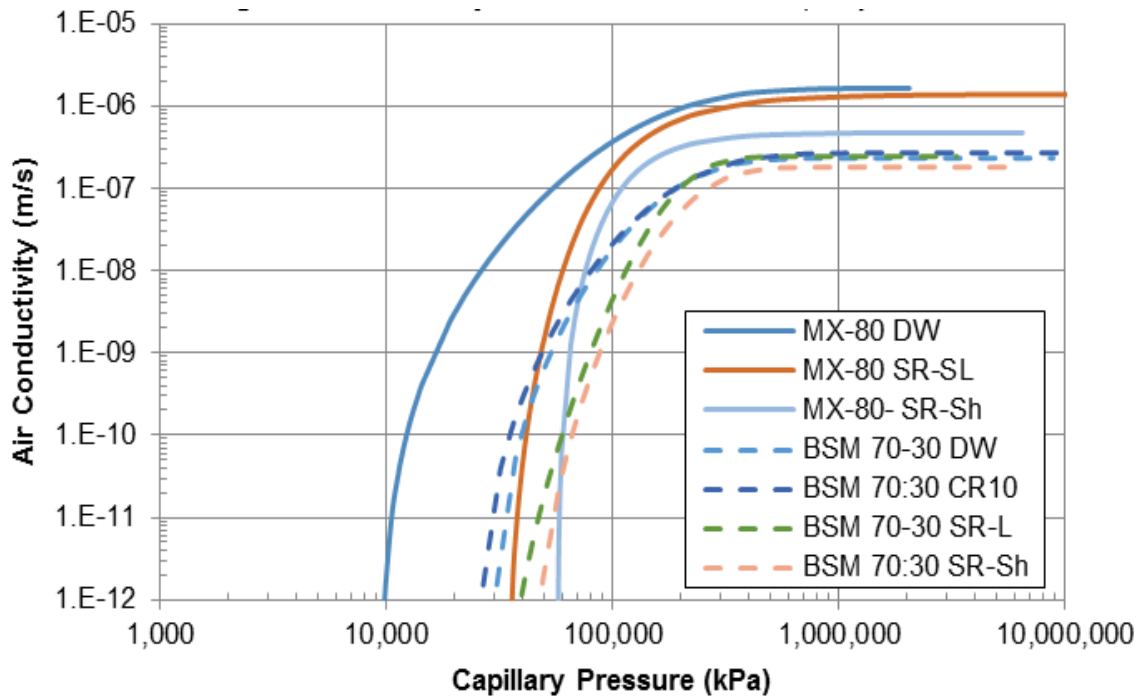


Figure 7.21: Summary of Fitted Air Permeability Results Based on Capillary Pressure
(using average of three readings)

8. MECHANICAL PROPERTIES TESTING

8.1 BACKGROUND

As-fabricated samples of the reference clay seal material prepared using the four different reference water solutions were tested to determine their mechanical properties. These parameters are of importance with respect to prediction of the ability of bentonite and bentonite-sand materials to support a UFC and also predict how they will deform under conditions of higher compressive load.

The parameters measured included:

- Bulk Modulus (K) and elastic-plastic parameters (κ and λ). Isotropic triaxial consolidation tests are used to determine the Bulk Modulus (K) and the elastic-plastic parameters κ and λ . These tests traditionally require saturation at a cell pressure equal to the swelling pressure to prevent swelling from the as-fabricated condition. Following saturation, the specimens are incrementally loaded (similar to an oedometer test) to define the p' , V curve;
- Shear Modulus (G) was determined using isotropically consolidated undrained (CI \bar{U}) triaxial tests. These tests were done at the Royal Military College (RMC) using the high pressure systems at RMC designed specifically for testing bentonite-based materials with high swelling pressures.
- Young's Modulus (E) was determined using isotropically consolidated drained (CID) triaxial tests. These tests were completed at both RMC's and Golder's Mississauga testing laboratories.
- One-dimensional (1-D) consolidation tests were used to supplement the elastic and hardening parameters determined above. These 1D tests provide compression indices including volume compressibility (m_v), Swelling Index (C_s) and Compression Index (C_c). The testing matrix associated with this work was provided in Table 1.1. There were two laboratories involved in completion of this work, Royal Military College of Canada (RMC), who as a subcontractor to Golder, undertook testing of specimens that required very high confinement in order to prevent swelling and the Golder Mississauga laboratory. The Golder testing began in early 2015 and was completed in early 2016. Testing at RMC began in the spring of 2015 and was completed in the summer of 2018. Completion of testing at RMC was delayed as the result of unexpectedly long times needed to achieve specimen saturation before compression testing could be undertaken.

8.2 ISOTROPIC TRIAXIAL CONSOLIDATION TESTS (K, κ , λ)

8.2.1 Isotropic Consolidation Test Setup

Isotropic triaxial consolidation tests were performed to determine the Bulk Modulus (K) and the elastic-plastic parameters (κ and λ). As per the methodology of Blatz et al. (2008), each specimen was built into the triaxial systems at their prescribed composition, density and pore fluid. Specimens were manufactured to nominal dimensions of 50 mm diameter and 100 mm length at as high an initial water content as possible ($S_r \sim 95\%$) and then sealing the sample in a latex membrane with a saturated filter paper and saturated porous stone placed on the top and bottom of the sample. The first phase was saturation at an effective stress equal to the swelling pressure to prevent swelling from the as-fabricated condition. Saturated specimens were required to measure volume change during incremental loading and shearing later in the test.

Specimens were considered saturated when $B\text{-value} \geq 0.95$ were achieved. Following saturation, specimens were incrementally loaded. Isotropic consolidation tests were split between RMC's and Golder's laboratories to expedite the testing program and utilize the high-pressure systems at RMC for the materials with higher swelling pressures. Due to the extended time required to achieve specimen saturation, only one replicate per condition was performed. At the end of these tests, the specimens were sheared under drained conditions to provide a point on the strength envelope and supplement the Young's Modulus data (Section 8.3). These tests traditionally require saturation at a cell pressure equal to the swelling pressure to prevent swelling from the as-fabricated condition. Traditional testing methods are not however practical when testing bentonite materials such as those investigated in this study. The saturation of the as-built specimens is a slow process (many months to years to achieve saturation under the hydraulic gradients that can be used) and counteracting of swelling by the specimen (to maintain required density) is highly problematic as it requires very careful pressure control as well as a cell capable of applying very high confining pressures (1-10 MPa depending on material type, density and pore fluid TDS). Testing is usually begun on traditional soil materials when a saturation of $>90\%$ is achieved (as determined by B-tests) using a test setup similar to that shown in Figure 8.1.



Figure 8.1: Triaxial Test Apparatus at Golder's Mississauga Laboratory

In order to facilitate timely completion of the desired testing program a modified testing methodology was proposed by Golder and accepted by NWMO prior to initiation of this project. The modification involved the manner in which the test specimens were prepared and testing was initiated in order to avoid the need for extended saturation time and the very high confining pressures otherwise required. The conduct of typical tests involves construction of specimens at their optimal (or higher water content, typically $<80\%$ saturation) and then saturating them in a triaxial cell before isotropic consolidation testing begins. In this testing program the manufactured bentonite and bentonite-sand specimens were built to a known, initial degree of

saturation of $\geq 95\%$ and then were installed in the test cells. The specimens were then confined in the triaxial cell using incrementally increasing confining pressures (similar to an oedometer test) to define the p', V curve. Following completion of consolidation at the highest pressure increment, the specimens were sheared in order to provide a supplemental point on the strength envelope for a given material and pore fluid (Section 8.3).

8.2.2 Isotropic Consolidation Test Results (K , κ and λ)

The Bulk Modulus (K) was determined from the slope of the isotropic consolidation pressure-specific volume curve for each specimen (Figure 8.2). Volume strain was measured for each increment and the Bulk Modulus was calculated using the following equation:

$$K = \Delta p / \Delta \epsilon_v \quad (8-1)$$

The Bulk Modulus results are tabulated in Table 8.1, along with the isotropic stress increment used to determine the parameters. In two cases (i.e. specimens IsoComp-BSM7030-SR-L and IsoComp-BSM7030-SR-Sh), volume control was lost on the final increment and therefore that final point was not used in the determination of K . In general, stiffness decreased with increasing pore fluid salinity for both soil types. The decreased stiffness measured in the triaxial tests is likely due to the suppression of the diffuse double layer, which may result in more free water between particles. As expected, the bentonite-sand mixture is stiffer than 100% bentonite at a given pore fluid salinity. It should be noted that the appropriate value selected for any modelling purposes needs to consider the stress range since the soil may either be in the elastic or plastic region. This is considered further below in the interpretation of κ and λ .

The parameters κ and λ define the slope of the $\ln p', V$ plots for the elastic and plastic regions. The separation between the two was guided by the estimated isotropic preconsolidation pressure suggested by the yield loci presented below. The approximate isotropic preconsolidation pressures for each material are as follows:

- 6,000 kPa for 70:30 Bentonite:Sand Mixture;
- 4,000 kPa for 100% Bentonite; and
- 8,000 kPa for HCB.

These values were used to determine if a given test provided a κ or λ value, as presented in Table 8.1. This interpretation suggests that only two tests were conducted at high enough stresses to interpret λ (those being IsoComp-BSM7030-DW and IsoComp-BSM7030-CR10).

Table 8.1: Bulk Modulus (K) and elastic-plastic parameters (κ and λ)

Isotropic Consolidation Specimen ID	Soil Type	Pore Fluid	As-Built Dry		End of Test		Bulk Modulus, K (MPa)	κ	λ	Isotropic Stress Range (kPa)
			Density (Mg/m^3)	Degree of Saturation	Dry Density (Mg/m^3)					
IsoComp-BSM7030-DW	70:30 BSM	DW	1.82	96%	1.85	189	0.0372*	0.0784	5,500 to 14,500	
IsoComp-BSM7030-CR10	70:30 BSM	CR10	1.81	99%	1.86	308	0.0160*	0.0475	5,500 to 14,500	
IsoComp-BSM7030-SR-L	70:30 BSM	SR-L	1.74	94%	1.79	44.6	0.0384	0.0740*	1,000 to 1,200	
IsoComp-BSM7030-SR-Sh	70:30 BSM	SR-Sh	1.75	92%	1.79	34.4	0.0494	0.0650*	1,000 to 1,200	
IsoComp-Bent100-DW	100% Bentonite	DW	1.54	99%	1.49	53.8	0.104	0.0576*	2,000 to 4,000	
IsoComp-Bent100-SR-L	100% Bentonite	SR-L	1.52	95%	1.52	26	0.075	0.119*	800 to 1,400	
IsoComp-Bent100-SR-Sh	100% Bentonite	SR-Sh	1.58	94%	1.67	14.9	0.121	0.101*	800 to 1,400	

* calculated from 1D consolidation tests

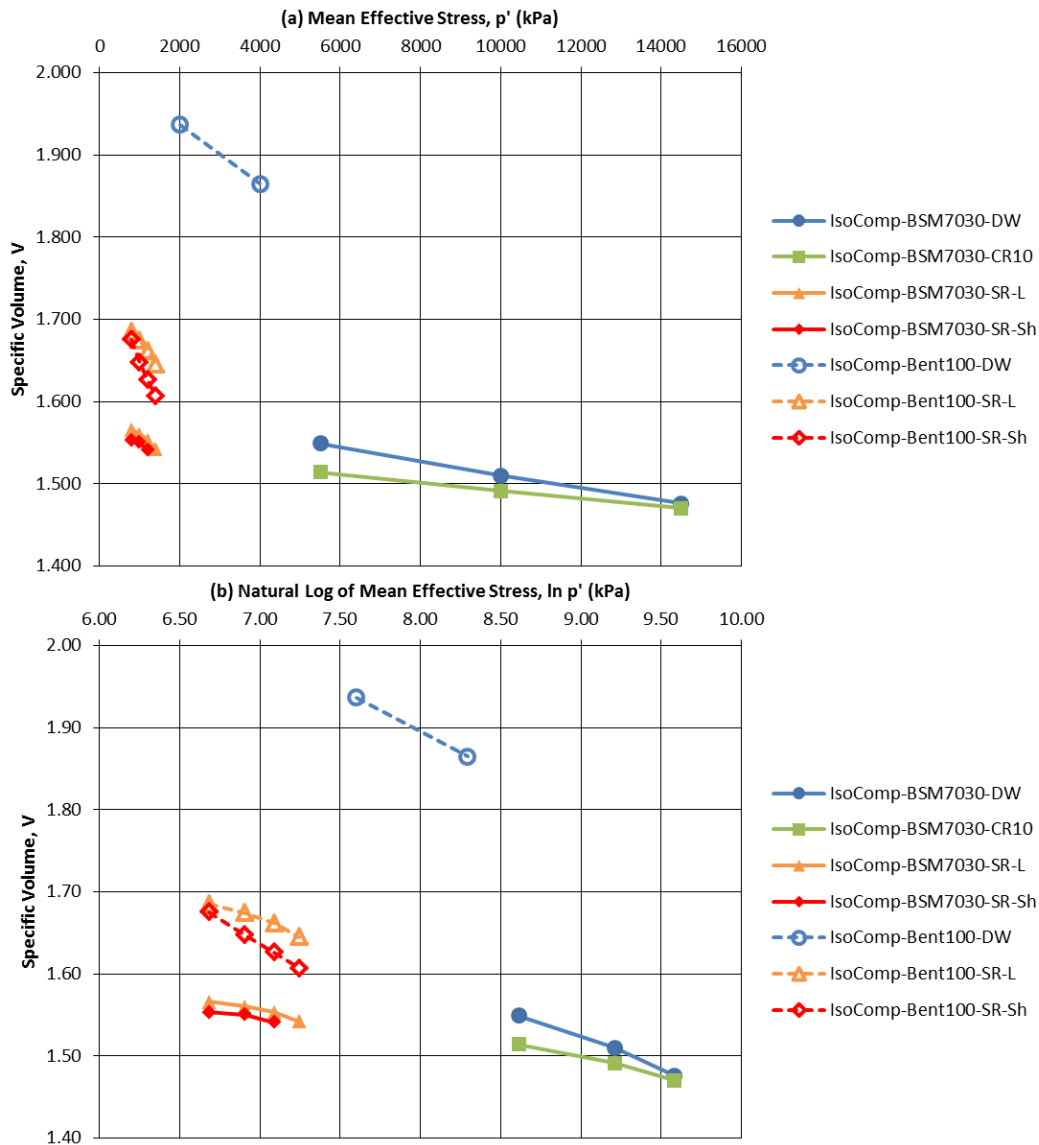


Figure 8.2: Isotropic Consolidation Test Results

8.3 ISOTROPICALLY CONSOLIDATED UNDRAINED (CI \bar{U}) TRIAXIAL TESTS (G)

8.3.1 CI \bar{U} Test Setup

Isotropically consolidated, undrained (CI \bar{U}) triaxial tests were performed to determine the Shear Modulus (G) (since $\varepsilon_v = \varepsilon_s$ when there is no volume change such as during a CI \bar{U} test). They also contribute to the characterization of the strength envelope.

As per the methodology of Blatz et al. (2008), each specimen was built into the triaxial systems at their prescribed composition, density and pore fluid. Specimens were manufactured to nominal dimensions of 50 mm diameter and 100 mm length at as high an initial water content as possible ($S_r \sim 95\%$) and then sealing the sample in a latex membrane with a saturated filter paper and saturated porous stone placed on the top and bottom of the sample. A cell pressure was applied that matched the expected swelling pressure of the material to prevent swelling

during saturation. Since porewater pressure measurements are required for CIU tests, shearing tests required saturated specimens ($B\text{-value} \geq 0.95$). Constructing the specimens at a high initial water content was an attempt to speed up saturation times that typically take very long periods of time for these materials. However, flow distances for saturation to occur were the same as for previous testing programs. Combined with low hydraulic conductivities, long saturation times were still expected. Due to very long saturation periods expected for these specimens, only two tests were scheduled, one for BSM and one for HCB, both using freshwater as the porefluid. After saturation, the shearing rate selected was sufficiently slow to ensure pore pressure equilibrium across the specimen (approximately a two-week shearing phase). The Shear Modulus (G) was determined from the elastic portion of the stress-strain curves established from these tests.

The limited number of triaxial tests completed was also the need for a highly specialized system for testing of clay-based materials with high swelling pressures. It must be able to monitor the internal pore pressures of a fluid-saturated specimen as well as the high confining pressures applied to the surface of specimen by the fluid outside the flexible membrane. This is particularly challenging for bentonite which when in contact with a source of free water will swell unless confined by an external pressure equal to the sum of the pore fluid pressure and the swelling pressure. Dense bentonite specimens of the type tested in this program can require pressures of 5 MPa to 10 MPa in order to counteract the swelling of the specimens. The RMC is one of the few laboratories that have cells capable of providing sufficient confinement to allow for testing of the dense bentonites examined in this study. Figure 8.3 provides a photograph of the test setup with a specimen installed (excluding the thick metal sleeve required to provide fluid confinement).



Figure 8.3: Triaxial Test Apparatus used at RMC

8.3.2 CIŪ Test Results (G)

CIŪ triaxial tests were conducted on one specimen of 70:30 bentonite:sand mixture prepared with deionized water, and on one specimen of highly compacted bentonite also prepared with deionized water. Additionally, all of the isotropic consolidation tests presented in Section 8.2 were sheared under undrained conditions after completion of the final consolidation increment. The stress-strain curves for the CIŪ tests are provided in Figure 8.4. Note that cell pressure control issues were experienced during the shearing of the specimen made with the 70:30 bentonite:sand mixture containing deionized water (specimen IsoComp-BSM7030-DW). However, this occurred after peak failure and the required information could be extracted from this test.

The Shear Modulus (G) was determined from the slope of the elastic region of the stress versus axial strain plots, prior to yielding of the specimen using the following equation:

$$G = \delta q / 3\delta \varepsilon_1$$

Where q is the deviator stress and ε_1 is axial strain. This equation can be used since $\varepsilon_v = 0$ for an undrained test and therefore $\varepsilon_1 = \varepsilon_{\text{shear}}$. The slope of the stress-strain curve was selected at about $q = 1/3q_{\text{max}}$, where the curve was approximately linear.

The Shear Modulus results are presented in Table 8.2. Based on the available results, it appears that the final consolidation pressure (p'_c), at which the specimen was sheared, influences the Shear Modulus to a greater degree than the type of pore fluid. Where similar consolidation pressures were used, similar stiffness was measured regardless of soil type. This applies to the higher pore fluid concentrations (SR-L and SR-Sh) where lower consolidation pressures could be used. At these lower pressures, the addition of sand did not significantly increase the shear stiffness. For parameter selection during stress-deformation modelling, it is recommended that the operating stress in the model be considered to determine an appropriate value or range of values.

Table 8.2: Shear Modulus (G) Results

Isotropic Consolidation Specimen ID	Soil Type	Pore Fluid	As-Built Dry		End of Test		
			Density (Mg/m ³)	Degree of Saturation	Dry Density (Mg/m ³)	Shear Modulus, G (MPa)	Isotropic Stress, p' _c (kPa)
CIU-BSM7030-DW	70:30 BSM	DW	1.82	100%	1.79	109	5589
IsoComp-BSM7030-DW	70:30 BSM	DW	1.82	96%	1.85	285	14585
IsoComp-BSM7030-CR10	70:30 BSM	CR10	1.81	99%	1.86	201	14742
IsoComp-BSM7030-SR-L	70:30 BSM	SR-L	1.74	94%	1.79	19.0	1400
IsoComp-BSM7030-SR-Sh	70:30 BSM	SR-Sh	1.75	92%	1.79	24.6	1400
IsoComp-Bent100-DW	100% Bentonite	DW	1.54	99%	1.49	31.0	4009
IsoComp-Bent100-SR-L	100% Bentonite	SR-L	1.52	95%	1.52	16.4	1400
IsoComp-Bent100-SR-Sh	100% Bentonite	SR-Sh	1.58	94%	1.67	16.2	1400
CIU-HCB-DW	HCB	DW	1.71	94%	1.63	60.3	7922

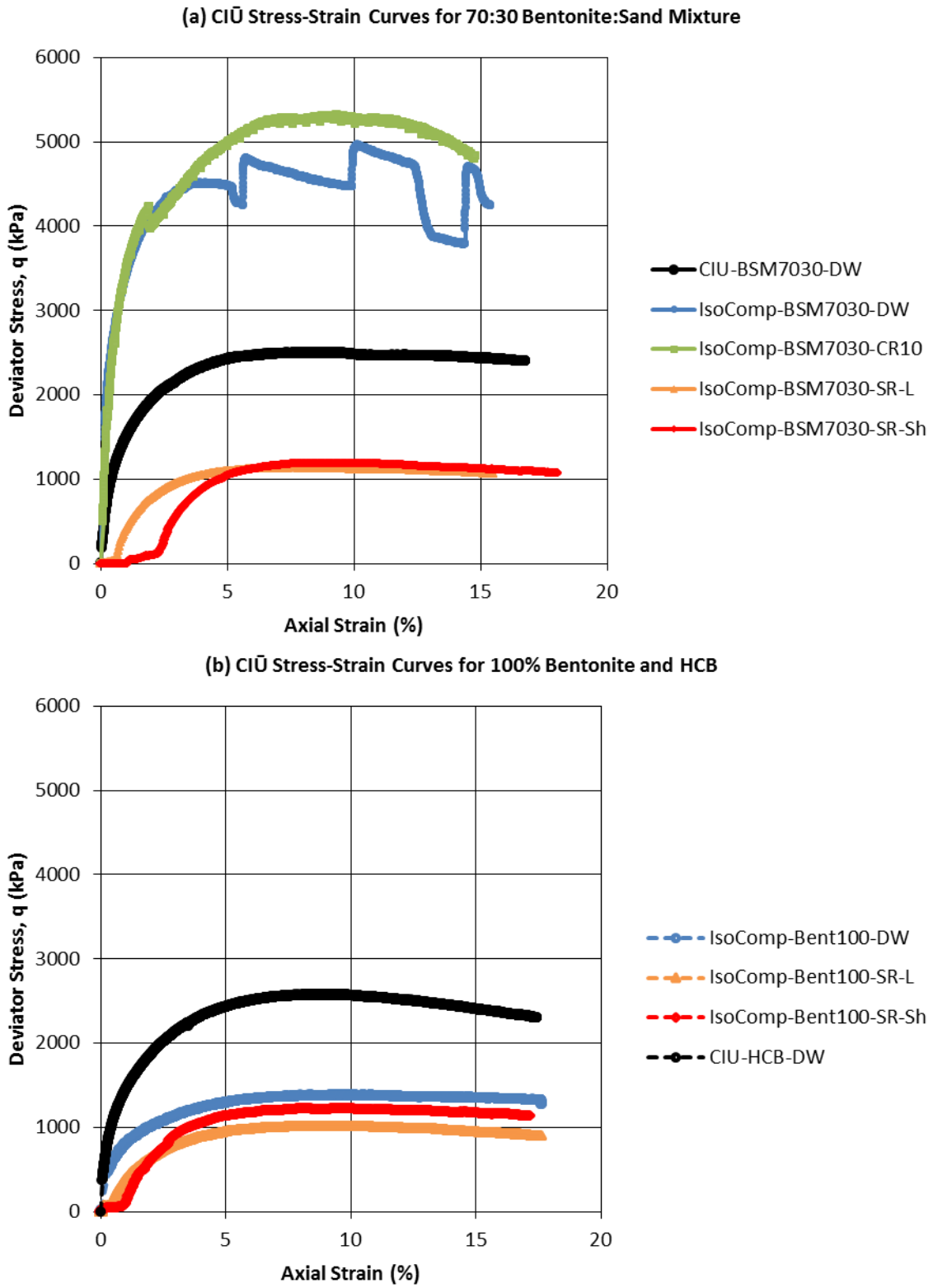


Figure 8.4: Stress-Strain Curves from CIŪ Tests

8.4 ISOTROPICALLY CONSOLIDATED DRAINED (CID) TRIAXIAL TESTS

8.4.1 CID Test Setup

CID triaxial tests were performed to determine the Young's Modulus (E). As for the CI \bar{U} tests, each specimen was built into the triaxial systems at their prescribed composition, density and pore fluid. For the purposes of determining consistency of measurements, three replicates each of BSM and HCB were prepared using freshwater and then tested using identical consolidation and shearing processes. The procedure generally followed that of Blatz et al. (2008), with the primary exception of keeping the drainage leads open during shearing to allow volume change during that phase of the test. This sends the specimen along a different stress path (with a 3:1 slope in p',q space) than in undrained tests. Specimens were manufactured to nominal dimensions of 50 mm diameter and 100 mm length at as high an initial water content as possible ($S_r \sim 95\%$) and then sealing the sample in a latex membrane with a filter paper and a dry porous stone placed on the top and bottom of the sample. After an equilibration period, the specimens were sheared with no back pressure. No back pressure was supplied to the CID test specimens so that they were sheared in their as-fabricated state, providing information on the longer-term behaviour of materials exposed to gradually increasing mechanical loading. The rate of shearing was sufficiently slow to prevent the build-up of pore pressures in the specimen during shearing (approximately a two-week shearing phase). Young's Modulus was determined from the elastic portion of the stress-strain curves established from these tests.

The same challenges regarding preventing specimen swelling are present in these tests as mentioned above. The CID tests are even more problematic with respect to control of specimen volume since traditional methodology would provide a water-saturated drainage pathway via the filter stones. This therefore would provide a source of free water to the specimen (which would induce specimen water uptake and swelling rather than drainage and require very high confining pressure to counteract this process. The same initial conditions (saturation $>90\%$) is defined as being required to start these tests and so the same approach as described in Section 8.2 was adopted to facilitate testing. Specimens were constructed to a known ($>95\%$) initial degree of saturation so that the minimum required initial-state conditions for start of testing were immediately present. The filter-drains at the top and bottom of the specimen were also not water saturated as that would induce specimen swelling and water uptake. The drainage of water induced by the confinement was not a factor due to the low confining pressure (approximately 1,500 kPa and 5,500 kPa was used for HCB and 70:30 BSM, respectively) and drainage induced by shearing was allowed via the dry filter stones at the top and base of the specimens (all fluid movement was out of the specimen). Following installation and equilibration under nominal confinement, shearing was initiated. Low strain rates (0.06 %/hour with total shearing times in the order of 100 hours) were used so that pore pressures could be assumed to be zero during the shearing phase.

8.4.2 CID Test Results (E)

Young's Modulus was determined from the slope of the elastic region of the stress versus axial strain plot, prior to yielding of the specimen using the following equation:

$$E = \delta\sigma_1' / \delta\varepsilon_1 \quad (8-3)$$

Where σ_1' is the principal effective stress and ε_1 is axial strain.

Three replicate CID tests were conducted on both 70:30 bentonite:sand mixture and HCB. All replicate specimens were made with deionized water. The stress-strain curves for these tests are shown on Figure 8.5, and Table 8.3 and summarize the Young's Modulus results determined from the early linear portions of the stress-strain curves. These data show the very similar stress-strain behaviour for the BSM materials, providing confidence in the values obtained. The BSM specimens displayed elastic-plastic behaviour, with a small degree of strain softening. Strain softening is characterized by a drop in shearing resistance after peak strength is reached. As expected, due to the absence of sand particles, greater strain softening was observed for the HCB specimens. The HCB behaviour was quite similar with respect to the maximum deviator stress required to induce failure, however one test exhibited rapid failure rather than the more gradual behaviour observed for the other two. This is attributed to complete rupture of the specimen without the formation of a shear plane. The other two specimens reached critical state with generally good agreement. As expected, the BSM displayed greater stiffness than the HCB.

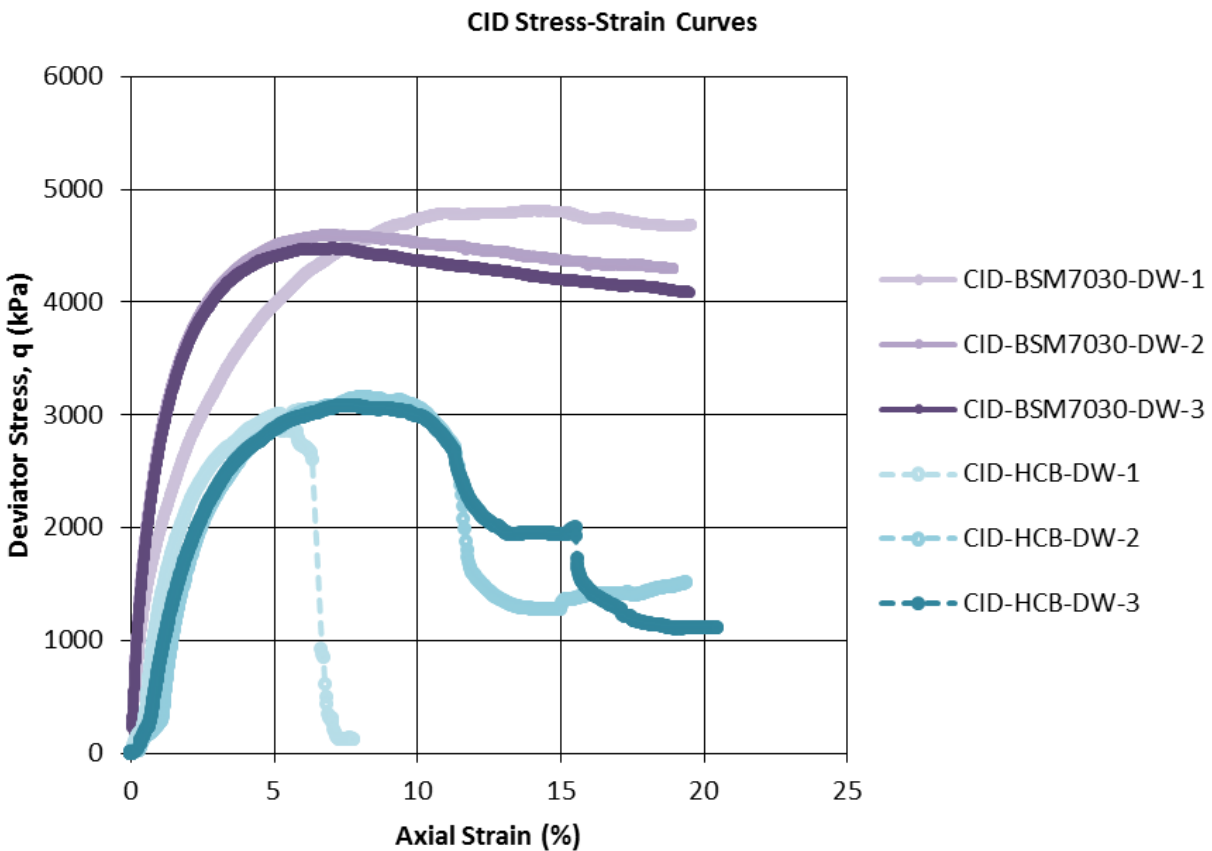


Figure 8.5: Stress-Strain Curves from CID Tests

Table 8.3: Young's Modulus (E) Results

Isotropic Consolidation Specimen ID	Soil Type	Pore Fluid	As-Built Dry		End of Test	Young's	Isotropic Stress, p'_c (kPa)
			Density (Mg/m ³)	Degree of Saturation	Dry Density (Mg/m ³)	Modulus, E (MPa)	
CID-BSM7030-DW-1	70:30 BSM	DW	1.75	87%	1.87	278	5533
CID-BSM7030-DW-2	70:30 BSM	DW	1.81	99%	1.84	367	5534
CID-BSM7030-DW-3	70:30 BSM	DW	1.82	100%	1.83	427	5512
CID-HCB-DW-1	HCB	DW	1.63	100%	1.63	214	1489
CID-HCB-DW-2	HCB	DW	1.62	97%	1.55	192	1488
CID-HCB-DW-3	HCB	DW	1.62	99%	1.42	150	1499

8.5 TRIAXIAL SHEAR STRENGTH AND YIELD LOCUS

Shear strength and yielding data obtained in this study are presented in Figure 8.6 within a critical state soil mechanics framework. The Critical State Line, with slope M , is defined by post-peak, steady-state behaviour. Detailed presentation of this concept can be found in Budhu (2011). The results for each test, and the calculated effective friction angle, ϕ' are presented in Table 8.4.

Upon inspection of Table 8.4, it is reasonable to conclude that shear strength increases when higher pore fluid TDS concentrations are present. The slope of the Critical State Line (CSL) was about $M = 1$ for SR-L and SR-Sh pore fluids for both 70:30 BSM and 100% Bentonite. For these same materials prepared with deionized water as the pore fluid, M values ranged from 0.3 to 0.6. It should be noted that operating confining stress needs to be considered when using these parameters for modelling purposes. This is especially the case for when a critical state model, requiring a yield locus, is employed. The following provides further discussion for each material with reference to Figure 8.6a for 70:30 BSM and Figure 8.6b for 100% bentonite and HCB.

70:30 Bentonite: Sand Mixture

Comparing specimens of 70:30 BSM made with SR-L and SR-Sh (Figure 8-6), there was no significant difference in strength at these high concentrations. Both of these tests were conducted at relatively low isotropic consolidation pressures and help define the shape of the yield locus at low stress. Compared to the other M values, these two specimens were significantly higher at $M = 1.0$ ($\phi' = 25^\circ$). It is possible that the high pore fluid concentrations reduced the diffuse double layers of the clay component, allowing greater interparticle contact between sand grains. However, there were no tests conducted on specimens made with DW in this low stress range so direct comparison was not possible. Conversely, there were no tests conducted with SR-L or SR-Sh pore fluids at higher isotropic consolidation pressures.

The stress path for specimen CIU-BSM7030-DW (Figure 8-6) initially displayed the expected behaviour for an elastic and isotropic material under undrained conditions (i.e. a vertical stress path). The vertical stress path indicates that the specimen was in the elastic region during shearing and the isotropic preconsolidation pressure (p'_c) is further to the right along the p' axis. This suggests the compaction effort used in preparing the specimens imparts an isotropic preconsolidation pressure greater than 5589 kPa (which was the isotropic compression pressure used for this specimen). The "hooked" stress path near peak strength helps define the

shape of the as-built yield locus with DW as the pore fluid. This specimen reached a Critical State Line (CSL) with an M value of 0.40. Based on the available tests, this is considered representative for the as-built conditions for this material.

Three replicate CID tests on this material made with DW as the porefluid were also conducted from the same initial isotropic consolidation pressure as specimen CIU-BSM7030-DW. The three replicates showed generally good agreement. Beyond the peak reached for CIU-BSM7030-DW, the CID specimens underwent hardening, thus expanding the yield locus for these specimens. Upon reaching peak strength, these specimens displayed some strain softening. These specimens did not strain soften back to the CSL defined by specimen CIU-BSM7030-DW. Instead, they reached a CSL with an average M value of 0.62. It is unclear why these specimens did not strain soften to the same CSL as the specimens tested at higher isotropic consolidation pressures (discussed below). It is likely that the presence of the sand affects the strain-softening behaviour of this material.

Table 8.4: Summary of Shear Strength Test Results

Isotropic Consolidation Specimen ID	Soil Type	Pore Fluid	As-Built Dry		End of Test		ϕ'	Isotropic Stress, p'_c (kPa)
			Density (Mg/m^3)	Degree of Saturation	Dry Density (Mg/m^3)	M		
70:30 Bentonite:Sand Mixture								
CIU-BSM7030-DW	70:30 BSM	DW	1.82	100%	1.79	0.40	10.8	5589
IsoComp-BSM7030-DW	70:30 BSM	DW	1.82	96%	1.85	0.28	7.7	14585
CID-BSM7030-DW-1	70:30 BSM	DW	1.75	87%	1.87	0.66	17.3	5533
CID-BSM7030-DW-2	70:30 BSM	DW	1.81	99%	1.84	0.61	16.1	5534
CID-BSM7030-DW-3	70:30 BSM	DW	1.82	100%	1.83	0.60	15.8	5512
IsoComp-BSM7030-CR10	70:30 BSM	CR10	1.81	99%	1.86	0.32	8.7	14742
IsoComp-BSM7030-SR-L	70:30 BSM	SR-L	1.74	94%	1.79	1.00	25.4	1400
IsoComp-BSM7030-SR-Sh	70:30 BSM	SR-Sh	1.75	92%	1.79	1.00	25.4	1400
Bentonite								
IsoComp-Bent100-DW	100% Bentonite	DW	1.54	99%	1.49	0.31	8.5	4009
IsoComp-Bent100-SR-L	100% Bentonite	SR-L	1.52	95%	1.52	0.84	21.6	1400
IsoComp-Bent100-SR-Sh	100% Bentonite	SR-Sh	1.58	94%	1.67	1.09	27.5	1400
CID-HCB-DW-1	HCB	DW	1.63	100%	1.63	0.51	13.6	1489
CID-HCB-DW-2	HCB	DW	1.62	97%	1.55	0.66	17.3	1488
CID-HCB-DW-3	HCB	DW	1.62	99%	1.42	0.59	15.6	1499
CIU-HCB-DW	HCB	DW	1.71	94%	1.63	0.28	7.7	7922

At the higher end of isotropic compression pressures, there was little observed difference between DW and CR10 (IsoComp-BSM7030-DW vs IsoComp-BSM7030-CR10). The specimen made with CR10 showed only a slightly higher peak strength. Both of these specimens displayed some strain softening (despite some pressure control variations experienced during the testing of the specimen made with DW). Based on these observations, the estimated yield locus for as-built 70:30 BSM with DW as the pore fluid is shown on Figure 8.6a. In order to better define the yield locus, and the effect of pore fluid chemistry, further testing would be required.

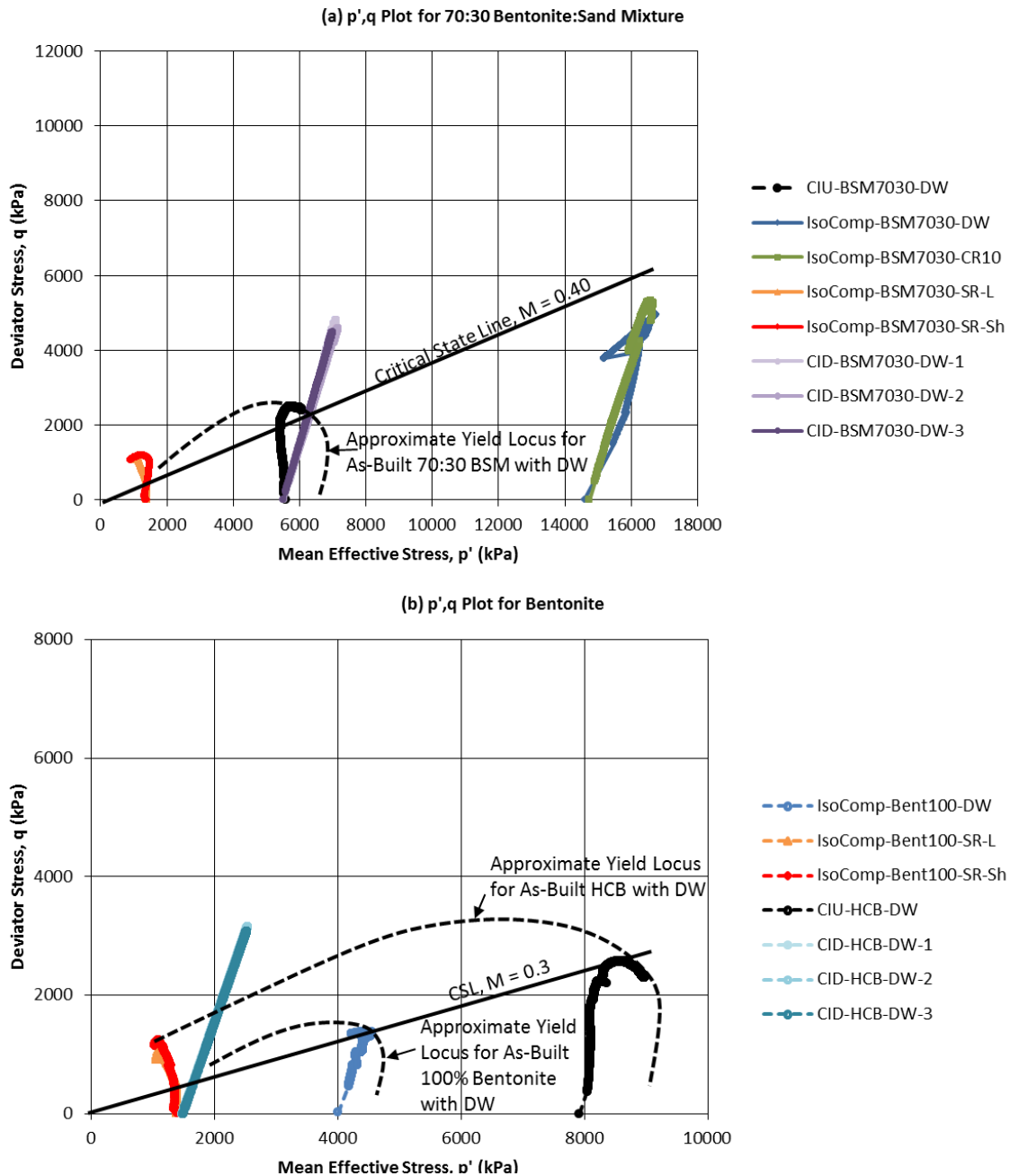


Figure 8.6: p', q Plots from Triaxial Tests

100% Bentonite and HCB

Comparing specimens of 100% bentonite made with SR-L and SR-Sh, the higher concentration resulted in a slightly higher shear strength. Both specimens displayed similar stress-strain curves with limited strain softening. Post-peak deviator stress values were similar to the CID tests (discussed below) that started from the same isotropic consolidation pressure. This provides confidence in defining the yield locus at these lower pressures, and suggests that post-peak, critical state behaviour is not significantly influenced by pore fluid chemistry (in contrast to 70:30 BSM).

Three replicate CID tests on HCB made with DW (specimens CID-HCB-DW-1,2 and 3) were also conducted from the same initial isotropic consolidation pressure as the specimens made with SR-L and SR-Sh. The three replicates showed generally good agreement. One sample crumbled after peak and did not reach what would be considered critical state (i.e. specimen CID-HCB-DW-1). Beyond the peak reached for the CI \bar{U} tests that started at the same isotropic consolidation pressure, the CID specimens underwent hardening, thus expanding the yield locus for these specimens. Upon reaching peak strength, these specimens displayed significant strain softening and reached values close to the neighboring CI \bar{U} tests. This behaviour agrees with classic critical state models and as mentioned above, the critical state behaviour appears to not be influenced by pore fluid chemistry.

Two additional CI \bar{U} tests were conducted at higher pressures. In the mid-range, one of these tests was conducted on 100% bentonite. The test with the highest isotropic consolidation pressure was conducted on a specimen of HCB. Comparing the two tests implies that 100% bentonite and HCB have different yield loci. This is expected due to the higher compaction effort applied when making HCB. The approximate yield loci for the two materials are shown on Figure 8.6b. As for 70:30 BSM, further testing would be required to confirm the shape of the yield loci under the range of pore fluid conditions.

8.6 SUMMARY OF STRESS-STRAIN BEHAVIOUR DETERMINED BY TRIAXIAL TESTING

The triaxial testing program was designed to establish initial stress-deformation models for the two materials within an elastic-plastic, or critical state soil mechanics framework. Various stress paths were examined including isotropic consolidation, drained shearing (CID tests), and undrained shearing (CI \bar{U} tests). A compilation of the results is provided in Table 8.5.

These models require a number of elastic-plastic parameters which were extracted from the results. The Bulk Modulus was determined from the Specific Volume, p' plots from the isotropic consolidation tests. Similarly, the parameters κ and λ were determined from the slope of the $\ln p', V$ plots. Determination of κ and λ depends on obtaining sufficient points along the consolidation curve both before and after yielding. Since final isotropic stress increments were specified and largely limited by the capacity of the equipment, only two of the high pressure samples were conducted into a stress range that would be considered beyond the isotropic preconsolidation pressure. Those two tests provided λ . The remainder of the tests were conducted over stress ranges that would be representative of κ . This interpretation is guided by the collective results combined into the yield loci in p', q space. The new insight towards the shape of the yield loci can be used to guide future testing and further definition of the elastic-plastic model. In general, stiffness decreased with increasing pore fluid salinity for both soil types. As expected, the bentonite-sand mixture is stiffer than 100% bentonite at a given pore fluid salinity.

The CI \bar{U} tests were used to determine the Shear Modulus, G . The results of this testing program suggest that the final consolidation pressure (p'_c), at which the specimen was sheared, influences the Shear Modulus to a greater degree than the type of pore fluid. The CID tests were used to determine Young's Modulus. The presence of sand in the BSM resulted in higher stiffness than the HCB.

It should be noted that the appropriate parameter values selected for any modelling purposes needs to consider the stress range since the soil may either be in the elastic or plastic region.

Table 8.5: Summary of mechanical properties parameters derived from triaxial testing

Specimen Name	Material	EOT Dry Density (Mg/m ³)	Pore Fluid	M	ϕ' (°)	p'_c (MPa)	E (MPa)	G (MPa)	K (MPa)	κ	λ
IsoComp-Bent100-DW	MX80	1.49	DW	0.31	8.5	2-4	NR (<146)*	31	53.8	0.104	-
IsoComp-Bent100-SR-L	MX80	1.52	SR-L	0.84	21.6	0.8-1.4	NR	16.4	26	0.075	-
IsoComp-Bent100-SR-Sh	MX80	1.67	SR-Sh	1.09	27.5	0.8-1.4	NR	16.2	14.9	0.121	-
CID-HCB-DW-1	HCB	1.63	DW	0.51	13.6	1.5	214	NR	NR	NR	NR
CID-HCB-DW-1	HCB	1.55	DW	0.66	17.3	1.5	192	NR	NR	NR	NR
CID-HCB-DW-1	HCB	1.42	DW	0.59	15.6	1.5	150	NR	NR	NR	NR
CIU-HCB-DW	HCB	1.63	DW	0.28	7.7	7.9	NR	60.3 (80.6)*	NR	NR	NR
CIU-BSM7030-DW	BSM	1.79	DW	0.4	10.8	5.6	NR	109	NR	NR	NR
IsoComp-BSM7030-DW	BSM	1.85	DW	0.28	7.7	5.5-14.6	NR	285	189	-	0.0784
CID-BSM7030-DW-1	BSM	1.87	DW	0.66	17.3	5.5	278	NR	NR	NR	NR
CID-BSM7030-DW-2	BSM	1.84	DW	0.61	16.1	5.5	367	NR	NR	NR	NR
CID-BSM7030-DW-3	BSM	1.83	DW	0.60	15.8	5.5	427	NR	NR	NR	NR
IsoComp-BSM7030-CR10	BSM	1.85	CR10	0.32	8.5	5.5-14.7	NR	201	308	-	0.0475
IsoComp-BSM7030-SR-L	BSM	1.79	SR-L	1	21.6	0.8-1.4	NR	19.0	44.6	0.0384	-
IsoComp-BSM7030-SR-Sh	BSM	1.79	SR-Sh	1	27.5	0.8-1.4	NR	24.6	34.4	0.0494	-

NR- parameter not part of testing matrix, cannot be determined from this type of test or data collected, alternative method to determine κ and λ values are provided in Section 8.7

- parameter could not be derived from test data.

* value in brackets obtained from literature (Dixon 2018)

The yield loci presented in Figure 8.6 (a) and (b) can be used to help guide that parameter selection. These p',q plots show anisotropic yield loci for the tested materials. Anisotropy is likely imparted during the sample compaction procedure. The shapes of the yield loci are largely guided by tests conducted on specimens made with deionized water. Further testing would be required to confirm the effect of pore fluid chemistry on yielding. These plots include critical state strength envelopes defined by the slope, M . For BSM, a value of $M = 0.4$ was obtained. For 100% bentonite and HCB, a value of $M = 0.3$ was obtained. Note that the higher compaction effort imparted on HCB resulted in an expanded yield locus relative to 100% bentonite with lower density. Both yield loci show similar shapes and can be considered a family of curves within the same model.

8.7 ONE-DIMENSIONAL CONSOLIDATION (OEDOMETER) TESTS

8.7.1 Oedometer Test Setup

One dimensional consolidation tests were performed using ASTM D2435M-11 “Standards for oedometer tests” as the guideline for testing pre-conditioned material that was compacted directly into the testing rings and tested in standard lever-arm oedometer frames as shown in Figure 8.7. Compaction directly into the test cell allowed for greater confidence in the as-built condition and also minimized the potential effects of specimen defects on subsequent consolidation behaviour that might arise from use of precompacted and then trimmed-to-fit specimens. The very high loads required to confine and consolidate bentonite-based materials (particularly when low salinity pore fluid is present), required use of testing rings that were slightly smaller in diameter than traditionally used for consolidation testing and application of loads that were in some cases higher than typically used.

As per the test matrix provided in Table 1.1, there were two soil materials examined in this part of the testing program. The first was the 70:30 bentonite:sand mixture, compacted to a target dry density of 1.8 Mg/m^3 and the second was 100% MX80 bentonite compacted to a target dry density of 1.5 Mg/m^3 . The 70:30 material was tested in triplicate using DW, CR-10, SR-L and SR-Sh fluids and the MX80 clay-only materials were tested using DW, SR-L and SR-Sh.

Previous experience with consolidation testing of MX80-based materials (Barone et al. 2014) provided estimated swelling pressure values for the specimens. This allowed for preselection of initial seating loads that were sufficient to limit or prevent specimen swelling during the first loading step(s). This was important as it meant that the specimens did not undergo microstructural changes caused by swelling and realignment of the clay particles. In order to minimize the effects of pore fluid composition and to greatly reduce the time required for the specimens to achieve saturation, each test was constructed to a pre-selected density at a high pre-defined degree of saturation ($>90\%$). The same fluid was used in the construction of the specimen as was used in the fluid reservoir surrounding the test.

The one-dimensional (1-D) consolidation tests are useful as they provide supplemental data regarding the elastic and hardening parameters determined from the triaxial tests described in Section 8.1. The 1D tests provide values for deformation indices including the coefficient of consolidation (C_v), coefficient of volume compressibility (m_v), Compression Index (C_c) and Swelling Index (C_s or C_r), which are needed in some mechanical models for soil deformation and performance. For the purposes of this study the symbol C_r is used to describe the swelling index. How these are extracted from the test data for conventional materials is shown in

Figure 8.8. Tests were conducted following ASTM D2435M-11 “Standards for oedometer tests”, using loads and load increments required to resist substantial initial strain due to clay swelling and induce sufficient consolidation to allow for determination of the required parameters.



Figure 8.7: Lever-Arm Oedometers Used in 1-D Consolidation Testing.

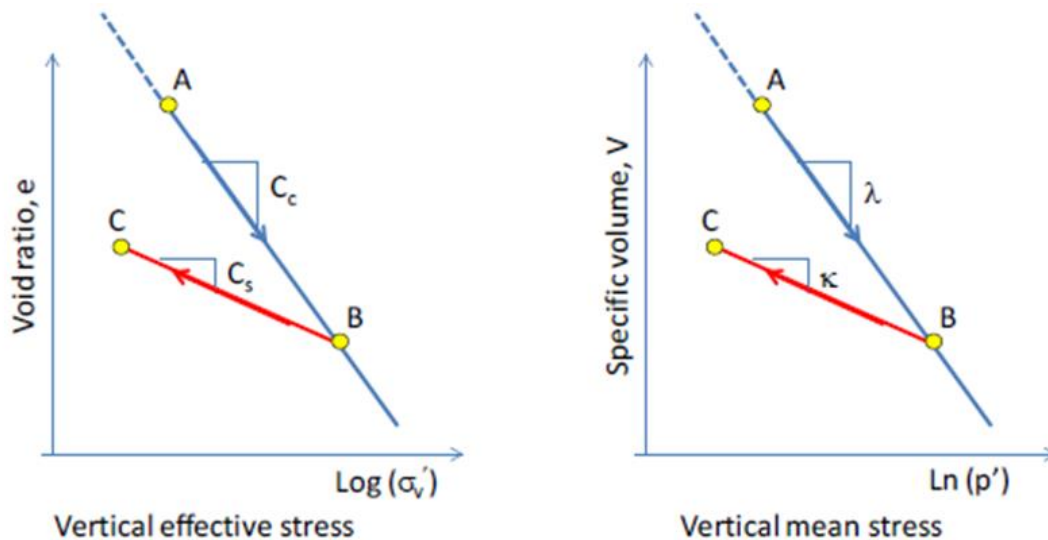


Figure 8.8: Derivation of the Parameters of C_c , C_s (sometimes referred to as C_r) in 1D Consolidation Tests and the Lambda and Kappa Parameters from Triaxial Testing. (Figure from Priyanto et al. 2013).

In addition to deformation properties, the consolidation (oedometer) tests can also be used to generate swelling pressure versus density and hydraulic conductivity estimates to supplement the direct measurements made using the rigid-wall swelling pressure cells. The swelling

pressure and hydraulic conductivity data generated using the oedometers were presented in Sections 6.2.2 (Figure 6.3) and 6.3.2 (Figure 6.4) respectively. The oedometer data was very comparable with respect to swelling pressure but tended to provide higher hydraulic conductivity values than direct flow measurements provided. Greater confidence should be placed on the results of the direct flow measurements. One-dimensional consolidation tests can also be used to generate estimates of the Lambda (λ) and Kappa (κ) parameters needed to evaluate the deformation behaviour (Bhudu 2011). These two parameters are typically generated through conduct of triaxial testing but can be problematic to obtain in high-swelling capacity materials such as bentonite. Bhudu (2011) provides the following equations to describe the relationship between the consolidation parameters C_c and C_r (or C_s) and λ and κ , respectively.

$$\lambda = 0.434 C_c \quad (8-4)$$

$$\kappa = 0.434 C_r \quad (8-5)$$

8.7.2 Oedometer Test Results

The results of the 1-D tests completed as part of the current study are summarized in Table 8.5 and the full set of e-Log σ_v' plots and calculated parameter values for each test are provided in Appendix I. Figure 8.9 provides example plots of the 1D consolidation data for the 70:30 specimens using low salinity (CR10) and brine (SR-L) pore fluids and how the coefficient of consolidation (C_c), rebound coefficient (C_r) and apparent preconsolidation pressure (σ_p') are determined for each specimen. These two plots show the two clearly different deformation behaviours observed in this testing activity, one for the low salinity systems where initial volume was fully (or returned to higher than initial volume), recovered during unloading and systems where rebound (swelling) was much lower, more in keeping with a conventional soil having limited swelling capacity.

Figure 8.9 clearly shows how salinity affects the consolidation behaviour of bentonite-based materials. The load required to achieve a given void ratio (e) is much higher in a low salinity system than for a saline system (swelling pressure is higher at low salinity and must be overcome before compression can occur). The swelling capacity of the low salinity system is also much higher, with full recovery of volume during the unloading cycle in the CR10 system.

The deformation parameter values obtained for each of the tests completed are summarized in Table 8.5 and data are shown in Figures 8.10 and 8.11. Plots for each individual test done as part of this project are provided in Appendix I. The data shows generally good consistency in the values obtained for replicate specimens, particularly those tested under saline conditions, providing confidence in the reproducibility of the test results. The shape of the e-log σ_v' plots are consistent with what is expected for the type of materials tested. The initial seating and maximum loads required to prevent swelling and induce consolidation respectively are much higher than are required for normal (non-swelling soils). Tests done using freshwater fluids tended to show a greater degree of variability in their results, primarily as a result of the very high swelling capacity of these systems and challenges in controlling/achieving adequate consolidation during loading and subsequently swelling during unloading.

Figures 8.10 and 8.11 present the C_v and m_v data derived from the consolidation tests in terms of both dry density and EMDD. From the data presented in Table 8.5 it can be concluded that C_v is not discernibly affected by either density or pore fluid composition for MX80-only or MX80-

aggregate mixtures (30% sand) for the range of densities of interest. In general, the replicate tests provided C_v values that were similar and averaged $1 \times 10^{-8} \text{ m}^2/\text{s}$ (plus or minus $\frac{1}{2}$ -order of magnitude). Two of the low salinity tests provided data points that were inconsistent (higher) than the main body of data. This was attributed to the challenges associated with confining and consolidating low salinity systems (very high swelling pressure develops, together with large strains under low-load conditions), as a result these data are not considered to be reliable.

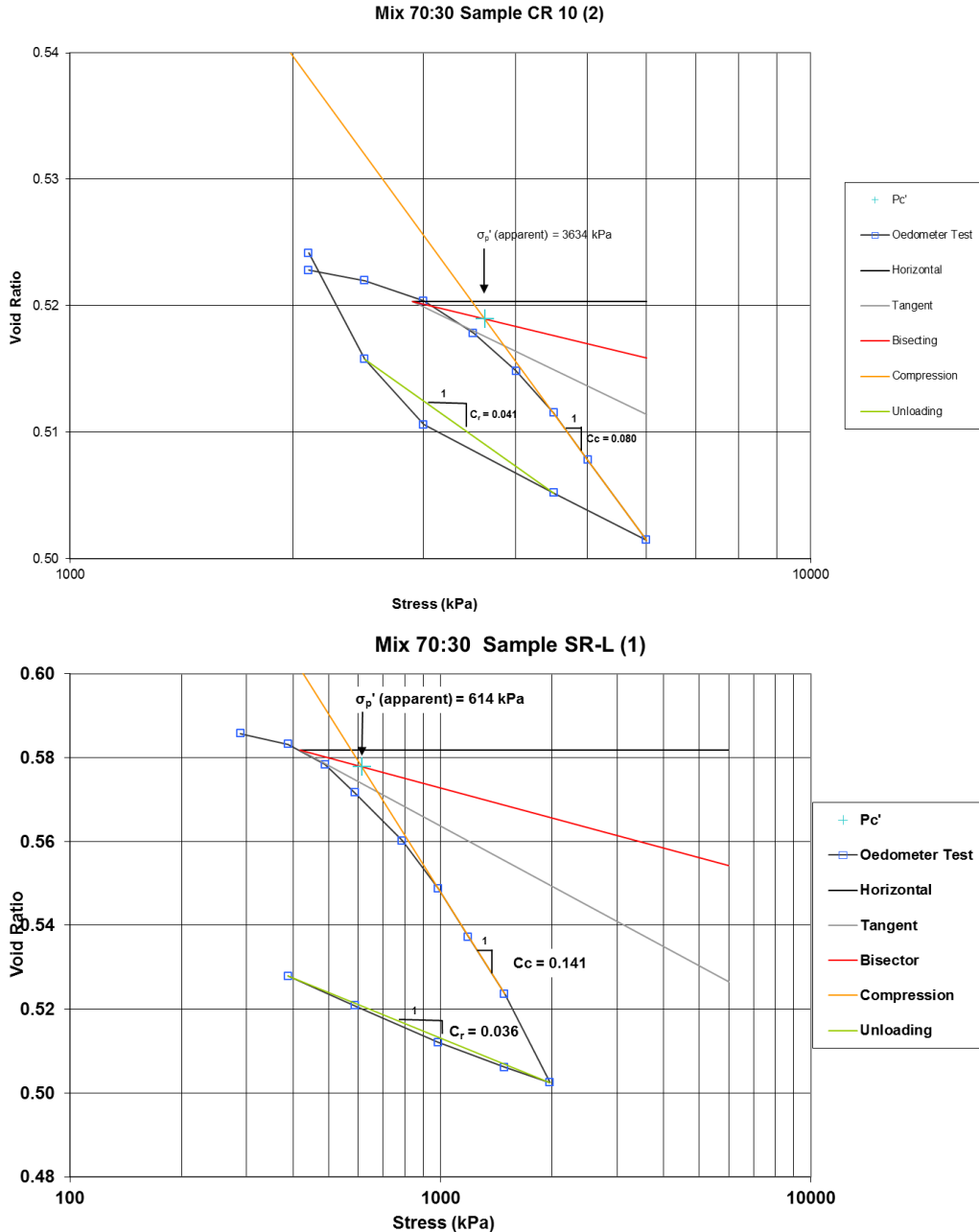


Figure 8.9: Consolidation Tests Showing Effect of Salinity on Rebound Behaviour.

The coefficient of volume compressibility (m_v) presented in Figure 8.10 shows a very different pattern of behaviour than was observed for the C_v parameter. In general, these data show an

apparent insensitivity to changes in density but a strong dependence on pore fluid salinity and the presence of an aggregate component. For the 70:30 materials, the m_v value shifts from $\sim 4 \times 10^{-6} \text{ m}^2/\text{KN}$ to $\sim 3 \times 10^{-5} \text{ m}^2/\text{KN}$ when salinity is increased from the DW-CR10 range ($< 11 \text{ g/L}$ TDS) to the SR-L - SR-Sh ($> 223 \text{ g/L}$ TDS) range. As with other data, there appears to be little effect of behaviour when the TDS goes from 223 to 335 g/L. The MX80 materials show a similar behaviour change with change in pore fluid salinity but tend to exhibit slightly higher parameter values, $\sim 1 \times 10^{-5} \text{ m}^2/\text{KN}$ at low salinity, increasing to $\sim 5 \times 10^{-5} \text{ m}^2/\text{KN}$ at high TDS.

The data presented in Figure 8.11 is for determination of the C_c and C_r parameters. These data show the same type of behavioural sensitivity to salinity, again providing two separate data groupings for each material based on TDS. At high TDS the C_c parameter is approximately twice the value obtained for low TDS materials, illustrative of the effect of the reduced swelling pressure (and hence resistance to consolidation). The data generated by the current study is not entirely clear as to possible effects of the sand component on C_c , there is a considerable overlap in the data values. The 70:30 mixture at low TDS materials exhibits a C_c value of approximately $0.08 (\pm \sim 0.01)$ and the brine systems exhibited values in the order of $0.16 (\pm \sim 0.02)$. For the bentonite-only materials there is the same increase in C_c value for increasing TDS, but the data shows a larger degree of scatter than observed for the bentonite-sand mixture. The C_c averages $\sim 0.14 (\pm 0.05)$ at low TDS and increases to $\sim 0.275 (\pm 0.075)$.

As noted above, the consolidation behaviour of the bentonite-sand material is strongly influenced by the pore fluid salinity and this is also reflected in the swelling/rebound parameter (C_r) in Figure 8.11. The low salinity systems exhibited consistently higher C_s values (~ 0.085 for 70:30 material and $\sim 0.18 (\pm \sim 0.06)$ for the MX80-only material for DW conditions. In these tests the presence of only a low salinity (CR10 at $\sim 11 \text{ g/L}$ TDS) seemed to be sufficient to strongly affect the unloading/swelling behaviour of both systems, resulting in a very consistent C_r value ($\sim 0.05 \pm 0.02$). It should be noted that the CR10 systems did show an ability to recover almost all of its original volume as it was stepwise unloaded to its initial state while the higher TDS systems were not able to swell to this degree (see load-unload data plots in Appendix I).

8.7.3 Summary of One-Dimensional Consolidation Test Results

From the plots provided in Figures 8.10 and 8.11 it can be concluded that:

For C_v :

- There is little effect of salinity on the materials examined;
- Over the range of density (dry or EMDD), there is no discernible influence of sand on the C_v parameter value; and
- C_v can be considered to be constant ($\sim 1 \times 10^{-8} \text{ m}^2/\text{s} \pm \sim 1/2$ order of magnitude)

For m_v :

- Salinity has a substantial effect on the m_v . Low salinity systems show approximately an order of magnitude lower value than comparable materials tested at high salinity;
- m_v shows little change with the presence of sand (30%) indicating that the clay component is controlling behaviour; and
- The m_v parameter value at a given pore fluid TDS content is not discernibly affected by density (dry or EMDD) over the range examined in this study.

For C_c :

- C_c is influenced by pore fluid salinity with value increasing with increasing TDS (up to some value <223 g/L after which it is a constant);
- There is a clear difference in behaviour between sand-bentonite and bentonite-only systems. Bentonite-only systems show substantially higher C_c values at a given density (dry or EMDD) and salinity than are observed in bentonite-sand material; and
- C_c will need to be defined for each salinity and bentonite-sand ratio considered.

For C_r :

- C_r is influenced by pore fluid salinity when low (<11 g/L TDS) conditions are present.
- For freshwater conditions, C_r of 70:30 material is lower ($\sim 0.09 \pm 0.01$) than for MX80 ($\sim 0.18 \pm 0.06$).
- For saline conditions C_r is constant ($\sim 0.04 \pm 0.01$) and density insensitive for MX80 and MX80-sand materials.

8.8 SUMMARY OF MECHANICAL PROPERTIES

Sections 8.2 through 8.7 have examined the mechanical properties of the three materials under investigation in this testing program (100% bentonite at ~ 1.5 Mg/m³; HCB at >1.7 Mg/m³ and BSM at >1.7 Mg/m³ dry density). These tests allowed for the determination of some of the parameters important to the development of deformation models for use in predicting the short- and long-term behaviour of these materials.

Table 8.6 provides a summary of these parameters. It should however be noted that some of these parameter values are based on very limited data sets and do not consider factors such as temperature on behaviour. Technical literature contains information on the effects of temperature on the behaviour of bentonite and BSM and should be consulted when defining parameter values for use in modelling (e.g. Tsato and Marelli (2013); Borgesson et al. (2010), Eloranta (2017) and Lingnau et al. (1996)), but evaluation of temperature or other environmental effects on stress-strain behaviour is beyond the scope of the current study. Other effects on mechanical parameters such as microbial activity, mineralogical changes or longer-term processes such as cementation (or dissolution) of clay materials are also not considered as part of this study. If deformation properties beyond the level of accuracy provided by the current study are required there will need to be detailed evaluation of literature and further laboratory testing.

Table 8.6: Summary of Oedometer Test Results

Test	Avg Stress* (MPa)	Avg Density* (Mg/m ³)	EMDD (Mg/m ³)	Avg. Void Ratio*	Avg. Cv* (m ² /s)	Avg mv* (m ² /kN)	Cc	Cr Cs	Avg k* (m/s)	Pc (kPa)	e @ Pc
70-30 DW (1)	5.17	1.820	1.462	0.563251	3.40E-08	3.61E-06	0.082	0.089	1.20E-10	4364	0.571
70-30 DW (2)	5.17	1.823	1.465	0.558742	2.03E-08	3.70E-06	0.082	0.087	7.72E-13	4510	0.566
70-30 DW (3)	6.01	1.858	1.506	0.531872	7.68E-08	3.05E-06	0.089	0.061	1.95E-12	5447	0.538
MX80 DW (1)	3875	1.534	1.388	0.851046	1.313E-08	2.759E-06	0.071	0.232	2.341E-13	4000	0.850
MX80 DW (2)	3875	1.534	1.388	0.849218	5.953E-09	8.648E-06	0.138	0.192	4.769E-13	4000	0.840
MX80 DW (3)	3875	1.552	1.407	0.826621	3.838E-09	1.182E-05	0.189	0.122	4.373E-13	3500	0.830
70-30 CR-10 (1)	5.146	1.826	1.469	0.5165	1.33E-08	4.12E-06	0.084	0.04	5.38E-13	4094	0.527
70-30 CR-10 (2)	5.170	1.841	1.486	0.5045	1.12E-08	4.41E-06	0.08	0.041	4.83E-13	3634	0.519
70-30 CR-10 (3)	5.170	1.844	1.489	0.5025	1.88E-07	3.98E-06	0.095	0.0498	7.23E-12	4372	0.512
70-30 SR-L (1)	1.550	1.824	1.466	0.513	1.22E-08	2.76E-05	0.141	0.036	3.30E-12	614	0.577
70-30 SR-L (2)	1.551	1.853	1.500	0.4905	5.61E-09	3.28E-05	0.17	0.038	1.80E-12	630	0.566
70-30 SR-L (3)	1.554	1.892	1.546	0.459	7.20E-09	3.24E-05	0.169	0.047	2.30E-12	607	0.537
MX80 SR-L (1)	1.207	1.607	1.463	0.698704	1.45E-08	5.56E-05	0.282	0.059	7.83E-12	646	0.785
MX80 SR-L (2)	1.225	1.634	1.491	0.6715	1.11E-08	6.75E-05	0.346	0.061	7.30E-12	648	0.775
MX80 SR-L (3)	1.229	1.606	1.462	0.6995	1.16E-08	3.97E-05	0.198	0.045	4.56E-12	659	0.760
70-30 SR-Sh (1)	1.547	1.850	1.496	0.5025	5.04E-09	2.99E-05	0.157	0.031	1.46E-12	584	0.577
70-30 SR-Sh (2)	1.550	1.857	1.505	0.497	7.48E-09	2.92E-05	0.145	0.034	2.13E-12	585	0.567
70-30 SR-Sh (3)	1.550	1.869	1.519	0.4875	6.34E-09	2.80E-05	0.146	0.037	1.75E-12	604	0.555
MX80 SR-Sh (1)	1.200	1.813	1.681	0.4615	6.36E-09	4.72E-05	0.232	0.049	2.95E-12	764	0.516
MX80 SR-Sh (2)	1.218	1.701	1.562	0.558	7.89E-09	4.85E-05	0.236	0.045	3.77E-12	778	0.613
MX80 SR-Sh (3)	1.199	1.687	1.547	0.571354	4.92E-09	4.71E-05	0.232	0.048	2.29E-12	732	0.630

* Values based on average of final two load increments.

Shaded boxes identify results that were based on limited responses or that deviate substantially from other replicate tests. This is associated with very high swelling capacity of low salinity systems.

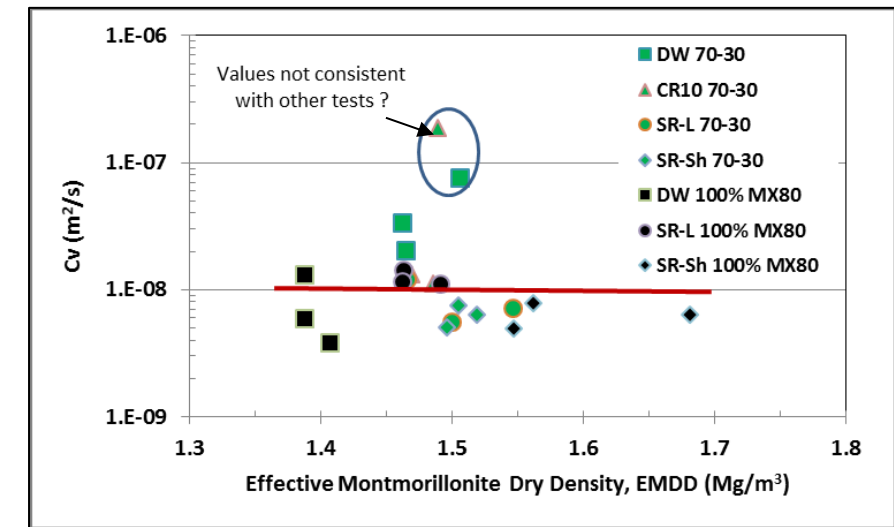
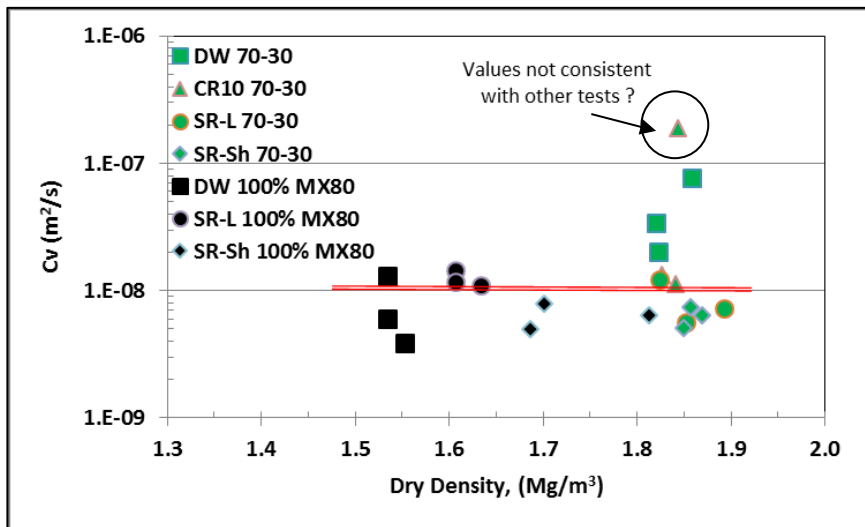
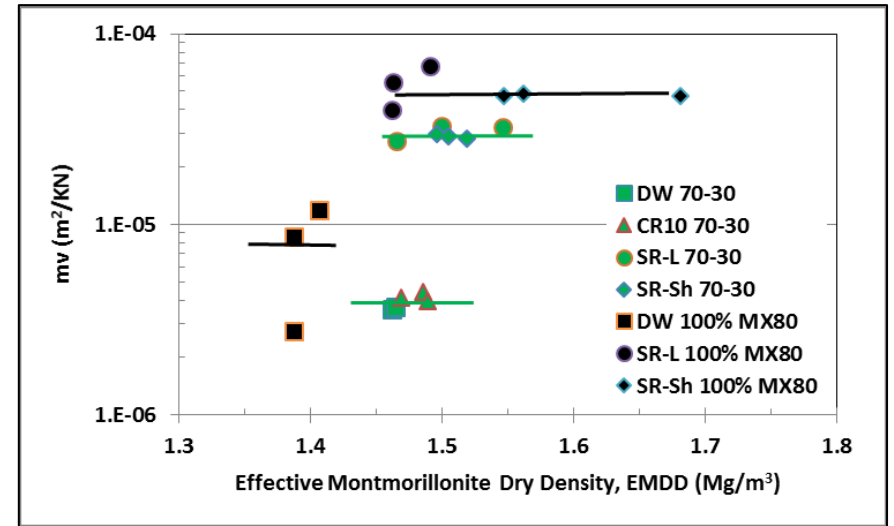
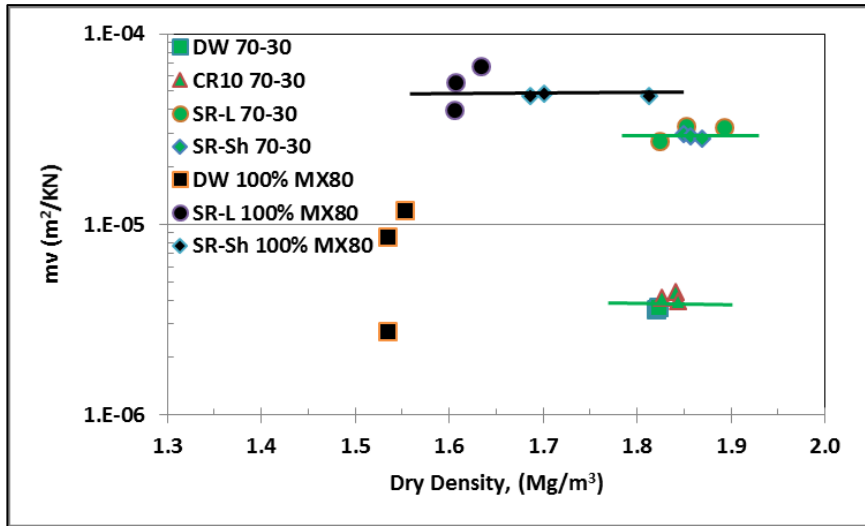


Figure 8.10: Effect of Pore Fluid Composition on Volume Compressibility (mv) and Swelling Index (C_s) Properties of 70:30 MX80:Sand Specimens and 100% MX80 clay.

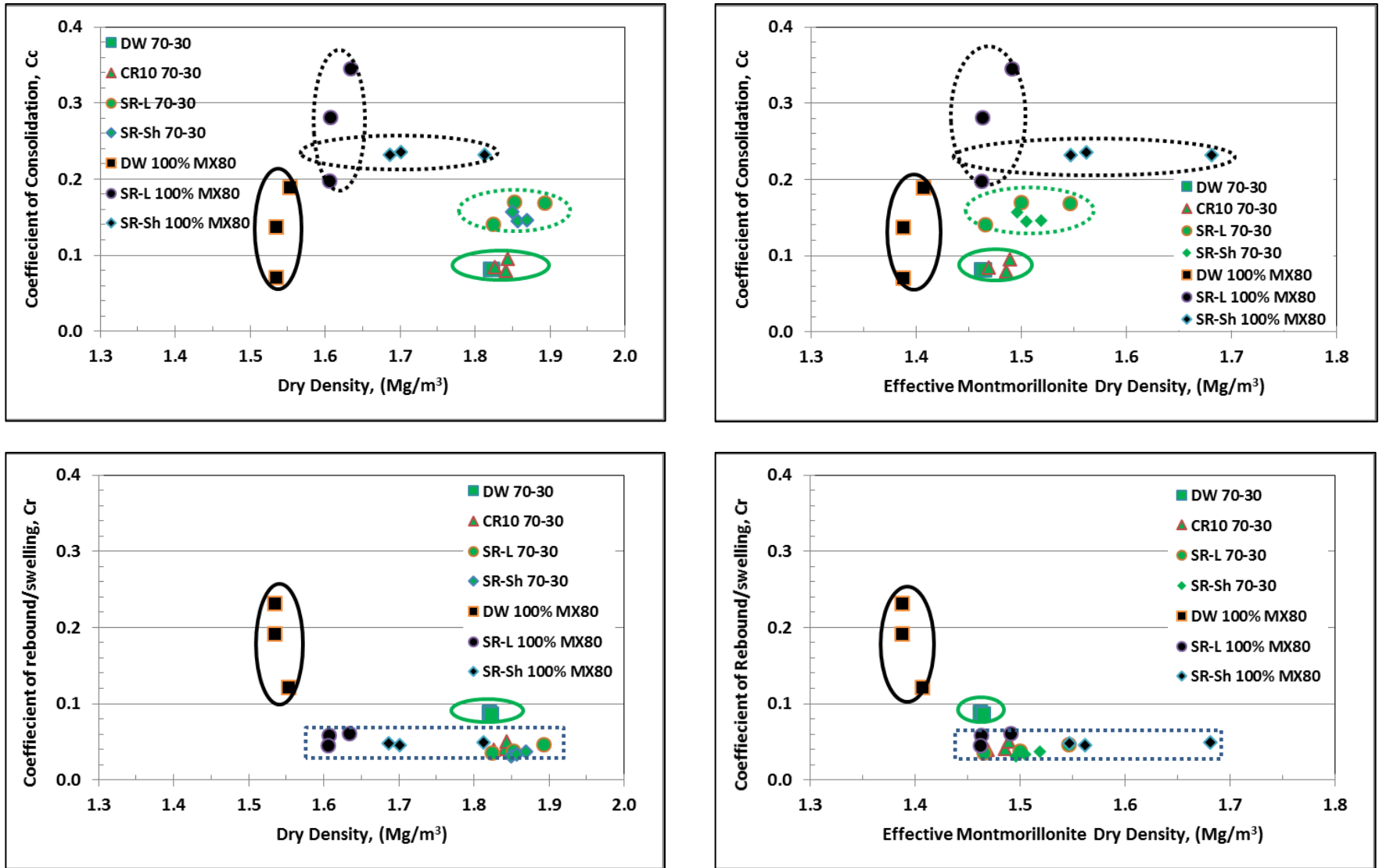


Figure 8.11: Effect of Pore Fluid Composition on Consolidation (Cc) and Swelling (Cr) Properties of 70:30 MX80:Sand Specimens and 100% MX80 Clay.

9. THERMAL PROPERTIES TESTING

9.1 BACKGROUND

The DGR will contain heat-generating UFCs and so the temperature of the materials surrounding them will increase for a period of time following installation. The ability of the materials closest to the UFCs will be HCB and further from the UFC there will be granular or pelletized bentonite gap fill. The BSM is not intended for use in the vicinity of the placement room and so will be less effected by the heat-generating UFCs and will also have a lesser effect on regional temperature development. Knowing the ability of the materials surrounding the UFC to conduct the heat outwards to the surrounding rock mass is vital in predicting the temperatures that will develop within the placement room.

The thermal conductivity and specific heat capacity of the two bentonite densities specified, using freshwater as the pore fluid have been measured using NWMO's Hot Disk Thermal Constants Analyzer (Model TPS1500). The system operates under non-steady state principles using a transient plane source (TPS) sensor sandwiched between two pucks of the material to be tested. The TPS supplies a quantity of heat over a set time and records the dissipation of the heat by the material tested. The rate of change of temperature measured in the material is used to determine the thermal conductivity. Operation of this device is described in a previous study by Martino and Man (2010).

Specimens were tested at degrees of saturation ranging from 0 to 100%, (in triplicate) from the lowest degree of saturation that allows for coherent specimens to be manufactured through to as close to 100% saturation as possible with as-built conditions. Three separate series of measurements were completed in order to obtain a measure of the repeatability of the specimen manufacture and test results.

9.2 THERMAL TESTING SETUP

9.2.1 Thermal Constants Analyzer (TPS1500) Description

The TPS1500 device (Hot Disk Thermal Constants Analyzer¹) operates by supplying a pulse of constant power via the sensor during the heating period. This power application results in heat generation and as a result, a temperature change occurs in the specimen. The change in temperature following this heating period is then measured using the same sensor. The resistance change in the sensor is recorded and internally analyzed by the device so that both the thermal conductivity and thermal diffusivity can be determined from a single recording.

Martino and Man (2010) used exactly the same device and testing method in an earlier study of sealing materials and described the system operation as follows:

“The system is based on a specially designed Wheatstone bridge with the Hot Disk sensor located in one of the arms. A Keithley 2400 source meter supplies a constant voltage across the bridge. Before the measurement, the bridge is automatically balanced and as the resistance of the sensor increases the bridge becomes increasingly unbalanced. A Keithley 2000 digital

¹ Hot Disk Constants Analyzer, TPS2500, manufactured by Hot Disk AB, Chalmers Science Park, Chalmers University of Technology, Sven Hultins gata 9 A, SE-412 88 Gothenberg, Sweden

voltmeter equipped with a scanner or multiplexing card, records the unbalanced voltage. From these recorded voltages it is possible to determine the temperature increase of the sensor and consequently the thermal transport properties of the material under test.

The sensor itself consists of an electrical conducting pattern in the shape of a double spiral etched out of a thin sheet of nickel. The nickel foil is chosen because of its high and well-known temperature coefficient of resistivity (TCR). The TCR for nickel is stable above and below temperatures of the 350°C and 400°C temperature. The current test series is done at ambient temperature (20°C to 23°C). The elevated temperatures for testing are planned to be no higher than 150°C.

The conducting pattern is supported on both sides with a thin insulating material. Thin Polyimide (Kapton) films with a thickness of 12.7 µm or 25 µm are used from cryogenic temperatures to about 500 K. This gives a total thickness of the sensor between 60 and 80 µm (including the thickness of the adhesive bonding the nickel to the Kapton). For measurements in a temperature range from 500 K to 1000 K, a special Mica insulation is employed. This insulation material is somewhat thicker (around 0.1 mm), which means the total thickness of the sensor is approximately 0.25 mm. The Kapton insulated sensors were used in testing for this programme” (Figure 9.1).

“There are four electrical connections to the double spiral in each sensor” (Figure 9.1). “Two of these contacts carry the electrical current. The other two have much thinner leads and are for sensing or controlling the voltage drop across the spiral. The four contact design permits measurement of resistance variations during the transient heating of the sample. Different materials will often require sensors of different radii. The radius of the sensor must always be considerably larger than the porosity or the void structure of the sample if the material is not dense or homogenous.”



Figure 9.1: Hot Disk Sensor Used in Current Thermal Testing

9.2.2 Testing Method

In order to accurately determine thermal conductivity and thermal diffusivity, the thickness of a specimen should not be less than the radius of the hot disk sensor. The sensor used in this testing program was 9.87 mm in diameter. The individual 50.6 mm diameter by 25 mm high clay disks used in testing were produced by compressing moisture-conditioned material into a

compaction cylinder using a hydraulic press and then extruding the disk. With the exception of the 0% saturation specimens (prepared at a small water content and then oven-dried to desaturate so-as to provide a specimen that could be handled and tested), all specimens were tested at their as-built condition. The sensor was placed horizontally between two identical disks. The timing of the test calls for measurement to be approximately equal to a^2/K , where “ a ” is the radius of the sensor and K is the thermal diffusivity of the material that is being tested. The MX80 clays tested in this study is known to have thermal diffusivity of approximately 0.4 to 0.7 mm²/s. From this estimation, the time required for completion of a reading should be between 116 to 270 seconds. In order to achieve stable readings (indicated by the device as green lights on the display) testing was done for 160 seconds for these two-sided (sandwich-type) tests.

Specimens were installed at room temperature (~20°C) into a stainless steel specimen holder with the sensor as shown in Figure 9.2. The assembled specimen-sensor assemblies used in this study were 50.6 mm diameter and 50 mm in thickness (two disks stacked vertically with sensor between them). A cylindrical cover (protection against temperature disturbances caused by air draft past the sample during the transient recording) is then placed over the assembly.



Figure 9.2: Thermal Test Setup Showing Sensor and Specimen installation.

9.2.3 Calculation of Thermal Properties

Specific heat is measured directly by this device and is defined as the amount of heat, measured in calories required to raise the temperature of one unit mass of material by one degree Kelvin (K). The Hot Disk programming expresses the value as volumetric heat capacity or (MJ/m³•K); where MJ is megajoules.

The derivation of thermal conductivity is based on the assumption that the sensor is located in an infinite material. As a result, the time available for the completion of a transient recording is limited by the size of the sample since the thermal disturbance induced by the sensor must not reach the exterior of the specimen during the test. An estimation of how far this thermal wave has proceeded in the sample during a recording is defined as the probing depth as follows:

$$\Delta p = 2 \cdot \sqrt{(K \cdot t)} \quad (9-1)$$

where: Δp is the probing depth (i.e., the shortest distance from sensor edge to specimen edge), K is the thermal diffusivity; and t is the measuring time.

This means that the distance from any point of the sensor to any point on the surface of the specimens must exceed Δp if the total measuring time is t . In order to determine both the thermal conductivity and thermal diffusivity with good accuracy, the thickness of a flat sample should not be less than the radius of the hot disk sensor.

The probing depth only provides an estimate of the required sample size as the thermal diffusivity of the material is unknown but can be estimated from known properties of materials. In practice the determination is by an iterative process.

As the Hot Disk sensor is electrically heated, the resistance increase as a function of time is given by:

$$R(t) = R_0\{1 + \alpha[\Delta T_i + \Delta T_{ave}(\tau)]\} \quad (9-2)$$

where: R_0 is the resistance of the disk prior to heating and time $(t) = 0$;
 α is the temperature coefficient of resistivity (TCR);
 ΔT_i is the constant temperature difference that develops nearly immediately over the insulation on the sensors; and
 $\Delta T_{ave}(\tau)$ is the average temperature increase of the sample surface in contact with the sensor.

The temperature increase recorded by the sensors can be represented by:

$$\Delta T_{ave}(\tau) + \Delta T_i = (1/\alpha) * (R(t)/R_0 - 1) \quad (9-3)$$

ΔT_i becomes a constant after a short time Δt_i , which can be estimated as:

$$\Delta t_i = (\delta^2/\kappa_i) \quad (9-4)$$

where: δ is the thickness of the insulating layer; and
 κ_i is the thermal diffusivity of the layer material

The time dependent temperature increase is given by:

$$\Delta T_{ave}(\tau) = (P_0/\pi^{3/2} a \Lambda) D(\tau) \quad (9-5)$$

where: P_0 is the power output from the sensor;
 a is the overall radius of the disk;
 Λ is the thermal conductivity of the sample; and
 $D(\tau)$ is a dimensionless time dependent function with:

$$\tau = \sqrt{t/\Theta} \quad (9-6)$$

where: t is the time measured from the start of measurement; and
 Θ is the "characteristic time"

The characteristic time is defined by:

$$\Theta = a^2/\kappa \quad (9-7)$$

By plotting the recorded temperature increase versus $D(\tau)$ a straight line is produced, the intercept of which is ΔT_i and the slope is $P_0/(\pi^{3/2} \cdot a \cdot \Lambda)$ using testing times longer than Δt_i .

Because this thermal diffusivity not known before testing the final straight line is determined through iteration.” (Martino and Man 2010).

9.3 RESULTS OF THERMAL CHARACTERIZATION TESTING

Using the materials and methods described above, two test series were completed to provide thermal information on compacted MX80 bentonite materials prepared using deionized water. These tests examined a full range of initial degrees of water saturation (~0 to ~100%) in order to fully assess the role of water saturation on behaviour.

The results of thermal testing and analysis are provided in Figure 9.3 through Figure 9.5 (Specific Heat (SH), thermal conductivity (TC) and thermal diffusivity (TD) respectively) and data values are provided in Appendix L. In addition to the results of the current testing series, data presented by Martino and Man (2010) for specimens prepared to a dry density of 1.5 Mg/m^3 using powdered (200 mesh) Wyoming bentonite of similar mineralogical composition are also provided for comparison and discussion purposes.

The plots of SH measurements provided in Figure 9.3 show that the MX80 specimens all showed very similar values for a given degree of water saturation and were not particularly sensitive to dry density (1.5 to 1.7 Mg/m^3 range). The values range from $\sim 1.25 \text{ MJ/m}^3\text{K}$ at 0% water saturation to approximately $3.0 \text{ MJ/m}^3\text{K}$ once a degree of saturation exceeding 60% has been achieved. 60% is approximately the point at which the water phase becomes continuously connected in the specimens (see also air conductivity behaviour discussed in Section 7.4). The data produced by Marino and Man (2010) track parallel to the MX80 data but are offset by approximately $0.6 \text{ MJ/m}^3\text{K}$ lower (1.0 to $\sim 2.25 \text{ MJ/m}^3\text{K}$ for saturations of 0 and 100%) than the current test results. As these two sets of data were conducted using the same measuring device and method and essentially mineralogically-identical bentonite, the differences are attributable to the textural differences in the materials tested. The 2010 study used a 200-mesh (powdered) Wyoming bentonite in the manufacture of the test specimens while the current study used a coarsely ground (80 mesh) material. These materials would be expected to exhibit different inter-aggregate pore size distributions and hence differences in how water and air are distributed, potentially causing differences in their SH values.

In Figure 9.4 the thermal conductivity measurements collected for the test specimens are plotted, as are the data from Martino and Man (2010). There is very limited scatter in the replicate measurements, providing confidence in the saturation-thermal conductivity trend lines presented. The denser (1.7 Mg/m^3 dry density) MX80 materials exhibit slightly higher TCs than the 1.5 Mg/m^3 materials at the same degree of saturation. This is attributable to the higher proportion of more thermally conductive mineral solids in the denser specimen, resulting in a slight increase in the ability of the material to conduct heat through it. The data from Martino and Man (2010) show slightly lower TC values for a given degree of saturation at moderate degrees of water saturation (~20-80% water saturation) than are observed for the MX80 material of similar dry density. At degrees of saturation outside of this range, behaviour was virtually identical to the MX80 material. As concluded previously, the differences at intermediate degree of saturation is likely the result of differences in pore structure with the coarser-grained materials having greater macro-pore interconnection and hence greater thermal conductivity.

The thermal conductivities observed at >80% and <20% degrees of saturation for all the 1.5 Mg/m^3 materials are comparable and can be attributed to the effects of a continuous air

phase at <20% saturation. At >80% saturation a continuous water phase is present and TC is dominated by the pore filling. At very low degree of water saturation (<10%) the data for all the specimens tested show insensitivity to change in saturation, at these very low water contents, heat transfer is determined by the contacts between minerals and any water present is tightly-held to the mineral surfaces and would behave as part of the mineral itself. It may also be attributed to micro-cracking of the specimen as the result of extreme drying.

The thermal diffusivity values for all tests are presented in Figure 9.5, TD is a ratio of the TC and the SH parameter values and so given the roughly opposite trends observed for those parameters. It is reasonable to expect that the TD values would show some change with changing degree of saturation for a given material density. This is seen in Figure 9.5, where there is little change in the TD with saturation until saturation exceeds approximately 60%. Beyond the 60% saturation value there is only a gradual increase in TD.

The TD of the materials reported by Martino and Man (2010) for 1.5 Mg/m³ dry density materials show a similar pattern of lack of change until saturation exceeds ~60% but the TD values observed are slightly higher than observed for the MX80 materials. As noted in discussion of TC data, it is unlikely that the slight increase in TD at very low degree of water saturation is a result of actual change in material behaviour, rather it is more likely a relict of the test method.

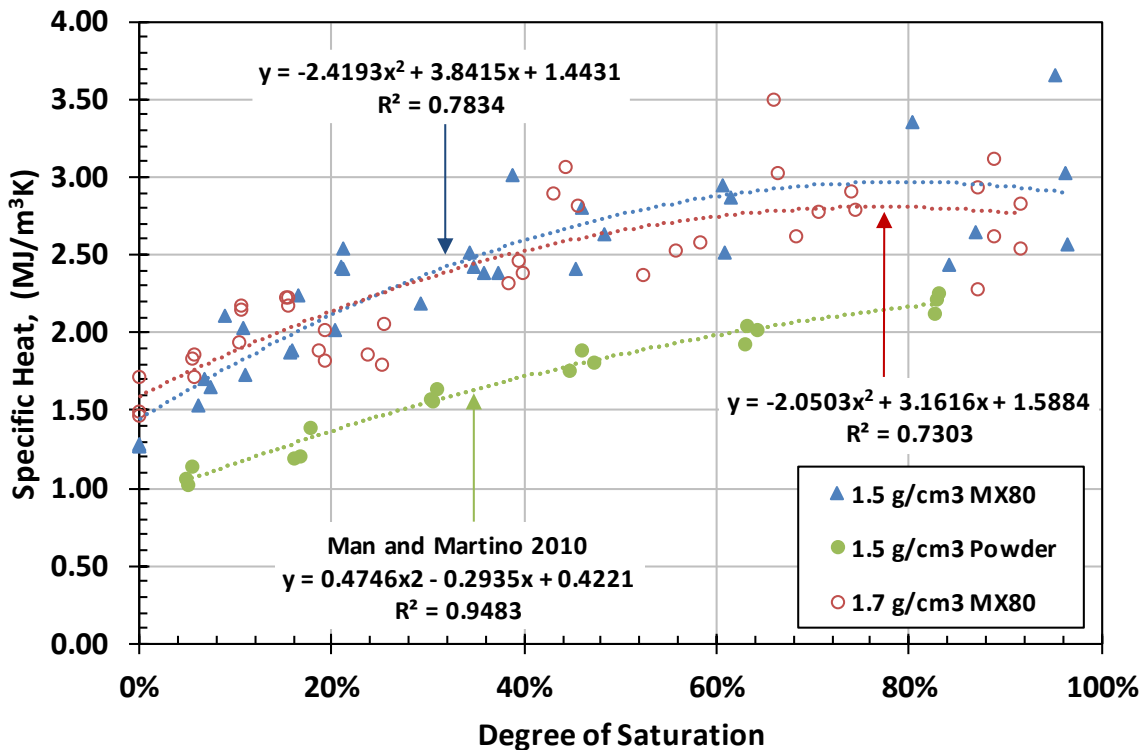


Figure 9.3: Specific Heat of MX80 and 200 Mesh Wyoming Bentonite Compacted Using Fresh Water.

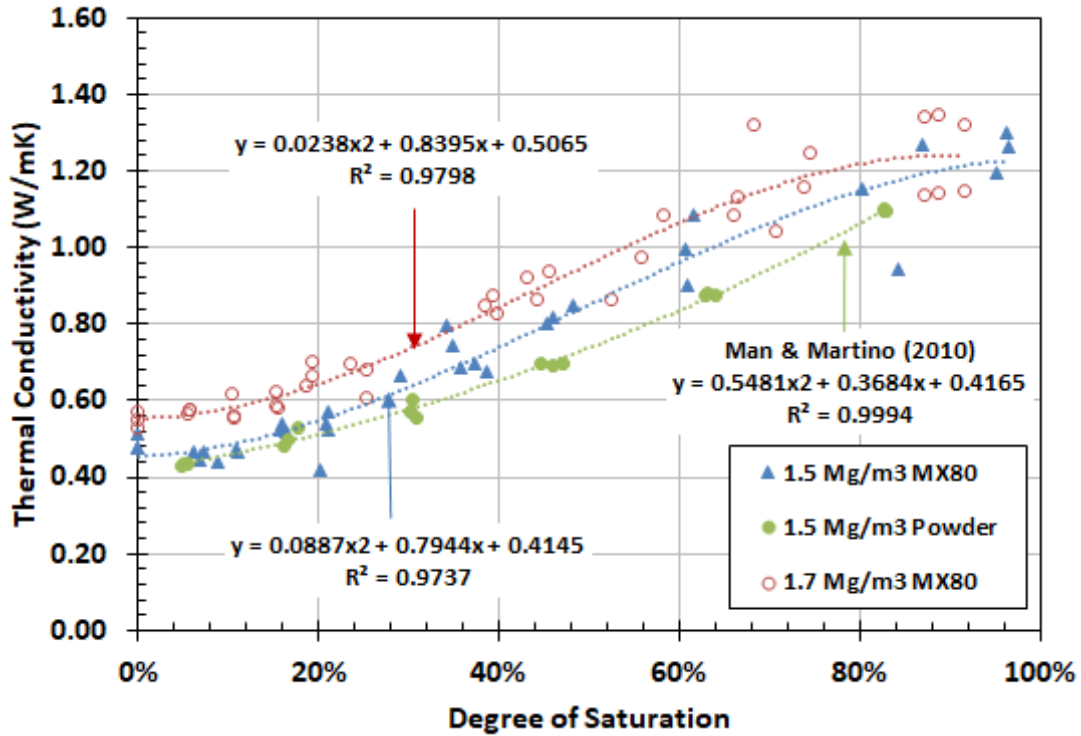


Figure 9.4: Thermal Conductivity of MX80 Bentonite and 200 Mesh Wyoming Bentonite Compacted Using Fresh Water (average of three readings).

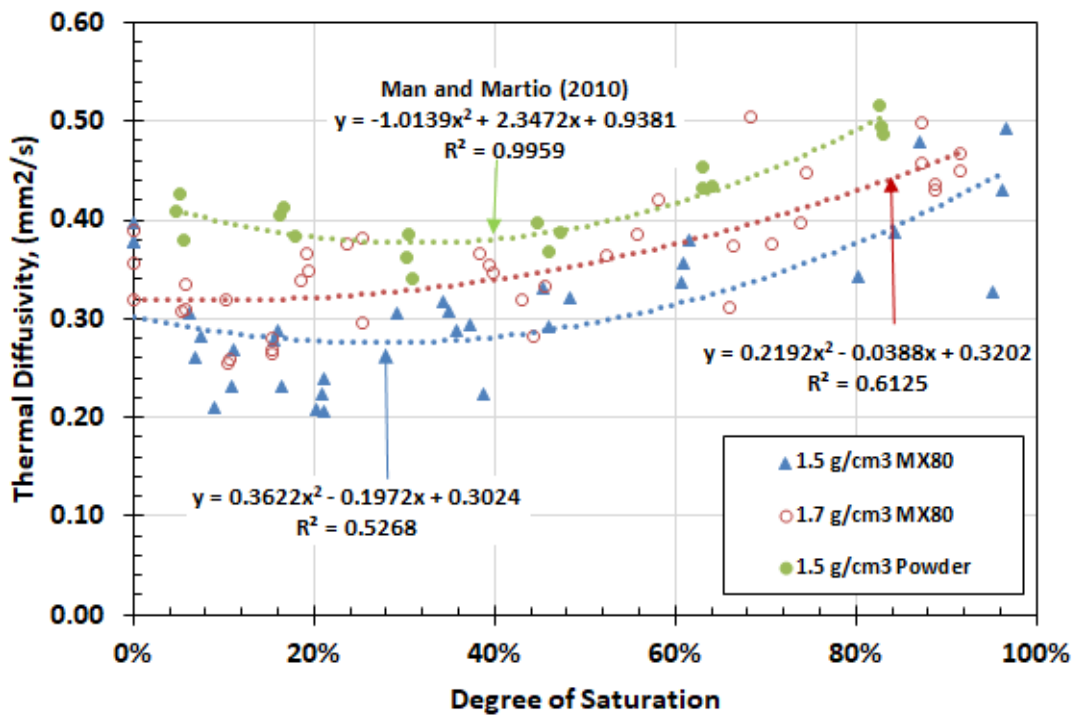


Figure 9.5: Thermal Diffusivity of MX80 and 200 Mesh Wyoming Bentonite Compacted Using Fresh Water (average of three readings).

9.4 SUMMARY OF THERMAL CHARACTERIZATION TESTS

The thermal characterisation testing was successful with very consistent results being obtained for most of the specimens. A complete set of analytical measurements are provided in Appendix L and from these data and the summary plots provided above it can be concluded that the following bounds and variabilities can be placed on the thermal behaviour of compacted MX80 bentonite:

- Dry density variability of replicate specimens is typically $\pm 0.02 \text{ Mg/m}^3$;
- Degree of saturation determined by replicate specimens typically varied within $\pm 3\%$ range;
- Specific heat in 1.5 Mg/m^3 specimens ranged from 1.25 to $3.0 \text{ MJ/m}^3\text{K}$ for 0 to 100% water saturation;
- Standard deviation of SH values (for 1.5 Mg/m^3 specimens) was typically $\sim 8\%$ of the average for a given degree of saturation;
- Specific heat in 1.7 Mg/m^3 specimens ranged from 1.25 to $3.0 \text{ MJ/m}^3\text{K}$ for 0 to 100% water saturation;
- Standard deviation of SH values (for 1.7 Mg/m^3 specimens) was typically $\sim 5\%$ of the average for a given degree of saturation;
- Thermal conductivity of 1.5 Mg/m^3 specimens 0.40 to 1.3 W/mK for 0 to 100% saturation;
- Standard deviation of TC values (for 1.5 Mg/m^3 specimens) can be as much as 12% of the average value for a given degree of saturation but data typically was within $\sim 5\%$;
- Thermal conductivity of 1.7 Mg/m^3 specimens ranged from 0.50 to $\sim 1.35 \text{ W/mK}$;
- Standard deviation of TC values (for 1.7 Mg/m^3 specimens) can be as much as 9% of the average value for a given degree of saturation but are typically about 5%;
- Thermal diffusivity in 1.5 Mg/m^3 specimens ranged from 1.25 to $3.0 \text{ MJ/m}^3\text{K}$ for 0 to 100% water saturation;
- Standard deviation of SH values (for 1.5 Mg/m^3 specimens) can be as much as 16% of the average value for a given degree of saturation but are typically about 8%;
- Thermal diffusivity in 1.7 Mg/m^3 specimens ranged from 1.25 to $3.0 \text{ MJ/m}^3\text{K}$ for 0 to 100% water saturation;
- Standard deviation of SH values (for 1.5 Mg/m^3 specimens) can be as much as 15% of the average value for a given degree of saturation but are typically about 7%; and
- There is an apparent effect of granularity of the raw materials used to manufacture the compacted bentonite on thermal properties. Previously completed tests using the same equipment and preparation methods but using a powdered bentonite rather than the current coarser grained MX80 exhibited slightly lower SH and TC, and slightly higher TD.

10. SUMMARY: COMPILATION OF PARAMETER VALUES

This report contains a large body of characterisation data associated with the bentonite and bentonite-sand materials being considered for use in NWMO deep geological repository concepts. Testing focussed on completion of materials properties and behaviour characterisation tests with triplicate tests completed when-ever possible for each parameter measured in order to develop a better sense of the variability that can be expected when measurements are made. These data provide improved bounding values for parameters that may need to be input into safety assessment and other models and also identify which parameters are most sensitive to changes in local conditions.

The data collected is summarised below in Table 10.1 through Table 10.3, providing where-ever possible averages, standard deviations and basic descriptive equations for the parameters measured. For the air permeability, air conductivity and SWCC trend lines, their more complex behaviour required use of Van Genuchten-type equations to describe their behaviour. The fitting parameters associated with these equations for each material and pore fluid tested are provided in Tables 10.1 through 10.3.

The MX80 bentonite used in this study contains the following x-ray detectable mineral components: Montmorillonite $87\pm 8\%$, Illite $tr-7\%$; Quartz $2.5\pm 1\%$; Feldspars $3-7\%$; Calcite $2.9\pm 0.7\%$; others $\sim 4.5\%$ as determined from raw material. For the purposes of conservative estimation of swelling behaviour, a value at the lower end of the range of measured montmorillonite content (80%) was used in derivation of the EMDD parameter for test specimens. Mineralogical composition showed no discernible change as the result of 18 months of soaking in CR10, SR-L or SR-Sh saline solutions. Slight changes to the chemical composition of the specimens was observed and were associated with soluble cations (Na, K, Ca) and are attributed to cation exchange on the clay surfaces. A further analysis of these materials following ~ 4 years of further interaction is planned by NWMO as part of a successor testing program.

The compaction properties of MX80 and 70:30 BSM are little effected by the salinity of the water used to hydrate the clay to be compacted. The maximum compaction dry density (modified compaction density) of the BSM is approximately 12% higher than for a 100% clay system.

Salinity of the porefluid will strongly affect the volumetric swelling capacity (free swell, FS) as well as the Consistency (Atterberg) Limits of bentonite (and hence bentonite-aggregate materials). Commonly used as a quality check for bentonite quality it should be noted that even small increase in TDS (from ~ 0 to 11 g/L) results in substantial reduction in these values and so could be interpreted as compositionally substandard rather than as a result of change in the TDS in the material. Liquid Limit (LL) of materials examined in this study decreased from ~ 350 to 48 %. It would also appear that at high TDS conditions (>225 g/L), the effect of a further increase in TDS, results in limited further reduction in free swell or consistency limits. Even when tested by experienced laboratories, the LL and FS values measured for identical materials can vary 5 to 6 % of the measured value.

The swelling pressure (Ps) developed by the MX80 and BSM is critical to achieving the desired system performance. A positive contact must be present at the interface between the clay and the surrounding rock mass once saturation is achieved. Literature-derived values are very comparable to the results obtained in the current study, providing confidence in the repeatability

of these measurements. There is considerable scatter in the available data, but this can be reduced through use of normalizing parameters such as EMDD that account for known differences in the swelling clay content in different batches of MX80. Data shows clear trends of increasing Ps with increasing dry density as well as a strong effect of salinity. For the materials and densities examined in this study, there is almost a one-order-of-magnitude reduction in Ps when salinity is increased from 0-11 g/L to >100 g/L (NaCl) with limited further effect when salinity increases beyond approximately 100 g/L.

The hydraulic conductivity (k) of MX80 and BSM is another key parameter in assessing performance of the sealing systems. The fluid-saturated MX80 and BSM must maintain diffusion-dominated mass transport characteristics ($k < 10^{-10}$ m/s) under all potential environmental conditions. k is strongly influenced by density (> density the lower is k), over the range of density of interest in a DGR. It is also influenced by the porefluid TDS and hence changes to its surroundings. For a given density and material composition, k increases markedly with increase of TDS. For a TDS of < 11 g/L the k can be as much as 1 to 2 orders of magnitude lower than for a material exposed to a fluid having TDS of 100-335 g/L, with difference increasing with decreasing specimen density. While TDS strongly affects k, it should be noted that even in a brine environment, a k of $< 10^{-10}$ m/s will be achieved in MX80 having a dry density of > 1.2 Mg/m³ dry density (EMDD ~ 1.06 Mg/m³). In a 70:30 BSM this would be accomplished at a dry density of approximately 1.45 Mg/m³. As density increases beyond these lower limit values, k decreases substantially reaching 10^{-11} (brine) to 10^{-13} (fresh water) m/s for the reference dry densities for HCB and BSM.

The movement of air (gas) through the clay-based sealing materials needs to be understood in order to evaluate how gases generated within the DGR will move or develop pressures within confined volumes in the repository. Gas can be generated by a variety of means, including radiolysis, microbial activity and corrosion of the iron components within the repository. In order to assess gas movement there are several parameters that need to be developed, including drying shrinkage, soil-water characteristic curves, and then directly measured gas flow measurements.

Tests to determine drying shrinkage behaviour observed that 70:30 BSM exhibits very limited shrinkage, a maximum of approximately 7-8 % when high salinity is present and only slightly higher (~8.5%) for freshwater systems. The result of shrinkage is increased density of the material if it remains intact during drying. MX80 in freshwater dried to a final density of ~1.95 Mg/m³ and where saline porefluid was present a final dry density of ~1.82 Mg/m³ was achieved. The drying of BSM resulted in achieving final dry densities of approximately 1.96 Mg/m³ and 1.92 Mg/m³ where freshwater and brine porefluids were present respectively. The difference in shrinkage behaviour in high TDS materials is attributed to the formation of salt crystals in the soil matrix as drying progresses, resulting in an inability for the soil particles to move closer together. These data show the same pattern of behaviour with respect to elevated salinity as have been observed for other parameters with limited, or no incremental effect of increasing salinity at high TDS levels (e.g. 223 and 335 g/L). These data indicate that there is potential for drying shrinkage in both the HCB and BSM materials and in an environment where complete desiccation occurs there could be change in the UFC's location in a placement room. It should be noted that this requires the as-placed materials to undergo complete drying with no compensating support as the result of swelling of perimeter materials.

The Soil Water Characteristic Curve (SWCC) is a measure of the relationship between the quantity of water held by the soil and the negative porewater pressure (suction) that is needed to remove this fluid. This parameter is important as it describes the amount of water that will be held in the clay and the force with which the clay or BSM will draw water from adjacent regions (e.g. rock). This will influence both material shrinkage potential as well as the thermal, hydraulic and mechanical behaviour of the MX80 or BSM as the suction forces act to hold the material together and resist desaturation. This will therefore also influence gas movement since gas movement requires contiguous dry pores to allow for its movement through the barrier materials. The SWCCs measured show a lower degree of fluid retention in low TDS systems than in brine. The behaviour of MX80 and BSM are discernibly different and may be attributed to differences in their porosity and also their pore size distributions.

Air (gas) permeabilities of MX80 at 1.5 Mg/m³ dry density and BSM at 1.8 Mg/m³ dry density were determined for a range of specimen degrees of saturation and also where freshwater and brine porefluids are present. The ~1.5 Mg/m³ dry density MX80 has an air conductivity at least one order of magnitude higher than the ~1.8 Mg/m³ BSM at low (<~20%) degree of water saturation. This difference is attributable to the different porosities (and perhaps pore size distribution) of bentonite-only (~0.45) versus bentonite-sand systems (~0.35), that could result in easier air movement. The data also indicate that at greater than approximately 75% water saturation, the pore spaces containing air become discontinuous and the ability of air/gas to pass through the soil becomes increasingly restricted. The higher viscosity of brine versus low salinity water may also be a contributor to the observed behaviour. It can be concluded that the AC and AP of MX80 and the 70:30 MX80:sand materials is determined by the porosity (dry density) and degree of fluid saturation of the systems. The clay:sand ratio and pore fluid TDS of these materials play secondary roles in determining the movement of air.

Triaxial tests were completed on a limited number of MX80, HCB and BSM materials in order to determine some of their key mechanical properties. These are of particular importance with respect to prediction of their ability to support the UFC and also how the sealing materials will deform under UFC or other externally-applied (e.g. rock movement-induced) loadings. The parameters of particular importance in developing an understanding (and hence ability to predict) the mechanical behaviour of the MX80 and BSM materials and the deformation-describing results obtained from the testing described in Section 8 are: Bulk Modulus (K); Elastic-plastic parameters (κ and λ); Shear Modulus (G) and Young's Modulus (E).

Consolidation behaviour of the MX80 is important to determining the potential for the UFC to move vertically from its as-placed location as the result of swelling pressure developed by the bentonite or load-induced compression of the underlying HCB. There are a number of deformation parameters that need to be known in order to undertake such estimations and some of these can be determined using one-dimensional compression tests. These data also provide supplemental information regarding the elastic and hardening parameters from triaxial tests. The parameters derived from these tests are:

- Coefficient of Consolidation C_c : Influenced by salinity, bentonite-only systems show higher values than for the BSM for the same dry density. This parameter will need to be defined for each salinity and BSM formulation considered
- Rebound Coefficient C_r : Is strongly influenced by salinity at low TDS. MX80 has a C_r or ~0.18, twice than for the BSM examined. It is relatively insensitive to TDS change once high TDS conditions where values are similar for the compacted bentonite and BSM

(0.04) examined in this study. This behavioural pattern is related to the reduction in swelling capacity under high TDS conditions.

- Apparent Preconsolidation Pressure σ_p' : Is very dependent on density and porefluid salinity. For swelling clay systems this parameter is very much related to swelling pressure, which increases with density and EMDD over the range considered in this study. This parameter's value is in the order of 600 to 775 kPa for high TDS systems and 3600 to 5450 kPa for low TDS systems of the type and density examined.
- Volume Compressibility mv : Is essentially constant at $\sim 4E-5$ mm²/kN for the low TDS systems examined and is approximately one order of magnitude higher under brine conditions. The presence of a 30% sand content does not seem to substantially effect this parameter.
- Coefficient of Volume Change C_v : Is little effected by salinity or the presence of a sand component over the range of density and materials examined. It can be assumed to be a constant of $1E-8$ m²/s (with an uncertainty of approximately ½ order of magnitude).

Thermal characterization done in this study was for MX80 bentonite only, at dry densities of 1.5 and 1.7 Mg/m³ with freshwater as the porefluid. The parameters of specific heat (SH), thermal conductivity (TC) and thermal diffusivity (TD) were all determined and equations describing their behaviour were generated.

- SH increases with increasing degree of saturation until saturation exceeds approximately 50% and is relatively insensitive to further increase in saturation. It is not discernibly affected by change in dry density (1.5 and 1.7 Mg/m³ dry density) and appears to be sensitive to soil texture with materials prepared from powdered bentonite having a discernibly lower SH.
- TC increases with dry density and also degree of saturation. The TC of specimens prepared using powdered bentonite was 10-25% lower than those prepared from coarser-grained MX80 at the same dry density and degree of saturation. This is attributed to differences in the pore-size distribution as well as differences in the interparticle contacts. These data if confirmed by further testing, highlight the need to use a consistent bentonite material for production of the sealing system components.
- TD increases $\sim 10-15\%$ with increase in bentonite dry density from 1.5 to 1.7 Mg/m³. Tests of compacted materials made from a powdered rather than fine granular showed a 30% increase in TD values for the 1.5 Mg/m³ bentonite. For a given dry density TD changes very little with degree of water saturation with a slight increase being observed when degree of saturation exceeds approximately 50%.

Table 10.1: Summary of Materials Properties and Behaviour Data (MX80 at ~1.5 Mg/m³ Dry Density, EMDD = 1.35 Mg/m³)

Parameter	DW	CR10	SR-L	SR-Sh
Swelling Pressure, Ps (MPa)	4.06 Ps=0.003*e ^{5.329*EMDD}	2.55 Ps=0.0008e ^{5.9635*EMDD}	0.60 Ps=0.00005e ^{6.9442*EMDD}	0.67 Ps=0.0001e ^{6.5134*EMDD}
Hydraulic Conductivity, k (m/s)	1.48E-13 k=6E-13*EMDD ^{-4.635}	1.38E-13 k=1E-12*EMDD ^{-6.552}	1.48E-12 k=8E-11*EMDD ^{-13.27}	2.1E-11 k=2E-9*EMDD ^{-15.07}
Water Permeability, K (m ²)	1.51E-20 K=6E-20*EMDD ^{-4.635}	1.43E-20 K=9E-20*EMDD ^{-5.684}	2.48E-19 K=1E-17*EMDD ^{-13.27}	4.04E-18 K=3E-16*EMDD ^{-15.07}
Free Swell (cc/g)**	16.3	3.6	2.1	1.8
Drying Shrinkage (vol. %)	~23	NM	< 18	< 18
Specific density of solids: Bentonite	2.72	2.72	2.72	2.72
Porosity (vol voids / total vol.)	0.449	0.449	0.449**	0.449**
Void ratio, e (vol. voids / vol. solids)	0.815	0.815**	0.815**	0.815**
Shrinkage (Table 7.1)	A _{sh} = 0.41 B _{sh} = 0.15 C _{sh} = 3.38	NM	A _{sh} = 0.52 B _{sh} = 0.19 C _{sh} = 2.17	A _{sh} = 0.50 B _{sh} = 0.18 C _{sh} = 1.83
SWCC (Table 7.2)	m = 4.46 n = 1.02 α (1/Pa) = 2.91E-9 S _{ir} = 0.01	NM	m = 0.47 n = 3.57 α (1/Pa) = 1.68E-8 S _{ir} = 0.01	m = 0.52 n = 3.99 α (1/Pa) = 1.35E-8 S _{ir} = 0.01
Air Permeability (AP) (m ²) Saturation vs AP plots (Table 7.3)	m = 1.24 S _{gr} = 0.11 K _a = 1.759E-6 S _{ir} = 0	NM	m = 1.34 S _{gr} = 0.06 K _a = 1.513E-6 S _{ir} = 0	m = 1.02 S _{gr} = 0.14 K _a = 4.872E-7 S _{ir} = 0
Air conductivity (m/s)	AC = AP * 6.40E+5	NM	AC = AP * 6.40E+5	AC = AP * 6.40E+5
Bulk Modulus***, K = δp'/δε _v	53.8	NM	26	14.9
κ	0.104 0.079+++	NM	0.075 0.024+++	0.121 0.021+++
λ	0.0576+++	NM	0.119+++	0.101+++
Shear Modulus, G = δq/3δε ₁	31	NM	16.4	16.2
Young's Modulus, E = δσ ₁ '/δε ₁	NM	NM	NM	NM
M	0.31	NM	0.84	1.09
Φ'	8.5	NM	21.6	27.5
Cc	0.133	NM	0.275	0.233*

Parameter	DW	CR10	SR-L	SR-Sh
Cs (Cr)	0.182	NM	0.055	0.047 ⁺
Cv (m ² /s)	7.6E-9 (average) (0.4 to 1.5E-8) range	NM	1.2E-8 (average) (1 to 2E-8) range	6.4E-9 (average) ⁺ (5 to 8E-9) range
Mv (m ² /KN)	7.7E-6 (average) (0.3 to 1.2E-5) range	NM	5.5E-5 (average) (4 to 6.8E-5) range	4.7E-5 ⁺ (4.7-4.9E-5) range
Thermal Conductivity (TC) (W/mK)	= 0.0887S ² + 0.7944S + 0.4145 (0.4 to ~1.3) range	NM	NM	NM
Thermal Diffusivity (TD) (mm ² /s)	= 0.335S ² - 0.1765S + 0.3032 (~0.2 to ~0.45) range	NM	NM	NM
Specific Heat Capacity (SHC)	= -2.4755S ² + 3.9067S + 1.4394 (1.25 to ~3) range	NM	NM	NM

* Density referenced is the initial density of specimens. This may change in the course of testing (e.g. drying shrinkage, consolidation).

** does not take into account any precipitated salts;

*** values are strongly affected by confining pressures

⁺ Specimen was higher density than targeted when it reached the state where values could be derived (~1.7 Mg/m³)

⁺⁺ Free swell of loose clay in large volume of solution.

⁺⁺⁺ Value derived from 1-D oedometer test

NM not measured, not part of testing matrix or cannot be derived from test results;

S is degree of saturation (%);

Table 10.2: Summary of Materials Properties and Behaviour Data (MX80 at ~1.7 Mg/m³ Dry Density, EMDD = 1.56 Mg/m³)

Parameter	DW	CR10	SR-L	SR-Sh
Swelling Pressure, Ps (MPa)	12.3 $Ps = 0.003 \cdot e^{5.329 \cdot EMDD}$	8.8 $Ps = 0.0008e^{5.9635 \cdot EMDD}$	2.6 $Ps = 0.00005e^{6.9442 \cdot EMDD}$	2.6 $Ps = 0.0001e^{6.5134 \cdot EMDD}$
Hydraulic Conductivity, k (m/s)	7.6E-14 $k = 6E-13 \cdot EMDD^{-4.635}$	5.4E-14 $k = 1E-12 \cdot EMDD^{-6.552}$	2.2E-13 $k = 8E-11 \cdot EMDD^{-13.27}$	2.4E-12 $k = 2E-9 \cdot EMDD^{-15.07}$
Water Permeability, K (m ²)	7.8E-21 $K = 6E-20 \cdot EMDD^{-4.635}$	5.6E-21 $K = 9E-20 \cdot EMDD^{-5.684}$	3.8E-20 $K = 1E-17 \cdot EMDD^{-13.27}$	4.7E-19 $K = 3E-16 \cdot EMDD^{-15.07}$
Drying Shrinkage (vol. %)	See table 10.1	See table 10.1	See table 10.1	See table 10.1
Specific density of solids: Bentonite	2.72	2.72	2.72	2.72
Porosity (vol voids / total vol.)	0.375	0.375	0.375	0.375
Void ratio e (vol voids/vol soil solids)	0.600	0.600	0.600	0.600
Shrinkage	See table 10.1	NM	See table 10.1	See table 10.1
SWCC	See table 10.1	NM	See table 10.1	See table 10.1
Air Permeability (m ²)	NM	NM	NM	NM
Air conductivity (m/s)	$AC = AP \cdot 6.40E+5$	$AC = AP \cdot 6.40E+5$	$AC = AP \cdot 6.40E+5$	$AC = AP \cdot 6.40E+5$
Bulk Modulus***, $K = \delta p' / \delta \epsilon_v$	NM	NM	NM	NM
κ	See table 10.1	NM	See table 10.1	0.101+++
λ	See table 10.1	NM	See table 10.1	See table 10.1
Shear Modulus, $G = \delta q / 3 \delta \epsilon_1$	60.3	NM	NM	NM
Young's Modulus, $E = \delta \sigma_1' / \delta \epsilon_1$	150-214	NM	NM	NM
M	0.51-0.66	NM	NM	NM
Φ' (°)	13.6-17.3	NM	NM	NM
Cc	0.06-0.2 estimated	NM	0.2 - 0.34 estimated	0.233+
Cs (Cr)	0.2 estimated	NM	0.55 estimated	0.047+
Cv (m ² /s)	1E-8 estimated	NM	1E-8 estimated	6.4E-9 (average) + (5 to 8E-9) range
Mv (m ² /KN)	1E-5 estimated	NM	5E-5 estimated	4.7E-5+ (4.7 - 4.9E-5) range

Parameter	DW	CR10	SR-L	SR-Sh
Air Permeability (AP)** (m ²) From saturation vs AP plots Data from Barone et al. (2014) (Van Genuchten fitting functions provided in Table 7.3)	m = 1.19 S _{gr} = 0.01 K _a = 1.0E-7 S _{ir} = 0	m = 1.30 S _{gr} = 0.01 K _a = 1.4E-7 S _{ir} = 0	<u>SR160 solution</u> m = 1.08 S _{gr} = 0.10 K _a = 5.0E-8 S _{ir} = 0	<u>SR270 solution</u> m = 0.90 S _{gr} = 0.10 K _a = 3.0E-8 S _{ir} = 0
Thermal Conductivity, TC (W/mK)	= 0.0238S ² + 0.8395S + 0.5065 (0.5 to ~1.35) range	NM	NM	NM
Thermal Diffusivity, TD (mm ² /s)	= 0.2233S ² - 0.0408S + 0.3204 (~0.25 to ~0.5) range	NM	NM	NM
Specific Heat Capacity, SH (MJ/m ³ K)	= -1.8304S ² + 2.9413S + 1.6128 (~1.5 to ~3) range	NM	NM	NM

* Density referenced is the initial density of specimens. This may change in the course of testing (e.g. drying shrinkage, consolidation).

** does not take into account any precipitated salts;

*** value strongly affected by confining pressure

+ Specimen not part of original testing matrix, specimens were not able to be reliably tested at lower density.

+++ Value derived from 1-D Oedometer test

S is degree of saturation (%);

NM not measured, not part of assigned testing matrix or cannot be determined from test data;

Estimated = value based on extrapolation of lab test data

Table 10.3: Summary of Properties and Behaviour Data (70:30 MX80:Sand at ~1.7 Mg/m³ Dry Density; EMDD ~1.37 Mg/m³)

Parameter	DW	CR10	SR-L	SR-Sh
Swelling Pressure, Ps (MPa)	3.5 $P_s = 0.003 * e^{5.329 * EMDD}$	2.2 $P_s = 0.0008e^{5.9635 * EMDD}$	0.5 $P_s = 0.00005e^{6.9442 * EMDD}$	0.57 $P_s = 0.0001e^{6.5134 * EMDD}$
Hydraulic Conductivity, k (m/s)	1.6E-13 $k = 6E-13 * EMDD^{-4.635}$	1.6E-13 $k = 1E-12 * EMDD^{-6.552}$	1.9E-12 $k = 8E-11 * EMDD^{-13.27}$	2.8E-11 $k = 2E-9 * EMDD^{-15.07}$
Water Permeability, K (m ²)	1.7E-20 $K = 6E-20 * EMDD^{-4.635}$	1.6E-20 $K = 9E-20 * EMDD^{-5.684}$	3.2E-19 $K = 1E-17 * EMDD^{-13.27}$	5.4E-18 $K = 3E-16 * EMDD^{-15.07}$
Free Swell (cc/g)	9.4	2.7	1.9	1.5
Max. Drying Shrinkage (vol. %)	<8 8.5% ⁺	<8 6.3% ⁺	<8 5.6% ⁺	<8 4.5% ⁺
Specific density of solids mixture	2.70	2.70	2.70	2.70
Porosity (vol voids / total vol.)	0.370	0.370	0.370	0.370
Void ratio e (vol voids/vol soil solids)	0.588	0.588	0.588	0.588
Shrinkage (Table 7.1)	A _{sh} = 0.39 B _{sh} = 0.15 C _{sh} = 4.90	A _{sh} = 0.38 B _{sh} = 0.14 C _{sh} = 6.13	A _{sh} = 0.40 B _{sh} = 0.15 C _{sh} = 3.14	A _{sh} = 0.41 B _{sh} = 0.15 C _{sh} = 2.94
SWCC (Table 7.2)	m = 5.90 n = 1.36 α (1/Pa) = 2.60E-9 S _{ir} = 0.01	m = 4.37 n = 1.25 α (1/Pa) = 3.18E-9 S _{ir} = 0.01	m = 4.70 n = 2.11 α (1/Pa) = 3.87E-9 S _{ir} = 0.01	m = 4.90 n = 1.77 α (1/Pa) = 3.87E-9 S _{ir} = 0.01
Air Permeability (AP) (m ²) Saturation vs AP plots (Table 7.3)	m = 1.34 S _{gr} = 0.14 K _a = 2.557E-7 S _{ir} = 0	m = 1.40 S _{gr} = 0.15 K _a = 2.97E-7 S _{ir} = 0	m = 1.57 S _{gr} = 0.04 K _a = 2.856E-7 S _{ir} = 0	m = 1.54 S _{gr} = 0.12 K _a = 2.181E-7 S _{ir} = 0
Air Permeability (AP) ⁺⁺ (m ²) Data from Barone et al. (2014)	m = 1.19	m = 1.30	<u>SR160 solution</u> m = 1.08	<u>SR270 solution</u> m = 0.90

Parameter	DW	CR10	SR-L	SR-Sh
(van Genuchten fitting functions used in Equation provided in Section 7.4.1)	$S_{gr} = 0.01$ $K_a = 1.0E-7$ $S_{ir} = 0$	$S_{gr} = 0.01$ $K_a = 1.4E-7$ $S_{ir} = 0$	$S_{gr} = 0.10$ $K_a = 5.0E-8$ $S_{ir} = 0$	$S_{gr} = 0.10$ $K_a = 3.0E-8$ $S_{ir} = 0$
Air conductivity, AC (m/s)	$AC = AP * 6.40E+5$			
Bulk Modulus, $K = \delta p' / \delta \epsilon_v$	189	308	44.6	34.4
κ	0.0372+++	0.0315+++	0.0384 0.018+++	0.0494 0.015+++
λ	0.0784 0.0366+++	0.0475 0.015+++	0.074+++	0.065+++
Shear Modulus, $G = \delta q / 3\delta \epsilon_1$	109-285	201	19	24.6
Young's Modulus, $E = \delta \sigma_1' / \delta \epsilon_1$	278-427	NM	NM	NM
M^{***}	0.28-0.66	0.32	1	1
Φ' (°)	7.7-16.3	8.7	25.4	25.4
Cc	0.084	0.087	0.160	0.149
Cs (Cr)	0.079	0.044	0.040	0.034
Cv (m ² /s)	4.4E-8	1.2E-8+++	8.3E-9	6.3E-9
Mv (m ² /KN)	3.5E-6	4.2E-6	3.1E-5	2.9E-5
Thermal Conductivity (W/mK)	NM	NM	NM	NM
Thermal Diffusivity (mm ² /s)	NM	NM	NM	NM
Specific Heat Capacity	NM	NM	NM	NM

* Density referenced is the initial density of specimens. This may change in the course of testing (e.g. drying shrinkage, consolidation).

** does not take into account any precipitated salts

*** value strongly effected by confining pressure

+ Data from Barone et al. (2014) for 70:30 BSM at ~1.5-1.65 Mg/m³ initial dry density.

++ Data from Barone et al. (2014) for MX80 at 1.75-1.8 Mg/m³ density

+++ Data derived from 1-D oedometer test

NM not measured, not measurable in this testing program or not part of testing matrix;

S degree of water saturation (%).

11. CLOSURE

Extensive materials properties testing has been completed in support of developing a reference database of key thermal, hydraulic and mechanical parameters for MX80 bentonite at target dry densities of 1.5 and 1.7 Mg/m³ and 70:30 BSM at >1.7 Mg/m³ dry density. The data generated provide reference values for behavioural parameters and the means to estimate change in behaviour as the materials evolve following placement in a DGR.

Testing established that the quality of the swelling clays (e.g. swelling clay content) of the materials tested in this study can be reliably determined using conventional and fairly rapid characterization tests (e.g. free swell, consistency limits) requiring 1-2 days to get results. When in conjunction with a rapid (almost immediate results) test such as methylene blue (not done in this study) a reliable means of establishing bentonite quality is available. More detailed tests such as XRD provide for a semi quantitative measure of actual mineral content but are also slow to do (typ. >2 days to prepare materials and get results) and are prone to interpretive variations between laboratories. XRF provides accurate and detailed chemical compositional information and allows for accurate identification of gross changes in bentonite chemical composition, but as it is typically done in conjunction with XRD, it requires about 2 days to obtain results.

The test data and generated behavioural predictive relationships identifies the importance of groundwater salinity in determining the behaviour of these materials. Salinity was determined to be substantial factor in determining most thermal, hydraulic and mechanical properties of the materials examined. The texture (granularity) of the bentonite used will also affect thermal and gas conductivity properties of these compacted materials. The use of a BSM compacted to >1.7 Mg/m³ provides a material that shows some differences from that of MX80 compacted to the same dry density (e.g. reduced drying shrinkage, higher TC and k, lower PS and AC). The 70:30 BSM compacted to > 1.7 Mg/m³ dry density will meet the established performance requirements for the sealing systems located beyond the placement rooms in the DGR.

The data collected in this study show that while some parameters can be quite reliably estimated based on large existing databases, there is however a need for further evaluation of some parameters including:

- Establishing the effects of porefluid salinity and granularity of material used in production of compacted materials on thermal behaviour and air permeability),
- The hydraulic conductivity under highly saline conditions should also be more thoroughly evaluated through conduct of additional tests to provide for a more comprehensive data base and allow better predictive equations to be developed.
- Stress-strain behaviour of dense bentonite materials has limited information available and so deformation parameters used in deformation modelling have an unknown degree of uncertainty associated with them. Further evaluation literature-derived information is needed in order to determine what information is still needed, particularly with respect to behaviour under highly saline groundwater conditions.

REFERENCES

- ASTM D5890-11. Standard test method for swell index of clay mineral component of geosynthetic clay liners. Am. Soc. Testing Materials. West Conshohocken, Pennsylvania, USA.
- ASTM D4318-10. Standard test methods for Liquid Limit, Plastic Limit, and Plasticity Index of soils. Am. Soc. Testing Materials. West Conshohocken, Pennsylvania, USA.
- ASTM D2216-10. Test methods for laboratory determination of water (moisture) content of soil and rock by mass. Am. Soc. Testing Materials. West Conshohocken, Pennsylvania, USA.
- ASTM D1557-12. Modified compaction test. Standard test methods for laboratory compaction characteristics of soil using modified effort (56,000 ft-lbf/ft³ (2,700 kN-m/m<sup>3

Barbour, L. 1990. The impact of sodium-chloride solutions on the geotechnical properties of clay soils: A review of clay-brine interactions, Minerals and Groundwater Program. Saskatchewan Research Council. Saskatoon, Canada.

Barone, F., J. Stone and A. Man. 2014. Geotechnical properties of candidate shaft backfill. Nuclear Waste Management Organization Report NWMO-TR-2014-12. Toronto, Canada.

Baumgartner, P. 2006. Generic thermal-mechanical-hydraulic (THM) data for sealing materials: Volume 1: soil-water relationships. Ontario Power Generation Report 06819-REP-01300-10122-R00. Toronto, Canada.

Börgesson, L., A. Dueck and L. E. Johannesson. 2010. Material model for shear of the buffer. Evaluation of laboratory test results. Swedish Nuclear Fuel and Waste Management Company Technical Report SKB TR-10-31. Stockholm, Sweden.

Brooks, R.H. and A.T. Corey. 1964. Hydraulic properties of porous medium. Colorado State University, Hydrology Paper, Nr. 3. March. Fort Collins, USA.

Budhu, M. 2011. Soil mechanics and foundations. John Wiley & Sons. Hoboken, USA.

Dixon, D.A. and M.N. Gray. 1985. The engineering properties of buffer material – Research at Whiteshell Nuclear Research Establishment. Atomic Energy of Canada Technical Record TR-350. Chalk River, Canada.

Dixon, D.A. 1994. Sodium bentonites of Canada, the United States and Mexico: Sources, reserves and properties. ed. A.M. Crawford, H.S. Radhakrishna, M. Goutama and K.C. Lau, CSCE Special Technical Publication of the Engineering Materials Division. Montreal, Canada.

Dixon, D.A. 1995. Towards an understanding of water structure and water movement through dense clays. Ph.D thesis, Department of Civil and Geological Engineering, University of Manitoba. Winnipeg, Canada.</sup>

- Dixon, D.A., M.N. Gray and A.W. Thomas. 1985. A study of the compaction properties of potential clay-sand buffer mixtures for use in nuclear fuel waste disposal. *Eng.Geol.*, 21:247-255.
- Dixon, D.A. and S. Miller. 1995. Comparison of the mineralogical composition, physical, swelling and hydraulic properties of untreated sodium bentonites from Canada, the United States and Japan. Atomic Energy of Canada Limited Report AECL-11301, COG-95-156. Chalk River, Canada.
- Eloranta, A. 2012. Experimental methods for measuring elasto-plastic parameters of bentonite clay. Master Thesis, University of Jyväskylä. Finland.
- Fredlund, D.G. and A. Xing. 1994. Equations for the soil-water characteristic curve. *Canadian Geotechnical Journal*. Vol. 31, pp. 521-532.
- Fredlund, M.D., G.W. Wilson and D.G. Fredlund. 2002. Representation and estimation of the shrinkage curve. UNSAT 2002, Proceedings of the Third International Conference on Unsaturated Soils, Recife, Brazil, March 10-13, pp. 145-149.
- Kiviranta, L. and S. Kumpulainen. 2011. Quality control and characterization of bentonite materials. Posiva Oy Working Report, 2011-84. Olkiluoto, Finland.
- Karnland, O., S. Olsson and U. Nilsson. 2006. Mineralogy and sealing properties of various bentonites and smectite-rich clay materials. Swedish Nuclear Fuel and Waste Management Company Technical Record SKB TR-06-30, Stockholm, Sweden.
- Karnland, O. 2010. Chemical and mineralogical characterization of the bentonite buffer for the acceptance control procedure in a KBS-3 repository. Swedish Nuclear Fuel and Waste Management Company Technical Record SKB TR-10-60, Stockholm, Sweden.
- Lingnau, B., J. Graham, D. Yarechewski, N. Tanaka and M.N. Gray. 1996. Effects of temperature on strength and compressibility of sand-bentonite buffer. *Eng. Geol.* 41(1) pp. 103-115.
- Priyanto, D.G., C.S. Kim and D.A. Dixon. 2013. Geotechnical characterization of a potential shaft backfill material. Nuclear Waste Management Organization Report NWMO-TR-2013-03. Toronto, Canada.
- Tisato, N. and S. Marelli. 2013. Laboratory measurements of the longitudinal and transverse wave velocities of compacted bentonite as a function of water content, temperature and confining pressure. *J. Geophys. Res. Solid Earth*. V118, pp. 3380-3393.

APPENDIX A: CHEMICAL COMPOSITION OF SALINE SOLUTIONS

ANALYSIS OF SALT SOLUTIONS

Each of the test solutions developed for use in this work were formulated to meet, so far as possible the specifications provided by NWMO and provided in Section 2.1 of this document. Following formulation and preparation of trial batches using the formulation developed, samples of each of the three saline solutions CR-10, SR-L and SR-Sh were submitted to a commercial laboratory (ALS-Saskatoon) for analysis. The results provided by this laboratory are provided below.



Golder Associates Ltd.
ATTN: Crystal Rinas
1721 8th Street East
Saskatoon SK S7H 0T4

Date Received: 20-AUG-14
Report Date: 27-AUG-14 16:09 (MT)
Version: FINAL

Client Phone: 306-665-7989

Certificate of Analysis

Lab Work Order #: L1505441
Project P.O. #: NOT SUBMITTED
Job Reference: 13-1380-0101/1000
C of C Numbers:
Legal Site Desc:

A handwritten signature in black ink that reads "B. Morgan".

Brian Morgan
Account Manager

[This report shall not be reproduced except in full without the written authority of the Laboratory.]

ADDRESS: #819-58th St E., Saskatoon, SK S7K 6X5 Canada | Phone: +1 306 668 8370 | Fax: +1 306 668 8383
ALS CANADA LTD Part of the ALS Group A Campbell Brothers Limited Company

ALS ENVIRONMENTAL ANALYTICAL REPORT

Sample Details/Parameters	Result	Qualifier*	D.L.	Units	Extracted	Analyzed	Batch
L1505441-1 CR-10 Sampled By: CLIENT on 19-AUG-14 Matrix: BRINE							
Routine Water Analysis							
Alkalinity by Auto. Titration							
Bicarbonate (HCO ₃)	21.0		20	mg/L		20-AUG-14	R2927888
Hydroxide (OH)	<10.		10	mg/L		20-AUG-14	R2927888
Carbonate (CO ₃)	<10.		10	mg/L		20-AUG-14	R2927888
Alkalinity, Total (as CaCO ₃)	<20		20	mg/L		20-AUG-14	R2927888
Chloride (Cl)							
Chloride (Cl)	6080	DLA	150	mg/L	20-AUG-14	20-AUG-14	R2925496
Conductivity (Automated)							
Conductivity	17900		10	uS/cm		20-AUG-14	R2927888
ICP Cations							
Calcium (Ca)	2030	DLA	30	mg/L	21-AUG-14	21-AUG-14	R2925355
Potassium (K)	85	DLA	30	mg/L	21-AUG-14	21-AUG-14	R2925355
Magnesium (Mg)	67	DLA	30	mg/L	21-AUG-14	21-AUG-14	R2925355
Sodium (Na)	1850	DLA	60	mg/L	21-AUG-14	21-AUG-14	R2925355
Sulfur (as SO ₄)	923	DLA	90	mg/L	21-AUG-14	21-AUG-14	R2925355
Ion Balance Calculation							
Cation - Anion Balance	-0.4			%		25-AUG-14	
TDS (Calculated)	11000			mg/L		25-AUG-14	
Hardness (as CaCO ₃)	5340			mg/L		25-AUG-14	
Nitrate, Nitrite and Nitrate+Nitrite-N							
Nitrate-N	<0.50		0.50	mg/L	20-AUG-14	20-AUG-14	R2925014
Nitrite-N	<0.050		0.050	mg/L	20-AUG-14	20-AUG-14	R2925014
Nitrate+Nitrite-N	<0.50		0.50	mg/L	20-AUG-14	20-AUG-14	R2925014
pH by Meter (Automated)							
pH	7.88		0.10	pH		20-AUG-14	R2927888
L1505441-2 SR-L-2013 Sampled By: CLIENT on 19-AUG-14 Matrix: BRINE							
Routine Water Analysis							
Alkalinity by Auto. Titration							
Bicarbonate (HCO ₃)	142.		20	mg/L		20-AUG-14	R2927888
Hydroxide (OH)	<10.		10	mg/L		20-AUG-14	R2927888
Carbonate (CO ₃)	<10.		10	mg/L		20-AUG-14	R2927888
Alkalinity, Total (as CaCO ₃)	117		20	mg/L		20-AUG-14	R2927888
Chloride (Cl)							
Chloride (Cl)	138000	DLA	5000	mg/L	20-AUG-14	20-AUG-14	R2925496
Conductivity (Automated)							
Conductivity	180000		10	uS/cm		20-AUG-14	R2927888
ICP Cations							
Calcium (Ca)	20300	DLA	200	mg/L	21-AUG-14	21-AUG-14	R2925355
Potassium (K)	18000	DLA	200	mg/L	21-AUG-14	21-AUG-14	R2925355
Magnesium (Mg)	4530	DLA	200	mg/L	21-AUG-14	21-AUG-14	R2925355
Sodium (Na)	43500	DLA	400	mg/L	21-AUG-14	21-AUG-14	R2925355
Sulfur (as SO ₄)	830	DLA	600	mg/L	21-AUG-14	21-AUG-14	R2925355
Ion Balance Calculation							
Cation - Anion Balance	-2.3			%		25-AUG-14	
TDS (Calculated)	225000			mg/L		25-AUG-14	
Hardness (as CaCO ₃)	69300			mg/L		25-AUG-14	
Nitrate, Nitrite and Nitrate+Nitrite-N							
Nitrate-N	0.55		0.50	mg/L	20-AUG-14	20-AUG-14	R2925014

* Refer to Referenced Information for Qualifiers (if any) and Methodology.

13-1380-0101/1000

L1505441 CONTD....

PAGE 3 of 5

Version: FINAL

ALS ENVIRONMENTAL ANALYTICAL REPORT

Sample Details/Parameters	Result	Qualifier*	D.L.	Units	Extracted	Analyzed	Batch
L1505441-2 SR-L-2013 Sampled By: CLIENT on 19-AUG-14 Matrix: BRINE Nitrate, Nitrite and Nitrate+Nitrite-N							
Nitrite-N	0.076		0.050	mg/L	20-AUG-14	20-AUG-14	R2925014
Nitrate+Nitrite-N	0.62		0.50	mg/L	20-AUG-14	20-AUG-14	R2925014
pH by Meter (Automated) pH	6.73		0.10	pH		20-AUG-14	R2927888
L1505441-3 SR-SH-2013 Sampled By: CLIENT on 19-AUG-14 Matrix: BRINE Routine Water Analysis							
Alkalinity by Auto. Titration							
Bicarbonate (HCO3)	484.		20	mg/L		20-AUG-14	R2927888
Hydroxide (OH)	<10.		10	mg/L		20-AUG-14	R2927888
Carbonate (CO3)	<10.		10	mg/L		20-AUG-14	R2927888
Alkalinity, Total (as CaCO3)	397		20	mg/L		20-AUG-14	R2927888
Chloride (Cl)							
Chloride (Cl)	204000	DLA	20000	mg/L	20-AUG-14	20-AUG-14	R2925496
Conductivity (Automated) Conductivity	186000		10	uS/cm		20-AUG-14	R2927888
ICP Cations							
Calcium (Ca)	45000	DLA	250	mg/L	21-AUG-14	21-AUG-14	R2925355
Potassium (K)	20800	DLA	250	mg/L	21-AUG-14	21-AUG-14	R2925355
Magnesium (Mg)	5660	DLA	250	mg/L	21-AUG-14	21-AUG-14	R2925355
Sodium (Na)	51700	DLA	500	mg/L	21-AUG-14	21-AUG-14	R2925355
Sulfur (as SO4)	<750	DLA	750	mg/L	21-AUG-14	21-AUG-14	R2925355
Ion Balance Calculation							
Cation - Anion Balance	-2.4			%		25-AUG-14	
TDS (Calculated)	327000			mg/L		25-AUG-14	
Hardness (as CaCO3)	136000			mg/L		25-AUG-14	
Nitrate, Nitrite and Nitrate+Nitrite-N							
Nitrate-N	0.59		0.50	mg/L	20-AUG-14	20-AUG-14	R2925014
Nitrite-N	0.092		0.050	mg/L	20-AUG-14	20-AUG-14	R2925014
Nitrate+Nitrite-N	0.68		0.50	mg/L	20-AUG-14	20-AUG-14	R2925014
pH by Meter (Automated) pH	6.43		0.10	pH		20-AUG-14	R2927888

* Refer to Referenced Information for Qualifiers (if any) and Methodology.

Reference Information

Qualifiers for Sample Submission Listed:

Qualifier	Description
EXTEMP	Samples Received with temperature >15 Degrees C

Sample Parameter Qualifier Key:

Qualifier	Description
DLA	Detection Limit adjusted for required dilution

Test Method References:

ALS Test Code	Matrix	Test Description	Method Reference**
---------------	--------	------------------	--------------------

ALK-PCT-SK	Water	Alkalinity by Auto. Titration	APHA 2320 Alkalinity
------------	-------	-------------------------------	----------------------

This analysis is carried out using procedures adapted from APHA Method 2320 "Alkalinity". Total alkalinity is determined by potentiometric titration to a pH 4.5 endpoint. Bicarbonate, carbonate and hydroxide alkalinity are calculated from phenolphthalein alkalinity and total alkalinity values.

CL-COL-SK	Water	Chloride (Cl)	APHA 4500-CL E
-----------	-------	---------------	----------------

Chloride in aqueous matrices is determined colorimetrically by auto-analyzer.

EC-PCT-SK	Water	Conductivity (Automated)	APHA 2510 Auto. Conduc.
-----------	-------	--------------------------	-------------------------

This analysis is carried out using procedures adapted from APHA Method 2510 "Conductivity". Conductivity is determined using a conductivity electrode.

ETL-ROUTINE-ICP-SK	Water	ICP Cations	APHA 3120 B-ICP-OES-ROU
--------------------	-------	-------------	-------------------------

These ions are determined directly y ICP-OES.

Reference

Greenberg, Arnold E., Cleseri, Lenore S., Eaton, Andrew D., Standard Methods For The Examination of Water and Wastewater, 18th Edition, 1992, Method 3120B.

IONBALANCE-OP03-SK	Water	Ion Balance Calculation	APHA 1030-E
--------------------	-------	-------------------------	-------------

N2/N3-SK	Water	Nitrate, Nitrite and Nitrate+Nitrite-N	APHA 4500 NO3F
----------	-------	--	----------------

Nitrate is quantitatively reduced to nitrite by passage of the sample through a copperized cadmium column. The nitrite (reduced nitrate plus original nitrite) is then determined by diazotizing with sulfanilamide followed by coupling with N-(1-naphthyl)ethylenediamine dihydrochloride. The resulting water-soluble dye has a magenta color, which is measured at 520nm. Original nitrite can also be determined by removing the cadmium column and following the same procedure. Nitrate-N, Nitrite-N and NO3+NO2-N are reported.

Reference

Greenberg, Arnold E., Cleseri, Lenore S., Eaton, Andrew D., Standard Methods For The Examination of Water and Wastewater, 18th Edition, 1992, Method 4500NO3-F.

PH-PCT-SK	Water	pH by Meter (Automated)	APHA 4500-H pH Value
-----------	-------	-------------------------	----------------------

This analysis is carried out using procedures adapted from APHA Method 4500-H "pH Value". The pH is determined in the laboratory using a pH electrode

It is recommended that this analysis be conducted in the field.

** ALS test methods may incorporate modifications from specified reference methods to improve performance.

The last two letters of the above test code(s) indicate the laboratory that performed analytical analysis for that test. Refer to the list below:

Laboratory Definition Code	Laboratory Location
SK	ALS ENVIRONMENTAL - SASKATOON, SASKATCHEWAN, CANADA

Chain of Custody Numbers:

Reference Information

Test Method References:

ALS Test Code	Matrix	Test Description	Method Reference**
---------------	--------	------------------	--------------------

GLOSSARY OF REPORT TERMS

Surrogates are compounds that are similar in behaviour to target analyte(s), but that do not normally occur in environmental samples. For applicable tests, surrogates are added to samples prior to analysis as a check on recovery. In reports that display the D.L. column, laboratory objectives for surrogates are listed there.

mg/kg - milligrams per kilogram based on dry weight of sample

mg/kg wwt - milligrams per kilogram based on wet weight of sample

mg/kg lwt - milligrams per kilogram based on lipid-adjusted weight

mg/L - unit of concentration based on volume, parts per million.

< - Less than.

D.L. - The reporting limit.

N/A - Result not available. Refer to qualifier code and definition for explanation.

Test results reported relate only to the samples as received by the laboratory.

UNLESS OTHERWISE STATED, ALL SAMPLES WERE RECEIVED IN ACCEPTABLE CONDITION.

Analytical results in unsigned test reports with the DRAFT watermark are subject to change, pending final QC review.



Quality Control Report

Workorder: L1505441

Report Date: 27-AUG-14

Page 1 of 4

Client: Golder Associates Ltd.
1721 8th Street East
Sasktoon SK S7H 0T4

Contact: Crystal Rinas

Test	Matrix	Reference	Result	Qualifier	Units	RPD	Limit	Analyzed
ALK-PCT-SK	Water							
Batch	R2927888							
WG1934999-2	LCS							
Alkalinity, Total (as CaCO ₃)			97.8		%		85-115	20-AUG-14
WG1934999-3	MB							
Alkalinity, Total (as CaCO ₃)			<20		mg/L		20	20-AUG-14
CL-COL-SK	Water							
Batch	R2925496							
WG1935048-2	DUP	L1505441-2						
Chloride (Cl)		138000	139000		mg/L	0.7	20	20-AUG-14
WG1935048-4	LCS							
Chloride (Cl)			102.8		%		85-115	20-AUG-14
WG1935048-1	MB							
Chloride (Cl)			<1.0		mg/L		1	20-AUG-14
EC-PCT-SK	Water							
Batch	R2927888							
WG1934999-2	LCS							
Conductivity			99.9		%		90-110	20-AUG-14
WG1934999-3	MB							
Conductivity			<10		uS/cm		10	20-AUG-14
ETL-ROUTINE-ICP-SK	Water							
Batch	R2925355							
WG1935122-3	LCS							
Calcium (Ca)			97.2		%		80-120	21-AUG-14
Potassium (K)			98.3		%		80-120	21-AUG-14
Magnesium (Mg)			97.0		%		80-120	21-AUG-14
Sodium (Na)			98.5		%		80-120	21-AUG-14
Sulfur (as SO ₄)			94.0		%		90-110	21-AUG-14
WG1935122-1	MB							
Calcium (Ca)			<1.0		mg/L		1	21-AUG-14
Potassium (K)			<1.0		mg/L		1	21-AUG-14
Magnesium (Mg)			<1.0		mg/L		1	21-AUG-14
Sodium (Na)			<2.0		mg/L		2	21-AUG-14
Sulfur (as SO ₄)			<3.0		mg/L		3	21-AUG-14
N2/N3-SK	Water							
Batch	R2925014							
WG1935046-1	DUP	L1505441-2						
Nitrate-N		0.55	0.61		mg/L	11	20	20-AUG-14



Quality Control Report

Workorder: L1505441

Report Date: 27-AUG-14

Page 2 of 4

Test	Matrix	Reference	Result	Qualifier	Units	RPD	Limit	Analyzed
N2/N3-SK	Water							
Batch	R2925014							
WG1935046-1	DUP	L1505441-2						
Nitrite-N		0.076	0.076		mg/L	0.0	25	20-AUG-14
Nitrate+Nitrite-N		0.62	0.69		mg/L	9.6	20	20-AUG-14
WG1935046-3	LCS							
Nitrate-N			2.93		mg/L		2.55-3.45	20-AUG-14
Nitrite-N			0.498		mg/L		0.425-0.575	20-AUG-14
Nitrate+Nitrite-N			3.43		mg/L		3-4	20-AUG-14
WG1935046-2	MB							
Nitrate-N			<0.50		mg/L		0.5	20-AUG-14
Nitrite-N			<0.050		mg/L		0.05	20-AUG-14
Nitrate+Nitrite-N			<0.50		mg/L		0.5	20-AUG-14
PH-PCT-SK	Water							
Batch	R2927888							
WG1934999-2	LCS							
pH			6.89		pH		6.76-6.96	20-AUG-14

APPENDIX B: RESULTS OF XRD AND XRF ANALYSES OF MINERALS TESTED

XRD and XRF analyses were completed by three analytical laboratories on identical samples of the MX80 bentonite and the quartz sand. The analytical reports provided by these laboratories are provided below. Also included are text sections extracted directly from the analytical reports that describe the methods used in the analysis and the results obtained.

Following 18 months of soaking in a high-fluid content environment, samples of MX80 bentonite were desalinated, dried, crushed and submitted for re-analysis by the same laboratories as were used for the initial analysis. The analytical reports for these tests are also provided below.

It should be noted that each laboratory used different (but still correct) methods to undertake the XRD analyses, specifically the radiation used to generate the diffraction patterns. Cu and Co radiation were both used, resulting in different diffraction patterns due to their differing wavelengths. The result was diffraction peaks that occurred at different angles, making the graphs appear substantially different. However, evaluation of these patterns results in very similar mineralogical determinations.

B-1: Activation Laboratories Ltd.

The X-ray diffraction analysis was performed on a Panalytical X'Pert Pro diffractometer equipped with Cu X-ray source and an X'Celerator detector and operating at the following conditions: 40 kV and 40 mA; range 5 - 70 deg 2θ for the bulk specimen and 3 – 35 deg 2θ for the oriented specimen; step size 0.017 deg 2θ ; time per step 50.165 sec; fixed divergence slit, angle 0.5° or 0.25° ; sample rotation 1 rev/sec.

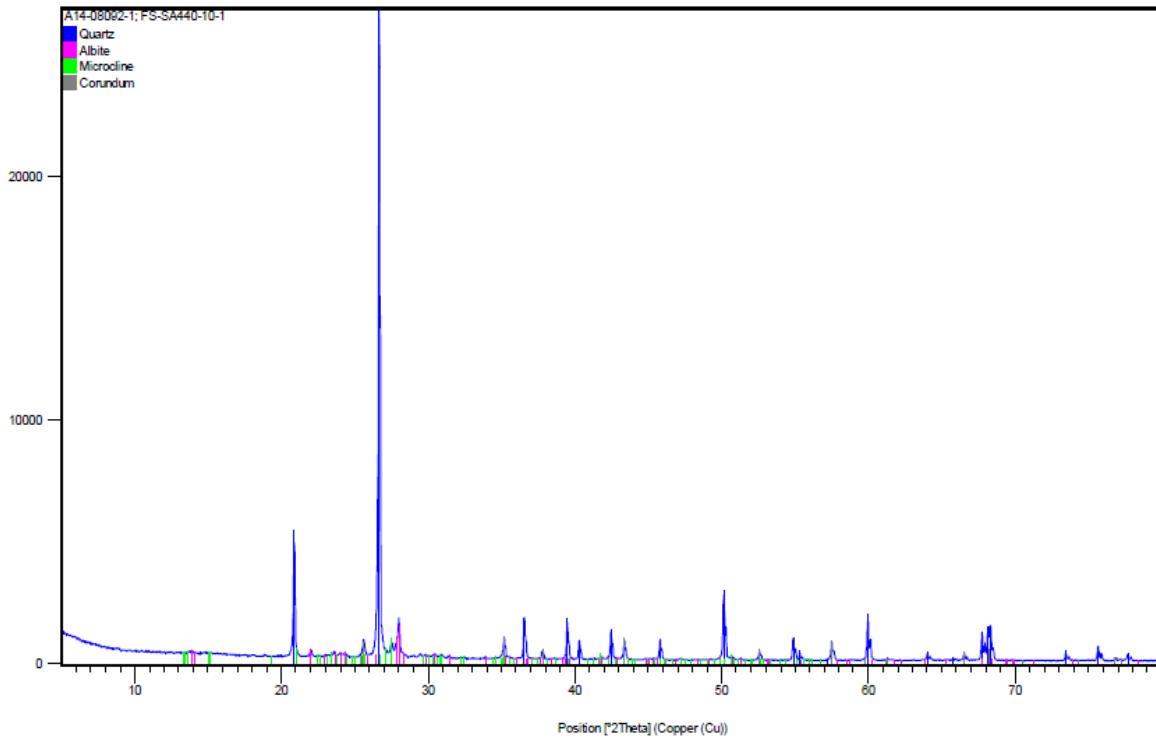
The X'Pert HighScore plus software along with the PDF4/Minerals ICDD database were used for mineral identification. The quantities of the crystalline mineral phases were determined using Rietveld method. The Rietveld method is based on the calculation of the full diffraction pattern from crystal structure information. The amount of poorly crystalline minerals such as smectite could not be calculated by the Rietveld refinement. Instead, the amounts of the crystalline minerals were recalculated based on a known percent of corundum and the remainder to 100 % was considered poorly crystalline and X-ray amorphous material.

Initial Sample: Quartz Sand XRD Analysis

The XRD analysis of sample FS-SA440-10-1 showed that the sample contains predominantly quartz (75.9 wt %) and minor amounts of plagioclase (15.5 wt %) and K feldspar (8.6 wt %).

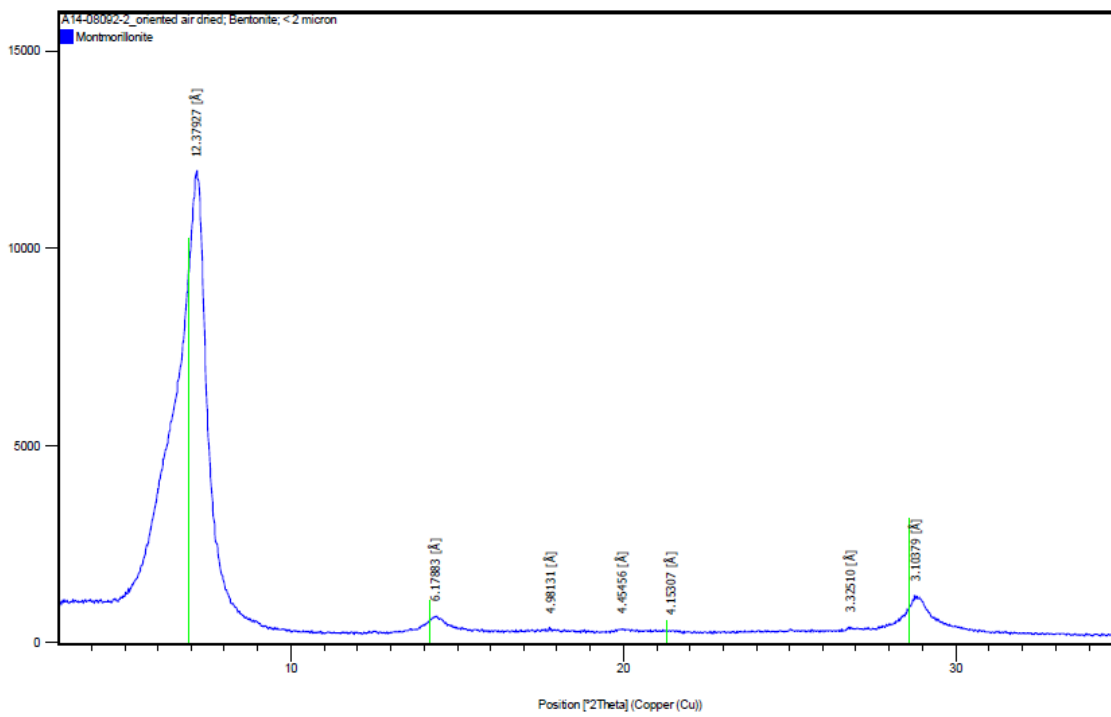
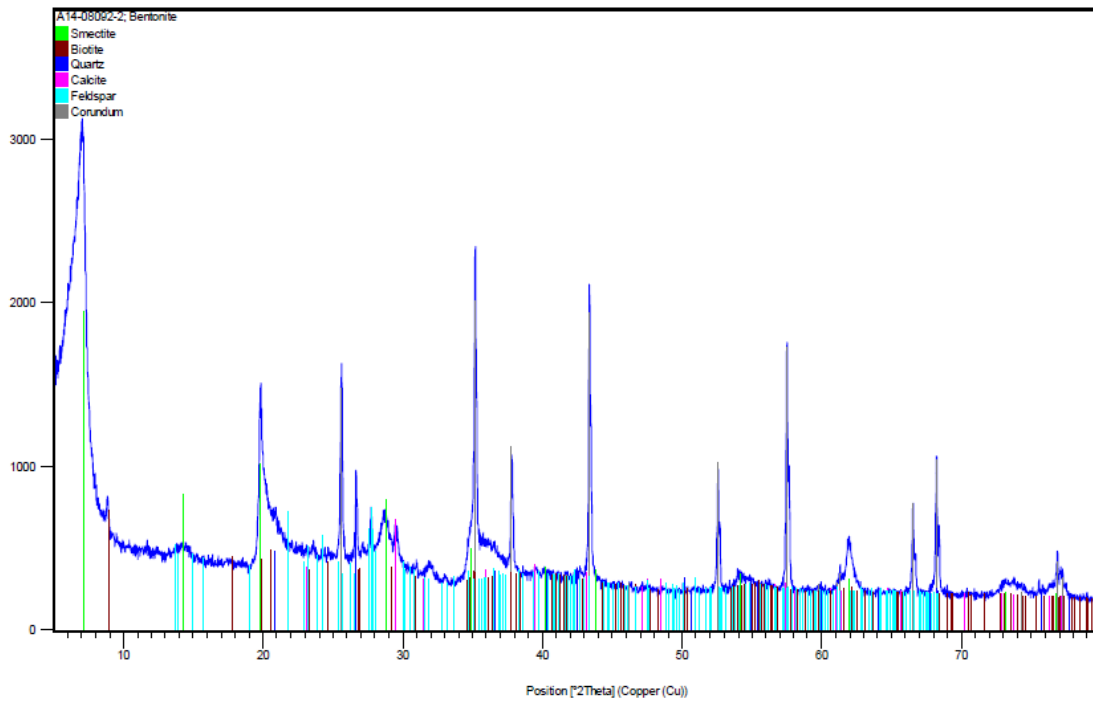
The bulk sample bentonite is composed of montmorillonite/beidellite (94.8 wt %) and contains traces of calcite (2.2 wt %), quartz (1.6 wt %), biotite (1.4 wt %) and possibly feldspar. Biotite may include other mica minerals. The sample may contain X-ray amorphous material, which could not be calculated separately from smectite. The $< 2 \mu\text{m}$ size fraction is composed of montmorillonite/beidellite. A mineral from the smectite group was identified on the basis of a peak at 12.4 \AA in the diffraction pattern of the air-dried oriented specimen, which shifts to 16.5 \AA after saturation with ethylene glycol, as well as peaks at 8.33, 5.57 and 3.35 \AA . The peak at 1.50 \AA in the diffraction pattern of the random specimen indicates that the smectite mineral is dioctahedral from the montmorillonite-beidellite series.

Initial Sample: Quartz Sand XRF



Analyte Symbol	Unit Symbol	Detection Limit	FS-SA440-10-1
Co3O4	%	0.005	< 0.005
CuO	%	0.005	< 0.005
NiO	%	0.003	< 0.003
SiO2	%	0.01	89.38
Al2O3	%	0.01	4.84
Fe2O3(T)	%	0.01	1.22
MnO	%	0.001	0.016
MgO	%	0.01	0.3
CaO	%	0.01	1.11
Na2O	%	0.01	1.03
K2O	%	0.01	1.33
TiO2	%	0.01	0.09
P2O5	%	0.01	0.05
Cr2O3	%	0.01	< 0.01
V2O5	%	0.003	< 0.003
LOI	%		1.03
Total	%	0.01	100.4

Initial Sample: Bentonite XRD Analysis

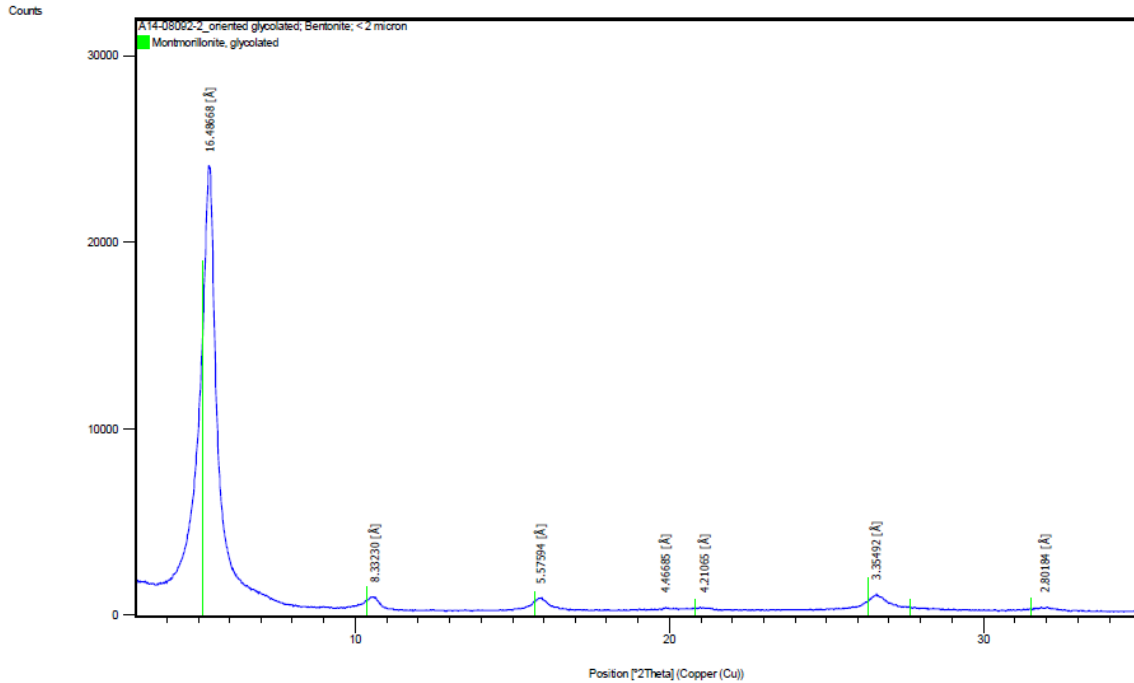


Initial Sample: Bentonite XRF Analysis

Date: 11/12/2014 Time: 3:25:51 PM

File: A14-08092-2_oriented glycolated

User: xrd-inst-xpert



Report Number: A14-08092

Report Date: 13/11/2014

Analysis Method: FUS-XRF

Analyte Symbol		Unit Symbol	Detection Limit	BENTONITE
Co3O4		%	0.005	< 0.005
CuO		%	0.005	< 0.005
NiO		%	0.003	< 0.003
SiO2		%	0.01	51.46
Al2O3		%	0.01	18.57
Fe2O3(T)		%	0.01	3.78
MnO		%	0.001	0.015
MgO		%	0.01	3.16
CaO		%	0.01	2.07
Na2O		%	0.01	1.87
K2O		%	0.01	0.73
TiO2		%	0.01	0.16
P2O5		%	0.01	0.1
Cr2O3		%	0.01	< 0.01
V2O5		%	0.003	< 0.003
LOI		%		17.41
Total		%	0.01	99.31

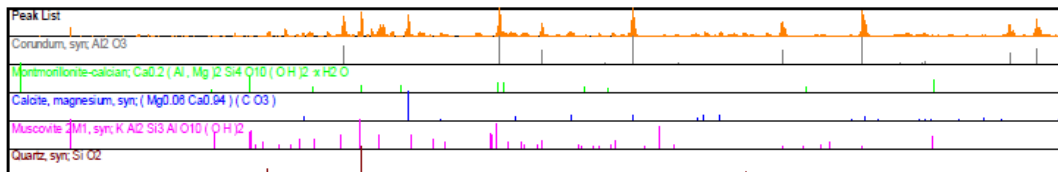
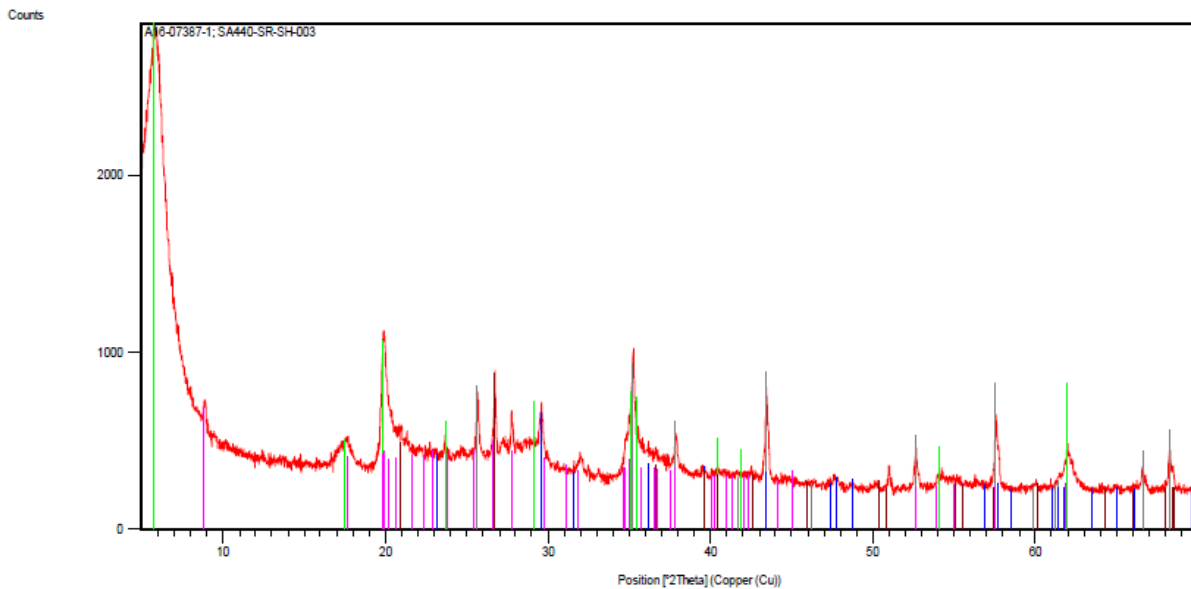
Desalinized Sample: Bentonite XRD Analysis

The bulk sample SA440-SR-SH-003 is composed predominantly of montmorillonite/beidellite (84.6 wt %) with minor amounts of feldspar (8.3 wt %), calcite (3.1 wt %), quartz (2.4 wt %) and mica (1.7 wt %). The sample may contain X-ray amorphous material, which could not be calculated separately from smectite. The < 4 μm size fraction contains montmorillonite/beidellite. A mineral from the smectite group was identified on the basis of the peaks at 16.9 \AA , 8.51, 5.61 and 3.39 \AA in the diffraction pattern of the glycolated specimen. The peak at 1.50 \AA in the diffraction pattern of the random specimen indicates that the smectite mineral is dioctahedral from the montmorillonite-beidellite series.

Date: 8/11/2016 Time: 12:29:16 PM

File: A16-07387-1

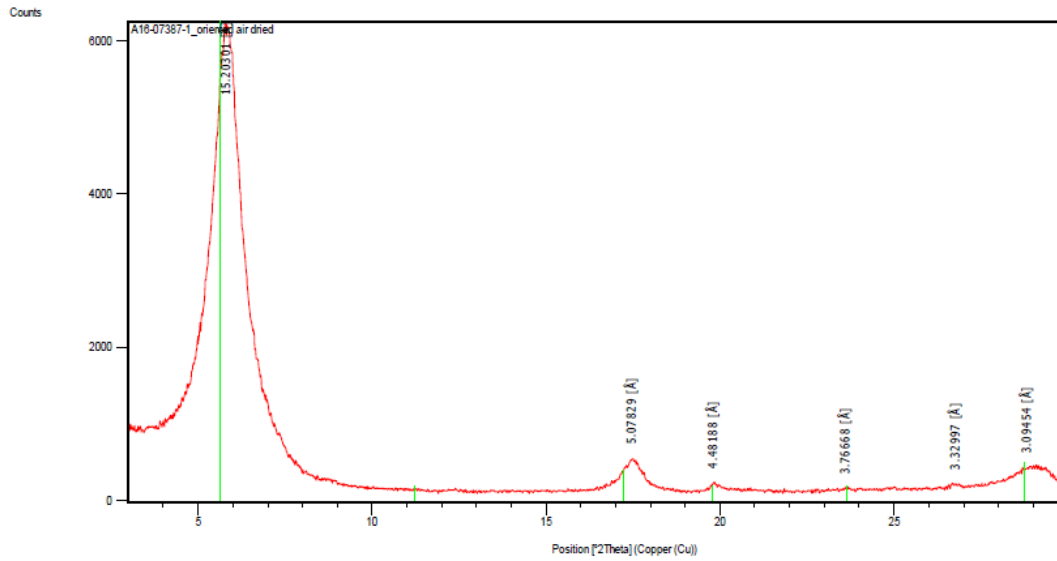
User: hrischevae



Date: 8/11/2016 Time: 12:25:23 PM

File: A16-07387-1_oriented air dried_1

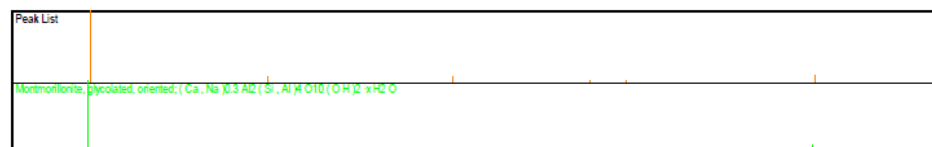
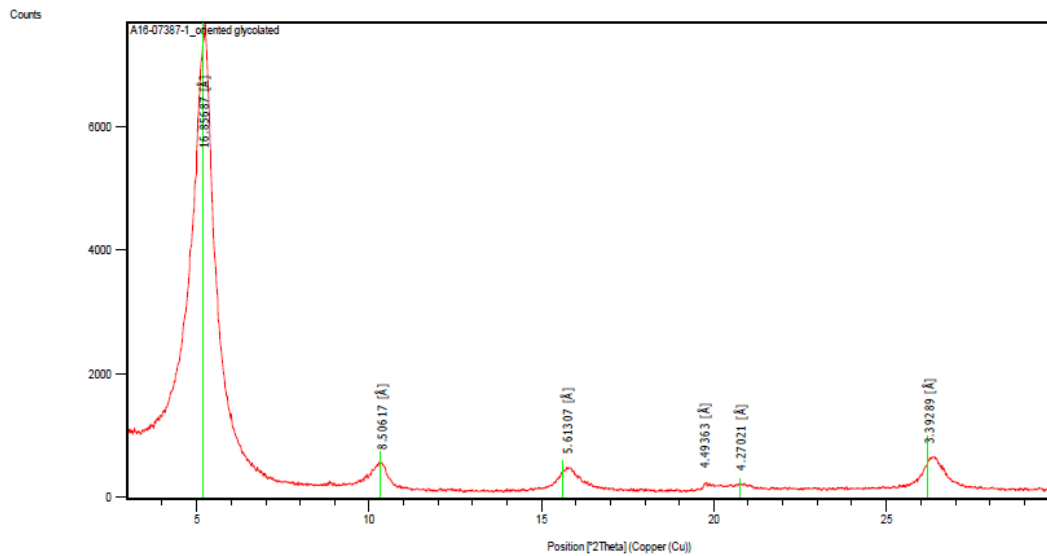
User: hrischevae



Date: 8/11/2016 Time: 12:21:33 PM

File: A16-07387-1_oriented glycolated

User: hrischevae



Desalinated Specimen: XRF Analysis

Report Number: A16-07387			
Report Date: 11/8/2016			
Analyte Symbol	Unit Symbol	Detection Limit	SA440-SR-SH-003
Co3O4	%	0.005	< 0.005
CuO	%	0.005	< 0.005
NiO	%	0.003	< 0.003
SiO2	%	0.01	51.35
Al2O3	%	0.01	18.22
Fe2O3(T)	%	0.01	5.09
MnO	%	0.001	0.026
MgO	%	0.01	3.03
CaO	%	0.01	3.35
Na2O	%	0.01	0.45
K2O	%	0.01	1.17
TiO2	%	0.01	0.16
P2O5	%	0.01	0.07
Cr2O3	%	0.01	< 0.01
V2O5	%	0.003	< 0.003
LOI	%		16.68
Total	%	0.01	99.6

B-2: James Hutton Limited (UK)

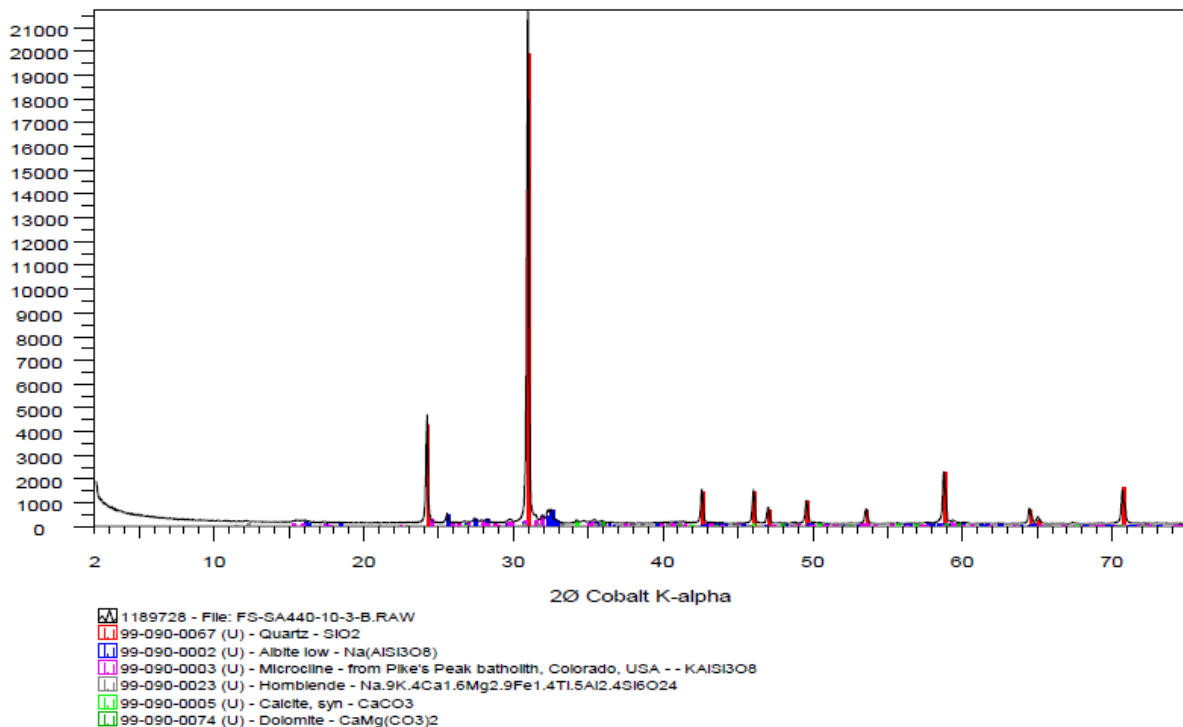
The bulk sample was wet ground (in ethanol) in a McCrone mill and spray dried to produce a random powder. The X-ray powder diffraction (XRPD) pattern was recorded from 2-75°2 θ using Cobalt K α radiation. Quantitative analysis was done by a normalised full pattern reference intensity ratio (RIR) method. Unless stated otherwise, expanded uncertainty using a coverage factor of 2, i.e. 95% confidence, is given by $\pm X0.35$, where X = concentration in wt.%, e.g. 30 wt.% ± 3.3 . Note also that for phases present at the trace level (<1%) there may also be uncertainty as to whether or not the phase is truly present in the sample. This is both phase and sample dependent. It arises because at trace concentrations identification is often based on the presence of a single peak and the judgement of the analyst in assigning that peak to a likely mineral.

The XRPD pattern is identified by a labcode and by a name based on customer supplied identifiers, plus the suffix 'B' for bulk sample.

Original Sample: Quartz Sand XRD

Sample 'FS-SA440-10-3' is dominated by quartz (82%) with plagioclase, K-feldspar, calcite, a trace of amphibole and a possible trace of dolomite.

Labcode	Sample ID	Quartz	Plagioclase	K-feldspar	Calcite	Dolomite	Siderite	Pyrite	Gypsum	Amphibole	Muscovite	Smectite(Di)	Total
1189727	BENTONITE-3-B	2.3	0.0	3.0	3.0	trace	1.9	0.6	0.4	0.0	0.3	88.5	100
1189728	FS-SA440-10-3-B	81.7	10.9	6.01	0.7	trace?	0.0	0.0	0.0	0.7	0.0	0.0	100



Original Samples: Quartz Sand XRF

The chemical analyses made by XRF appear to be fully compatible with the mineralogy as determined by XRPD, noting that the analysis of the 'bentonite' will include moisture in the LOI.

For the 'sand' the alumina content suggests the possible presence of some clay minerals/phyllsilicates at or below detection limits since it cannot be fully accounted for by feldspars and amphibole alone.

3421983
1189728 SAND

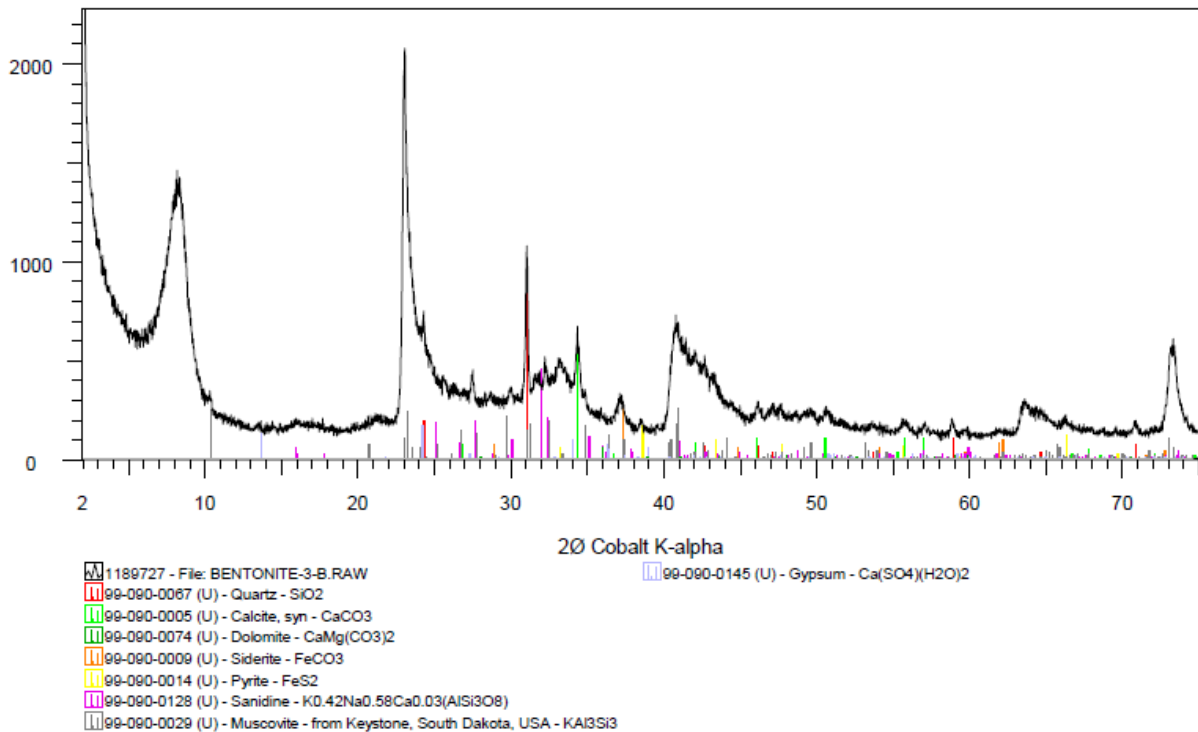
LOI@1000°C	0.93	%
Na2O	1.10	%
MgO	0.32	%
Al2O3	4.51	%
SiO2	90.22	%
P2O5	<0.05	%
K2O	1.27	%
CaO	1.08	%
TiO2	0.09	%
Mn3O4	<0.05	%
V2O5	<0.05	%
Cr2O3	<0.05	%
Fe2O3	0.90	%
BaO	<0.05	%
ZrO2	<0.05	%
ZnO	<0.05	%
SrO	<0.05	%
XRF/LOI Total	100.42	%

END OF REPORT

Original Sample: Bentonite XRD Analysis

Sample 'Bentonite 3' is dominated by dioctahedral smectite (89% with smaller amounts of quartz, Kfeldspar, calcite, dolomite, siderite, pyrite, gypsum and muscovite).

Labcode	Sample ID	Quartz	Plagioclase	K-feldspar	Calcite	Dolomite	Siderite	Pyrite	Gypsum	Amphibole	Muscovite	Smectite(Di)	Total
1189727	BENTONITE-3-B	2.3	0.0	3.0	3.0	trace	1.9	0.6	0.4	0.0	0.3	88.5	100



Original Samples: Bentonite XRF Analysis

3421982
1189727 BENTONITE CLAY

LOI@1000°C	17.19 %
Na ₂ O	1.98 %
MgO	3.09 %
Al ₂ O ₃	18.24 %
SiO ₂	51.78 %
P ₂ O ₅	0.07 %
K ₂ O	0.61 %
CaO	2.21 %
TiO ₂	0.16 %
Mn ₃ O ₄	<0.05 %
V ₂ O ₅	<0.05 %
Cr ₂ O ₃	<0.05 %
Fe ₂ O ₃	3.86 %
BaO	<0.05 %
ZrO ₂	<0.05 %
ZnO	<0.05 %
SrO	<0.05 %
XRF/LOI Total	99.19 %

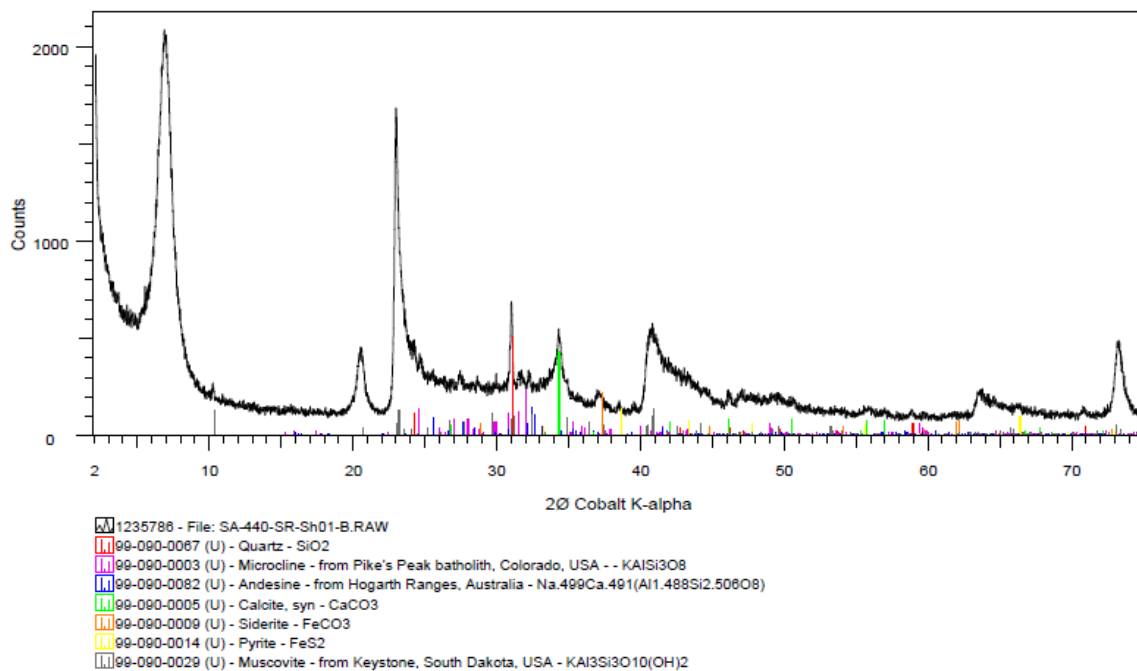
Desalinated Sample: Bentonite XRD

The XRPD pattern is identified by a labcode and by a name based on customer supplied identifiers, plus the suffix 'B' for bulk sample. The sample is a mixture of dioctahedral smectite (88.6%) with smaller amounts of quartz, calcite, siderite, plagioclase, K-feldspar, pyrite, muscovite and kaolinite. Traces of trioctahedral mica may also be present.

Table 1: XRPD Bulk Mineralogy (weight %) by RIR Method

Labcode	Sample ID	Quartz	Plagioclase	K-feldspar	Calcite	Siderite	Pyrite	Muscovite	Smectite(Di)	Kaolinite	Total
1235786	SA-440-SR-Sh01-B	1.4	0.3	1.2	4.3	1.9	0.4	1.8	88.6	0.1	100

Smectite(Di) = Dioctahedral smectite



Desalinized Sample: Bentonite XRF Analysis for Mineral Chemical Composition



4119

ITRI Ltd
Unit 3, Curo Park
Frogmore
St Albans
Hertfordshire, AL2 2DD

Phone: +44(0)1727 87 55 44
Fax: +44(0)1727 87 13 41
Email: info@itri.com
Web: www.itri-innovation.com



innovation
Job Number: 2016-23821

WD-XRF Analysis Certificate(LTM2)									
ITRI No:	L16-354	Complete Report:	YES	Report Status:	Original				
Customer:	James Hutton Limited	Contact :	Ian Phillips	Customer order No:	CB/0000215				
Address:	Craigiebuckler Aberdeen AB15 8QH			No. of Samples	1				
				Page	1 of 1				
Sample Number	L16-354-1								
Sample Drying at 110°C	C.No.	1235786							
Silicon Dioxide ^x	SiO ₂	58.558							
Titanium dioxide ^x	TiO ₂	0.178							
Aluminium Oxide ^x	Al ₂ O ₃	20.602							
Iron Oxide ^x	Fe ₂ O ₃	3.971							
Manganese (II,III) Oxide	Mn ₃ O ₄	0.020							
Magnesium Oxide ^x	MgO	3.143							
Calcium Oxide ^x	CaO	3.142							
Sodium Oxide ^x	Na ₂ O	0.226							
Potassium Oxide ^x	K ₂ O	1.189							
Phosphorus Pentoxide ^x	P ₂ O ₅	0.063							
Vanadium Oxide	V ₂ O ₅	<0.01							
Chromium (III) Oxide ^x	Cr ₂ O ₃	<0.01							
Strontium (II) Oxide	SrO	0.089							
Zirconium Oxide	ZrO ₂	0.022							
Barium Oxide ^x	BaO	0.050							
Nickel Oxide	NiO	<0.01							
Copper Oxide	CuO	<0.01							
Zinc Oxide	ZnO	<0.01							
Lead Oxide	PbO	<0.01							
Hafnium (IV) Oxide	HfO ₂	<0.01							
LOI (@1000°C)		8.46							
XRF + LOI Total		99.713							

LTM2 WD-XRF Test Method was used for the testing. ^x Elements within scope of LTM 2. Units are % unless specified

This report is issued in accordance with the Conditions of Business of ITRI Limited and relates only to the sample(s) tested. No responsibility is taken for the accuracy of the sampling unless this is done under our own supervision. This report shall not be reproduced in part without the written approval of ITRI Limited.

Mark Dowling (Quality Manager)

End of Test Report

B-3: Saskatchewan Research Council (SRC)

Samples were irradiated with Cu K α radiation ($\lambda=1.54056 \text{ \AA}$) in a Bruker D4 Endeavor X-ray diffractometer (XRD) operating at 1.6 kW power (40 kV accelerating potential and 40 mA current). The XRD is outfitted with a high speed LynxEye silicon strip detector with fluorescence background suppression. Samples were measured from 3.5 to 70° 2 θ with a 0.02° step size and 0.5 seconds dwell time with a 0.300° divergence slit. An anti-air-scattering filter is used to further suppress the background at low 2 θ angles.

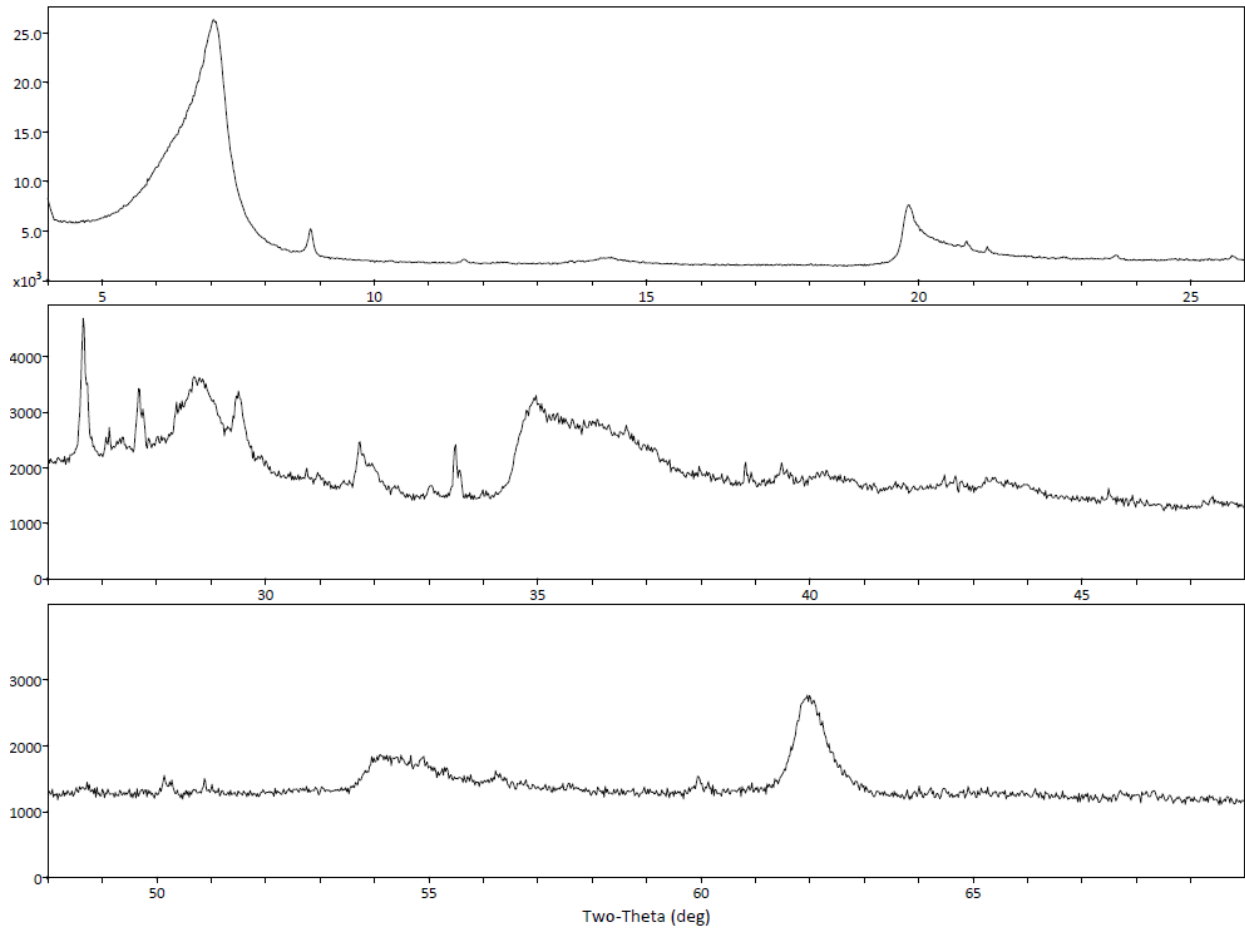
Quantitative mineralogy is done using whole pattern fitting Rietveld analysis for randomly oriented bulk samples. Data analysis is done using algorithms in MDI Products JADE v. 9 software and reference spectra from the International Centre Diffraction Data Pattern Diffraction File 4+2009 (ICDD PDF4+2009). The practical limit of detection is 1 weight percent depending on the degree of crystallinity and symmetry of the minerals present.

Semi-oriented sample: The raw diffraction data was processed using MDI Products Jade software for mineral identification and quantification. Minerals were identified based on the observed interatomic spacing of the crystal lattices present constrained by common mineral associations. All mineral abundances were calculated using whole-pattern fitting algorithms with peak intensities scaled with internally-consistent relative intensity ratios. Non-orientable mineral abundances were quantified using patterns derived from the American Mineralogist Crystal Structure Database (AMCSD). Clay mineral abundances were quantified using reference spectra proprietary to SRC because the preferred orientation and glycol solvation precludes the use of published (e.g. ICDD, AMCSD) mineral reference databases.

Bulk sample: The raw diffraction data from the bulk sample is interpreted in the same manner as the semi-oriented with the exception of the use of bulk clay patterns from the AMCSD. Detection and precision limits.

The detection limit of XRD analysis is controlled by the abundance and symmetry of all the minerals present in the sample. Low symmetry minerals are harder to detect in the presence of higher symmetry minerals. The estimated detection limit for most minerals is 1-3 wt.%. Based on repeat analyses of a secondary standards, the estimated accuracy of the clay analysis is $\pm 3 \text{ wt.}\%$.

Original Sample: Bentonite XRD Analysis



SRC Advanced Microanalysis Centre -- microlab@src.sk.ca

XRD Analysis

Backpacked Random Mount

Sample	Montmorillonite wt%	Muscovite wt%	Albite wt%	Foshagite wt%	Quartz wt%	Anorthite wt%	Microcline wt%	Orthoclase wt%	Sum wt%
Bentonite	79.00	7.10	6.80	3.60	3.50	-	-	-	100

Bentonite XRF Analysis for Mineral Chemical

XRF Analysis 40 mm Glass Bead

Samples	Na ₂ O Wt%	MgO Wt%	Al ₂ O ₃ Wt%	SiO ₂ Wt%	P ₂ O ₅ Wt%	K ₂ O Wt%	CaO Wt%	TiO ₂ Wt%	MnO Wt%	Fe ₂ O ₃ Wt%	S Wt%	LOI Wt%	Sum Wt%
Bentonite	1.49	2.25	18.8	54.4	0.055	0.430	1.82	0.186	0.029	4.20	0.160	15.8	99.62
Bentonite dup	1.56	2.26	18.8	53.1	0.061	0.410	1.87	0.175	0.025	4.54	0.170	15.9	98.87

Desalinated Sample: Bentonite XRD Analysis

Amorphous material was observed in the sample. The broad amorphous hump in the baseline was modelled using a Pearson VII peak function with fitting parameters (centroid, FWHM, peak intensity, etc.) iteratively refined with the Whole Pattern Fitting routine. Attempts to quantify the abundance of amorphous material from XRD data have not yet proven reliable enough for inclusion in routine analyses.

Results

The following pages contain the results of the XRD mineral identification and quantitative mineral abundances. A summary spreadsheet of the mineralogy and whole-rock chemical composition, measured by XRF, are also included.

A comparison of the data from the bulk and semi-oriented mounts shows a number of interesting features.

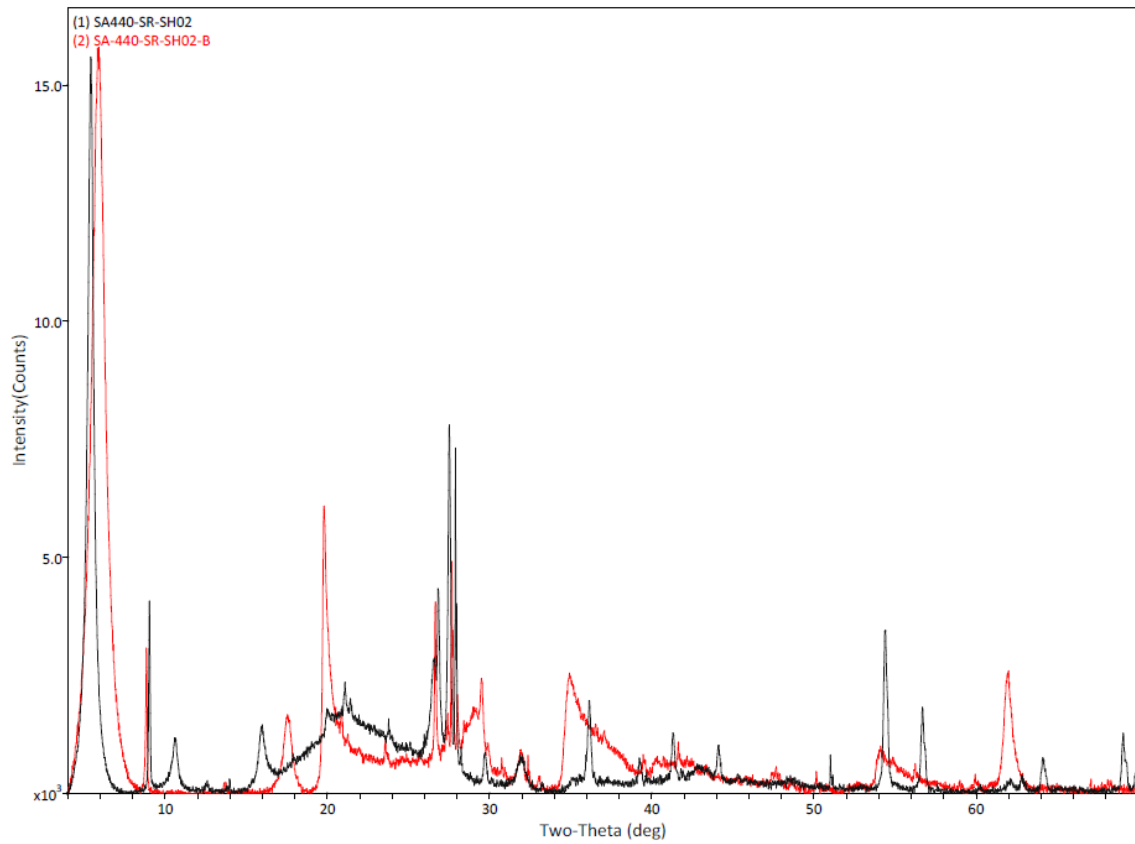
1. There is an anticipated peak shift in the smectite (001) to higher d-spacing and the appearance of smectite (002) and (003) due to glycolation;
2. The shift of illite (002) possibly due to interlayering of smectite in the illite structure;
3. Suppression of some broad humps, at approximately 29° , 35° , and $55^\circ 2\theta$, observed in the bulk data but not in the semi-oriented data;
4. Enhanced sensitivity of rutile peaks in the semi-oriented mount (due to preferred orientation of tetragonal rutile) – rutile peaks are unresolved in the bulk sample;
5. Suppression of the illite (060) peak (at $\sim 62^\circ 2\theta$) in the semi-oriented mount confirming the strong orientation of the clay minerals.

Calcite and quartz were added into the whole-pattern-fitting (WPF) routine at the suggestion of the client. The peak intensities for these two minerals are very weak and there is no strong justification for their inclusion in the data analysis. Despite being below the stated detection limit, the strong rutile peaks justify its retention in the WPF and is consistent with TiO_2 in the whole-rock XRF data.

Whole Pattern Fitting and Rietveld Refinement

FILE: [SA440-SR-SH02-B.raw] SA-440-SR-SH02-B				
SCAN: 4.0/69.9946/0.01997/49.7[sec], Cu(40kV,40mA), I(p)=18659, 08/16/16 09:27a				
PROC: [WPF Control File]				
<input checked="" type="checkbox"/> K-alpha2 Peak Present	[Diffractometer LP] Two-Theta Range of Fit = 5.0 - 70.0(deg)			
<input checked="" type="checkbox"/> Allow Negative Isotropic B	<input checked="" type="checkbox"/> Specimen Displacement - Cos(Theta) = 0.11721(0.015546)			
<input checked="" type="checkbox"/> Allow Negative Occupancy	<input type="checkbox"/> Monochromator Correction for LP Factor = 1.0			
<input checked="" type="checkbox"/> Apply Anomalous Scattering	<input type="checkbox"/> K-alpha2/K-alpha1 Intensity Ratio = 0.5			
Profile Shape Function (PSF) for All Phases: Pearson-VII, Fixed-BG, Lambda=1.54059Å (Cu/K-alpha1)				
Phase ID (4)	Source	I/Ic	Wt%	#L
 Montmorillonite - $\text{Al}_2\text{Si}_4\text{O}_{12}\text{Ca}_5$	PDF#98-091-1941	1.10(5%)	87.8 (6.0)	90
 Muscovite - $\text{K}_{0.9}\text{Na}_{0.01}\text{Si}_{3.2}\text{Al}_{2.5}\text{Ti}_{0.02}\text{Fe}_{0.16}\text{Mg}_{0.16}\text{H}_{0.34}\text{O}_{12}$	PDF#98-091-2035	0.30(5%)	11.2 (0.9)	199
 Calcite - CaCO_3	PDF#98-090-3364	3.12(5%)	0.8 (0.1)	19
 Quartz - SiO_2	PDF#98-091-4802	4.48(5%)	0.2 (0.1)	18
NOTE: Fitting Halted at Iteration 18(4): R=13.08% (E=2.02%, R/E=6.49, P=37, EP5=0.5)				

SA440-SR-SH02



SRC Advanced Microanalysis Centre -- microlab@src.sk.ca

Desalinated Sample: Bentonite XRF Analysis for Mineral Chemical Composition

XRF Analysis Loose Powder

Samples	Na ₂ O Wt%	MgO Wt%	Al ₂ O ₃ Wt%	SiO ₂ Wt%	P ₂ O ₅ Wt%	K ₂ O Wt%	CaO Wt%	TiO ₂ Wt%	MnO Wt%	Fe ₂ O ₃ Wt%	S Wt%	Total
GSP-2	2.48	0.87	14.31	66.48	0.23	5.34	1.97	0.63	0.04	4.49	0.03	96.86
SA440-SR-SH02	0.22	2.24	15.96	50.54	0.07	1.02	3.14	0.19	0.03	4.48	0.09	77.97

APPENDIX C: MODIFIED COMPACTION TEST DATA

APPENDIX D: CORRECTION FOR SALT CONTENT IN SATURATED SOIL

Determining Actual Dry Density of Clays Containing High Salinity Porewater

Based on technique from Barbour (1990)

Materials:

30% quartz sand by dry mass

70% bentonite clay by dry mass

	CR10 – 11 g/L Ca-Na Cl	1005.8 g/cc solution density
Saline porefluid:	SR160 - 160 g/L Na-Ca Cl	1100 g/cc solution density
	SR270 - 270 g/L Na-Ca Cl	1186 g/cc solution density
	SR-L – 223 g/L Na-Ca Cl	1152.8 g/cc solution density
	SR-Sh – 334.6 g/L Na-Ca Cl	1218.6 g/cc solution density

Calculations:

Specimen – assumed to be water-saturated at end of testing

Wet weight = W_T g

Oven Dry Weight = W_d g includes salt

$M_w = W_T - W_d$ g

$G_w =$ density of fresh water = 1000 kg/m³

$C_w =$ density solution – $C_s = 1182-270 = 912$

Apparent water content $W_{app} = M_w / (M_s + M_{salt})$

$W_{true} / W_{app} = 1 + W_{app} \times C_s / C_w$

$W_{true} = W_{app} \times (1 + W_{app} \times C_s / C_w)$

$e_{true} = W_{true} \times G_s \times G_w / C_w$

$e_{app} = W_{app} \times G_s$

$e_{true} / e_{app} = Z$

Dry Density_{app} = $M_s / V_t = G_s \times G_w / (1 + e_{true})$

Dry Density_{true} / Dry density_{app} = $1 / (1 + W_{true} \times C_s / C_w) = Q$

Dry Density_{true} = Q x Dry Density_{app}

APPENDIX E : SWELLING PRESSURE AND HYDRAULIC CONDUCTIVITY TEST DATA

Name	Porefluid	Dry Density (Mg/m ³)	EMDD (Mg/m ³)	Swelling Pressure (kPa)	Hydraulic Conductivity (m/s)	Permeability (m ²)
DW- MX80 1.45-1	DW	1.46	1.30	2050	NM*	NM*
DW- MX80 1.45-1A	DW	1.40	1.24	1280	2.6E-13	2.65E-20
DW- MX80 1.45-2	DW	1.42	1.28	3150	1.14E-13	1.16E-20
CR10 MX80 1.45-1A	CR10	1.43	1.27	1200	3.07E-13	3.18E-20
CR10 MX80 1.45-1B	CR10	1.30	1.14	600	3.09E-13	3.20E-20
CR10 MX80 1.45-2A	CR10	1.44	1.28	1200	4.58E-13	4.74E-20
CR10 MX80 1.45-2B	CR10	1.28	1.12	700	3.65E-13	3.78E-20
CR10 MX80 1.45-3A	CR10	1.44	1.28	1400	2.06E-13	2.13E-20
CR10 MX80 1.45-3B	CR10	1.33	1.17	700	2.07E-13	2.11E-20
SR-L MX80 1.50-1	SR-L	1.50	1.33	380	6.41E-13	1.07E-19
SR-L MX80 1.50-2	SR-L	1.42	1.26	610	3.63E-12	6.08E-19
SR-L MX80 1.50-3	SR-L	1.50	1.33	480	9.73E-12	1.63E-19
SR-Sh MX80 1.50-1	SR-Sh	1.49	1.32	580	1.28E-11	2.46E-18
SR-Sh MX80 1.50-2	SR-Sh	1.52	1.35	600	2.26E-12	4.34E-19
SR-Sh MX80 1.50-3	SR-Sh	1.57	1.37	840	1.65E-12	3.17E-19
SR-Sh MX80 1.50-4	SR-Sh	1.49	1.34	289	2.3E-11	4.42E-18
SR-Sh MX80 1.50-5	SR-Sh	1.48	1.33	150	3.65E-11	7.02E-18
DW- MX80 1.75-1A	DW	1.70	1.56	7420	1.22E-13	1.24E-20
DW- MX80 1.75-1B	DW	1.44	1.29	2540	3.9E-13	3.98E-20
DW- MX80 1.75-2	DW	1.70	1.56	8250	1.26E-13	1.28E-20
SR-L MX80 1.8-1A	SR-L	1.76	1.62	5320	NM*	NM*
SR-L MX80 1.8-1B	SR-L	1.73	1.59	3150	6.07E-14	1.02E-21
SR-L MX80 1.8-2A	SR-L	1.84	1.70	6750	NM*	NM*
SR-L MX80 1.8-2B	SR-L	1.69	1.55	3420	1.94E-13	3.25E-20
SR-L MX80 1.8-3	SR-L	1.68	1.53	2820	8.2E-14	1.37E-20
SR-L MX80 1.8-4	SR-L	1.69	1.55	1258	4.38E-13	7.34E-20
DW- 70-30 MX80 1.75-1A	DW	1.70	1.33	980	2.17E-13	2.21E-20
DW- 70-30 MX80 1.75-1B	DW	1.55	1.16	450	2.81E-13	2.86E-20
DW- 70-30 MX80 1.75-2	DW	1.70	1.33	2750	7.74E-14	7.89E-21
CR10- 70/30 1.75-1	CR10	1.67	1.28	1950	9.4E-14	1.81E-20
CR10- 70/30 1.75-2	CR10	1.70	1.32	2710	7.94E-14	1.53E-20
CR10- 70/30 1.75-3	CR10	1.72	1.34	2630	7.5E-14	1.44E-20
SR-L 70/30 1.75-1	SR-L	1.70	1.32	270	NM*	NM*
SR-L 70/30 1.75-2	SR-L	1.72	1.34	1220	1.68E-12	2.81E-19
SR-L 70/30 1.75-3	SR-L	1.68	1.29	670	3.91E-12	6.55E-19
SR-L 70/30 1.75-4	SR-L	1.72	1.34	299	NM*	NM*
SR-Sh 70/30 1.75-1	SR-Sh	1.69	1.31	410	1.68E-12	3.23E-19
SR-Sh 70/30 1.75-2	SR-Sh	1.74	1.35	960	1.39E-12	2.67E-19
SR-Sh 70/30 1.75-3	SR-Sh	1.73	1.35	1140	1.41E-12	2.71E-19

* NM - Not measured in this test. Leak in cell did not allow for flow measurement

APPENDIX F: DRYING VOLUME CHANGE (SHRINKAGE) DATA

Table F-4: Drying Volume Change for 70:30 MX80:Sand (1.80 Mg/m³ with DW pore fluid)

BSM 70-30 DW #1				BSM 70-30 DW #2				BSM 70-30 DW #3				BSM 70-30 DW Average			
Measured				Measured				Measured				Measured			
water content (apparent)	water content (true)	void ratio	Dry density (g/cm ³)	water content (apparent)	water content (true)	void ratio	Dry density (g/cm ³)	water content (apparent)	water content (true)	void ratio	Dry density (g/cm ³)	Average Density (g/cm ³)	Average water content (%)	Average void ratio	
(%)	(%)		(g/cm ³)	(%)	(%)		(g/cm ³)	(%)	(%)		(g/cm ³)	(g/cm ³)	(%)		
18.4	18.4	0.50	1.802	18.4	18.4	0.50	1.801	18.4	18.4	0.50	1.802	1.802	18.4	0.50	
16.8	16.8	0.47	1.839	16.9	16.9	0.47	1.831	17.1	17.1	0.48	1.829	1.833	16.9	0.47	
15.5	15.5	0.47	1.833	15.4	15.4	0.47	1.834	15.5	15.5	0.47	1.834	1.834	15.5	0.47	
14.7	14.7	0.46	1.848	14.5	14.5	0.47	1.840	14.5	14.5	0.47	1.836	1.842	14.5	0.47	
14.5	14.5	0.45	1.867	14.4	14.4	0.44	1.871	14.3	14.3	0.45	1.863	1.867	14.4	0.45	
13.2	13.2	0.43	1.887	13.0	13.0	0.44	1.875	13.0	13.0	0.45	1.864	1.876	13.0	0.44	
12.0	12.0	0.43	1.891	11.8	11.8	0.43	1.894	11.7	11.7	0.43	1.893	1.893	11.8	0.43	
11.4	11.4	0.43	1.891	11.2	11.2	0.43	1.890	11.2	11.2	0.43	1.890	1.891	11.3	0.43	
9.5	9.5	0.41	1.915	9.4	9.4	0.42	1.902	9.4	9.4	0.42	1.905	1.907	9.4	0.42	
9.2	9.2	0.41	1.917	9.1	9.1	0.41	1.912	8.9	8.9	0.42	1.903	1.911	9.1	0.41	
9.0	9.0	0.41	1.915	8.8	8.8	0.41	1.916	8.7	8.7	0.41	1.916	1.916	8.8	0.41	
8.7	8.7	0.40	1.926	8.5	8.5	0.41	1.916	8.4	8.4	0.42	1.907	1.917	8.5	0.41	
8.6	8.6	0.41	1.914	8.4	8.4	0.40	1.931	8.3	8.3	0.42	1.906	1.917	8.5	0.41	
8.6	8.6	0.41	1.915	8.5	8.5	0.40	1.922	8.4	8.4	0.40	1.925	1.921	8.5	0.41	
8.6	8.6	0.40	1.927	8.5	8.5	0.40	1.930	8.4	8.4	0.40	1.928	1.929	8.5	0.40	
0.7	0.7	0.37	1.965	0.5	0.5	0.38	1.950	0.4	0.4	0.39	1.949	1.955	0.5	0.38	
0.6	0.6	0.38	1.955	0.5	0.5	0.39	1.948	0.4	0.4	0.39	1.949	1.951	0.5	0.38	
0.4	0.4	0.38	1.952	0.4	0.4	0.39	1.944	0.3	0.3	0.39	1.946	1.947	0.4	0.39	
0.4	0.4	0.38	1.962	0.2	0.2	0.38	1.953	0.3	0.3	0.39	1.944	1.953	0.3	0.38	
0.4	0.4	0.39	1.949	0.3	0.3	0.39	1.948	0.3	0.3	0.38	1.954	1.950	0.3	0.38	
Fitting Parameters															
				ash			bsh			csh					
BSM 70-30 DW #1				0.392			0.145			4.978					
BSM 70-30 DW #2				0.395			0.146			4.912					
BSM 70-30 DW #3				0.398			0.147			4.814					
average				0.395			0.146			4.901					

Table F-6: Drying Volume Change for 70:30 MX80:Sand (1.78 Mg/m³ with SR-L pore fluid)

BSM 70-30 SR-L #1				BSM 70-30 SR-L #2				BSM 70-30 SR-L #3				BSM 70-30 SR-L Average		
Measured				Measured				Measured				Measured		
Water content (apparent)	Water content (true)	void ratio	Dry density	Water content (apparent)	Water content (true)	void ratio	Dry density	Water content (apparent)	Water content (true)	void ratio	Dry density	Average Density	Average water content	Average void ratio
(%)	(%)		(g/cm ³)	(%)	(%)		(g/cm ³)	(%)	(%)		(g/cm ³)	(g/cm ³)	(%)	
16.1	16.9	0.52	1.781	16.2	16.9	0.51	1.783	16.2	16.9	0.52	1.781	1.782	16.9	0.52
14.8	15.5	0.51	1.790	15.0	15.7	0.50	1.794	15.2	15.9	0.52	1.778	1.787	15.7	0.51
13.5	14.1	0.49	1.807	13.7	14.3	0.50	1.801	13.7	14.4	0.50	1.796	1.801	14.3	0.50
13.5	14.1	0.48	1.819	13.5	14.1	0.49	1.813	13.7	14.3	0.50	1.800	1.811	14.2	0.49
12.7	13.2	0.50	1.802	12.8	13.4	0.49	1.812	12.9	13.5	0.48	1.819	1.811	13.4	0.49
12.0	12.5	0.47	1.841	12.2	12.8	0.47	1.835	12.3	12.8	0.47	1.837	1.838	12.7	0.47
11.5	12.0	0.46	1.848	11.8	12.3	0.46	1.849	11.8	12.4	0.47	1.838	1.845	12.2	0.46
10.1	10.6	0.45	1.860	10.4	10.8	0.45	1.868	10.5	11.0	0.45	1.861	1.863	10.8	0.45
9.7	10.2	0.44	1.879	10.0	10.5	0.44	1.875	10.2	10.6	0.44	1.870	1.875	10.4	0.44
9.2	9.6	0.42	1.901	9.4	9.8	0.44	1.879	9.6	10.0	0.44	1.875	1.885	9.8	0.43
8.8	9.2	0.43	1.888	9.0	9.4	0.43	1.883	9.2	9.7	0.43	1.890	1.887	9.4	0.43
8.1	8.5	0.42	1.901	8.3	8.7	0.42	1.900	8.5	8.9	0.42	1.899	1.900	8.7	0.42
7.9	8.3	0.43	1.888	8.1	8.5	0.42	1.899	8.3	8.7	0.42	1.899	1.895	8.5	0.42
7.7	8.1	0.42	1.901	7.9	8.2	0.43	1.894	8.1	8.4	0.42	1.897	1.897	8.2	0.42
7.7	8.0	0.42	1.897	7.8	8.2	0.43	1.891	8.0	8.3	0.43	1.890	1.892	8.2	0.43
7.6	7.9	0.42	1.904	7.7	8.1	0.43	1.891	7.8	8.2	0.43	1.888	1.894	8.1	0.43
7.5	7.9	0.42	1.904	7.7	8.0	0.42	1.900	7.8	8.1	0.43	1.893	1.899	8.0	0.42
7.4	7.7	0.42	1.900	7.5	7.8	0.42	1.901	7.6	8.0	0.42	1.902	1.901	7.8	0.42
7.4	7.7	0.41	1.917	7.5	7.9	0.41	1.914	7.6	7.9	0.42	1.906	1.913	7.8	0.41
7.2	7.5	0.42	1.903	7.3	7.7	0.42	1.908	7.4	7.7	0.42	1.905	1.905	7.6	0.42
7.1	7.4	0.41	1.909	7.3	7.6	0.42	1.895	7.3	7.7	0.42	1.898	1.901	7.6	0.42
7.0	7.3	0.41	1.910	7.2	7.6	0.41	1.909	7.3	7.6	0.41	1.909	1.909	7.5	0.41
7.2	7.5	0.41	1.908	7.3	7.7	0.42	1.903	7.4	7.7	0.42	1.904	1.905	7.6	0.42
6.6	6.9	0.42	1.905	6.9	7.2	0.42	1.907	6.8	7.1	0.42	1.908	1.907	7.0	0.42
6.2	6.5	0.41	1.916	6.5	6.8	0.41	1.913	6.3	6.6	0.41	1.911	1.913	6.6	0.41
5.8	6.0	0.40	1.925	6.0	6.2	0.41	1.916	5.8	6.1	0.41	1.917	1.920	6.1	0.41
4.6	4.9	0.40	1.926	4.9	5.1	0.40	1.922	4.7	5.0	0.40	1.923	1.924	5.0	0.40
4.3	4.5	0.40	1.926	4.6	4.8	0.41	1.919	4.4	4.6	0.40	1.927	1.924	4.6	0.40
3.8	4.0	0.40	1.928	4.1	4.3	0.40	1.924	3.9	4.1	0.40	1.925	1.926	4.1	0.40
3.2	3.4	0.42	1.897	3.8	4.0	0.41	1.916	3.6	3.7	0.40	1.929	1.914	3.7	0.41
3.0	3.1	0.41	1.914	3.4	3.6	0.41	1.919	3.2	3.3	0.41	1.918	1.917	3.3	0.41
2.9	3.0	0.40	1.935	3.3	3.5	0.40	1.924	3.0	3.2	0.41	1.915	1.925	3.2	0.40
2.7	2.8	0.40	1.930	3.1	3.2	0.39	1.936	2.8	2.9	0.40	1.929	1.932	3.0	0.40
2.5	2.6	0.39	1.942	2.9	3.0	0.40	1.932	2.6	2.7	0.40	1.925	1.933	2.8	0.40
2.4	2.5	0.40	1.926	2.7	2.8	0.40	1.928	2.4	2.5	0.40	1.922	1.925	2.6	0.40
2.4	2.5	0.39	1.938	2.7	2.8	0.40	1.931	2.4	2.5	0.40	1.925	1.931	2.6	0.40
1.4	1.5	0.40	1.931	1.5	1.5	0.40	1.930	1.3	1.4	0.40	1.929	1.930	1.5	0.40
1.1	1.2	0.40	1.930	1.2	1.3	0.40	1.924	1.3	1.4	0.40	1.926	1.927	1.3	0.40
0.7	0.7	0.40	1.924	0.8	0.8	0.41	1.917	0.7	0.7	0.41	1.913	1.918	0.8	0.41
0.6	0.7	0.40	1.935	0.7	0.8	0.40	1.929	0.7	0.7	0.40	1.924	1.929	0.7	0.40
0.6	0.6	0.41	1.913	0.7	0.8	0.41	1.921	0.7	0.7	0.41	1.917	1.917	0.7	0.41
0.5	0.6	0.40	1.932	0.7	0.8	0.40	1.929	0.7	0.7	0.40	1.923	1.928	0.7	0.40
0.5	0.5	0.40	1.928	0.7	0.8	0.41	1.912	0.7	0.7	0.41	1.909	1.917	0.7	0.41
0.5	0.5	0.40	1.934									1.934	0.5	0.40
Fitting Parameters														
				ash	bsh	csh								
BSM 70-30 SR-L #1				0.401	0.148	3.089								
BSM 70-30 SR-L #2				0.403	0.149	3.186								
BSM 70-30 SR-L #3				0.404	0.150	3.155								
average				0.402	0.149	3.143								

Table F-7: Drying Volume Change of 70:30 MX80:Sand (1.78 Mg/m³ with SR-Sh pore fluid)

BSM 70-30 SR-Sh #1				BSM 70-30 SR-Sh #2				BSM 70-30 SR-Sh #3				BSM 70-30 SR-Sh Average		
Measured				Measured				Measured				Measured		
Water content (apparent)	Water content (true)	void ratio	Dry density	Water content (apparent)	Water content (true)	void ratio	Dry density	Water content (apparent)	Water content (true)	void ratio	Dry density	Average Density	Average water content	Average void ratio
(%)	(%)		(g/cm ³)	(%)	(%)		(g/cm ³)	(%)	(%)		(g/cm ³)	(g/cm ³)	(%)	
14.5	15.6	0.52	1.772	14.5	15.5	0.51	1.793	14.6	15.6	0.51	1.784	1.783	15.6	0.51
13.6	14.6	0.50	1.797	13.8	14.8	0.50	1.805	13.6	14.5	0.49	1.813	1.805	14.6	0.50
12.9	13.8	0.49	1.812	12.9	13.8	0.49	1.818	12.9	13.8	0.49	1.814	1.815	13.8	0.49
12.4	13.3	0.49	1.808	12.2	13.1	0.49	1.817	12.8	13.7	0.49	1.809	1.812	13.4	0.49
12.4	13.2	0.49	1.814	12.2	13.0	0.48	1.819	12.2	13.0	0.48	1.821	1.818	13.1	0.49
11.8	12.7	0.49	1.816	11.6	12.4	0.48	1.828	11.7	12.5	0.48	1.826	1.823	12.5	0.48
11.5	12.3	0.48	1.822	11.2	11.9	0.47	1.833	10.9	11.6	0.47	1.838	1.831	11.9	0.47
10.7	11.5	0.47	1.842	10.4	11.1	0.46	1.852	9.1	9.8	0.44	1.869	1.854	10.8	0.46
9.0	9.7	0.44	1.880	8.9	9.5	0.44	1.871	8.7	9.4	0.44	1.876	1.876	9.5	0.44
8.5	9.1	0.44	1.869	8.4	9.0	0.43	1.883	8.3	8.9	0.43	1.892	1.881	9.0	0.44
8.3	8.8	0.44	1.879	8.1	8.7	0.44	1.880	7.6	8.1	0.42	1.895	1.884	8.6	0.43
7.6	8.2	0.43	1.884	7.4	7.9	0.43	1.885	7.4	8.0	0.42	1.899	1.889	8.0	0.43
7.5	8.0	0.42	1.896	7.3	7.8	0.42	1.905	6.6	7.1	0.41	1.910	1.904	7.6	0.42
6.8	7.3	0.42	1.903	6.4	6.9	0.41	1.912	6.1	6.5	0.42	1.903	1.906	6.9	0.42
6.3	6.7	0.42	1.903	6.0	6.4	0.42	1.901	6.0	6.4	0.41	1.909	1.905	6.5	0.42
6.2	6.6	0.43	1.893	5.9	6.3	0.41	1.911	6.0	6.4	0.41	1.911	1.905	6.4	0.42
6.1	6.5	0.42	1.898	5.9	6.3	0.42	1.903	5.8	6.2	0.41	1.913	1.905	6.3	0.42
6.0	6.4	0.43	1.893	5.8	6.2	0.42	1.906	5.8	6.2	0.41	1.916	1.905	6.3	0.42
6.0	6.4	0.43	1.894	5.8	6.2	0.42	1.907	5.5	5.9	0.41	1.916	1.906	6.2	0.42
5.6	6.0	0.43	1.895	5.4	5.8	0.42	1.904	4.4	4.7	0.41	1.917	1.905	5.5	0.42
4.5	4.9	0.42	1.904	4.2	4.5	0.41	1.913	4.1	4.4	0.41	1.918	1.912	4.6	0.41
4.4	4.7	0.41	1.911	4.0	4.3	0.41	1.919	4.0	4.3	0.41	1.916	1.915	4.4	0.41
4.3	4.6	0.42	1.908	4.0	4.2	0.41	1.917	3.6	3.9	0.40	1.925	1.917	4.3	0.41
3.8	4.1	0.41	1.909	3.5	3.7	0.41	1.917	3.4	3.7	0.40	1.925	1.917	3.8	0.41
3.7	3.9	0.42	1.895	3.2	3.4	0.41	1.917	3.1	3.4	0.40	1.926	1.913	3.6	0.41
3.3	3.5	0.42	1.907	2.9	3.1	0.41	1.920	3.0	3.2	0.40	1.933	1.920	3.3	0.41
3.2	3.4	0.42	1.906	2.9	3.1	0.40	1.922	2.7	2.9	0.40	1.933	1.920	3.1	0.41
2.8	3.0	0.40	1.925	2.5	2.7	0.41	1.922	2.4	2.6	0.39	1.941	1.929	2.8	0.40
2.2	2.4	0.41	1.915	2.3	2.4	0.40	1.929	2.3	2.5	0.40	1.935	1.926	2.4	0.40
2.3	2.5	0.42	1.908	2.2	2.3	0.40	1.929	2.3	2.5	0.39	1.943	1.927	2.4	0.40
2.3	2.4	0.41	1.917	2.1	2.3	0.40	1.928	2.3	2.4	0.41	1.921	1.922	2.4	0.40
2.3	2.5	0.42	1.907	2.2	2.3	0.40	1.924	1.9	2.0	0.40	1.931	1.921	2.3	0.41
1.9	2.0	0.42	1.907	1.7	1.9	0.40	1.927	1.5	1.6	0.39	1.946	1.927	1.8	0.40
1.6	1.7	0.42	1.899	1.4	1.5	0.40	1.928	1.4	1.5	0.40	1.928	1.918	1.6	0.41
1.4	1.5	0.42	1.905	1.3	1.4	0.40	1.928	0.8	0.9	0.40	1.935	1.923	1.3	0.40
0.9	1.0	0.41	1.914	0.8	0.8	0.41	1.921	0.8	0.8	0.40	1.927	1.921	0.9	0.41
0.8	0.9	0.41	1.911	0.7	0.8	0.41	1.917	0.6	0.7	0.40	1.927	1.918	0.8	0.41
0.7	0.7	0.42	1.904	0.6	0.6	0.40	1.927	0.6	0.7	0.40	1.926	1.919	0.7	0.41
0.7	0.7	0.42	1.907	0.6	0.6	0.40	1.925					1.916	0.7	0.41
Fitting Parameter														
				ash	bsh	csh								
BSM70-30 SR-Sh #1				0.413	0.153	3.025								
BSM70-30 SR-Sh #2				0.404	0.150	2.954								
BSM70-30 SR-Sh #3				0.399	0.148	2.855								
average				0.406	0.150	2.945								

Table F-8: Fitting parameters generated for each laboratory shrinkage test.

	a_{sh}	b_{sh}	C_{sh}
MX80 DW#1	0.4098	0.1506	3.5778
MX80 DW#2	0.4224	0.1553	3.1033
MX80 DW#3	0.4064	0.1494	3.4601
average	0.4129	0.1518	3.3804
	a_{sh}	b_{sh}	C_{sh}
MX80 SR-L #1	0.5469	0.2011	2.1648
MX80 SR-L #2	0.5080	0.1867	2.1321
MX80 SR-L #3	0.5086	0.1870	2.2133
average	0.5211	0.1916	2.1701
	a_{sh}	b_{sh}	C_{sh}
MX80 SR-Sh #1	0.5001	0.1839	1.8412
MX80 SR-Sh #2	0.5084	0.1869	1.8165
MX80 SR-Sh #3	0.4986	0.1833	1.8445
average	0.5024	0.1847	1.8341

	a_{sh}	b_{sh}	C_{sh}
BSM 70-30 DW #1	0.3921	0.1452	4.9776
BSM 70-30 DW #2	0.3951	0.1463	4.9119
BSM 70-30 DW #3	0.3976	0.1473	4.8141
average	0.3950	0.1463	4.9012
	a_{sh}	b_{sh}	C_{sh}
BSM 70-30 CR-10 #1	0.3822	0.1416	5.3303
BSM 70-30 CR-10 #2	0.3876	0.1435	6.5490
BSM 70-30 CR-10 #3	0.3802	0.1408	6.5089
average	0.3833	0.1420	6.1294
	a_{sh}	b_{sh}	C_{sh}
BSM 70-30 SR-L #1	0.4006	0.1484	3.0888
BSM 70-30 SR-L #2	0.4030	0.1493	3.1864
BSM 70-30 SR-L #3	0.4039	0.1496	3.1552
average	0.4025	0.1491	3.1435
	a_{sh}	b_{sh}	C_{sh}
BSM 70-30 SR-Sh #1	0.4134	0.1531	3.0249
BSM 70-30 SR-Sh #2	0.4043	0.1497	2.9544
BSM 70-30 SR-Sh #3	0.3989	0.1478	2.8551
average	0.4055	0.1502	2.9448

APPENDIX G: SOIL WATER CHARACTERISTIC CURVE (SWCC) DATA

MX80 DW #1							MX80 DW #2							MX80 DW #3						
Capillary pressure (kPa)	dry density (g/cm ³)	void ratio	porosity	Corrected gravimetric water content (%)	Volumetric fluid content (%)	Degree of liquid saturation (%)	Capillary pressure (kPa)	dry density (g/cm ³)	void ratio	porosity	Corrected gravimetric water content (%)	Volumetric fluid content (%)	Degree of liquid saturation (%)	Capillary pressure (kPa)	dry density (g/cm ³)	void ratio	porosity	Corrected gravimetric water content (%)	Volumetric fluid content (%)	Degree of liquid saturation (%)
100	1.461	0.86	0.46	32.0	46.8	101.0	200	1.479	0.84	0.46	30.3	44.8	98.2	200	1.471	0.85	0.46	30.1	44.3	96.5
200	1.447	0.88	0.47	32.8	47.4	101.3	450	1.472	0.85	0.46	30.5	44.9	98.0	450	1.463	0.86	0.46	30.4	44.4	96.1
400	1.442	0.89	0.47	33.2	47.8	101.7	700	1.458	0.86	0.46	30.9	45.0	97.1	700	1.452	0.87	0.47	30.7	44.5	95.5
700	1.433	0.90	0.47	33.8	48.4	102.3	1,000	1.457	0.87	0.46	30.9	45.0	96.8	1,000	1.448	0.88	0.47	30.8	44.5	95.3
1,450	1.440	0.89	0.47	33.7	48.5	103.1	1,450	1.443	0.89	0.47	31.4	45.2	96.3	1,450	1.441	0.89	0.47	31.0	44.7	95.1
16,600	1.490	0.83	0.45	23.9	35.7	78.9	16,570	1.490	0.83	0.45	23.9	35.7	78.9	17,110	1.490	0.83	0.45	23.9	35.7	78.9
31,650	1.487	0.83	0.45	20.9	31.1	68.6	32,270	1.487	0.83	0.45	20.9	31.1	68.6	34,220	1.487	0.83	0.45	20.9	31.1	68.6
71,700	1.465	0.86	0.46	15.0	22.0	47.8	71,850	1.465	0.86	0.46	15.0	22.0	47.8	71,210	1.465	0.86	0.46	15.0	22.0	47.8
119,770	1.458	0.87	0.46	9.0	13.1	28.3	120,590	1.458	0.87	0.46	9.0	13.1	28.3	120,610	1.458	0.87	0.46	9.0	13.1	28.3
206,540	1.487	0.83	0.45	3.1	4.7	10.3	203,840	1.487	0.83	0.45	3.1	4.7	10.3	202,450	1.487	0.83	0.45	3.1	4.7	10.3

Measured Data

Measured Data Graphs

Fitting Parameters:

	m	n	α (1/Pa)	S_{lr}
MX80 DW #1	4.63	1.01	2.89E-09	0.01
MX80 DW #2	4.67	1.02	2.89E-09	0.01
MX80 DW #3	4.67	1.04	2.95E-09	0.01
average	4.66	1.02	2.91E-09	0.01

Fitting Parameters

Fitted Curves Data

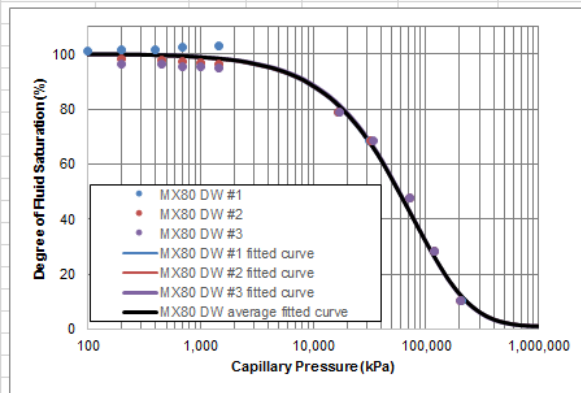


Figure G-1: SWCC data and curves for replicate tests of MX80 with DW pore fluid

MX80 SR-L #1							MX80 SR-L #2							MX80 SR-L #3						
Capillary pressure	dry density	void ratio	porosity	Corrected gravimetric water content	Volumetric fluid content	Degree of liquid saturation	Capillary pressure	dry density	void ratio	porosity	Corrected gravimetric water content	Volumetric fluid content	Degree of liquid saturation	Capillary pressure	dry density	void ratio	porosity	Corrected gravimetric water content	Volumetric fluid content	Degree of liquid saturation
(kPa)	(g/cm ³)			(%)	(%)	(%)	(kPa)	(g/cm ³)			(%)	(%)	(%)	(kPa)	(g/cm ³)			(%)	(%)	(%)
200	1.504	0.81	0.45	27.1	44.8	100.3	200	1.488	0.83	0.45	27.3	44.6	98.5	200	1.473	0.85	0.46	26.9	43.6	95.1
450	1.514	0.80	0.44	26.8	44.5	100.4	450	1.493	0.82	0.45	27.2	44.6	98.8	450	1.479	0.84	0.46	26.5	43.0	94.3
700	1.521	0.79	0.44	26.5	44.2	100.3	700	1.500	0.81	0.45	27.3	45.0	100.3	700	1.484	0.83	0.45	26.3	42.9	94.4
1,000	1.526	0.78	0.44	26.1	43.8	99.6	1,000	1.510	0.80	0.45	26.7	44.3	99.5	1,000	1.490	0.83	0.45	25.9	42.4	93.8
1,450	1.530	0.78	0.44	25.6	43.0	98.3	1,450	1.520	0.79	0.44	26.5	44.2	100.3	1,450	1.505	0.81	0.45	25.5	42.1	94.3
50,680	1.519	0.79	0.44	21.8	36.4	82.4	51,050	1.519	0.79	0.44	21.8	36.4	82.4	51,340	1.519	0.79	0.44	21.8	36.4	82.4
55,140	1.535	0.77	0.44	19.1	32.2	73.8	54,510	1.535	0.77	0.44	19.1	32.2	73.8	55,370	1.535	0.77	0.44	19.1	32.2	73.8
82,670	1.513	0.80	0.44	13.7	22.7	51.2	81,180	1.513	0.80	0.44	13.7	22.7	51.2	83,060	1.513	0.80	0.44	13.7	22.7	51.2
132,060	1.512	0.80	0.44	8.2	13.6	30.7	134,400	1.512	0.80	0.44	8.2	13.6	30.7	133,810	1.512	0.80	0.44	8.2	13.6	30.7
232,120	1.523	0.79	0.44	2.7	4.5	10.3	231,490	1.523	0.79	0.44	2.7	4.5	10.3	233,780	1.523	0.79	0.44	2.7	4.5	10.3

Measured Data

Measured Data Graphs

Fitting Parameters:

	m	n	α (1/Pa)	S_{lr}
MX80 SR-L #1	0.47	3.56	1.68E-08	0.01
MX80 SR-L #2	0.47	3.54	1.68E-08	0.01
MX80 SR-L #3	0.46	3.61	1.68E-08	0.01
average	0.47	3.57	1.68E-08	0.01

Fitting Parameters

Fitted Curves Data

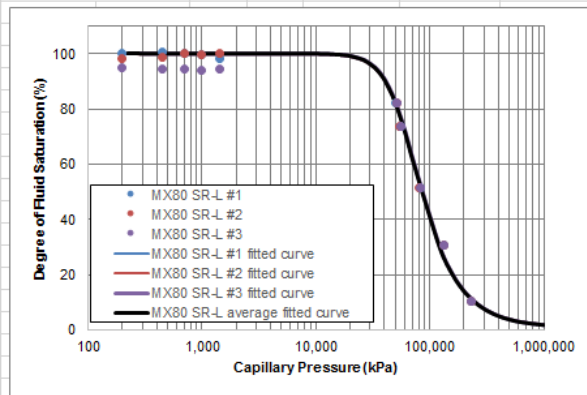


Figure G-2: SWCC data and curves for replicate tests of MX80 with SR-L pore fluid

MX80 SR-Sh #1							MX80 SR-Sh #2							MX80 SR-Sh #3						
Capillary pressure	dry density	void ratio	porosity	Corrected gravimetric water content	Volumetric fluid content	Degree of liquid saturation	Capillary pressure	dry density	void ratio	porosity	Corrected gravimetric water content	Volumetric fluid content	Degree of liquid saturation	Capillary pressure	dry density	void ratio	porosity	Corrected gravimetric water content	Volumetric fluid content	Degree of liquid saturation
(kPa)	(g/cm ³)			(%)	(%)	(%)	(kPa)	(g/cm ³)			(%)	(%)	(%)	(kPa)	(g/cm ³)			(%)	(%)	(%)
200	1.478	0.84	0.46	25.2	44.4	97.2	200	1.496	0.82	0.45	24.9	44.3	98.5	200	1.447	0.88	0.47	25.1	43.2	92.3
450	1.481	0.84	0.46	25.1	44.3	97.2	450	1.503	0.81	0.45	24.7	44.1	98.6	450	1.449	0.88	0.47	25.0	43.2	92.4
700	1.487	0.83	0.45	24.7	43.8	96.5	700	1.511	0.80	0.44	24.5	44.0	99.0	700	1.453	0.87	0.47	24.7	42.8	91.9
1,000	1.494	0.82	0.45	24.7	43.9	97.4	1,000	1.516	0.79	0.44	24.1	43.5	98.4	1,000	1.457	0.87	0.46	24.5	42.5	91.6
1,450	1.504	0.81	0.45	24.4	43.7	97.8	1,450	1.524	0.78	0.44	23.8	43.2	98.3	1,450	1.464	0.86	0.46	24.1	42.1	91.1
61,010	1.538	0.77	0.43	20.1	36.8	84.7	61,050	1.538	0.77	0.43	20.1	36.8	84.7	61,120	1.538	0.77	0.43	20.1	36.8	84.7
67,770	1.518	0.79	0.44	17.6	31.8	72.0	67,440	1.518	0.79	0.44	17.6	31.8	72.0	75,130	1.518	0.79	0.44	17.6	31.8	72.0
96,470	1.434	0.90	0.47	12.6	21.4	45.4	95,490	1.434	0.90	0.47	12.6	21.4	45.4	94,730	1.434	0.90	0.47	12.6	21.4	45.4
148,490	1.468	0.85	0.46	7.6	13.3	28.8	147,100	1.468	0.85	0.46	7.6	13.3	28.8	145,140	1.468	0.85	0.46	7.6	13.3	28.8
239,660	1.476	0.84	0.46	2.5	4.4	9.7	240,610	1.476	0.84	0.46	2.5	4.4	9.7	239,200	1.476	0.84	0.46	2.5	4.4	9.7

Measured Data

Measured Data Graphs

Fitting Parameters:

	m	n	α (1/Pa)	S_{lr}
MX80 SR-Sh #1	0.56	3.73	1.32E-08	0.01
MX80 SR-Sh #2	0.54	3.81	1.34E-08	0.01
MX80 SR-Sh #3	0.46	4.42	1.38E-08	0.01
average	0.52	3.99	1.35E-08	0.01

Fitting Parameters

Fitted Curves Data

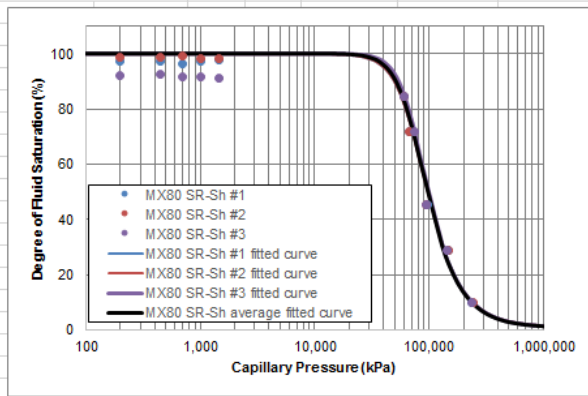


Figure G-3: SWCC data and curves for replicate tests of MX80 with SR-Sh pore fluid

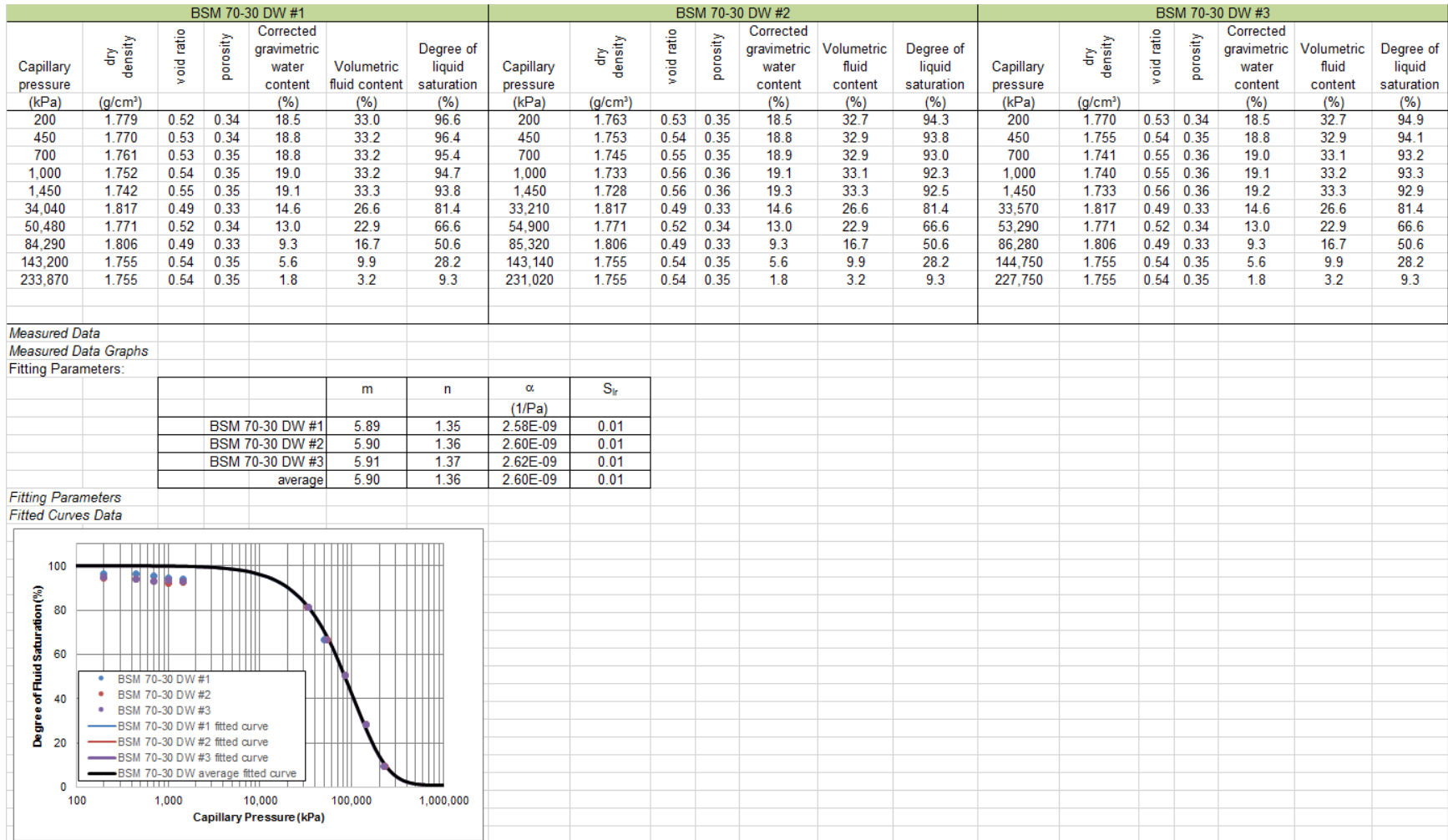


Figure G-4: SWCC data and curves for replicate tests of 70:30 BSM with DW pore fluid

BSM 70-30 CR-10 #1							BSM 70-30 CR-10 #2						BSM 70-30 CR-10 #3								
Capillary pressure (kPa)	dry density (g/cm ³)	void ratio	porosity	Corrected gravimetric water content (%)	Volumetric fluid content (%)	Degree of liquid saturation (%)	Capillary pressure (kPa)	dry density (g/cm ³)	void ratio	porosity	Corrected gravimetric water content (%)	Volumetric fluid content (%)	Degree of liquid saturation (%)	Capillary pressure (kPa)	dry density (g/cm ³)	void ratio	porosity	Corrected gravimetric water content (%)	Volumetric fluid content (%)	Degree of liquid saturation (%)	
200	1.785	0.51	0.34	18.5	33.3	98.2	200	1.805	0.50	0.33	18.6	33.9	102.1	200	1.799	0.50	0.33	18.5	33.5	100.3	
450	1.776	0.52	0.34	18.7	33.5	97.8	450	1.796	0.50	0.33	18.8	34.1	101.7	450	1.788	0.51	0.34	18.7	33.7	99.7	
700	1.762	0.53	0.35	19.0	33.7	97.1	700	1.780	0.52	0.34	19.1	34.2	100.4	700	1.770	0.53	0.34	19.1	34.0	98.6	
1,000	1.759	0.53	0.35	19.1	33.8	96.9	1,000	1.777	0.52	0.34	19.3	34.6	101.2	1,000	1.767	0.53	0.35	19.1	33.9	98.2	
1,450	1.750	0.54	0.35	19.2	33.8	96.2	1,450	1.770	0.53	0.34	19.5	34.7	100.6	1,450	1.761	0.53	0.35	19.4	34.3	98.7	
27,450	1.777	0.52	0.34	14.7	26.4	77.1	27,760	1.777	0.52	0.34	14.7	26.4	77.1	26,980	1.777	0.52	0.34	14.7	26.4	77.1	
51,960	1.811	0.49	0.33	12.9	23.5	71.5	52,250	1.811	0.49	0.33	12.9	23.5	71.5	51,640	1.811	0.49	0.33	12.9	23.5	71.5	
81,980	1.796	0.50	0.33	9.2	16.7	49.9	81,370	1.796	0.50	0.33	9.2	16.7	49.9	83,550	1.796	0.50	0.33	9.2	16.7	49.9	
139,340	1.730	0.56	0.36	5.6	9.7	27.0	138,530	1.730	0.56	0.36	5.6	9.7	27.0	140,140	1.730	0.56	0.36	5.6	9.7	27.0	
216,400	1.879	0.44	0.30	1.9	3.7	12.1	209,010	1.879	0.44	0.30	1.9	3.7	12.1	213,490	1.879	0.44	0.30	1.9	3.7	12.1	
<i>Measured Data</i>																					
<i>Measured Data Graphs</i>																					
Fitting Parameters:																					
					m	n					α	S_r									
											(1/Pa)										
					BSM 70-30 CR-10 #1	4.37	1.24				3.15E-09	0.01									
					BSM 70-30 CR-10 #2	4.39	1.27				3.24E-09	0.01									
					BSM 70-30 CR-10 #3	4.36	1.24				3.16E-09	0.01									
					average	4.37	1.25				3.18E-09	0.01									
<i>Fitting Parameters</i>																					
<i>Fitted Curves Data</i>																					

Figure G-5: SWCC data and curves for replicate tests of 70:30 BSM with CR10 pore fluid

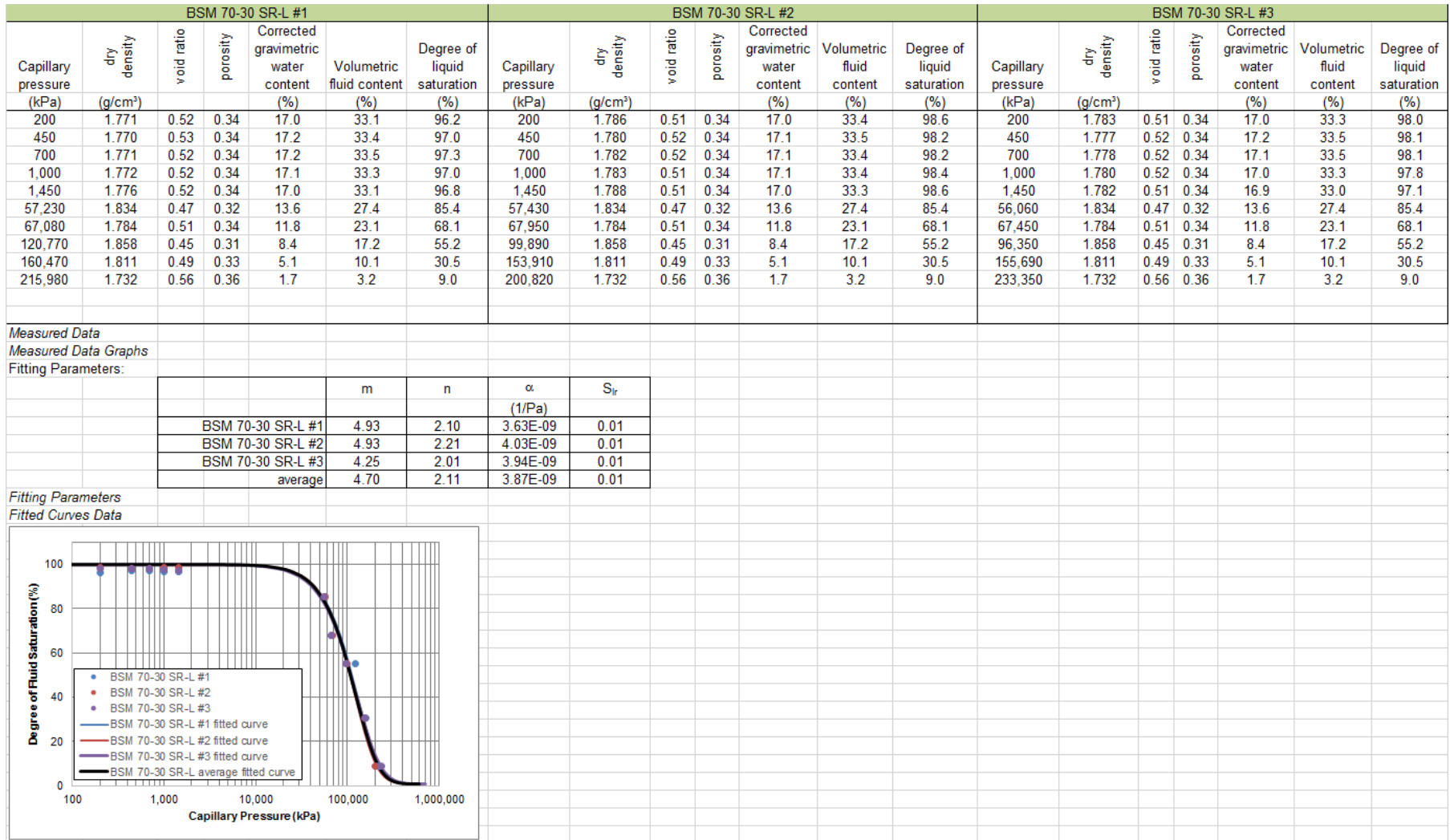


Figure G-6: SWCC data and curves for replicate tests of 70:30 BSM with SR-L pore fluid

BSM 70-30 SR-Sh #1							BSM 70-30 SR-Sh #2							BSM 70-30 SR-Sh #3						
Capillary pressure (kPa)	dry density (g/cm ³)	void ratio	porosity	Corrected gravimetric water content (%)	Volumetric fluid content (%)	Degree of liquid saturation (%)	Capillary pressure (kPa)	dry density (g/cm ³)	void ratio	porosity	Corrected gravimetric water content (%)	Volumetric fluid content (%)	Degree of liquid saturation (%)	Capillary pressure (kPa)	dry density (g/cm ³)	void ratio	porosity	Corrected gravimetric water content (%)	Volumetric fluid content (%)	Degree of liquid saturation (%)
200	1.753	0.54	0.35	15.5	32.4	92.3	200	1.791	0.51	0.34	15.6	33.2	98.6	200	1.746	0.55	0.35	15.6	32.3	91.5
450	1.749	0.54	0.35	15.9	33.1	93.9	450	1.787	0.51	0.34	15.7	33.3	98.5	450	1.744	0.55	0.35	15.5	32.2	91.0
700	1.749	0.54	0.35	15.8	33.0	93.6	700	1.783	0.51	0.34	15.9	33.7	99.4	700	1.744	0.55	0.35	15.4	32.1	90.6
1,000	1.749	0.54	0.35	15.9	33.1	93.9	1,000	1.784	0.51	0.34	15.7	33.3	98.2	1,000	1.747	0.55	0.35	15.6	32.3	91.6
1,450	1.751	0.54	0.35	15.9	33.0	94.0	1,450	1.786	0.51	0.34	15.7	33.3	98.4	1,450	1.749	0.54	0.35	15.4	32.2	91.3
68,220	1.750	0.54	0.35	12.4	25.9	73.7	67,650	1.750	0.54	0.35	12.4	25.9	73.7	67,060	1.750	0.54	0.35	12.4	25.9	73.7
79,730	1.774	0.52	0.34	10.9	23.0	67.0	80,190	1.774	0.52	0.34	10.9	23.0	67.0	78,850	1.774	0.52	0.34	10.9	23.0	67.0
113,030	1.772	0.52	0.34	7.8	16.4	47.8	112,730	1.774	0.52	0.34	7.8	16.4	47.9	114,340	1.772	0.52	0.34	7.8	16.4	47.8
167,470	1.724	0.57	0.36	4.7	9.6	26.5	168,910	1.723	0.57	0.36	4.7	9.6	26.5	168,890	1.724	0.57	0.36	4.7	9.6	26.5
250,640	1.754	0.54	0.35	1.6	3.2	9.3	249,520	1.754	0.54	0.35	1.6	3.2	9.3	250,580	1.754	0.54	0.35	1.6	3.2	9.3

Measured Data

Measured Data Graphs

Fitting Parameters:

	m	n	α (1/Pa)	S_{lr}
BSM 70-30 SR-Sh #1	4.93	1.77	3.14E-09	0.01
BSM 70-30 SR-Sh #2	4.92	1.77	3.14E-09	0.01
BSM 70-30 SR-Sh #3	4.84	1.75	3.15E-09	0.01
average	4.90	1.77	3.15E-09	0.01

Fitting Parameters

Fitted Curves Data

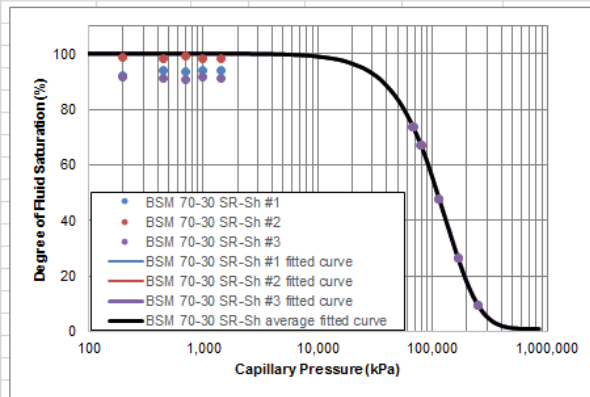


Figure G-7: SWCC data and curves for replicate tests of 70:30 BSM with SR-Sh pore fluid

APPENDIX H: AIR PERMEABILITY TEST DATA

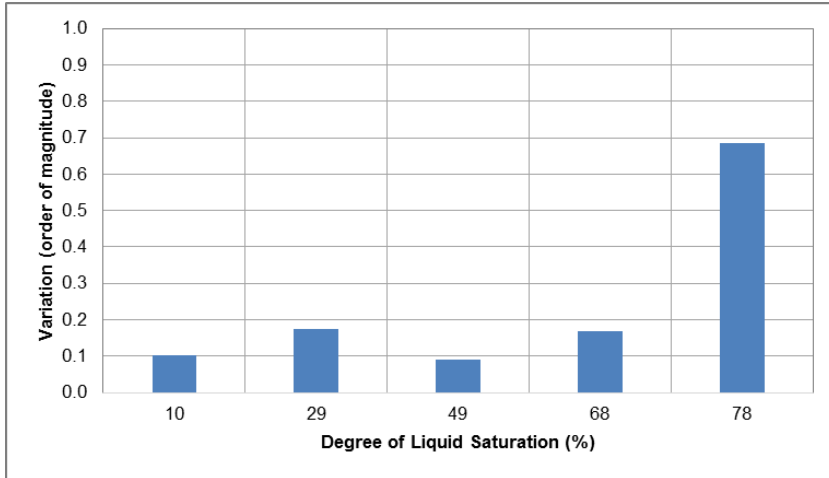
Table H-1: Air Permeability and Air Conductivity measurements of MX80 @ 1.5 Mg/m³ dry density

MX-80 DW #1						MX-80 DW #2						MX-80 DW #3						MX-80 DW Average						Log delta max-min, Coef. Of Air Perm.
Degree of Liquid Saturation	dry density	void ratio	porosity	Coefficient of Air Permeability	Air (gas) Conductivity	Degree of Liquid Saturation	dry density	void ratio	porosity	Coefficient of Air Permeability	Air (gas) Conductivity	Degree of Liquid Saturation	dry density	void ratio	porosity	Coefficient of Air Permeability	Air (gas) Conductivity	Degree of Liquid Saturation	dry density	void ratio	porosity	Coefficient of Air Permeability	Air (gas) Conductivity	
(%)	(g/cm ³)			(m ²)	(m/s)	(%)	(g/cm ³)			(m ²)	(m/s)	(%)	(g/cm ³)			(m ²)	(m/s)	(%)	(g/cm ³)			(m ²)	(m/s)	
77.2	1.477	0.84	0.46	8.7E-15	5.5E-09	78.7	1.490	0.83	0.45	5.3E-15	3.4E-09	78.6	1.489	0.83	0.45	1.8E-15	1.1E-09	78.2	1.485	0.83	0.45	5.3E-15	3.4E-09	0.69
67.6	1.478	0.84	0.46	3.2E-14	2.1E-08	68.0	1.481	0.84	0.46	2.7E-14	1.7E-08	68.0	1.482	0.84	0.46	2.2E-14	1.4E-08	67.9	1.480	0.84	0.46	2.7E-14	1.7E-08	0.17
47.8	1.467	0.85	0.46	2.4E-13	1.5E-07	48.6	1.478	0.84	0.46	2.0E-13	1.3E-07	49.9	1.497	0.82	0.45	2.0E-13	1.3E-07	48.8	1.481	0.84	0.46	2.1E-13	1.4E-07	0.09
28.5	1.464	0.86	0.46	9.4E-13	6.0E-07	29.7	1.492	0.82	0.45	6.6E-13	4.2E-07	30.0	1.498	0.82	0.45	6.3E-13	4.0E-07	29.4	1.485	0.83	0.45	7.5E-13	4.8E-07	0.17
9.7	1.474	0.85	0.46	1.4E-12	9.0E-07	9.7	1.476	0.84	0.46	1.7E-12	1.1E-06	9.9	1.493	0.82	0.45	1.4E-12	8.8E-07	9.8	1.481	0.84	0.46	1.5E-12	9.6E-07	0.10
MX-80 SR-L #1						MX-80 SR-L #2						MX-80 SR-L #3						MX-80 SR-L Average						Log delta max-min, Coef. Of Air Perm.
Degree of Liquid Saturation	dry density	void ratio	porosity	Coefficient of Air Permeability	Air (gas) Conductivity	Degree of Liquid Saturation	dry density	void ratio	porosity	Coefficient of Air Permeability	Air (gas) Conductivity	Degree of Liquid Saturation	dry density	void ratio	porosity	Coefficient of Air Permeability	Air (gas) Conductivity	Degree of Liquid Saturation	dry density	void ratio	porosity	Coefficient of Air Permeability	Air (gas) Conductivity	
(%)	(g/cm ³)			(m ²)	(m/s)	(%)	(g/cm ³)			(m ²)	(m/s)	(%)	(g/cm ³)			(m ²)	(m/s)	(%)	(g/cm ³)			(m ²)	(m/s)	
77.8	1.481	0.84	0.46	1.0E-14	6.4E-09	78.8	1.489	0.83	0.45	1.7E-15	1.1E-09	78.3	1.485	0.83	0.45	8.2E-15	5.3E-09	78.3	1.485	0.83	0.45	6.7E-15	4.3E-09	0.77
69.9	1.499	0.81	0.45	1.3E-14	8.2E-09	69.6	1.496	0.82	0.45	1.4E-14	9.0E-09	69.0	1.490	0.83	0.45	1.8E-14	1.1E-08	69.5	1.495	0.82	0.45	1.5E-14	9.4E-09	0.14
49.1	1.488	0.83	0.45	1.8E-13	1.1E-07	49.4	1.492	0.82	0.45	1.5E-13	9.5E-08	48.8	1.484	0.83	0.45	1.4E-13	8.9E-08	49.1	1.488	0.83	0.45	1.6E-13	9.9E-08	0.11
29.0	1.477	0.84	0.46	3.6E-13	2.3E-07	29.0	1.478	0.84	0.46	5.4E-13	3.5E-07	28.5	1.465	0.86	0.46	6.3E-13	4.0E-07	28.8	1.473	0.85	0.46	5.1E-13	3.3E-07	0.24
7.5	1.477	0.84	0.46	1.7E-12	1.1E-06	7.5	1.480	0.84	0.46	1.8E-12	1.2E-06	7.6	1.483	0.83	0.45	7.9E-13	5.0E-07	7.5	1.480	0.84	0.46	1.5E-12	9.3E-07	0.37
MX-80 SR-Sh #1						MX-80 SR-Sh #2						MX-80 SR-Sh #3						MX-80 SR-Sh Average						Log delta max-min, Coef. Of Air Perm.
Degree of Liquid Saturation	dry density	void ratio	porosity	Coefficient of Air Permeability	Air (gas) Conductivity	Degree of Liquid Saturation	dry density	void ratio	porosity	Coefficient of Air Permeability	Air (gas) Conductivity	Degree of Liquid Saturation	dry density	void ratio	porosity	Coefficient of Air Permeability	Air (gas) Conductivity	Degree of Liquid Saturation	dry density	void ratio	porosity	Coefficient of Air Permeability	Air (gas) Conductivity	
(%)	(g/cm ³)			(m ²)	(m/s)	(%)	(g/cm ³)			(m ²)	(m/s)	(%)	(g/cm ³)			(m ²)	(m/s)	(%)	(g/cm ³)			(m ²)	(m/s)	
79.0	1.492	0.82	0.45	1.2E-15	7.9E-10	79.3	1.495	0.82	0.45	1.4E-15	8.8E-10	78.5	1.487	0.83	0.45	3.0E-15	1.9E-09	78.9	1.491	0.82	0.45	1.9E-15	1.2E-09	0.38
69.6	1.496	0.82	0.45	1.3E-14	8.4E-09	69.5	1.495	0.82	0.45	1.5E-14	9.5E-09	69.2	1.492	0.82	0.45	1.2E-14	7.7E-09	69.4	1.495	0.82	0.45	1.3E-14	8.5E-09	0.09
49.2	1.489	0.83	0.45	1.1E-13	6.8E-08	48.8	1.484	0.83	0.45	1.0E-13	6.6E-08	49.0	1.486	0.83	0.45	1.1E-13	6.8E-08	49.0	1.486	0.83	0.45	1.0E-13	6.7E-08	0.01
29.1	1.479	0.84	0.46	2.3E-13	1.5E-07	29.2	1.482	0.84	0.46	2.9E-13	1.9E-07	29.4	1.486	0.83	0.45	3.0E-13	1.9E-07	29.2	1.482	0.83	0.46	2.7E-13	1.8E-07	0.11
9.6	1.470	0.85	0.46	5.4E-13	3.5E-07	9.7	1.477	0.84	0.46	5.7E-13	3.6E-07	9.7	1.478	0.84	0.46	5.5E-13	3.5E-07	9.6	1.475	0.84	0.46	5.5E-13	3.5E-07	0.02

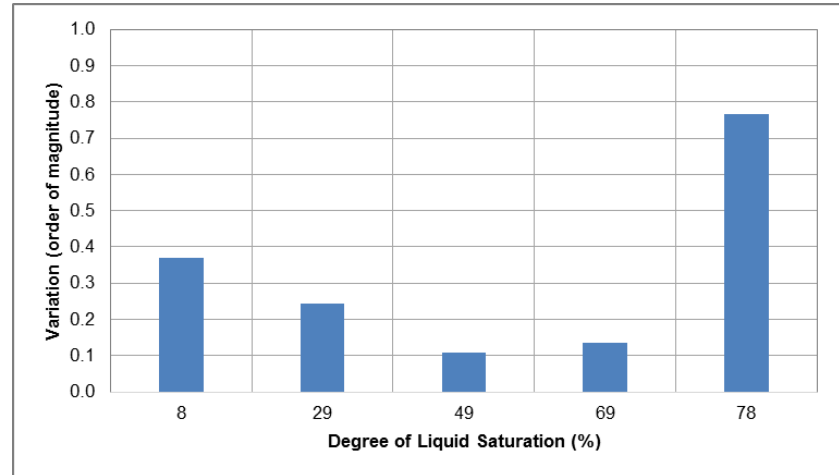
Table H-2: Air Permeability and Air Conductivity measurements of 70:30 Bentonite:Sand Mix @ ~ 1.8 Mg/m³ dry density

BSM 70-30 DW #1						BSM 70-30 DW #2						BSM 70-30 DW #3						BSM 70-30 DW Average						Log delta max-min, Coef. Of Air Perm.
Degree of Liquid Saturation	dry density	void ratio	porosity	Coefficient of Air Permeability	Air (gas) Conductivity	Degree of Liquid Saturation	dry density	void ratio	porosity	Coefficient of Air Permeability	Air (gas) Conductivity	Degree of Liquid Saturation	dry density	void ratio	porosity	Coefficient of Air Permeability	Air (gas) Conductivity	Degree of Liquid Saturation	dry density	void ratio	porosity	Coefficient of Air Permeability	Air (gas) Conductivity	
(%)	(g/cm ³)			(m ²)	(m/s)	(%)	(g/cm ³)			(m ²)	(m/s)	(%)	(g/cm ³)			(m ²)	(m/s)	(%)	(g/cm ³)			(m ²)	(m/s)	
78.8	1.798	0.50	0.33	9.5E-17	6.1E-11	78.5	1.795	0.50	0.34	1.2E-16	7.8E-11	78.3	1.795	0.50	0.34	9.8E-17	6.3E-11	78.5	1.796	0.50	0.33	1.1E-16	6.7E-11	0.11
67.6	1.785	0.51	0.34	1.4E-15	9.0E-10	68.5	1.793	0.51	0.34	1.3E-15	8.0E-10	68.7	1.794	0.51	0.34	1.1E-15	6.9E-10	68.3	1.790	0.51	0.34	1.2E-15	8.0E-10	0.12
48.8	1.791	0.51	0.34	1.9E-14	1.2E-08	47.7	1.778	0.52	0.34	2.7E-14	1.7E-08	48.4	1.787	0.51	0.34	1.5E-14	9.7E-09	48.3	1.785	0.51	0.34	2.0E-14	1.3E-08	0.25
27.8	1.758	0.54	0.35	8.5E-14	5.4E-08	31.4	1.832	0.47	0.32	9.5E-14	6.1E-08	28.1	1.765	0.53	0.35	9.5E-14	6.1E-08	29.1	1.785	0.51	0.34	9.2E-14	5.9E-08	0.05
9.5	1.764	0.53	0.35	1.7E-13	1.1E-07	9.5	1.766	0.53	0.35	1.7E-13	1.1E-07	9.4	1.759	0.53	0.35	1.8E-13	1.2E-07	9.5	1.763	0.53	0.35	1.7E-13	1.1E-07	0.04
BSM 70-30 CR-10 #1						BSM 70-30 CR-10 #2						BSM 70-30 CR-10 #3						BSM 70-30 CR-10 Average						Log delta max-min, Coef. Of Air Perm.
Degree of Liquid Saturation	dry density	void ratio	porosity	Coefficient of Air Permeability	Air (gas) Conductivity	Degree of Liquid Saturation	dry density	void ratio	porosity	Coefficient of Air Permeability	Air (gas) Conductivity	Degree of Liquid Saturation	dry density	void ratio	porosity	Coefficient of Air Permeability	Air (gas) Conductivity	Degree of Liquid Saturation	dry density	void ratio	porosity	Coefficient of Air Permeability	Air (gas) Conductivity	
(%)	(g/cm ³)			(m ²)	(m/s)	(%)	(g/cm ³)			(m ²)	(m/s)	(%)	(g/cm ³)			(m ²)	(m/s)	(%)	(g/cm ³)			(m ²)	(m/s)	
80.0	1.800	0.50	0.33	6.8E-17	4.3E-11	79.9	1.799	0.50	0.33	1.8E-17	1.1E-11	79.6	1.797	0.50	0.33	3.3E-17	2.1E-11	79.8	1.799	0.50	0.33	4.0E-17	2.5E-11	0.58
69.4	1.794	0.51	0.34	7.3E-16	4.7E-10	68.9	1.790	0.51	0.34	9.1E-16	5.8E-10	68.6	1.788	0.51	0.34	9.2E-16	5.9E-10	69.0	1.791	0.51	0.34	8.5E-16	5.4E-10	0.10
48.1	1.777	0.52	0.34	2.0E-14	1.3E-08	48.2	1.778	0.52	0.34	2.4E-14	1.5E-08	48.3	1.780	0.52	0.34	3.0E-14	1.9E-08	48.2	1.778	0.52	0.34	2.5E-14	1.6E-08	0.18
28.5	1.770	0.53	0.34	8.0E-14	5.1E-08	28.5	1.769	0.53	0.34	6.6E-14	4.2E-08	28.6	1.771	0.52	0.34	6.8E-14	4.3E-08	28.5	1.770	0.53	0.34	7.1E-14	4.5E-08	0.08
9.6	1.767	0.53	0.35	1.7E-13	1.1E-07	9.3	1.747	0.55	0.35	2.4E-13	1.6E-07	9.3	1.745	0.55	0.35	2.2E-13	1.4E-07	9.4	1.753	0.54	0.35	2.1E-13	1.3E-07	0.15
BSM 70-30 SR-L #1						BSM 70-30 SR-L #2						BSM 70-30 SR-L #3						BSM 70-30 SR-L Average						Log delta max-min, Coef. Of Air Perm.
Degree of Liquid Saturation	dry density	void ratio	porosity	Coefficient of Air Permeability	Air (gas) Conductivity	Degree of Liquid Saturation	dry density	void ratio	porosity	Coefficient of Air Permeability	Air (gas) Conductivity	Degree of Liquid Saturation	dry density	void ratio	porosity	Coefficient of Air Permeability	Air (gas) Conductivity	Degree of Liquid Saturation	dry density	void ratio	porosity	Coefficient of Air Permeability	Air (gas) Conductivity	
(%)	(g/cm ³)			(m ²)	(m/s)	(%)	(g/cm ³)			(m ²)	(m/s)	(%)	(g/cm ³)			(m ²)	(m/s)	(%)	(g/cm ³)			(m ²)	(m/s)	
79.1	1.793	0.51	0.34	1.5E-16	9.5E-11	79.7	1.797	0.50	0.33	4.4E-16	2.8E-10	79.1	1.793	0.51	0.34	4.8E-16	3.0E-10	79.3	1.795	0.50	0.34	3.6E-16	2.3E-10	0.51
69.3	1.794	0.51	0.34	1.1E-15	6.9E-10	69.7	1.798	0.50	0.33	7.4E-16	4.7E-10	68.7	1.788	0.51	0.34	2.4E-16	1.5E-10	69.2	1.793	0.51	0.34	6.8E-16	4.4E-10	0.66
48.2	1.778	0.52	0.34	2.9E-14	1.9E-08	49.1	1.789	0.51	0.34	1.7E-14	1.1E-08	49.4	1.792	0.51	0.34	9.9E-15	6.3E-09	48.9	1.787	0.51	0.34	1.9E-14	1.2E-08	0.47
28.5	1.770	0.53	0.34	5.9E-14	3.8E-08	28.9	1.779	0.52	0.34	7.5E-14	4.8E-08	28.5	1.769	0.53	0.34	6.0E-14	3.8E-08	28.7	1.773	0.52	0.34	6.5E-14	4.1E-08	0.11
9.3	1.754	0.54	0.35	1.6E-13	1.0E-07	9.3	1.755	0.54	0.35	1.6E-13	9.9E-08	9.4	1.763	0.53	0.35	1.6E-13	1.0E-07	9.3	1.757	0.54	0.35	1.6E-13	1.0E-07	0.01
BSM 70-30 SR-Sh #1						BSM 70-30 SR-Sh #2						BSM 70-30 SR-Sh #3						BSM 70-30 SR-Sh Average						Log delta max-min, Coef. Of Air Perm.
Degree of Liquid Saturation	dry density	void ratio	porosity	Coefficient of Air Permeability	Air (gas) Conductivity	Degree of Liquid Saturation	dry density	void ratio	porosity	Coefficient of Air Permeability	Air (gas) Conductivity	Degree of Liquid Saturation	dry density	void ratio	porosity	Coefficient of Air Permeability	Air (gas) Conductivity	Degree of Liquid Saturation	dry density	void ratio	porosity	Coefficient of Air Permeability	Air (gas) Conductivity	
(%)	(g/cm ³)			(m ²)	(m/s)	(%)	(g/cm ³)			(m ²)	(m/s)	(%)	(g/cm ³)			(m ²)	(m/s)	(%)	(g/cm ³)			(m ²)	(m/s)	
80.4	1.803	0.50	0.33	3.6E-17	2.3E-11	79.5	1.796	0.50	0.33	1.6E-17	1.0E-11	79.3	1.794	0.50	0.34	3.2E-17	2.1E-11	79.7	1.798	0.50	0.33	2.8E-17	1.8E-11	0.35
69.1	1.792	0.51	0.34	6.7E-16	4.3E-10	69.0	1.792	0.51	0.34	4.2E-16	2.7E-10	69.4	1.794	0.50	0.34	4.3E-16	2.7E-10	69.2	1.793	0.51	0.34	5.1E-16	3.3E-10	0.20
49.3	1.792	0.51	0.34	3.7E-15	2.3E-09	49.0	1.788	0.51	0.34	9.3E-15	5.9E-09	49.2	1.790	0.51	0.34	8.9E-15	5.7E-09	49.2	1.790	0.51	0.34	7.3E-15	4.6E-09	0.40
29.1	1.781	0.52	0.34	3.8E-14	2.4E-08	29.0	1.778	0.52	0.34	5.3E-14	3.4E-08	29.1	1.782	0.51	0.34	5.1E-14	3.3E-08	29.0	1.781	0.52	0.34	4.7E-14	3.0E-08	0.15
9.5	1.771	0.52	0.34	1.3E-13	8.4E-08	9.4	1.765	0.53	0.35	1.3E-13	8.3E-08	9.5	1.766	0.53	0.35	1.2E-13	7.6E-08	9.5	1.767	0.53	0.35	1.3E-13	8.1E-08	0.04

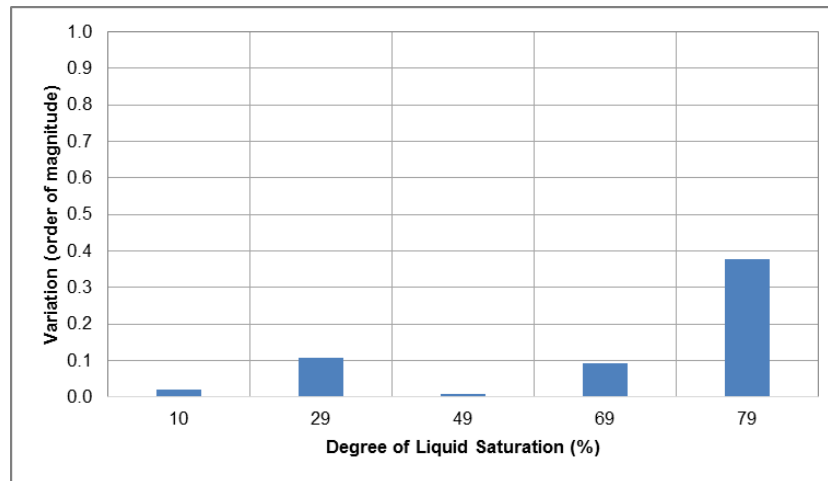
Figure H-1: Observed variability in replicate air permeability measurements (MX80)



MX80 – DW

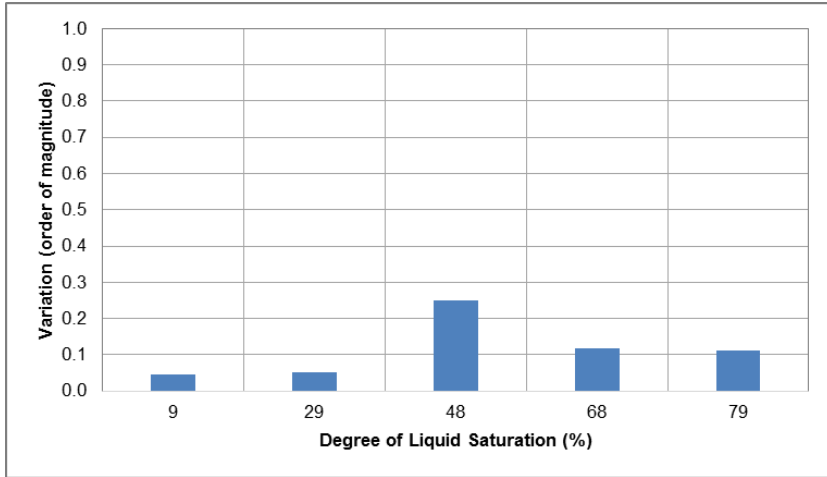


MX80 – SR-L

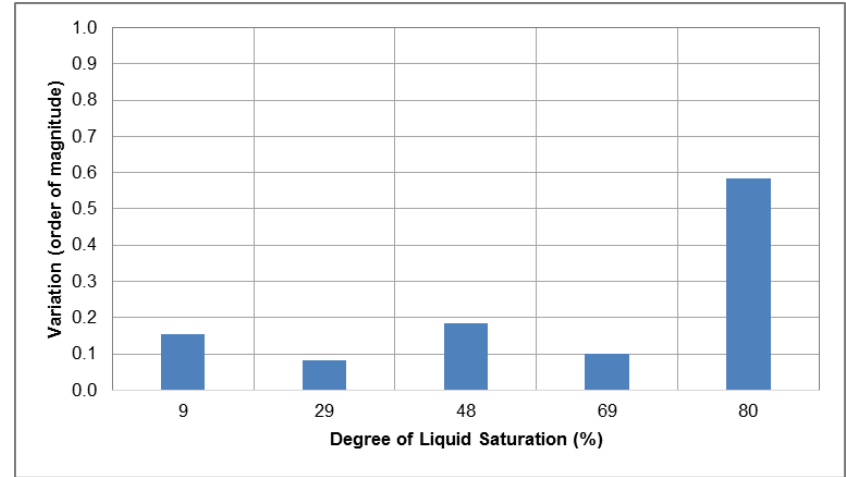


MX80 – SR-Sh

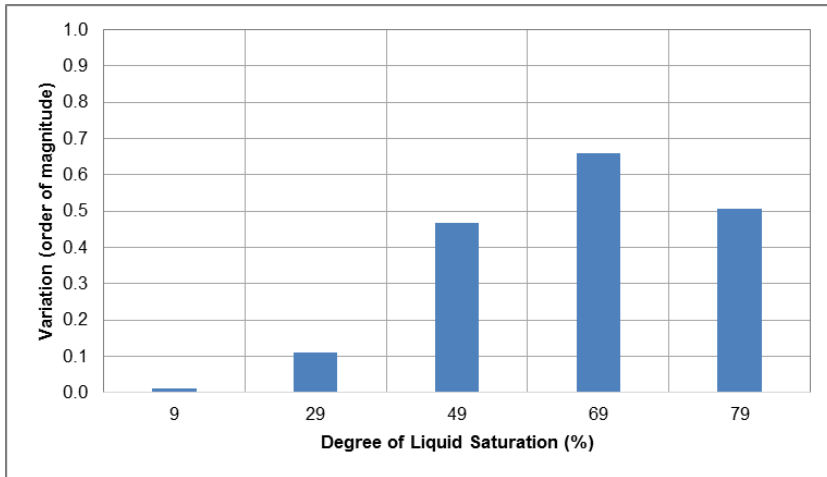
Figure H-2: Observed variability in replicate permeability measurements (BSM)



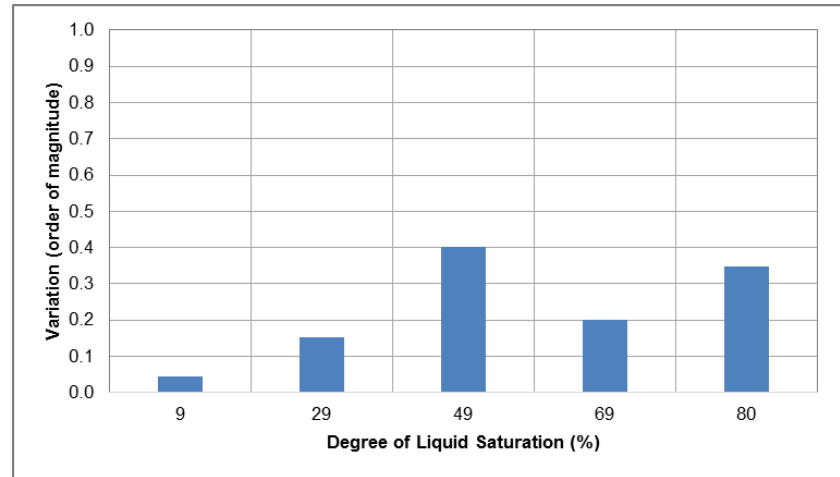
70:30 BSM : DW



70:30 BSM : CR10



70:30 BSM : SR-L



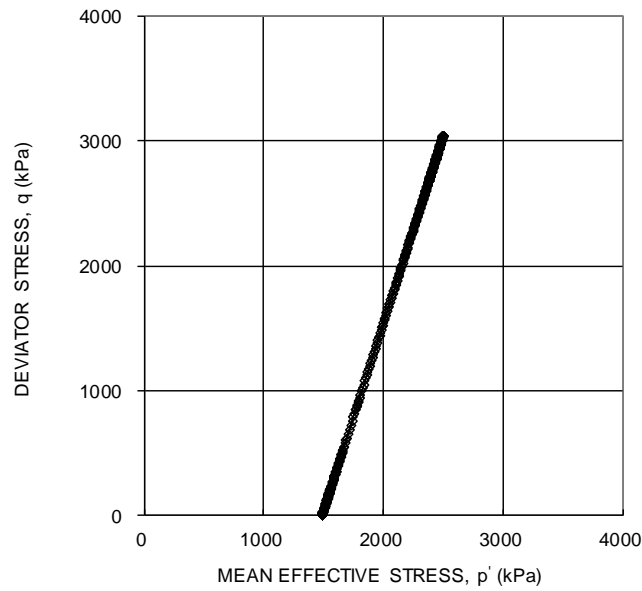
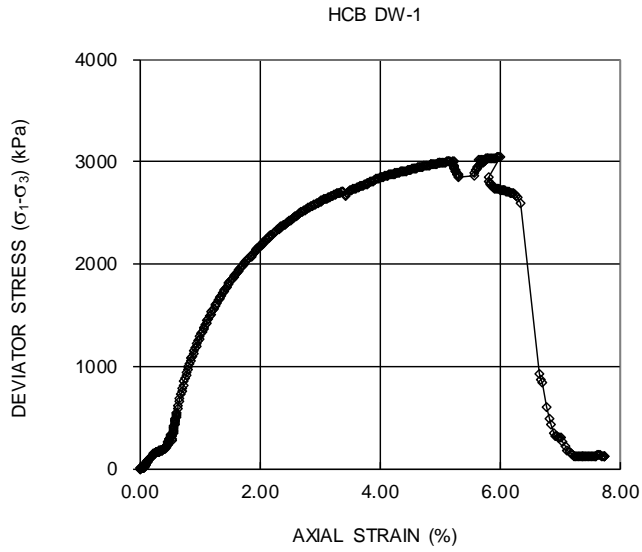
70:30 BSM : SR-Sh

Table H-3: Summary of air permeability and air conductivity measurements for three replicates as a function of degree of liquid saturation.

Degree of Liquid Saturation (%)	dry density (g/cm ³)	void ratio e	porosity n	Coefficient of Air Permeability (m ²)	Air (gas) Conductivity (m/s)
MX80 DW Average of 3 tests					
78.2	1.485	0.83	0.45	5.3E-15	3.4E-09
67.9	1.480	0.84	0.46	2.7E-14	1.7E-08
48.8	1.481	0.84	0.46	2.1E-13	1.4E-07
29.4	1.485	0.83	0.45	7.5E-13	4.8E-07
9.8	1.481	0.84	0.46	1.5E-12	9.6E-07
MX80 SR-L Average of 3 tests					
78.3	1.485	0.83	0.45	6.7E-15	4.3E-09
69.5	1.495	0.82	0.45	1.5E-14	9.4E-09
49.1	1.488	0.83	0.45	1.6E-13	9.9E-08
28.8	1.473	0.85	0.46	5.1E-13	3.3E-07
7.5	1.480	0.84	0.46	1.5E-12	9.3E-07
MX80 SR-Sh Average of 3 tests					
78.9	1.491	0.82	0.45	1.9E-15	1.2E-09
69.4	1.495	0.82	0.45	1.3E-14	8.5E-09
49.0	1.486	0.83	0.45	1.0E-13	6.7E-08
29.2	1.482	0.83	0.46	2.7E-13	1.8E-07
9.6	1.475	0.84	0.46	5.5E-13	3.5E-07
BSM 70-30 DW Average of 3 tests					
78.5	1.796	0.50	0.33	1.1E-16	6.7E-11
68.3	1.790	0.51	0.34	1.2E-15	8.0E-10
48.3	1.785	0.51	0.34	2.0E-14	1.3E-08
29.1	1.785	0.51	0.34	9.2E-14	5.9E-08
9.5	1.763	0.53	0.35	1.7E-13	1.1E-07
BSM 70-30 CR-10 Average of 3 tests					
79.8	1.799	0.50	0.33	4.0E-17	2.5E-11
69.0	1.791	0.51	0.34	8.5E-16	5.4E-10
48.2	1.778	0.52	0.34	2.5E-14	1.6E-08
28.5	1.770	0.53	0.34	7.1E-14	4.5E-08
9.4	1.753	0.54	0.35	2.1E-13	1.3E-07
BSM 70-30 SR-L Average of 3 tests					
79.3	1.795	0.50	0.34	3.6E-16	2.3E-10
69.2	1.793	0.51	0.34	6.8E-16	4.4E-10
48.9	1.787	0.51	0.34	1.9E-14	1.2E-08
28.7	1.773	0.52	0.34	6.5E-14	4.1E-08
9.3	1.757	0.54	0.35	1.6E-13	1.0E-07
BSM 70-30 SR-Sh Average of 3 tests					
79.7	1.798	0.50	0.33	2.8E-17	1.8E-11
69.2	1.793	0.51	0.34	5.1E-16	3.3E-10
49.2	1.790	0.51	0.34	7.3E-15	4.6E-09
29.0	1.781	0.52	0.34	4.7E-14	3.0E-08
9.5	1.767	0.53	0.35	1.3E-13	8.1E-08

APPENDIX I: TRIAXIAL TEST RESULTS

CONSOLIDATED DRAINED TRIAXIAL TEST		APPENDIX I
SHEET 2 OF 2		HCB DW-1
		Replicate 1

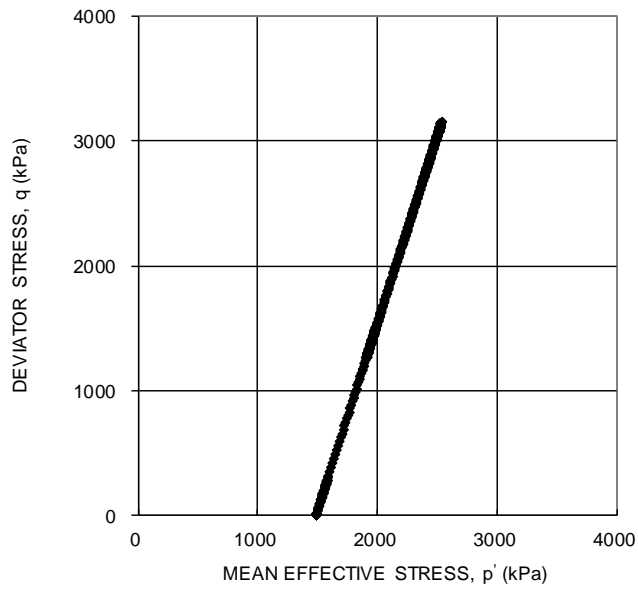
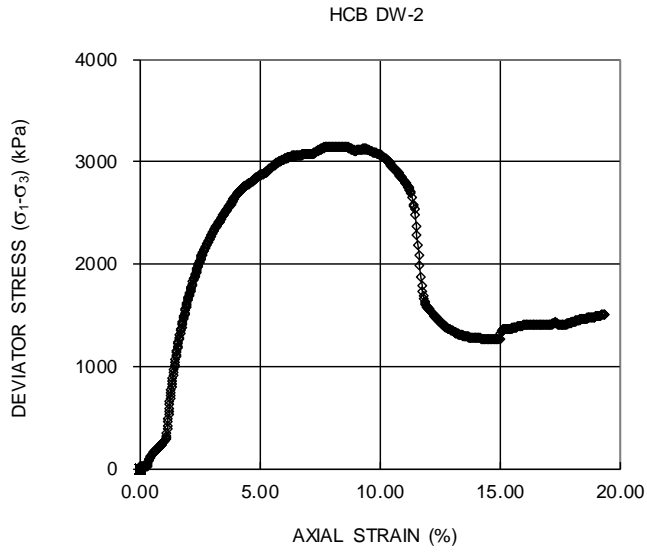


Date: 2015-08-26
 Project No. 13-1380-0101

Golder Associates

Prepared By: LH
 Checked By: AM

CONSOLIDATED DRAINED TRIAXIAL TEST		APPENDIX I
SHEET 2 OF 2		HCB DW-2
		Replicate 2



Date: 2015-09-02
 Project No. 13-1380-0101

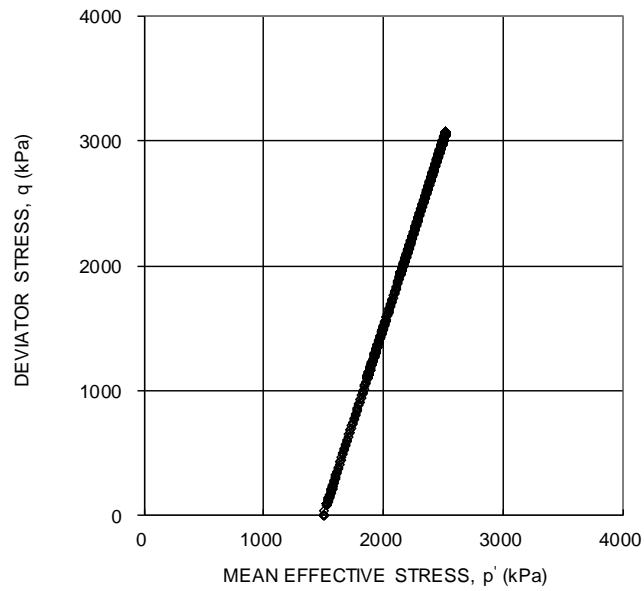
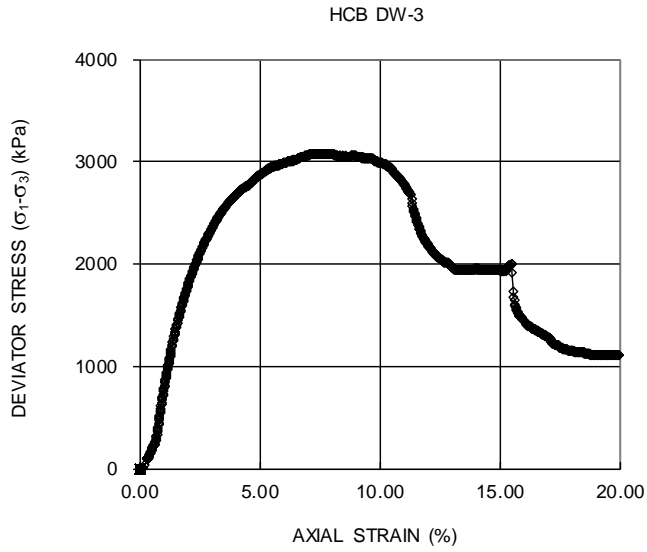
Golder Associates

Prepared By: LH
 Checked By: AM

CONSOLIDATED DRAINED TRIAXIAL TEST						APPENDIX I	
SHEET 1 OF 2						HCB DW-3	
						Replicate 3	
REPLICATE					3		
SAMPLE NUMBER					HCB DW-3		
SPECIMEN DIAMETER, cm					5.03		
SPECIMEN HEIGHT, cm					10.15		
INITIAL WATER CONTENT, %					24.8		
DRY DENSITY, Mg/m ³					1.62		
WATER CONTENT BEFORE CONSOLIDATION, %					24.8		
CELL PRESSURE, σ_3 , kPa					1490.0		
BACK PRESSURE, kPa					0.0		
PORE PRESSURE PARAMETER "B"					-		
CONSOLIDATION PRESSURE, σ_c , kPa					1490.0		
VOLUMETRIC STRAIN DURING CONSOLIDATION, %					0.0		
WATER CONTENT AFTER CONSOLIDATION, %					-		
AVERAGE RATE OF STRAIN, %/hr					0.06		
TIME TO FAILURE, HOURS					130		
WATER CONTENT AFTER TEST, %					33.9		
MAX. DEVIATOR STRESS, $(\sigma_1 - \sigma_3)$, kPa					3077.0		
AXIAL STRAIN AT $(\sigma_1 - \sigma_3)$ MAXIMUM, %					7.8		
STRENGTH ENVELOPE, M (q/p')					1.2		
MAX PRINCIPAL STRESS RATIO, (σ'_1/σ'_3) maximum					3.1		
FILTER DRAINS USED, y/n					y		
TEST NOTES:							
FAILURE PLANE NUMBER					1.0		
ANGLE OF FAILURE, DEGREES					55.0		
Date:	2015-09-09					Prepared By:	LH
Project No.	13-1380-0101					Checked By:	AM

Golder Associates

CONSOLIDATED DRAINED TRIAXIAL		APPENDIX I
SHEET 2 OF 2		HCB DW-3
		Replicate 3



Date: 2015-09-09
 Project No. 13-1380-0101

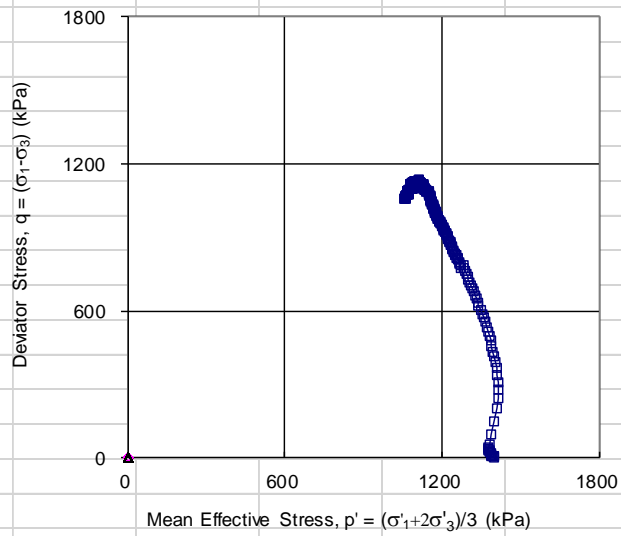
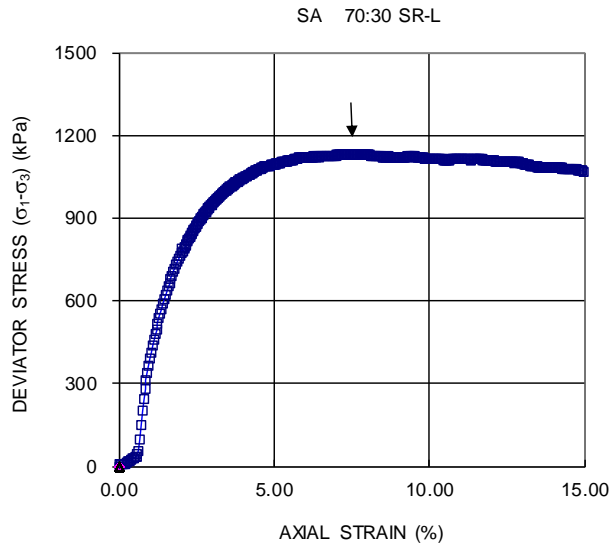
Golder Associates

Prepared By: LH
 Checked By: AM

Consolidated Undrained Tests

CONSOLIDATED UNDRAINED TRIAXIAL WITH PORE PRESSURE MEASUREMENTS ASTM D4767 SHEET 1 OF 4					APPENDIX I BSB -70:30 SR-L
TEST STAGE				A	
BOREHOLE NUMBER				-	
SAMPLE				70:30 SR-L	
DEPTH, m				-	
SPECIMEN DIAMETER, cm				5.10	
SPECIMEN HEIGHT, cm				10.12	
NATURAL WATER CONTENT, %				23.1	
DRY DENSITY, Mg/m ³				1.70	
WATER CONTENT AFTER SATURATION, %				32.4	
CELL PRESSURE, σ_3 , kPa				1600.0	
BACK PRESSURE, kPa				200.0	
PORE PRESSURE PARAMETER "B"				0.94	
EFFECTIVE CONSOLIDATION STRESS, σ_c , kPa				1400.0	
VOLUMETRIC STRAIN DURING CONSOLIDATION, %				16.1	
WATER CONTENT AFTER CONSOLIDATION, %				22.9	
AVERAGE RATE OF STRAIN, %/hr				0.060	
TIME TO FAILURE, HOURS				127.0	
WATER CONTENT AFTER TEST, %				20.0	
MAX. DEVIATOR STRESS, $(\sigma_1 - \sigma_3)$, kPa				1132.2	
AXIAL STRAIN AT $(\sigma_1 - \sigma_3)$ maximum, %				7.6	
MAX EFFECTIVE PRINCIPAL STRESS RATIO, (σ'_1 / σ'_3) maximum				2.6	
DEVIATOR STRESS AT (σ'_1 / σ'_3) maximum, kPa				1125.5	
AXIAL STRAIN AT (σ'_1 / σ'_3) maximum, %				8.2	
PORE PRESSURE PARAMETER, Af, AT $(\sigma_1 - \sigma_3)$ maximum				0.59	
PORE PRESSURE PARAMETER, Af, AT (σ'_1 / σ'_3) maximum				0.61	
FILTER DRAINS USED, y/n				y	
TEST NOTES:					
				Effective consolidation stresses are assigned by the client.	
FAILURE PLANE NUMBER				-	
ANGLE OF FAILURE PLANE, DEGREES				Bulged	
Date:	3/5/2018				Prepared By: LH
Project No.	13-1380-0101			Golder Associates	Checked By: AM

CONSOLIDATED UNDRAINED TRIAXIAL WITH PORE PRESSURE MEASUREMENTS ASTM D4767 SHEET 3 OF 4	FIGURE
--	---------------



Date: 3/5/2018
Project No. 13-1380-0101

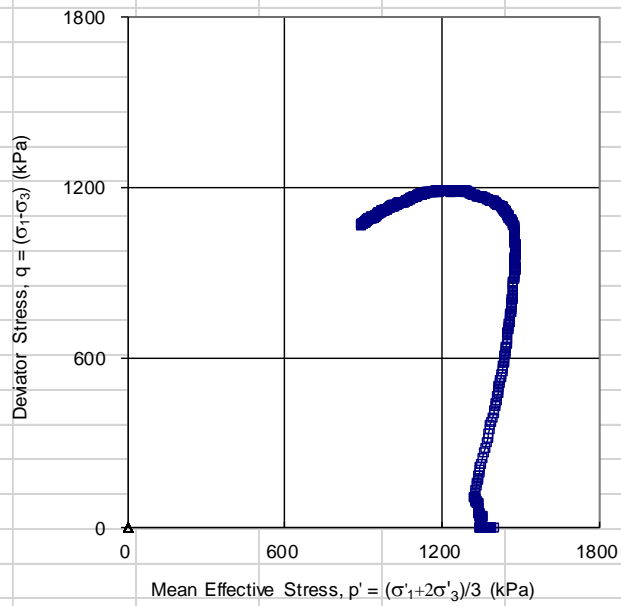
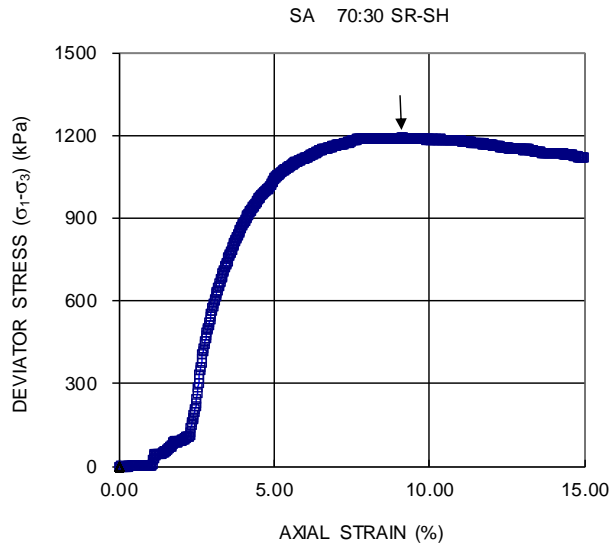
Golder Associates

Prepared By: LH
Checked By: AM

CONSOLIDATED UNDRAINED TRIAXIAL WITH PORE PRESSURE MEASUREMENTS ASTM D4767 SHEET 1 OF 4					APPENDIX I BSB 70:30 SR-Sh	
TEST STAGE				A		
BOREHOLE NUMBER				-		
SAMPLE				70:30 SR-SH		
DEPTH, m				-		
SPECIMEN DIAMETER, cm				5.10		
SPECIMEN HEIGHT, cm				10.22		
NATURAL WATER CONTENT, %				17.2		
DRY DENSITY, Mg/m ³				1.75		
WATER CONTENT AFTER SATURATION, %				24.9		
CELL PRESSURE, σ_3 , kPa				1600.0		
BACK PRESSURE, kPa				200.0		
PORE PRESSURE PARAMETER "B"				0.90		
EFFECTIVE CONSOLIDATION STRESS, σ_c , kPa				1400.0		
VOLUMETRIC STRAIN DURING CONSOLIDATION, %				16.4		
WATER CONTENT AFTER CONSOLIDATION, %				15.5		
AVERAGE RATE OF STRAIN, %/hr				0.054		
TIME TO FAILURE, HOURS				169.1		
WATER CONTENT AFTER TEST, %				18.9		
MAX. DEVIATOR STRESS, $(\sigma_1 - \sigma_3)$, kPa				1191.3		
AXIAL STRAIN AT $(\sigma_1 - \sigma_3)$ maximum, %				9.1		
MAX EFFECTIVE PRINCIPAL STRESS RATIO, (σ'_1 / σ'_3) maximum				2.8		
DEVIATOR STRESS AT (σ'_1 / σ'_3) maximum, kPa				1121.4		
AXIAL STRAIN AT (σ'_1 / σ'_3) maximum, %				14.8		
PORE PRESSURE PARAMETER, Af, AT $(\sigma_1 - \sigma_3)$ maximum				0.49		
PORE PRESSURE PARAMETER, Af, AT (σ'_1 / σ'_3) maximum				0.70		
FILTER DRAINS USED, y/n				y		
TEST NOTES:						
				Effective consolidation stresses are assigned by the client.		
FAILURE PLANE NUMBER				-		
ANGLE OF FAILURE PLANE, DEGREES				Bulged		
Date:	3/23/2018				Prepared By:	LH
Project No.	13-1380-0101			Golder Associates	Checked By:	AM

**CONSOLIDATED UNDRAINED TRIAXIAL
WITH PORE PRESSURE MEASUREMENTS
ASTM D4767
SHEET 3 OF 4**

**APPENDIX I BSB
70:30 70:30 SR-Sh**



Date: 3/23/2018
Project No. 13-1380-0101

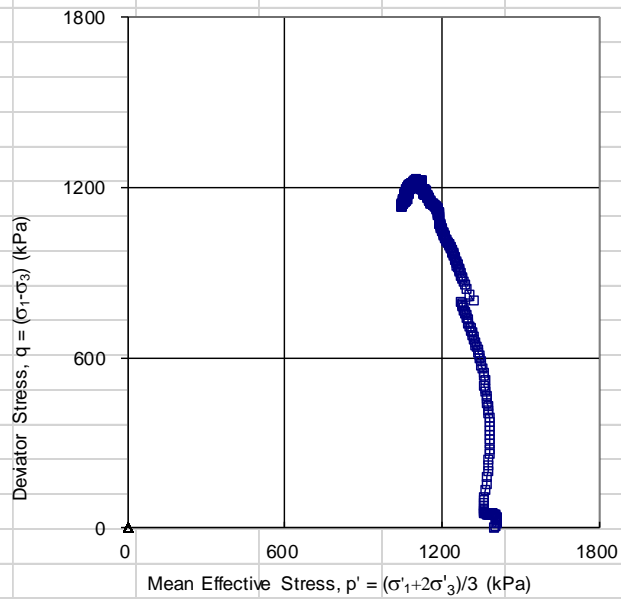
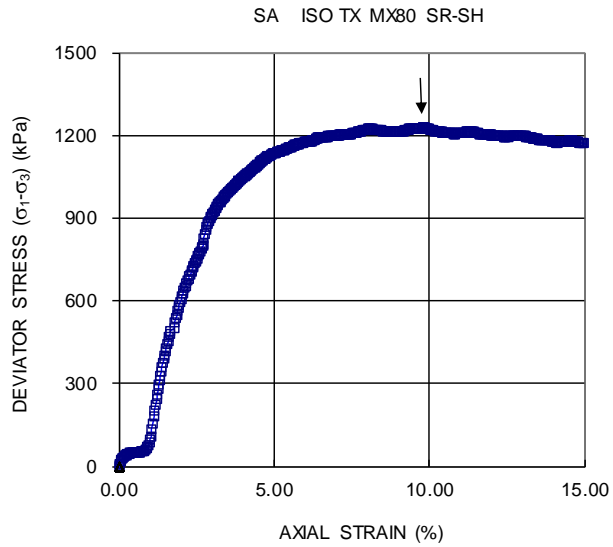
Golder Associates

Prepared By: LH
Checked By: AM

CONSOLIDATED UNDRAINED TRIAXIAL WITH PORE PRESSURE MEASUREMENTS ASTM D4767 SHEET 1 OF 4					APPENDIX I MX80 SR-Sh
TEST STAGE				A	
BOREHOLE NUMBER				-	
SAMPLE			ISO TX MX 80 SR-SH		
DEPTH, m				-	
SPECIMEN DIAMETER, cm				5.11	
SPECIMEN HEIGHT, cm				10.20	
NATURAL WATER CONTENT, %				28.1	
DRY DENSITY, Mg/m ³				1.54	
WATER CONTENT AFTER SATURATION, %				37.1	
CELL PRESSURE, σ_3 , kPa				1600.0	
BACK PRESSURE, kPa				200.0	
PORE PRESSURE PARAMETER "B"				0.91	
EFFECTIVE CONSOLIDATION STRESS, σ_c , kPa				1400.0	
VOLUMETRIC STRAIN DURING CONSOLIDATION, %				20.1	
WATER CONTENT AFTER CONSOLIDATION, %				24.6	
AVERAGE RATE OF STRAIN, %/hr				0.060	
TIME TO FAILURE, HOURS				164.2	
WATER CONTENT AFTER TEST, %				22.4	
MAX. DEVIATOR STRESS, $(\sigma_1 - \sigma_3)$, kPa				1228.0	
AXIAL STRAIN AT $(\sigma_1 - \sigma_3)$ maximum, %				9.9	
MAX EFFECTIVE PRINCIPAL STRESS RATIO, (σ'_1 / σ'_3) maximum				2.8	
DEVIATOR STRESS AT (σ'_1 / σ'_3) maximum, kPa				1209.2	
AXIAL STRAIN AT (σ'_1 / σ'_3) maximum, %				10.7	
PORE PRESSURE PARAMETER, Af, AT $(\sigma_1 - \sigma_3)$ maximum				0.58	
PORE PRESSURE PARAMETER, Af, AT (σ'_1 / σ'_3) maximum				0.60	
FILTER DRAINS USED, y/n				y	
TEST NOTES:					
				Effective consolidation stresses are assigned by the client.	
FAILURE PLANE NUMBER				-	
ANGLE OF FAILURE PLANE, DEGREES				Bulged	
Date:	3/26/2018				Prepared By: LH
Project No.	13-1380-0101			Golder Associates	Checked By: AM

**CONSOLIDATED UNDRAINED TRIAXIAL
WITH PORE PRESSURE MEASUREMENTS
ASTM D4767
SHEET 3 OF 4**

**APPENDIX I
MX80 SR-Sh**



Date: 3/26/2018
Project No. 13-1380-0101

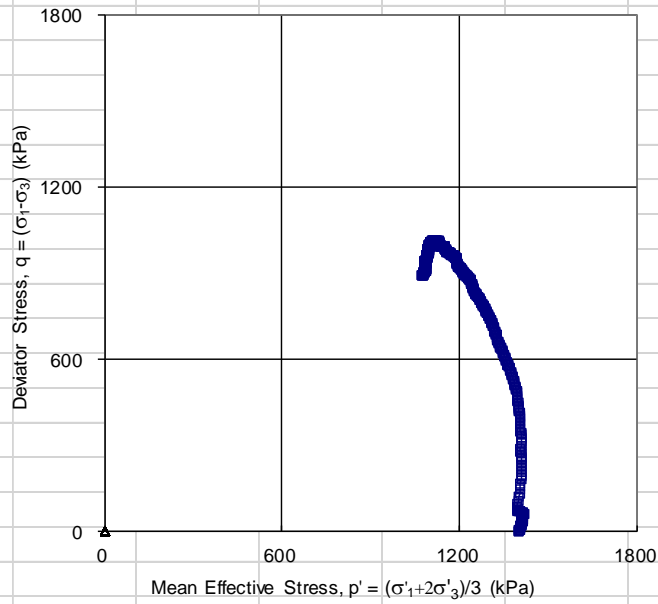
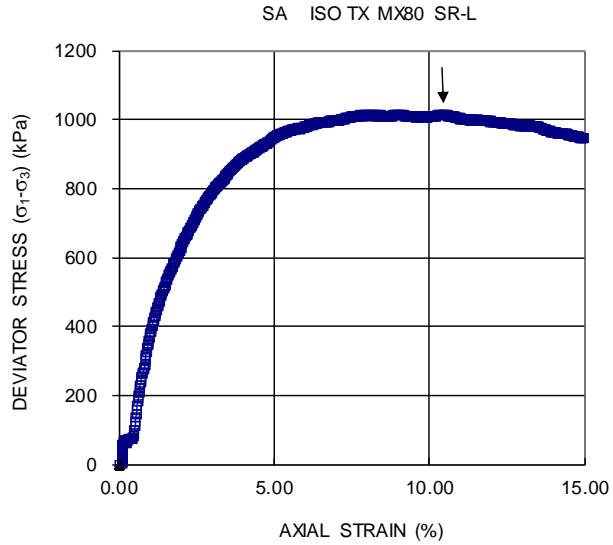
Golder Associates

Prepared By: LH
Checked By: AM

CONSOLIDATED UNDRAINED TRIAXIAL WITH PORE PRESSURE MEASUREMENTS ASTM D4767 SHEET 1 OF 4					APPENDIX I MX80 SR-L
TEST STAGE				A	
BOREHOLE NUMBER				-	
SAMPLE			ISO TX MX 80 SR-L		
DEPTH, m				-	
SPECIMEN DIAMETER, cm				5.11	
SPECIMEN HEIGHT, cm				10.15	
NATURAL WATER CONTENT, %				60.6	
DRY DENSITY, Mg/m ³				1.48	
WATER CONTENT AFTER SATURATION, %				32.9	
CELL PRESSURE, σ_3 , kPa				1600.0	
BACK PRESSURE, kPa				200.0	
PORE PRESSURE PARAMETER "B"				0.90	
EFFECTIVE CONSOLIDATION STRESS, σ_c , kPa				1400.0	
VOLUMETRIC STRAIN DURING CONSOLIDATION, %				8.5	
WATER CONTENT AFTER CONSOLIDATION, %				27.2	
AVERAGE RATE OF STRAIN, %/hr				0.060	
TIME TO FAILURE, HOURS				173.2	
WATER CONTENT AFTER TEST, %				25.1	
MAX. DEVIATOR STRESS, $(\sigma_1 - \sigma_3)$, kPa				1014.2	
AXIAL STRAIN AT $(\sigma_1 - \sigma_3)$ maximum, %				10.4	
MAX EFFECTIVE PRINCIPAL STRESS RATIO, (σ'_1 / σ'_3) maximum				2.3	
DEVIATOR STRESS AT (σ'_1 / σ'_3) maximum, kPa				1007.5	
AXIAL STRAIN AT (σ'_1 / σ'_3) maximum, %				9.6	
PORE PRESSURE PARAMETER, Af, AT $(\sigma_1 - \sigma_3)$ maximum				0.58	
PORE PRESSURE PARAMETER, Af, AT (σ'_1 / σ'_3) maximum				0.60	
FILTER DRAINS USED, y/n				y	
TEST NOTES:					
				Effective consolidation stresses are assigned by the client.	
FAILURE PLANE NUMBER				-	
ANGLE OF FAILURE PLANE, DEGREES				Bulged	
Date:	4/02/2018				Prepared By: LH
Project No.	13-1380-0101		Golder Associates		Checked By: AM

**CONSOLIDATED UNDRAINED TRIAXIAL
WITH PORE PRESSURE MEASUREMENTS
ASTM D4767
SHEET 3 OF 4**

**APPENDIX I
MX80 SR-L**



Date: 4/02/2018
Project No. 13-1380-0101

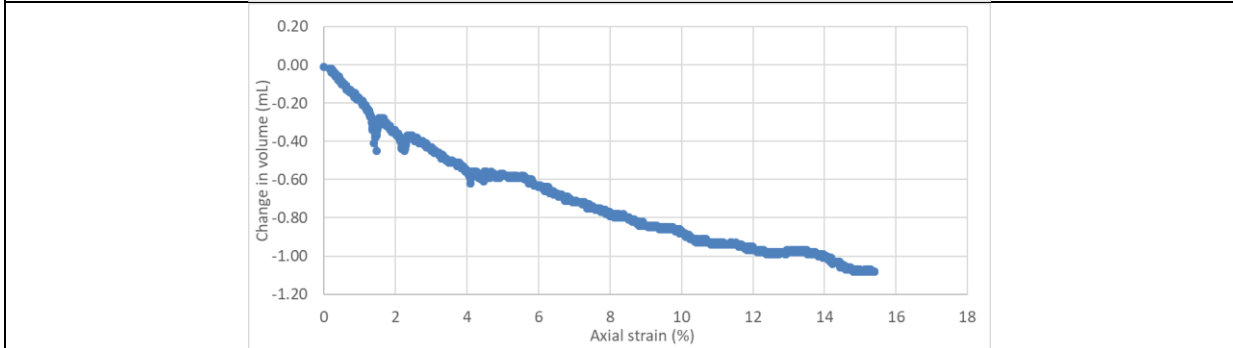
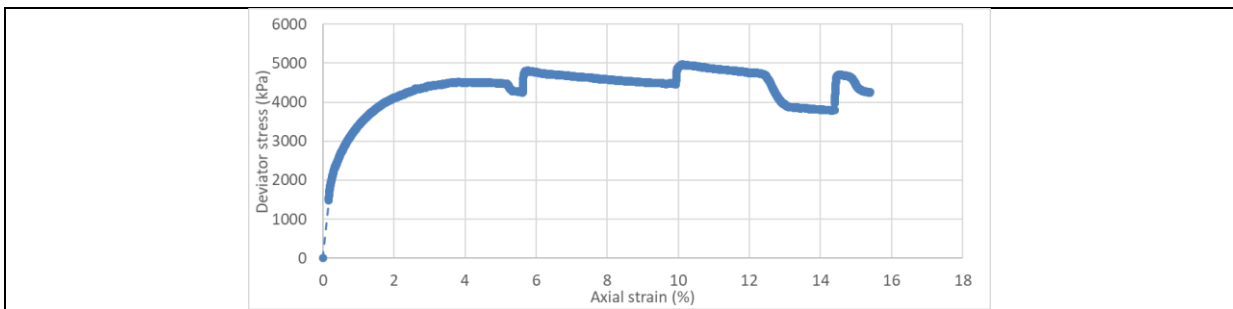
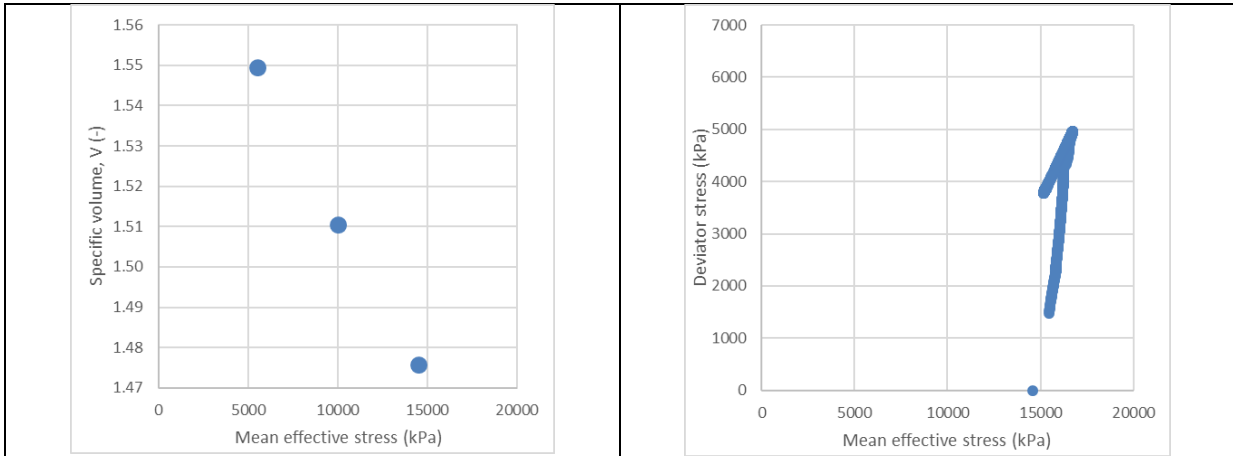
Golder Associates

Prepared By: LH
Checked By: AM

High Pressure Triaxial Tests (RMC)

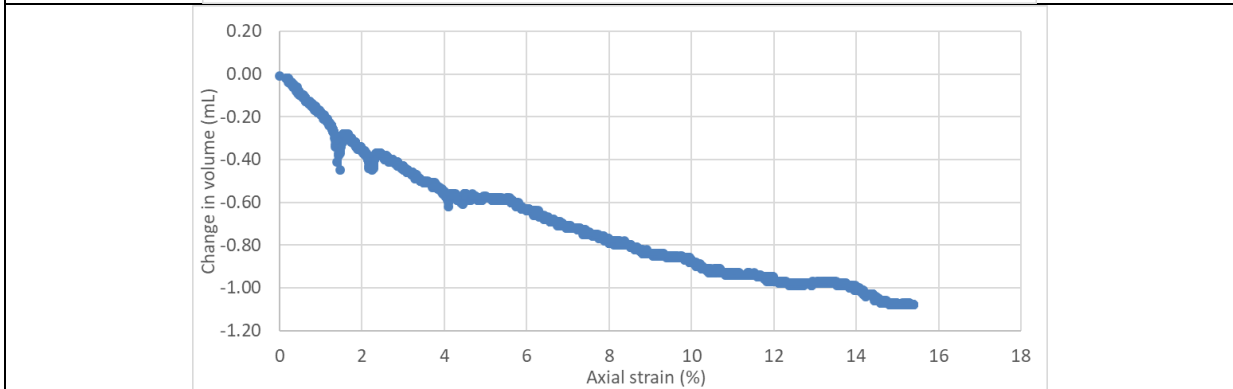
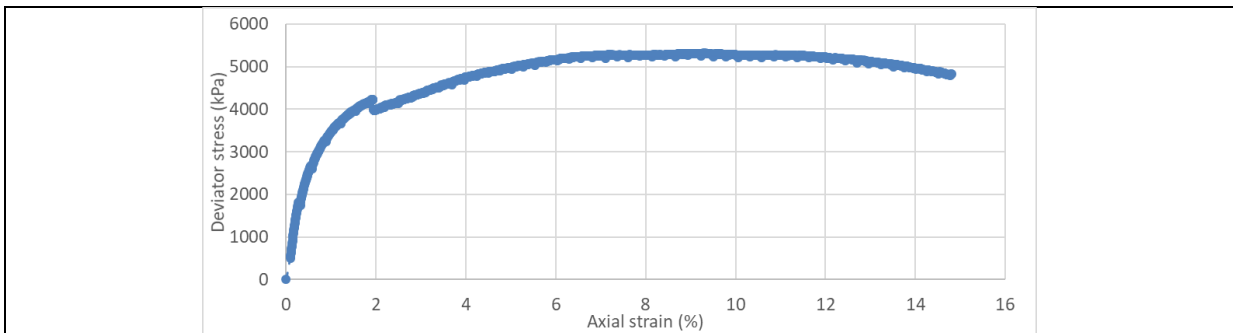
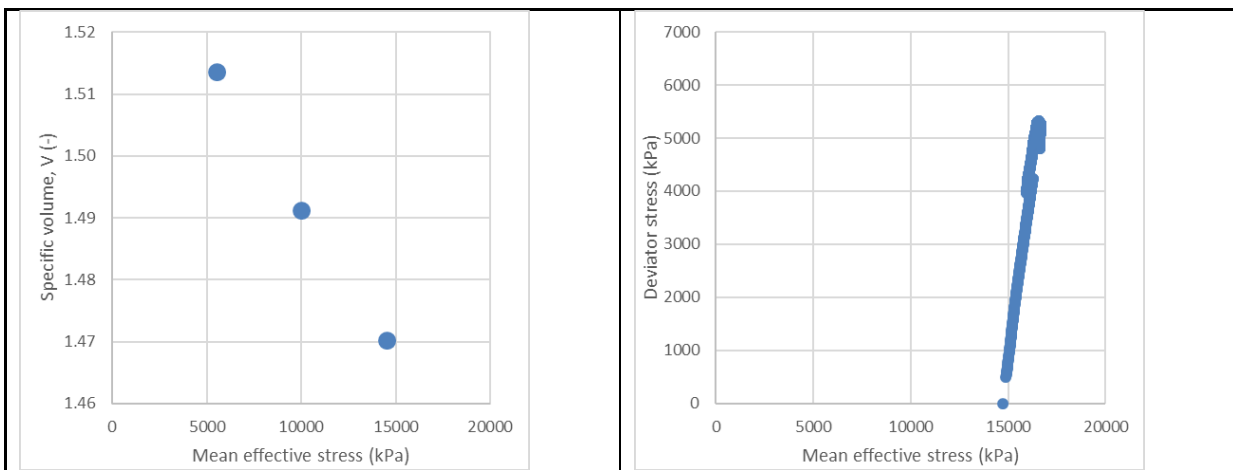
Project:	SA440
Test:	IsoComp-BSM7030-DW
Triaxial cell:	High pressure cell #1
Material:	BSM 70-30
Initial dry density:	1.8 Mg/m ³
Initial saturation:	95%
Preparation water:	Distilled water
Saturation water:	Distilled water

q_final	4252.38
p'_final	15795.53
M measured	0.269
phi	7.4
sin phi()	0.129
M calc	0.269
M_meas-M_calc	0.000

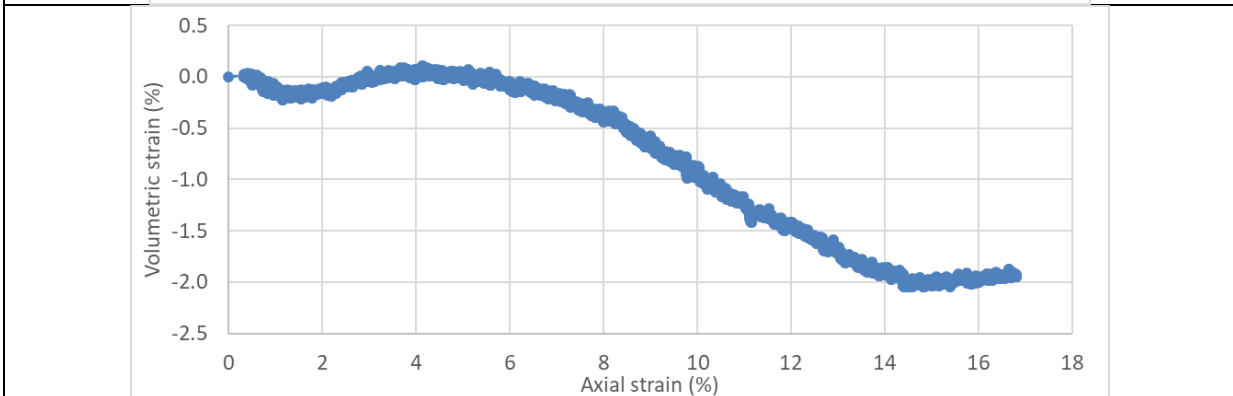
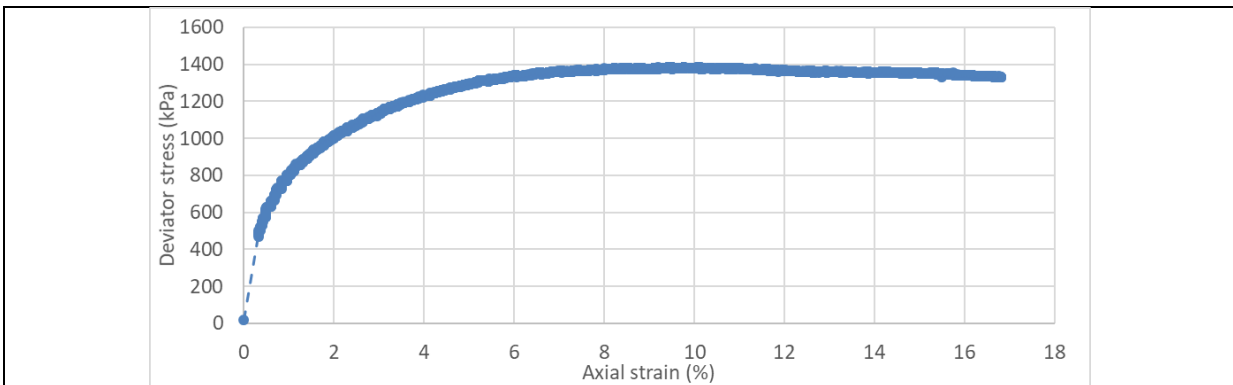
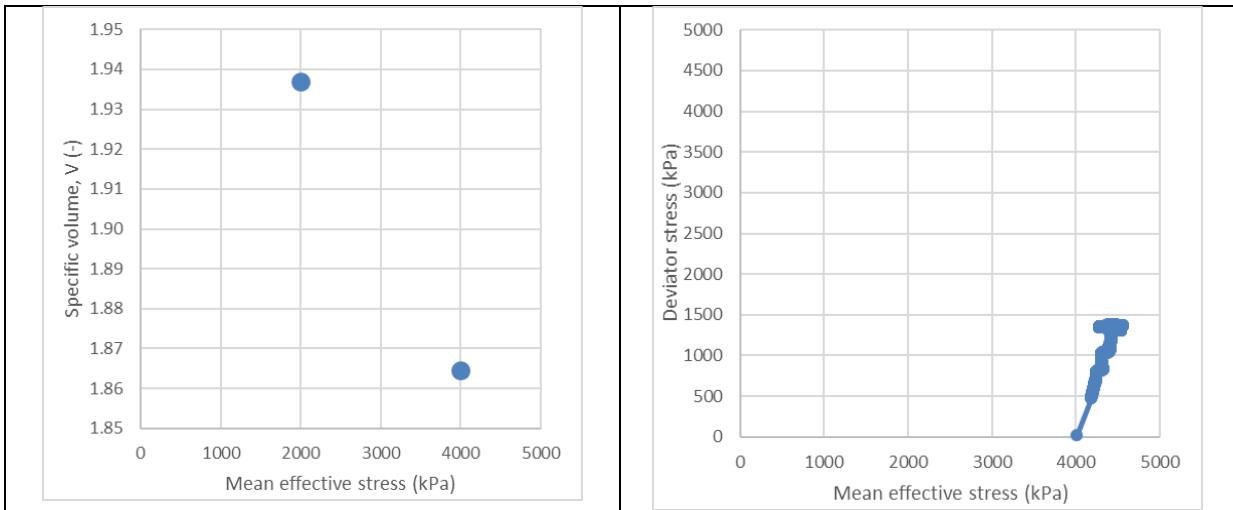


Project:	SA440
Test:	IsoComp-BSM7030-CR10
Triaxial cell:	High pressure cell #2
Material:	BSM 70-30
Initial dry density:	1.8 Mg/m3
Initial saturation:	95%
Preparation water:	CR10
Saturation water:	CR10

q_final	4795
p'_final	16601
M measured	0.289
phi	7.9
sin phi()	0.138
M calc	0.289
M_meas-M_calc	0.000

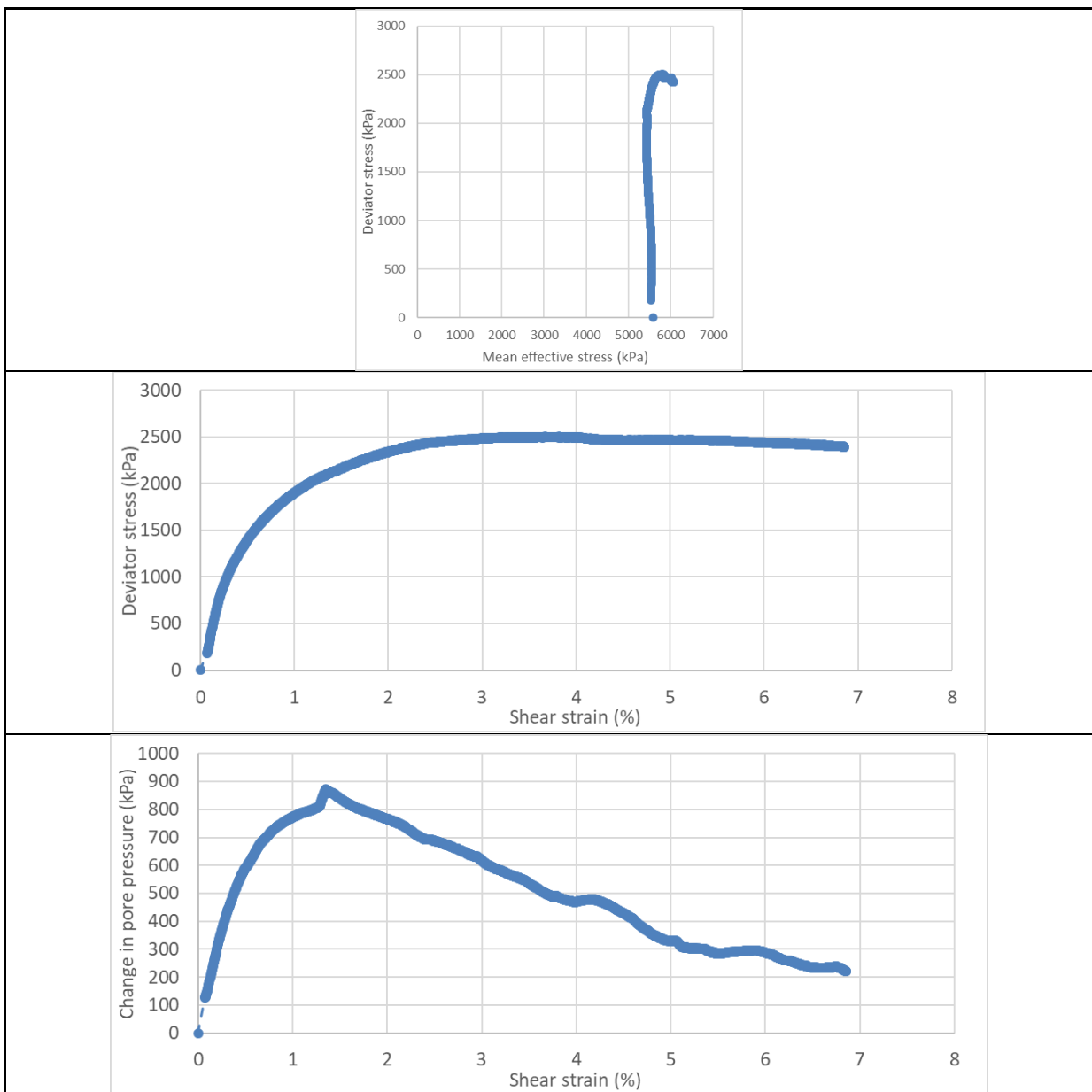


Project:	SA440
Test:	IsoComp-Bent100-DW
Triaxial cell:	Celco Cell #2
Material:	100% bentonite
Initial dry density:	1.5 Mg/m³
Initial saturation:	95%
Preparation water:	Distilled water
Saturation water:	Distilled water

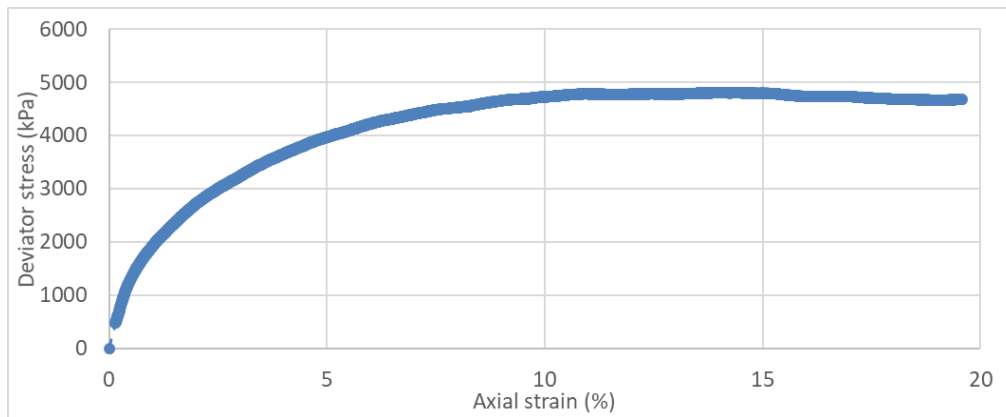


Project:	SA440
Test:	CIU-BSM7030-DW
Triaxial cell:	Celco cell #2
Material:	BSM 70-30
Initial dry density:	1.8 Mg/m³
Initial saturation:	95%
Preparation water:	Distilled water
Saturation water:	Distilled water

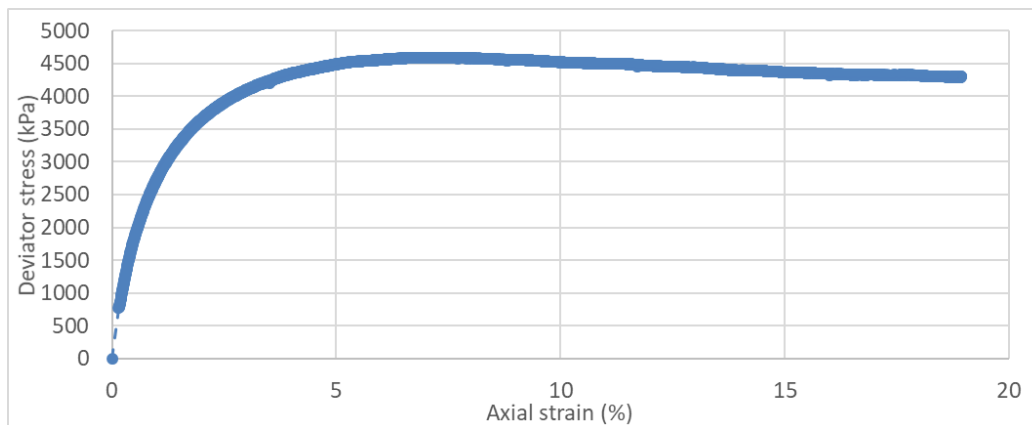
q_final	2396
p'_final	6068
M measured	0.395
phi	10.7
sin phi()	0.185
M calc	0.395
M_meas-M_calc	0.000



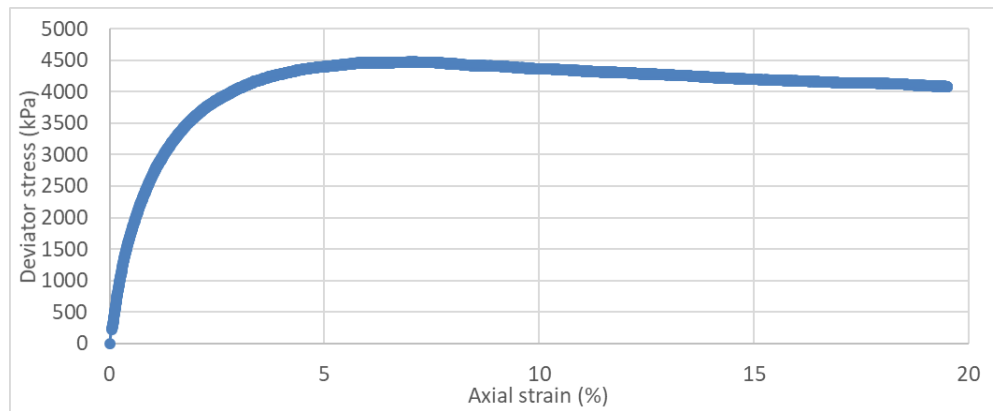
Project:	SA440
Test:	CID-BSM7030-DW_Test01
Triaxial cell:	Celco cell #1
Material:	BSM 70-30
Initial dry density:	1.8 Mg/m³
Initial saturation:	95%
Preparation water:	Distilled water
Saturation water:	N/A



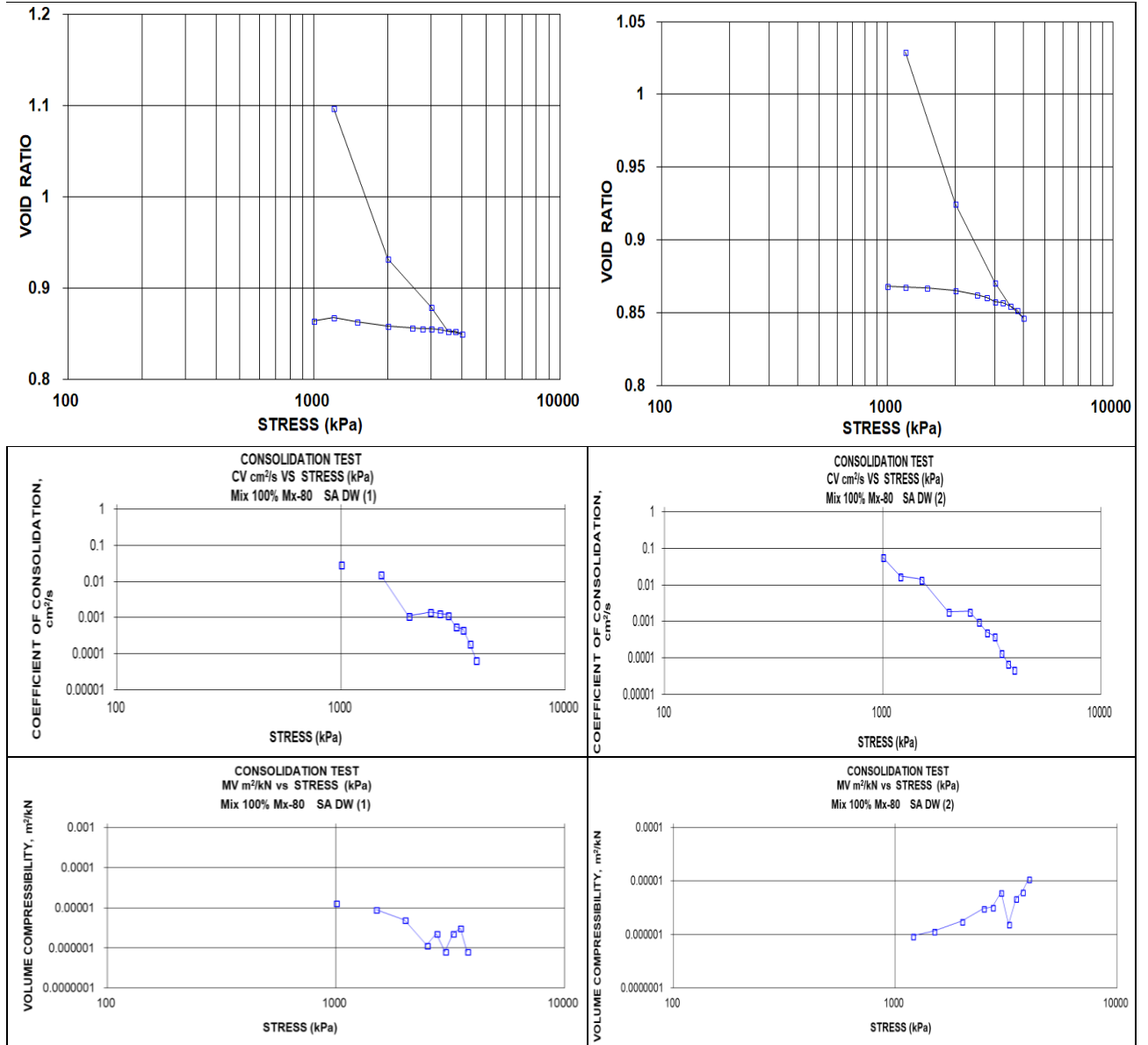
Project:	SA440
Test:	CID-BSM7030-DW_Test02
Triaxial cell:	Celco cell #1
Material:	BSM 70-30
Initial dry density:	1.8 Mg/m³
Initial saturation:	95%
Preparation water:	Distilled water
Saturation water:	N/A



Project:	SA440
Test:	CID-BSM7030-DW_Test03
Triaxial cell:	Celco cell #2
Material:	BSM 70-30
Initial dry density:	1.8 Mg/m3
Initial saturation:	95%
Preparation water:	Distilled water
Saturation water:	N/A



APPENDIX J: UNIAXIAL CONSOLIDATION (OEDOMETER) TEST RESULTS



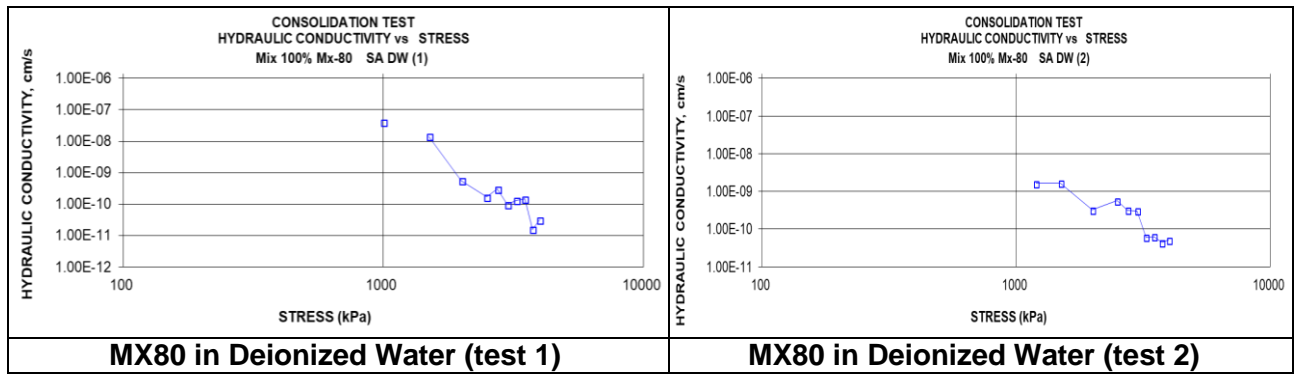


Figure J-1: Oedometer Tests on MX80 (1)

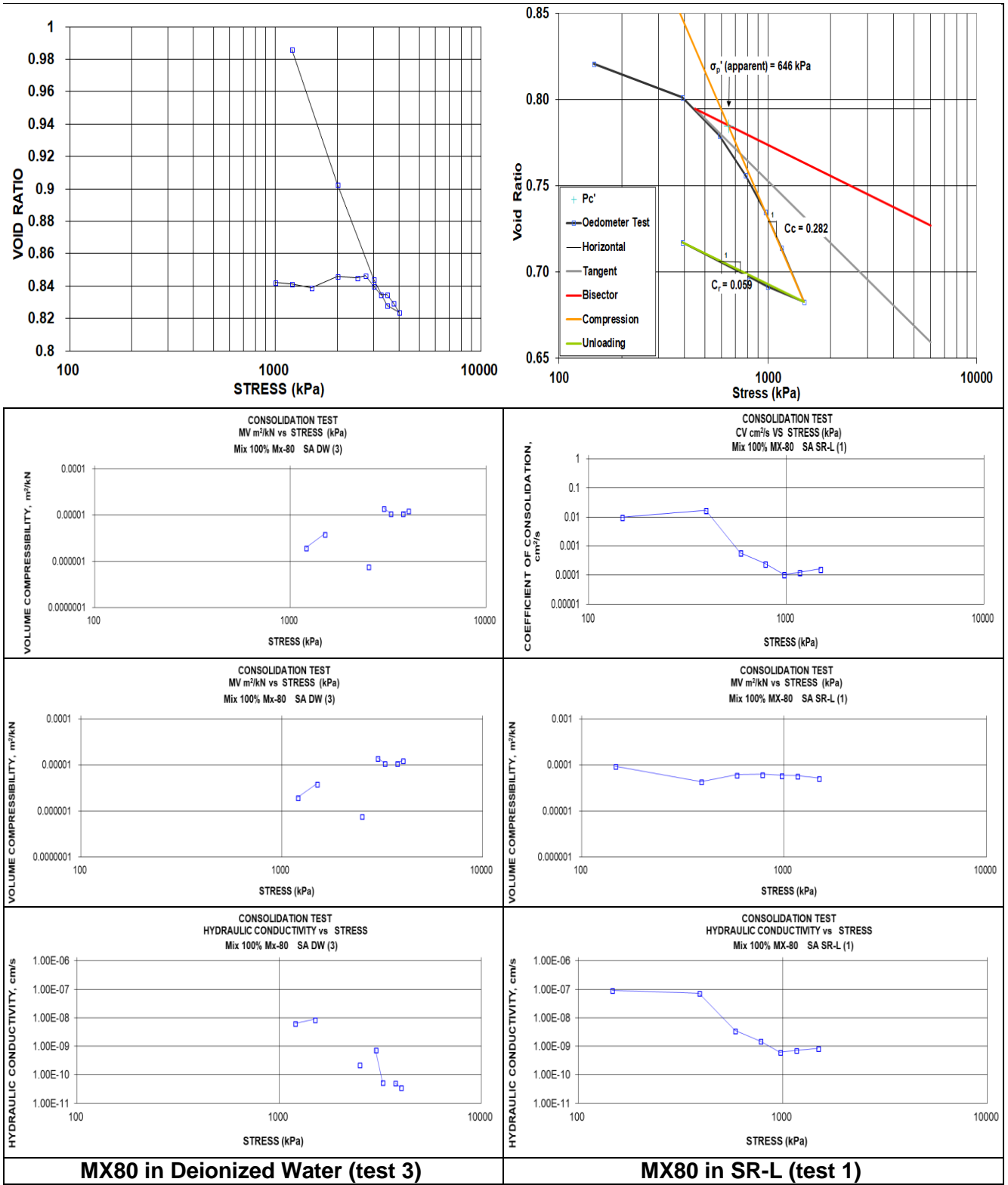


Figure J-2: Oedometer Tests on MX80 (2)

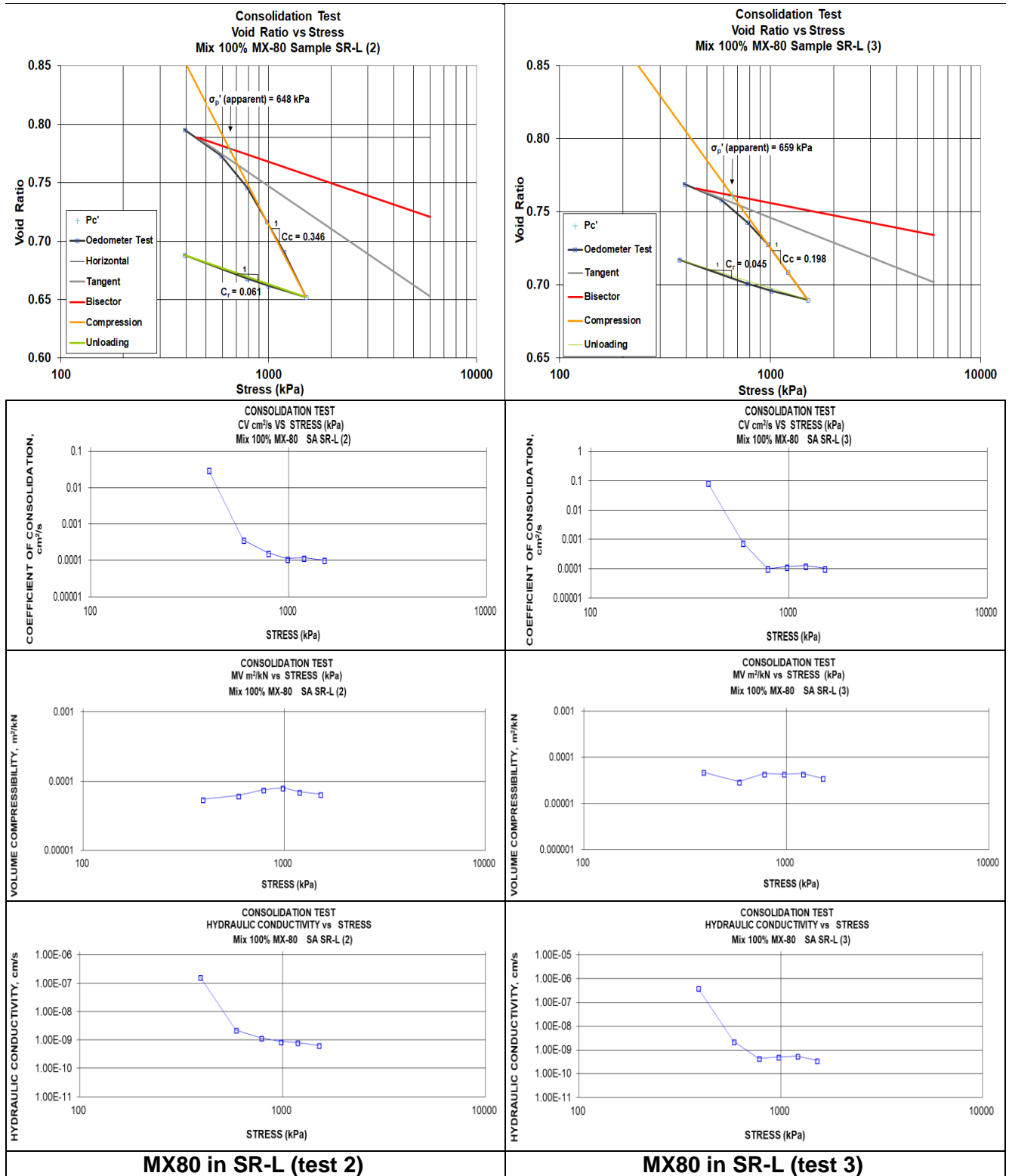


Figure J-3: Oedometer Tests on MX80 (3)

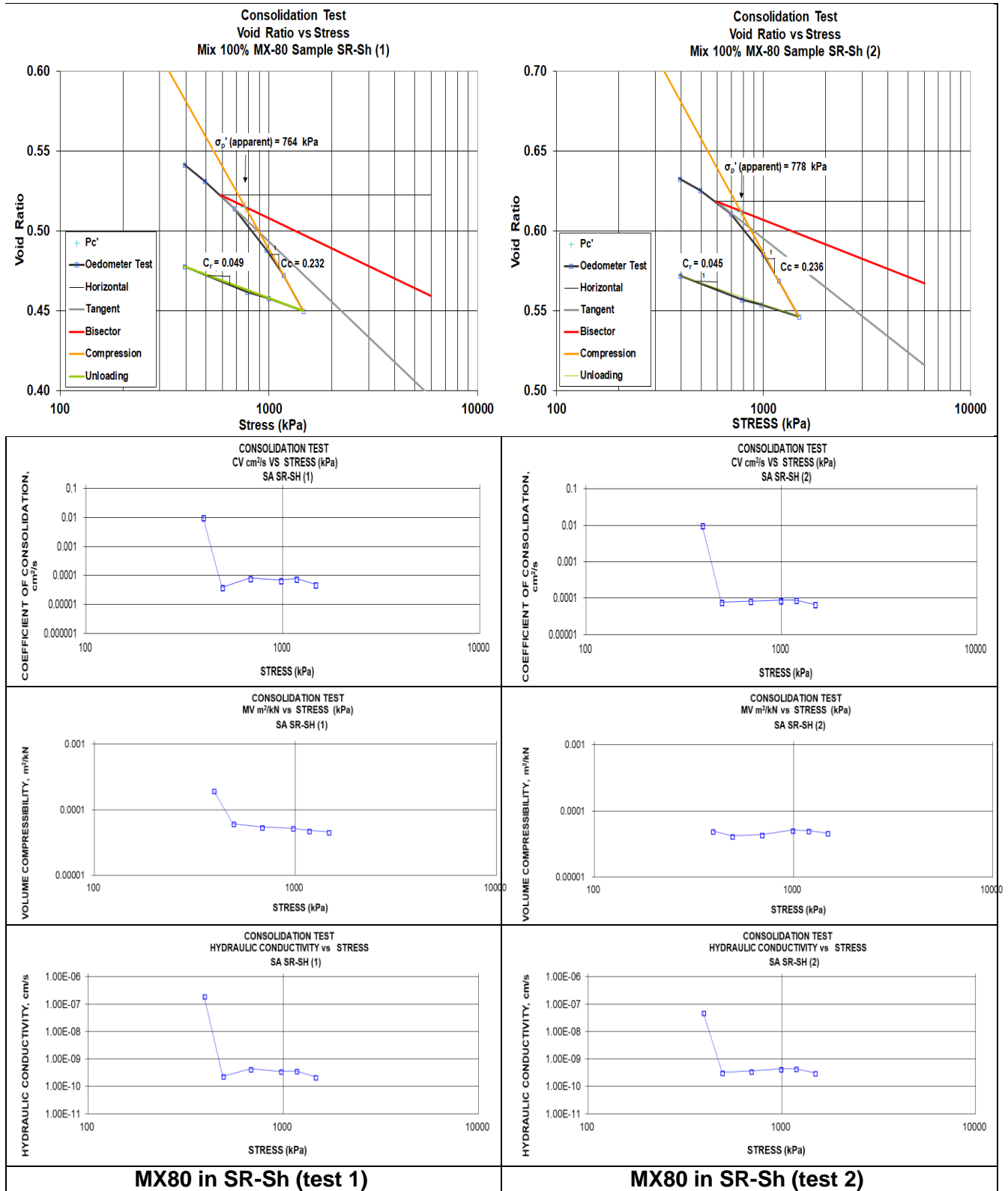


Figure J-4: Oedometer Tests on MX80 (4)

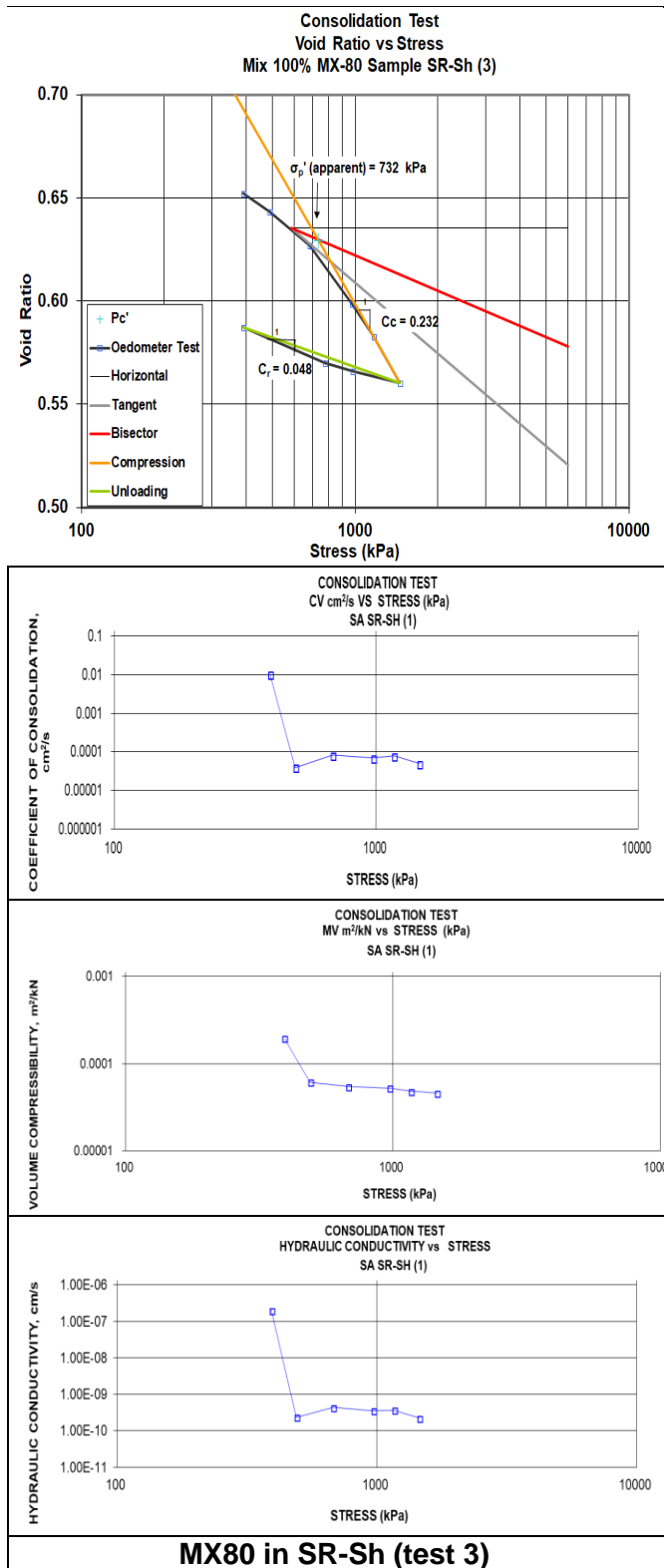


Figure J-5: Oedometer Tests on MX80 (5)

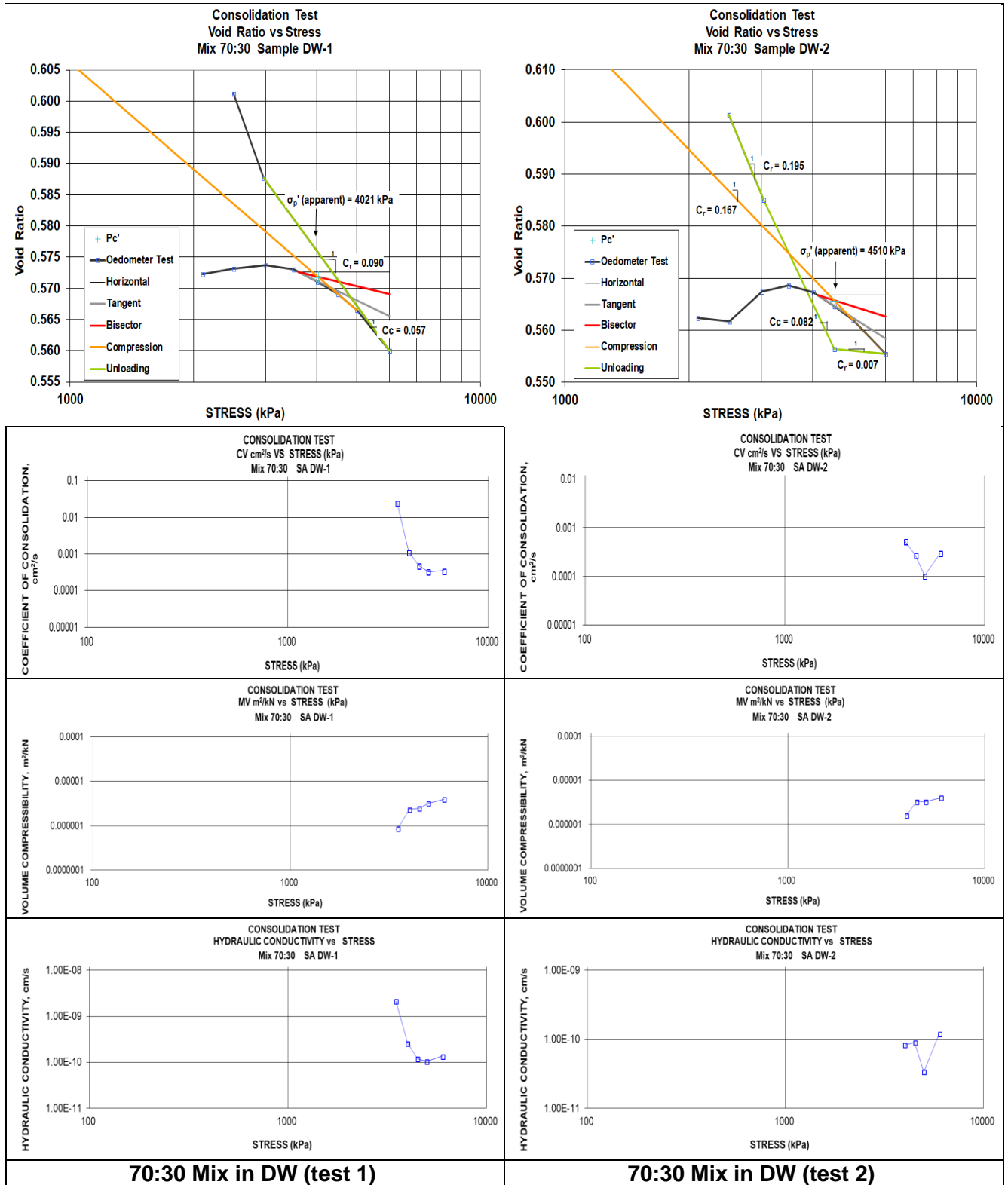


Figure J-6: Oedometer Tests on 70:30 BSM (1)

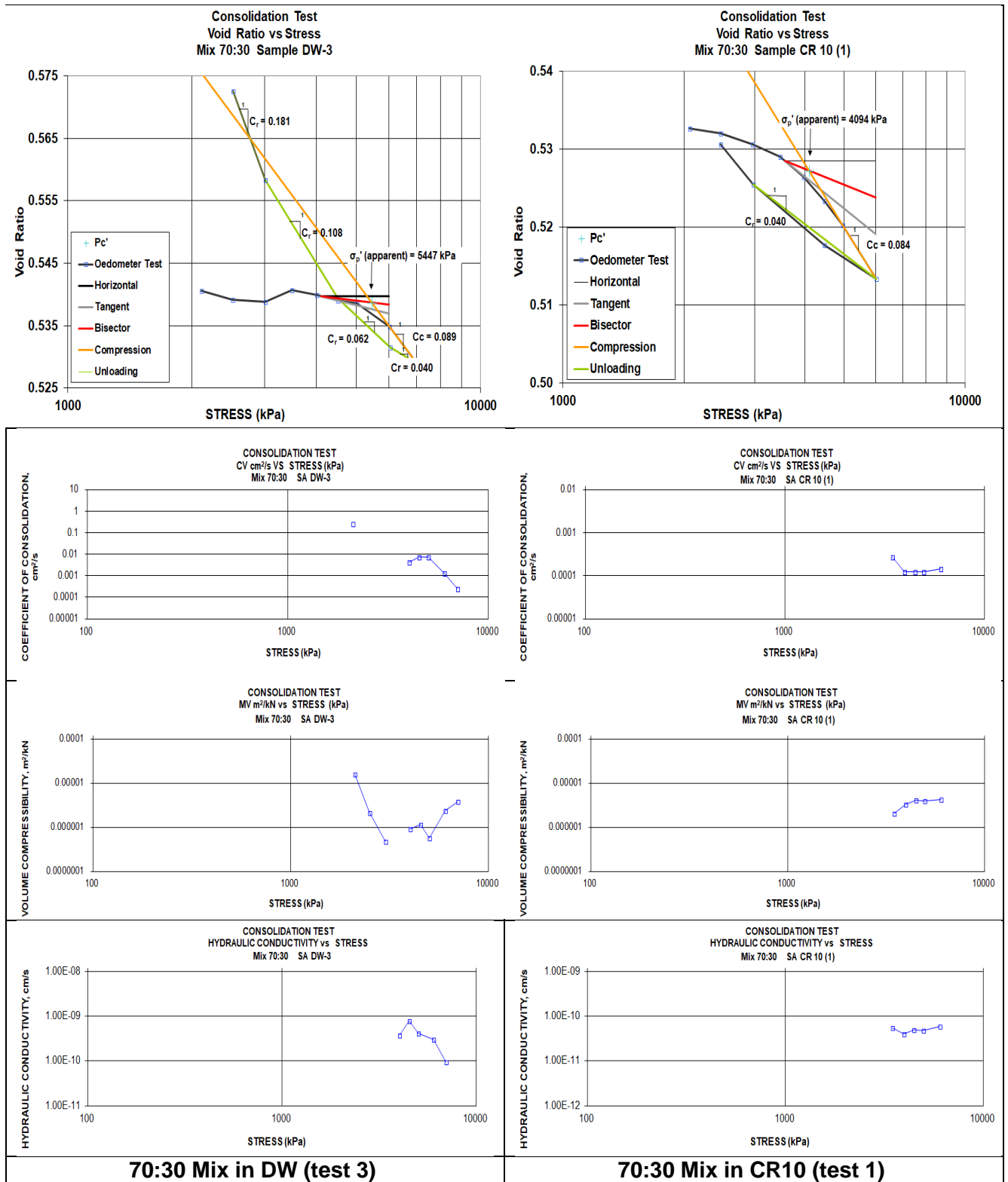


Figure J-7: Oedometer Tests on 70:30 BSM (2)

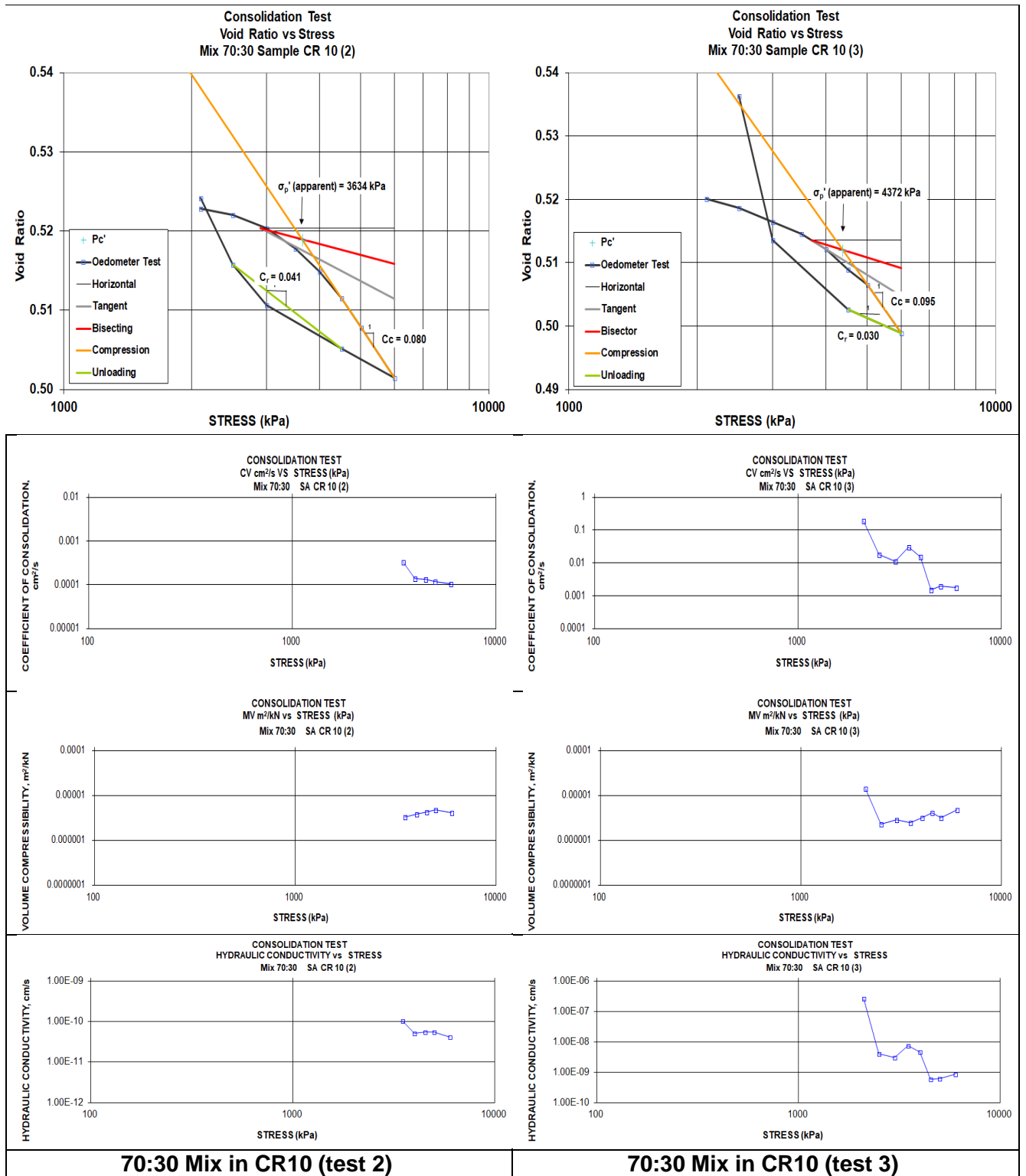


Figure J-8: Oedometer Tests on 70:30 BSM (3)

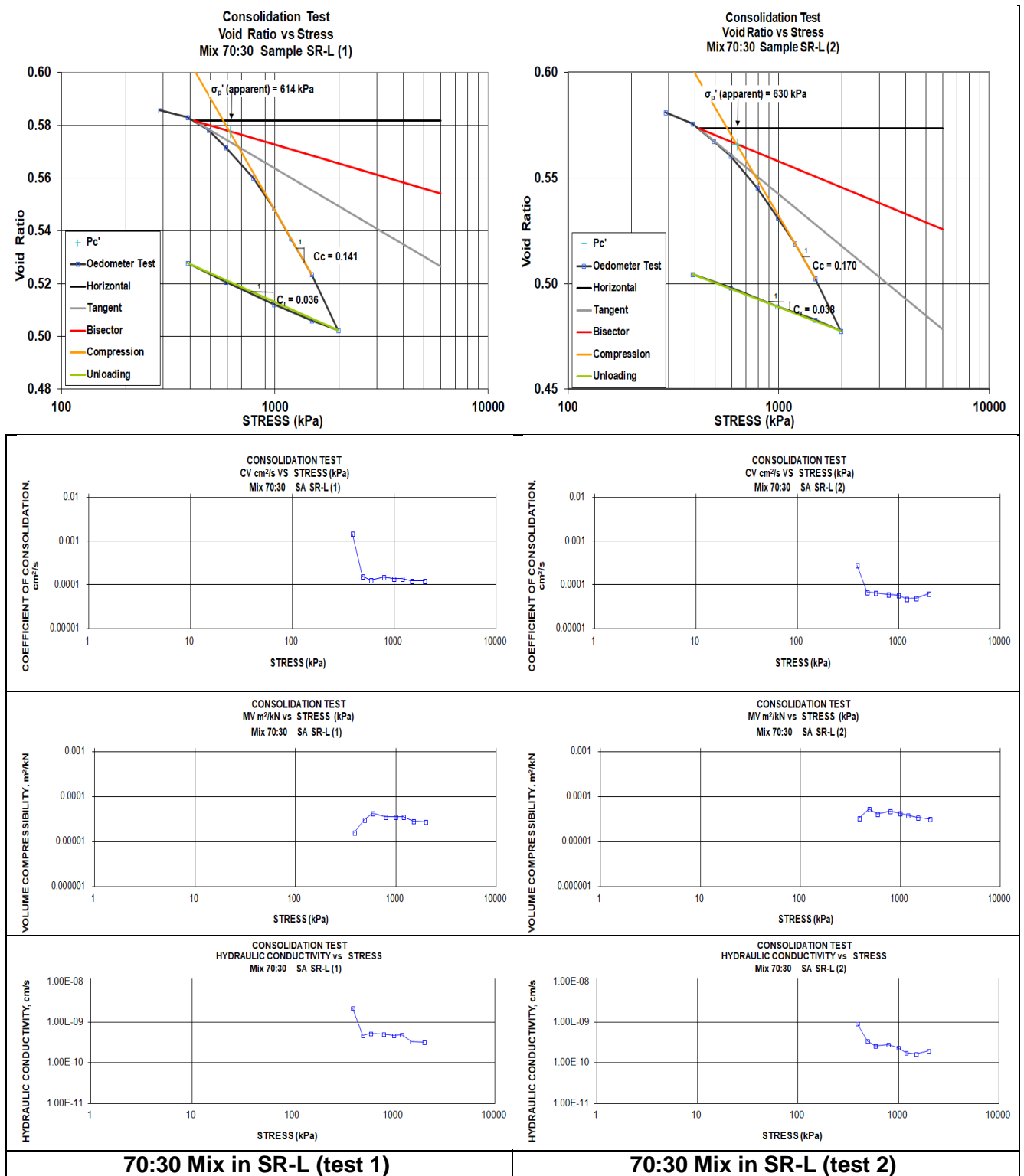


Figure J-9: Oedometer Tests on 70:30 BSM (4)

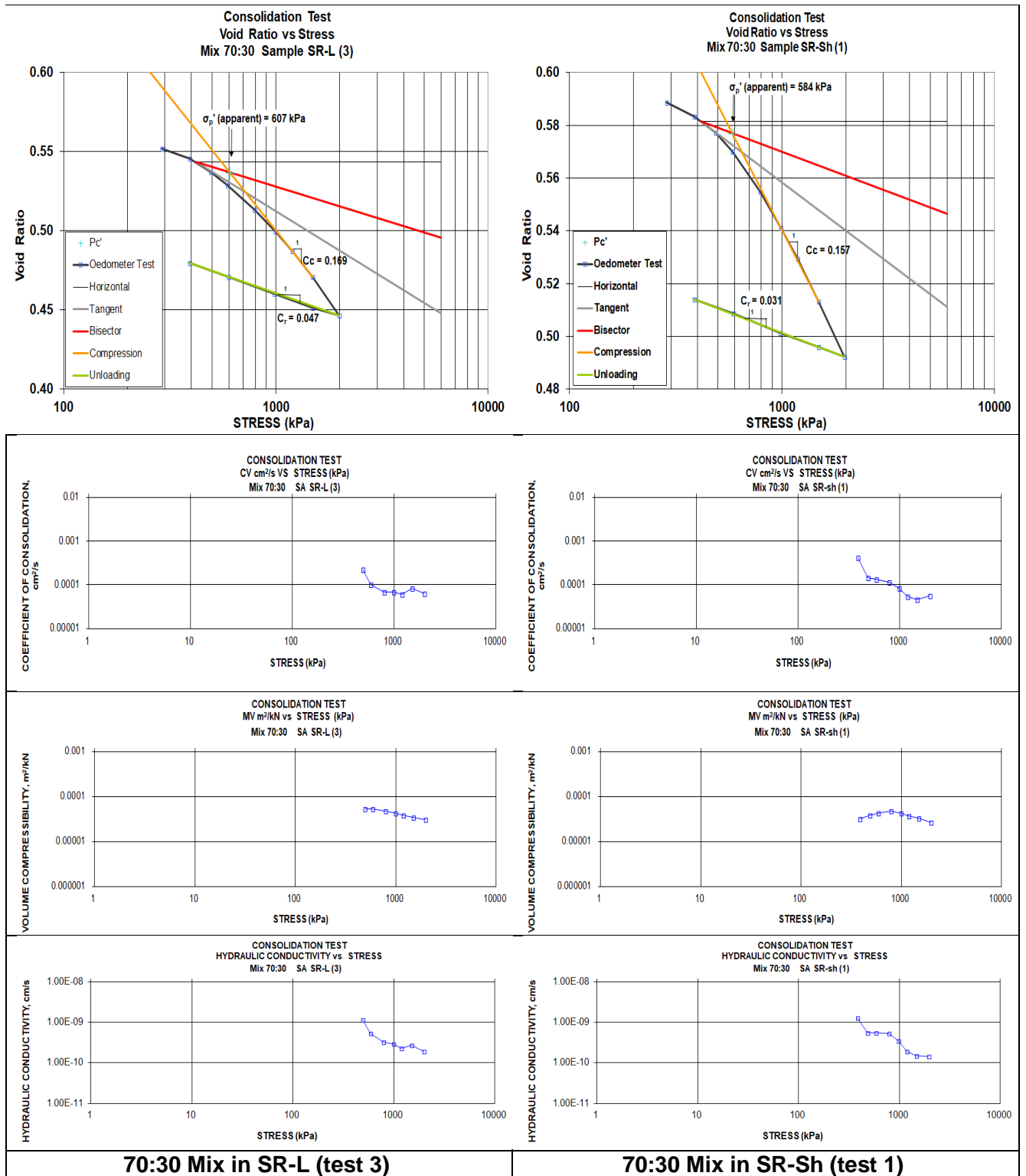


Figure J-10: Oedometer Tests on 70:30 BSM (5)

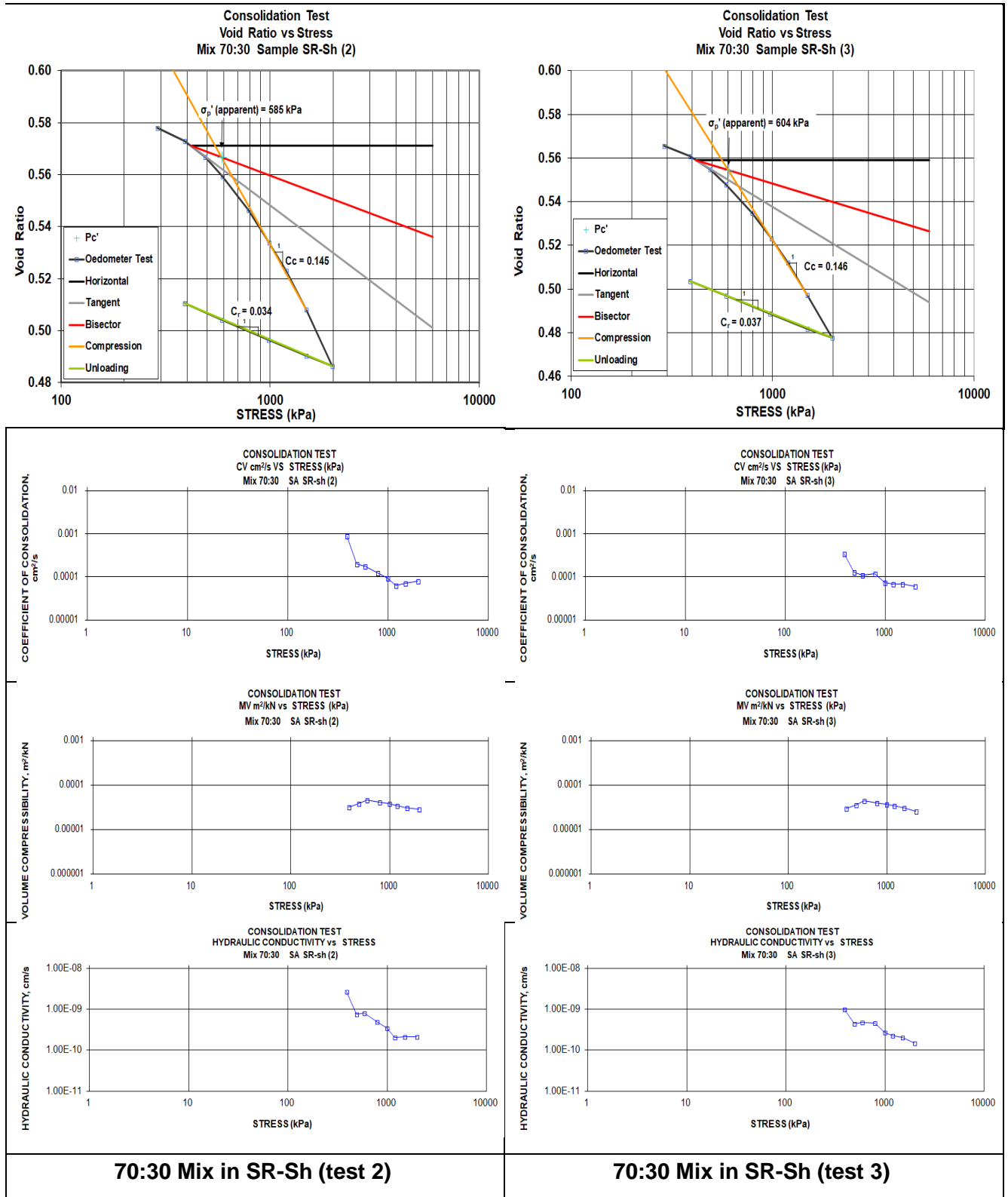


Figure J-11: Oedometer Tests on 70:30 BSM (6)

Table J-1: 1-D Consolidation (Oedometer) Test Results (1)

Test	Stress	Avg Stress	Dry Density	Avg Density	EMDD	Void Ratio	Avg e	t90	cv.	Avg. Cv	mv	Avg mv	Cc	Cr Cs	Lambda λ	Kappa κ	Avg k	Pc	e at Pc
	kPa	(MPa)	Mg/m ³	(Mg/m ³)	(Mg/m ³)	e		sec	m ² /s	(m ² /s)	m ² /kN	m ² /kN	MPa ⁻¹	MPa ⁻¹			(m/s)	(kPa)	
70-30 DW (1)	4496	5.17	1.815	1.820	1.460	0.569	0.563	2614	4.89E-08	3.40E-08	2.50E-06	3.61E-06	0.082	0.09	0.036	0.039	1.20E-12	4364	0.571
70-30 DW (1)	4999		1.818			0.566		3840	3.32E-08		3.22E-06								
70-30 DW (1)	6000		1.823			0.560		3650	3.47E-08		3.99E-06								
70-30 DW (2)	4508	5.17	1.817	1.823	1.463	0.565	0.559	4741	2.74E-08	2.03E-08	3.35E-06	3.70E-06	0.082	0.085	0.036	0.037	7.72E-13	4510	0.566
70-30 DW (2)	5006		1.820			0.562		12442	1.04E-08		3.31E-06								
70-30 DW (2)	6007		1.825			0.555		4267	3.01E-08		4.09E-06								
70-30 DW (3)	5018	6.01	1.852	1.860	1.506	0.539	0.532	167	7.41E-07	7.68E-08	5.60E-07	3.05E-06	0.089	0.082	0.039	0.036	1.95E-12	5447	0.538
70-30 DW (3)	6020		1.857			0.535		960	1.28E-07		2.36E-06								
70-30 DW (3)	7001		1.864			0.529		4860	2.52E-08		3.75E-06								
AVG DW		5.451		1.834	1.476		0.551			4.37E-08		3.45E-06	0.084	0.086	0.037	0.037	0.000	4774	0.558
MX80 DW (1)	3500	3.75	1.532	1.534	1.387	0.853	0.851	2828	4.71E-08	1.31E-08	3.13E-06	2.76E-06	0.071	0.232	0.031	0.101	2.34E-13	>4000	<0.85
MX80 DW (1)	3750		1.533			0.852		6827	1.95E-08		8.22E-07								
MX80 DW (1)	4000		1.534			0.850		19657	6.76E-09		4.70E-06								
MX80 DW (2)	3500	3.75	1.531	1.536	1.388	0.855	0.849	9597	1.36E-08	5.95E-09	4.72E-06	8.65E-06	0.138	0.192	0.060	0.083	4.77E-13	>4000	<0.84
MX80 DW (2)	3750		1.534			0.852		18259	7.15E-09		6.29E-06								
MX80 DW (2)	4000		1.538			0.847		27307	4.76E-09		1.10E-05								
MX80 DW (3)	3500	3.75	1.548	1.552	1.406	0.835	0.827	26740	4.90E-09	3.84E-09		1.18E-05	0.189	0.122	0.082	0.053	4.37E-13	>3500	<0.83
MX80 DW (3)	3750		1.550			0.830		27306	4.78E-09		1.10E-05								
MX80 DW (3)	4000		1.555			0.824		44827	2.89E-09		1.26E-05								
AVG DW		3.750		1.541	1.394		0.842			7.64E-09		7.74E-06	0.133	0.182	0.058	0.079	0.000	4000	0.840
70-30 CR-10 (1)	3964	5.146	1.815	1.826	1.461	0.527	0.517	10355	1.25E-08	1.33E-08	3.23E-06	4.12E-06	0.084	0.04	0.036	0.017	5.38E-13	4094	0.527
	4465		1.818			0.523		10314	1.25E-08		4.05E-06								
	4965		1.822			0.520		10355	1.24E-08		3.97E-06								
	6008		1.830			0.513		9011	1.42E-08		4.27E-06								
70-30 CR-10 (2)	4003	5.170	1.829	1.841	1.482	0.515	0.505	9127	1.38E-08	1.12E-08	3.81E-06	4.41E-06	0.08	0.041	0.035	0.018	4.83E-13	3634	0.519
	4503		1.833			0.512		9514	1.32E-08		4.21E-06								
	5003		1.837			0.508		10587	1.18E-08		4.76E-06								
	6004		1.845			0.501		11854	1.05E-08		4.05E-06								
70-30 CR-10 (3)*	4503	5.170	1.836	1.844	1.486	0.509	0.503	866	1.47E-07	1.74E-07	4.02E-06	3.98E-06	0.095	0.03	0.041	0.013	7.23E-12	4372	0.512
	5003		1.839			0.506		634	2.00E-07		3.15E-06								
	6004		1.848			0.499		714	1.76E-07		4.80E-06								
AVG CR-10		5.162		1.837	1.476		0.508			6.63E-08		4.17E-06	0.086	0.037	0.037	0.016	2.75E-12	4033	0.519

Table J-1: 1-D Consolidation (Oedometer) Test Results (2)

Test	Stress	Avg Stress	Dry Density	Avg Density	EMDD	Void Ratio	Avg e	t90	cv.	Avg. Cv	mv	Avg mv	Cc	Cr Cs	Lambda λ	Kappa κ	Avg k	Pc	e at Pc
	kPa	(MPa)	Mg/m ³	(Mg/m ³)	(Mg/m ³)	e		sec	m ² /s	(m ² /s)	m ² /kN	m ² /kN	MPa ⁻¹	MPa ⁻¹			(m/s)	(kPa)	
70-30 SR-L (1)	588	1.550	1.756	1.824	1.455	0.572	0.502	10048	1.30E-08	1.22E-08	4.18E-05	2.76E-05	0.141	0.036	0.061194	0.015624	3.30E-12	614	0.577
	788		1.769			0.56		8785	1.47E-08		3.55E-05								
	988		1.782			0.549		9375	1.36E-08		3.57E-05								
	1188		1.795			0.537		8930		3.57E-05								
	1488		1.811			0.524		10140	1.21E-08		2.80E-05								
	1974		1.837			0.502		9796	1.23E-08		2.71E-05								
70-30 SR-L (2)	588	1.551	1.768	1.853	1.486	0.561	0.478	10983	6.50E-09	5.61E-09	4.15E-05	3.28E-05	0.17	0.038	0.07378	0.016492	1.80E-12	630	0.566
	788		1.786			0.545		11793	5.97E-09		4.78E-05								
	988		1.802			0.531		12125	5.70E-09		4.25E-05								
	1188		1.817			0.519		14230	4.77E-09		3.78E-05								
	1488		1.837			0.503		13500	4.94E-09		3.41E-05								
	1976		1.868			0.478		10314	6.28E-09		3.15E-05								
70-30 SR-L (3)	591	1.554	1.805	1.892	1.532	0.529	0.483	6738	1.02E-08	7.20E-09	5.23E-05	3.24E-05	0.169	0.047	0.073346	0.020398	2.30E-12	607	0.537
	791		1.824			0.514		9967	6.77E-09		4.81E-05								
	991		1.840			0.5		9746	6.79E-09		4.31E-05								
	1191		1.856			0.487		10667	6.10E-09		3.78E-05								
	1491		1.876			0.471		7859	8.12E-09		3.40E-05								
	1980		1.908			0.447		9897	6.27E-09		3.08E-05								
AVG SR-L		1.552	1.819	1.856	1.491	0.518	0.488	10272	8.48E-09	8.34E-09	3.81E-05	3.09E-05	0.160	0.040	0.069	0.018	2.46E-12	617	0.560
MX80 SR-L (1)	778	1.207	1.554	1.607	1.452	0.757	0.699	2815	2.50E-08	1.45E-08	6.32E-05	5.56E-05	0.282	0.059	0.122388	0.025606	7.83E-12	646	0.785
	971		1.573			0.735		6490	1.06E-08		6.00E-05								
	1162		1.592			0.714		5352	1.25E-08		5.88E-05								
	1486		1.622			0.683		3961	1.64E-08		5.24E-05								
MX80 SR-L (2)	785	1.225	1.564	1.634	1.476	0.746	0.672	4335	1.60E-08	1.11E-08	7.55E-05	6.75E-05	0.346	0.061	0.150164	0.026474	7.30E-12	648	0.775
	981		1.590			0.717		6000	1.12E-08		8.10E-05								
	1185		1.615			0.691		5479	1.19E-08		7.01E-05								
	1508		1.652			0.652		6151	1.02E-08		6.49E-05								
MX80 SR-L (3)	777	1.229	1.566	1.606	1.453	0.743	0.709	12907	1.01E-08	1.16E-08	4.42E-05	3.97E-05	0.198	0.045	0.085932	0.01953	4.56E-12	659	0.760
	971		1.580			0.728		10845	1.18E-08		4.40E-05								
	1207		1.597			0.709		9885	1.27E-08		4.41E-05								
	1509		1.615					11760	1.05E-08		3.53E-05								
AVG SR-L		1.220		1.616	1.460		0.693			1.24E-08		5.43E-05	0.275	0.055	0.119	0.024	6.56E-12	651	0.773

Table J-1: 1-D Consolidation (Oedometer) Test Results (3)

Test	Stress	Avg Stress	Dry Density	Avg Density	EMDD	Void Ratio	Avg e	t90	cv.	Avg. Cv	mv	Avg mv	Cc	Cr Cs	Lambda λ	Kappa κ	Avg k	Pc	e at Pc
	kPa	(MPa)	Mg/m ³	(Mg/m ³)	(Mg/m ³)	e		sec	m ² /s	(m ² /s)	m ² /kN	m ² /kN	MPa ⁻¹	MPa ⁻¹			(m/s)	(kPa)	
70-30 SR-Sh (1)	586	1.547	1.770	1.850	1.484	0.570	0.492	9956	1.31E-08	5.04E-09	4.31E-05	2.99E-05	0.157	0.031	0.068	0.013	1.46E-12	584	0.577
	786		1.788			0.555		11142	1.15E-08		4.66E-05								
	987		1.804			0.541		15147	8.32E-09		4.23E-05								
	1186		1.818			0.529		23207	5.34E-09		3.67E-05								
	1486		1.837			0.513		26460	4.60E-09		3.30E-05								
	1970		1.863			0.492		21705	5.47E-09		2.67E-05								
70-30 SR-Sh (2)	588	1.550	1.783	1.857	1.492	0.559	0.486	7234	1.78E-08	7.48E-09	4.60E-05	2.92E-05	0.145	0.034	0.063	0.015	2.13E-12	585	0.567
	788		1.798			0.546		10314	1.23E-08		4.05E-05								
	988		1.812			0.534		13500	9.25E-09		3.85E-05								
	1188		1.825			0.523		19923	6.17E-09		3.40E-05								
	1488		1.843			0.508		16890	7.16E-09		3.04E-05								
	1975		1.870			0.486		15135	7.79E-09		2.79E-05								
70-30 SR-Sh (3)	588	1.550	1.796	1.869	1.507	0.548	0.488	11629	1.09E-08	6.34E-09	4.45E-05	2.80E-05	0.146	0.037	0.063	0.016	1.75E-12	604	0.555
	788		1.811			0.535		10667	1.17E-08		3.98E-05								
	987		1.825			0.523		16445	7.48E-09		3.64E-05								
	1188		1.838			0.512		18027	6.72E-09		3.44E-05								
	1488		1.857			0.497		17796	6.69E-09		3.09E-05								
	1975		1.881			0.478		19440	5.98E-09		2.51E-05								
AVG SR-Sh		1.549		1.859	1.494		0.489			6.28E-09		2.90E-05	0.149	0.034	0.065	0.015	1.78E-12	591	0.566
MX80 SR-Sh (1)	681	1.200	1.740	1.801	1.655	0.514	0.462	7707	8.13E-09	6.36E-09	5.48E-05	4.72E-05	0.232	0.049	0.101	0.021	2.95E-12	764	0.516
	972		1.765			0.489		8930	6.82E-09		5.26E-05								
	1168		1.790			0.473		7594	7.80E-09		4.82E-05								
	1460		1.813			0.450		11760	4.91E-09		4.62E-05								
MX80 SR-Sh (2)	692	1.218	1.637	1.690	1.538	0.611	0.558	8640	8.37E-09	7.89E-09	4.42E-05	4.85E-05	0.236	0.045	0.102	0.020	3.77E-12	778	0.613
	989		1.658			0.586		8074	8.73E-09		5.14E-05								
	1185		1.680			0.569		7661	8.96E-09		5.06E-05								
	1481		1.701			0.547		9830	6.81E-09		4.64E-05								
MX80 SR-Sh (3)	680	1.199	1.629	1.687	1.536	0.627	0.571	8560	8.34E-09	4.92E-09	4.88786E-05	4.71E-05	0.232	0.048	0.101	0.021	2.29E-12	732	0.630
	972		1.658			0.599		7935	8.75E-09		5.75954E-05								
	1166		1.674			0.583		10935	6.18E-09		4.86686E-05								
	1457		1.699			0.560		17957	3.67E-09		4.54794E-05								
AVG SR-Sh		1.206		1.726	1.576		0.530			6.39E-09		4.76E-05	0.233	0.047	0.101	0.021	3.00E-12	758	0.586

APPENDIX K: THERMAL PROPERTIES MEASUREMENTS

Table L-1: Thermal Properties of 100% Bentonite (1.5 Mg/m³) and HCB (1.7 Mg/m³)

Target Dry Density of 1.5 Mg/m ³						Target Dry Density of 1.7 Mg/m ³					
Sample Name	Dry Density ρ _d (g/cm ³)	Saturation S (%)	Specific Heat (MJ/m ³ K)	Thermal Conductivity (W/mK)	Thermal Diffusivity (mm ² /s)	Sample Name	Dry Density ρ _d (g/cm ³)	Saturation S (%)	Specific Heat (MJ/m ³ K)	Thermal Conductivity (W/mK)	Thermal Diffusivity (mm ² /s)
15-O-D	1.50	0%	1.27	0.48	0.38	17-O-D	1.70	0%	1.49	0.57	0.39
15-O-E	1.52	0%	1.26	0.48	0.38	17-O-E	1.71	0%	1.49	0.53	0.36
15-O-F	1.51	0%	1.29	0.51	0.40	17-O-F	1.72	0%	1.72	0.55	0.32
Avg	1.51	0.00	1.27	0.49	0.38	Avg	1.71	0.00	1.57	0.55	0.36
Stdev	0.01	0.00	0.01	0.02	0.01	Stdev	0.01	0.00	0.11	0.02	0.03
15-5-D	1.51	7%	1.65	0.46	0.28	17-5-D	1.70	6%	1.85	0.57	0.31
15-5-E	1.50	7%	1.71	0.44	0.26	17-5-E	1.68	5%	1.83	0.56	0.31
15-5-F	1.52	6%	1.53	0.47	0.30	17-5-F	1.72	6%	1.71	0.57	0.33
Avg	1.51	0.07	1.63	0.46	0.28	Avg	1.70	0.06	1.80	0.57	0.32
Stdev	0.01	0.01	0.08	0.01	0.02	Stdev	0.02	0.00	0.06	0.00	0.01
15-10-D	1.48	11%	1.73	0.46	0.27	17-10-D	1.69	11%	2.18	0.55	0.25
15-10-E	1.51	11%	2.03	0.47	0.23	17-10-E	1.67	11%	2.15	0.56	0.26
15-10-F	1.49	9%	2.10	0.44	0.21	17-10-F	1.68	10%	1.94	0.62	0.32
Avg	1.49	0.10	1.95	0.46	0.24	Avg	1.68	0.11	2.09	0.58	0.28
Stdev	0.01	0.01	0.16	0.01	0.02	Stdev	0.01	0.00	0.11	0.03	0.03
15-15-D	1.50	16%	1.88	0.52	0.28	17-15-D	1.69	15%	2.23	0.59	0.26
15-15-E	1.52	16%	1.88	0.54	0.29	17-15-E	1.69	15%	2.18	0.58	0.27
15-15-F	1.50	17%	2.24	0.52	0.23	17-15-F	1.70	15%	2.22	0.62	0.28
Avg	1.50	0.16	2.00	0.53	0.27	Avg	1.69	0.15	2.21	0.60	0.27
Stdev	0.01	0.00	0.17	0.01	0.02	Stdev	0.00	0.00	0.02	0.02	0.01
15-20-D	1.55	20%	2.01	0.42	0.21	17-20-D	1.68	19%	1.88	0.64	0.34
15-20-E	1.51	21%	2.40	0.57	0.24	17-20-E	1.71	19%	1.83	0.67	0.37
15-20-F	1.50	21%	2.42	0.54	0.22	17-20-F	1.71	19%	2.02	0.70	0.35
15-20-G	1.51	21%	2.54	0.52	0.21	Avg	1.70	0.19	1.91	0.67	0.35
Avg	1.52	0.21	2.34	0.51	0.22	Stdev	0.01	0.00	0.08	0.03	0.01
Stdev	0.02	0.00	0.20	0.06	0.01						
15-30-D	1.51	29%	2.19	0.67	0.31	17-30-D	1.70	25%	2.05	0.61	0.30
15-30-E	1.51	35%	2.42	0.74	0.31	17-30-E	1.76	25%	1.79	0.68	0.38
15-30-F	1.49	34%	2.51	0.80	0.32	17-30-F	1.70	24%	1.86	0.70	0.38
Avg	1.50	0.33	2.37	0.74	0.31	Avg	1.72	0.25	1.90	0.66	0.35
Stdev	0.01	0.03	0.14	0.05	0.01	Stdev	0.03	0.01	0.11	0.04	0.04
15-40-D	1.52	39%	3.01	0.67	0.22	17-40-D	1.72	39%	2.47	0.88	0.36
15-40-E	1.53	37%	2.38	0.70	0.29	17-40-E	1.73	40%	2.38	0.83	0.35
15-40-F	1.53	36%	2.88	0.69	0.29	17-40-F	1.71	38%	2.32	0.85	0.37
Avg	1.53	0.37	2.76	0.69	0.27	Avg	1.72	0.39	2.39	0.85	0.36
Stdev	0.00	0.01	0.27	0.01	0.03	Stdev	0.01	0.01	0.06	0.02	0.01
15-50-D	1.55	48%	2.64	0.85	0.32	17-50-A	1.64	43%	2.90	0.92	0.32
15-50-E	1.53	46%	2.80	0.82	0.29	17-50-B	1.63	44%	3.06	0.86	0.28
15-50-F	1.52	45%	2.41	0.80	0.33	17-50-C	1.65	46%	2.82	0.94	0.33
Avg	1.53	0.47	2.62	0.82	0.31	Avg	1.64	0.44	2.93	0.91	0.31
Stdev	0.01	0.01	0.16	0.02	0.02	Stdev	0.01	0.01	0.10	0.03	0.02
15-60-D	1.57	61%	2.52	0.90	0.36	17-60-A	1.69	58%	2.58	1.08	0.42
15-60-E	1.57	61%	2.95	0.99	0.34	17-60-B	1.66	56%	2.53	0.98	0.39
15-60-F	1.57	62%	2.87	1.09	0.38	17-60-C	1.62	52%	2.37	0.86	0.36
Avg	1.57	0.61	2.78	0.99	0.36	Avg	1.65	0.55	2.49	0.97	0.39
Stdev	0.00	0.00	0.19	0.08	0.02	Stdev	0.03	0.02	0.09	0.09	0.02
15-80-A	1.51	87%	2.65	1.27	0.48	17-80-A	1.67	74%	2.79	1.25	0.45
15-80-B	1.46	80%	3.36	1.15	0.34	17-80-B	1.66	74%	2.91	1.16	0.40
15-80-C	1.43	84%	2.43	0.94	0.39	17-80-C	1.66	68%	2.62	1.32	0.50
Avg	1.47	0.84	2.81	1.12	0.40	17-80-D	1.76	71%	2.78	1.05	0.38
Stdev	0.03	0.03	0.39	0.13	0.06	17-80-E	1.70	66%	3.49	1.09	0.31
						17-80-F	1.71	66%	3.03	1.13	0.37
15-100-A	1.41	97%	2.57	1.26	0.49	Avg	1.69	0.70	2.94	1.16	0.40
15-100-B	1.44	95%	3.65	1.20	0.33	Stdev	0.03	0.03	0.28	0.09	0.06
15-100-C	1.45	96%	3.00	1.30	0.43						
Avg	1.43	0.96	3.07	1.25	0.42	17-100-A-1	1.66	92%	2.83	1.32	0.47
Stdev	0.01	0.01	0.45	0.04	0.07	17-100-B-1	1.64	89%	3.12	1.35	0.43
						17-100-C-1	1.63	87%	2.94	1.34	0.46
						17-100-A-2	1.66	92%	2.45	1.15	0.45
						17-100-B-2	1.64	89%	2.62	1.14	0.44
						17-100-C-2	1.63	87%	2.28	1.14	0.50
						Avg	1.64	0.89	2.71	1.24	0.46
						Stdev	0.01	0.02	0.29	0.10	0.02

